AN INVESTIGATION OF MECHANICS OF COLLAGEN AND FIBRIL IN BONE AND INTERACTIONS IN SWELLING CLAYS: A MOLECULAR AND MULTISCALE MODELING STUDY

A Dissertation
Submitted to the Graduate Faculty
of the
North Dakota State University
of Agriculture and Applied Science

By

Shashindra Man Pradhan

In Partial Fulfillment of the Requirements
for the Degree of
DOCTOR OF PHILOSOPHY

Major Program: Engineering

October 2012

Fargo, North Dakota

North Dakota State University

Graduate School

Title

AN INVESTIGATION OF MECHANICS OF COLLAGEN AND FIBRIL IN BONE AND INTERACTIONS IN SWELLING CLAYS: A MOLECULAR AND MULTISCALE MODELING STUDY

By

Shashindra Man Pradhan

The Supervisory Committee certifies that this ***disquisition*** complies with North Dakota State University's regulations and meets the accepted standards for the degree of

DOCTOR OF PHILOSOPHY

SUPERVISORY COMMITTEE:

Dr. Dinesh Katti

Chair

Dr. Kalpana Katti

Dr. Achintya N. Bezbaruah

Dr. Eakalak Khan

Dr. Lawerence Reynolds

Approved:

11/08/2012

Date

Dr. Gary R. Smith

Department Chair

ABSTRACT

A fundamental study of the mechanics at the molecular scale and bridging it to the continuum level through multiscale modeling is the focus of this work. This work investigates how the material properties of nanoscale systems are influenced by the nonbonded interactions and molecular conformations. The molecular model is then bridged with the finite element model to link mechanics at nanoscale with the continuum scale. This work provides an unprecedented insight into how the interactions at the molecular scale influence mechanical properties at higher scales. Two materials are considered for the molecular modeling study: bone and Na-montmorillonite swelling clay. Bone is composed of composed of collagen molecules and hydroxyapatite in the molecular scale, which are organized into collagen fibril. The molecular dynamics study is carried out to study the nature of collagen-hydroxyapatite interface and the mechanics of collagen in bone. Furthermore, the molecular model of full-length collagen is built for the first time to show the differences in its conformation and deformation mechanism during pulling as compared to the short molecules, upon which the current understanding of is based. The mechanics of collagen is explained with the help of three-tier helical hierarchy not seen in short molecules. Two mechanisms of deformation and conformational stability of collagen are proposed: (i) interlocking gear analogy, and (ii) interplay between level-1 and level-2 hierarchies, the hydrogen bonds acting as an intermediary. The multiscale model of collagen fibril is developed by bridging nanomechanical molecular properties of collagen into the finite element model. This model shows that the molecular interactions between collagen and mineral significantly affect the mechanical response of collagen fibril. The deformation mechanism of collagen

fibril and the effect of collagen crosslinks are also elucidated in this study. In recent years Na-montmorillonite has been proposed for bone regenerative medicine, besides other existing engineering applications. The molecular dynamics study of Na-montmorillonite at different levels of hydration is carried out to understand the role played by molecular interactions in the swelling behavior of Na-montmorillonite. This study greatly adds to our understanding of clay swelling, and provides important insights for modeling exfoliation and particle breakdown in clay.

ACKNOWLEDGEMENTS

I would like to thank my advisor Dr. Dinesh Katti and co-advisor Dr. Kalpana Katti for their invaluable guidance and encouragement throughout my doctorate degree. This work would not have been possible without their support and inspiration.

I would like to acknowledge NDSU Presidential Doctoral Graduate Fellowship and ND EPSCoR Doctoral Dissertation Assistantship for supporting my graduate study. I acknowledge TeraGrid for computational resources at the NCSA Supercomputing Center. I also acknowledge NDSU Center for High Performance Computing (CHPC) for the computational resources, which was crucial for carrying out my work. I greatly appreciate Dr. Greg Wettstein, Dr. Hideaki Kikuchi, Matthew Piehl, and Bryan Mesich of CHPC/CCAST for their fantastic hardware and software support.

I extend my sincere thanks to my advisory committee members: Dr. Achintya N. Bezbaruah, Dr. Eakalak Khan, Dr. Lawerence Reynolds.

I would like to thank all my group members and close friends for their help, cooperation, and constructive advices throughout my study.

Finally, I would like to thank my family members for their incredible love and support, immeasurable sacrifices, and patience throughout my degree.

TABLE OF CONTENTS

LIST OF TABLES

LIST OF FIGURES

LIST OF APPENDIX FIGURES

CHAPTER 1. INTRODUCTION

The material properties of nanoscale systems are the result of a multiscale phenomenon that spans multiple scales ranging from the atomistic to the macroscopic scale. The study of the mechanics of material at the molecular scale is of great importance as the material properties are highly influenced by interactions at the molecular level. The studies presented in this dissertation deals with the investigation of the material behavior at the molecular level and bridging of molecular scale with the continuum scale through multiscale modeling. The studies presented in this dissertation can be divided into two basic subtopics, where the unifying theme is the investigation of the mechanics of material by probing different length scales. The first area of this dissertation deals with modeling the mechanics of material at the molecular scale for understanding the molecular deformation mechanisms and the material properties at the nanoscale. Two separate materials of different origin are considered for the molecular modeling study: bone and montmorillonite swelling clay. Bone is a biological tissue with high degree of hierarchical order that can teach us number of things about the role of organizations and interactions starting at the molecular scale and the redundancy of design employed by nature. In recent years clay has been proposed as a nanomaterial for regenerative medicine, besides its current applications for enhancing number of various material properties in nanocomposites, which depend on the molecular scale properties of clay. The second area of this dissertation deals with multiscale modeling to bridge molecular model with the continuum model of material. Bone is considered for the multiscale modeling study in which the nanomechanical properties of bone, obtained

from molecular simulations, is bridged with the finite element model of collagen fibril. The underlying hypothesis for the studies presented in this dissertation, which probe into the smallest scales of a material, is that the molecular interactions significantly affect the properties of human bone and other nanoscale systems.

1.1. Bone

Bone is an integral part of skeletal system designed to support and protect various body organs. In addition to the structural role, it has various mechanical, biological and chemical functions such as the production of red and white blood cells, movement of organs, and storage of minerals such as calcium and phosphorous necessary for bodily function. Light weight and adequate strength are two highly desirable properties of any structural material. Bone is both lightweight and strong due to the rich structural hierarchy spanning from the molecular to the macroscopic length scales and the porous design necessary for blood flow. Bone is a very complex biological-nanocomposite consisting of at least six levels of structural hierarchy, each of the structures existing at different length scales: (1) bone, (2) osteon, (3) concentric lamella, (4) collagen fiber, (5) collagen fibril, (6) collagen molecule, and hydroxyapatite nanocrystals [1-3]. Osteons are the structural units of compact bone, roughly cylindrical in shape and composed of concentric lamellas surrounding the central Haversian canal. The concentric lamellas consist of collagen fiber, which are in turn composed of collagen fibrils. The collagen fibrils are composed of the staggered arrangement of collagen molecules parallel to each other, and aligned along the longitudinal axis of bone. Collagen is the most abundant fibrous protein in our human body with superior mechanical properties that impart the tissue with necessary strength and toughness. Collagen is a very slender molecule with

very high aspect ratio, approximately 300 nm in length and 1.5 nm in diameter. The collagen molecule consists of three helical polypeptide chains, known as alpha chains, wrapped into a triple helical structure. Between the ends of collagen molecules is a gap zone where the hydroxyapatite nanocrystals nucleate. This kind of multi-level structural hierarchy starting at the molecular scale and the highly organized morphology present in bone are not found in synthetic nanocomposites.

The length scales characterizing each of the hierarchical structures of bone are shown in figure 1.1. The collagen molecules and hydroxyapatite nanocrystals exist in the molecular scale. At this scale the material behavior is governed by the molecular level bonded and nonbonded interactions, and the molecular conformation. The continuum methods used to describe the mechanics of larger structures are not applicable at this scale. There are extensive studies pertaining to the macroscopic and microscopic properties of bone, however the detailed studies of nanomechanics of collagen molecules and the molecular interactions at the collagen-mineral interface are scarce. Our previous Molecular Dynamics studies by Bhowmik et al. [4,5] show the presence of strong interactions between collagen molecule and mineral, which significantly affect the mechanical response of collagen. Similar observations have been made in our previous studies of organic-mineral interface in nacre [6] and polymer clay nanocomposite [7]. The arrangement of collagen molecules and hydroxyapatite in collagen fibril leads to a significant interfacial-area between collagen and mineral that affect the substantial volume of collagen. Depending on the relative orientation of collagen with respect to the mineral surface in the collagen fibril, different kinds of interfacial interactions take place, resulting in the directional dependence of collagen-hydroxyapatite interactions. Two

possible cases of the relative orientations between collagen and mineral are considered in this study: (i) collagen molecules placed normal to the hydroxyapatite (0001) surface, and (ii) collagen molecules parallel to the hydroxyapatite (10 $\bar{1}$ 0) surface. The collagen pulled normal to the mineral surface elucidates the mechanics of interaction between the end of collagen and the mineral located in the hole zone; whereas, the collagen pulled parallel to the mineral surface helps us understand the interaction between the surface of collagen and the intrafibrillar/interfibrillar mineral. This study is carried out by pulling the collagen molecule in the close proximity of mineral surface using Steered Molecular Dynamics. This is an important study that sheds light on the mechanics of collagen in various mineral environments inside collagen fibril, as well as, the effect of different crystallographic surface of mineral on collagen deformation.

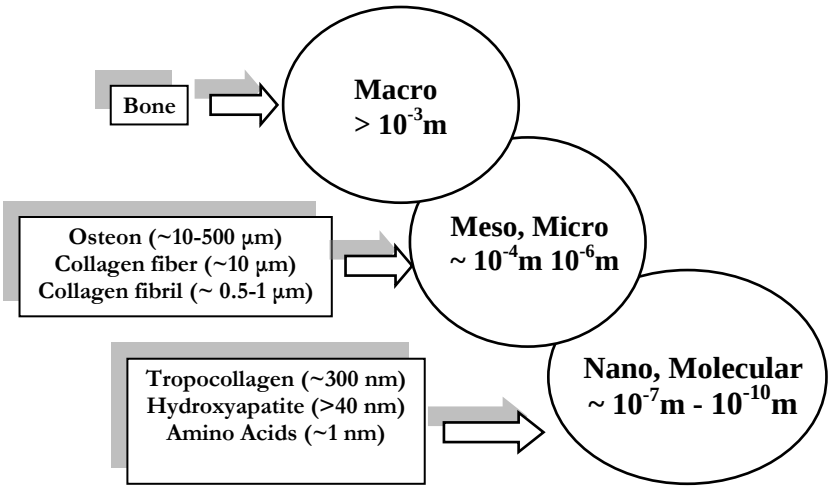

Figure 1.1. Length scales characterizing bone hierarchy and simulation/experimental methods applicable at these scales.

Collagen is an important protein that constitutes more than three quarters of the total proteins in the human body and provides structural integrity to various connective tissues such as bone, tendon, and skin. This long and slender molecule has exceptional mechanical properties of being highly elastic and able to undergo very large deformation, contributing to the strength and toughness of tissues. The current understanding of collagen mechanics is based on the Molecular Dynamics studies of shorter collagen approximately 8.5 nm in length, which is significantly shorter than the real collagen (~ 300 nm long). For a triple helical molecule such as collagen with multiple levels of helical hierarchy, the shorter molecule may not be able to able to capture its deformation mechanics in entirety. In this study the mechanical behavior of short and full length collagen is investigated using steered molecular dynamics at various loading conditions to compare to mechanisms with respect to unfolding of molecule and the resulting deformation response. This study captures the similarities and differences in the deformation mechanism of full-length collagen molecule, and deciphers the nuances of mechanical response of collagen in greater detail through simulation of the full-length collagen.

The molecular structure of collagen consists of three alpha chains left-handed helical in shape, each of which contain a repeating triplet of amino acids (Glycine-X-Y), where X and Y can be any amino acid - mostly proline and hydroxyproline. The three alpha chains are wrapped into triple helical structure forming inter-chain hydrogen bonds between them. In a collagen molecule glycine is situated near the center axis of collagen and the residues X and Y are exposed on the surface to allow close packing three alpha chains [8,9]. Furthermore, the collagen structure exhibits a new level of helical hierarchy, as

shown by our molecular dynamics simulation for the first time. Albeit the structure of collagen has been studied[9-14] extensively, there is a limited understanding of the molecular mechanisms of collagen deformation when subjected to a mechanical load. Here, we carry out steered molecular dynamics study to investigate how the structural hierarchies present in collagen contribute to collagen deformation. The conformational evolution of helical hierarchies, the interactions between different helical levels, and the role of inter-chain hydrogen bonds during deformation of collagen have been investigated in this study to explain the mechanics of collagen.

Each of the hierarchical structures of bone has unique set of properties that result from the structures existing at smaller length scales, all the way down to the molecular level. Due to this reason, the mechanics of bone can be understood only by bridging multiple hierarchical levels and linking the macroscopic scale to the molecular scale. This approach of connecting the interactions occurring at different length scales is known as multiscale modeling. In this study a hierarchical multiscale modeling has been carried out using a bottom-up-approach to investigate the deformation mechanics of collagen fibril using the combination of molecular dynamics and finite element (FEM) methods. For the first time, this multiscale model bridges together the molecular scale interactions with the deformation response of collagen fibril. A very important aspect of this model is that it takes into account the molecular interactions between mineral, hydroxyapatite, and water and incorporates them into our finite element model to study the mechanics of collagen fibril. The existing models do not incorporate these molecular interactions which limit their ability to accurately predict macroscopic property of bone. Our molecular simulations show that the molecular interactions between constituents of bone play a key

role in influencing the nanomechanical properties of collagen fibril. The mechanics of collagen fibril in the small and large deformation regime, as well as, the role of collagen crosslinks are investigated in this study.

This research is a principal step towards developing an accurate multiscale model of bone by bridging molecular scale properties and microstructure to the macroscopic response. This will help us better understand and model interactions-structure-property relations in bone that will allow for better understanding of the role of molecular level interactions and nano- & micro- structure on bone properties. This multiscale model will facilitate better prediction of how properties of bone are affected due to interactions at molecular and higher length scales. In brief, the broad objective of this research is to understand the role of molecular interactions and the hierarchical morphology in the microscopic and macroscopic response of bone. This knowledge is crucial for understanding bone in better light, which have great number of applications such as obtaining cues to the cure for various bone diseases and the design of better implant materials with desired properties.

1.2. Swelling Clay-Montmorillonite

Swelling clays are responsible for extensive damage to civil infrastructures every year in the United States and across the world. Smectite clays such as montmorillonite are well known for their expansive properties. The clay crystals are large sheets that are colloidal in dimension, with the lateral size of approximately 0.1 to 100 micrometers and the thickness of about 10Å. The large surface area to mass ratio and colloidal character of clay sheets impart it with the ability to swell, along with the highly reactive surface and high cation exchange capacity[15]. The clay minerals have various useful applications

such as in case of the borehole stabilization during drilling, drug delivery systems, cosmetics, polymer-clay-nanocomposite, and geoenvironmental engineering.

The swelling clays undergo large volumetric change when exposed to water. These clays result in considerable compressive stress, known as swelling pressure, when the swelling strain is restrained. Traditionally theories based on electric double layer have attempted to explain the swelling behavior of clay. Stern and Guoy theory is one of the earlier theories, known as diffuse double layer theory, which has attempted to explain interactions between the clay and water in the interlayer. However, it has number of limitations and is unable to explain the interlayer expansion and swelling behavior of montmorillonite[16]. Some of the limitations of these theories include the uniform distribution of surface charge, infinitely long clay particle, uniform dielectric permittivity throughout double layer, ions treated as point charge and ionic concentrations near the surface. Similarly, the DLVO (Derjaguin, Landau, Verwey and Overbeek) theory [17,18] is able to describe stability of clay colloidal suspension for larger spacing, but is not satisfactory for spacing smaller than 20Å. These limitations indicate that the swelling behavior can only be understood with the help of the molecular level study of clay water interactions in which both the clay and water are explicitly modeled using atoms.

There are various types of computational studies on hydrated smectite clays using molecular dynamics (MD) and Monte Carlo (MC) methods [19-26]. The computer simulation of interlayer water in 2:1 clays were carried out by Skipper et al. [19] using Monte Carlo and molecular dynamics methods. Delville [26,27] carried out Monte Carlo swelling clay to show that cations in the interlayer play an important role in the swelling behavior of clay. The computational studies were also carried out by Karaborni et al. [22]

using Monte Carlo and molecular dynamics methods. Tambach et al. [23] carried out molecular simulations to study different types of clay, water models and cations.

Despite the large number of theoretical and computational studies on swelling clays the mechanism of swelling behavior is not fully understood. The molecular dynamics study presented in this dissertation provides a detailed insight into the swelling and the stability of clay structure with increasing hydration. This work points to an important mechanisms that allows large interlayer swelling of these clays which has been observed experimentally but have not been not been clearly explained in the literature. This work significantly adds to the understanding of clay-water interaction and moves the state of knowledge in the field significantly further by providing a more complete description of molecular interactions during swelling.

1.3. Objectives of Research

The summary of the objectives of doctoral research described above in detail are as follows:

- To understand the effect of mineral-collagen interaction in the deformation response of collagen under fibrillar environment.
- To understand molecular mechanisms of collagen deformation by investigating the conformational evolution of its helical hierarchies.
- To develop the multiscale model of collagen fibril to link molecular mechanisms to continuum scale. This model seeks to understand mechanisms governing deformation response collagen fibril and the role of collagen-hydroxyapatite molecular interaction in the mechanical response of collagen fibril.

- To understand the role of molecular interactions in the swelling behavior of Na-montmorillonite

1.4. Dissertation Organization

The dissertation is organized into following chapters:

1) Chapter 1: Introduction
2) Chapter 2: This chapter presents review of literature on the structure of bone, the studies geared towards understanding the mechanics of bone, and molecular modeling studies of collagen.
3) Chapter 3: This chapter discusses the Computational Methods used in this study.
4) Chapter 4: The directional dependence of collagen deformation in collagen fibril is presented in this chapter.
5) Chapter 5: This chapter presents the steered molecular dynamics study of the deformation mechanics of short and full length collagen molecules.
6) Chapter 6: The role of structural hierarchies of in the deformation of collagen molecule is discussed in this chapter.
7) Chapter 7: The multiscale model of collagen fibril in the elastic regime is presented in this chapter.
8) Chapter 8: The mechanics of collage fibril in the small and large displacement regime, and the role of characteristic length and crosslinks are presented in this chapter.
9) Chapter 10: This chapter presents the molecular dynamics study of the swelling behavior of montmorillonite clay.

10) Chapter 10: This chapter presents summary and major conclusions of the research presented in this dissertation.

11) Chapter 11: The future directions for the research in this field are discussed in this chapter.

1.5. References

1. Landis, W.J., Song, M.J., Leith, A., McEwen, L. & McEwen, B.F. Mineral and organic matrix interaction in normally calcifying tendon visualized in three dimensions by high-voltage electron microscopic tomography and graphic image reconstruction. *Journal of structural biology* **110**, 39-54 (1993).
2. Weiner, S. & Wagner, H.D. The material bone: structure-mechanical function relations. *Annual Review of Materials Science* **28**, 271-298 (1998).
3. Weiner, S. & Traub, W. Bone structure: from angstroms to microns. *The FASEB journal official publication of the Federation of American Societies for Experimental Biology* **6**, 879-85 (1992).
4. Bhowmik, R., Katti, K.S. & Katti, D.R. Mechanics of molecular collagen is influenced by hydroxyapatite in natural bone. *Journal of Materials Science* **42**, 8795-8803 (2007).
5. Bhowmik, R., Katti, K.S. & Katti, D.R. Mechanisms of Load-Deformation Behavior of Molecular Collagen in Hydroxyapatite-Tropocollagen Molecular System: Steered Molecular Dynamics Study. *Journal of Engineering Mechanics-Asce* **135**, 413-421 (2009).

6. Ghosh, P., Katti, D.R. & Katti, K.S. Mineral Proximity Influences Mechanical Response of Proteins in Biological Mineral-Protein Hybrid Systems. *Biomacromolecules* **8**, 851-856 (2007).

7. Sikdar, D., Pradhan, S.M., Katti, D.R., Katti, K.S. & Mohanty, B. Altered phase model for polymer clay nanocomposites. *Langmuir* **24**, 5599-5607 (2008).

8. Ramachandran, G.N. & Kartha, G. Structure of Collagen. **176**, 593-595 (1955).

9. Bella, J., Eaton, M., Brodsky, B. & Berman, H.M. Crystal and molecular structure of a collagen-like peptide at 1.9 A resolution. **266**, 75-81 (1994).

10. Ramachandran, G.N. & Kartha, G. Structure of collagen. *Nature* **174**, 269-270 (1954).

11. Ramachandran, G.N. & Sasisekharan, V. Refinement of the structure of collagen. *Biochimica et Biophysica Acta (BBA) - Biophysics including Photosynthesis* **109**, 314-316 (1965).

12. Bhattacharjee, A. & Bansal, M. Collagen Structure: The Madras Triple Helix and the Current Scenario. *IUBMB Life* **57**, 161-172 (2005).

13. Berisio, R., Vitagliano, L., Mazzarella, L. & Zagari, A. Crystal structure of the collagen triple helix model [(Pro-Pro-Gly)10]3. *Protein Science* **11**, 262-270 (2002).

14. Brodsky, B. & Persikov, A.V. Molecular structure of the collagen triple helix. in *Fibrous Proteins: Coiled-Coils, Collagen and Elastomers*, Vol. 70 301-+ (2005).

15. Van Olphen, H.a.F., J. J. *Data handbook for clay materials and other non-metallic minerals*, (Pergamon Press, New York, 1979).

16. Jo, H.Y., Katsumi, T., Benson, C.H. & Edil, T.B. Hydraulic conductivity and swelling of nonprehydrated GCLs permeated with single-species salt solutions. *Journal of Geotechnical and Geoenvironmental Engineering* **127**, 557-567 (2001).

17. Verwey, E.J.W. Theory of the stability of lyophobic colloids. *Philips Research Reports* **1**, 33-49 (1945).

18. Verwey, E.J.W. Theory of the stability of lyophobic colloids. *Journal of Physical and Colloid Chemistry* **51**, 631-636 (1947).

19. Skipper, N.T., Refson, K. & McConnell, J.D.C. computer-simulation of interlayer water in 2-1 clays. *Journal of Chemical Physics* **94**, 7434-7445 (1991).

20. Skipper, N.T., Chang, F.R.C. & Sposito, G. Monte-carlo simulation of interlayer molecular-structure in swelling clay-minerals .1. Methodology. *Clays and Clay Minerals* **43**, 285-293 (1995).

21. Skipper, N.T., Sposito, G. & Chang, F.R.C. Monte-carlo simulation of interlayer molecular-structure in swelling clay-minerals .2. Monolayer hydrates. *Clays and Clay Minerals* **43**, 294-303 (1995).

22. Karaborni, S., Smit, B., Heidug, W., Urai, J. & vanOort, E. The swelling of clays: Molecular simulations of the hydration of montmorillonite. *Science* **271**, 1102-1104 (1996).

23. Tambach, T.J., Hensen, E.J.M. & Smit, B. Molecular simulations of swelling clay minerals. *Journal of Physical Chemistry B* **108**, 7586-7596 (2004).

24. Smith, D.E., Wang, Y. & Whitley, H.D. Molecular simulations of hydration and swelling in clay minerals. *Fluid Phase Equilibria* **222**, 189-194 (2004).

25. Smith, D.E., Wang, Y., Chaturvedi, A. & Whitley, H.D. Molecular simulations of the pressure, temperature, and chemical potential dependencies of clay swelling. *Journal of Physical Chemistry B* **110**, 20046-20054 (2006).

26. Delville, A. Modeling the clay water interface. *Langmuir* **7**, 547-555 (1991).

27. Delville, A. Structure of liquids at a solid interface - an application to the swelling of clay by water. *Langmuir* **8**, 1796-1805 (1992).

CHAPTER 2. REVIEW OF LITERATURE

2.1. Hierarchical Structure of Bone

Bone is an extraordinary material with a hierarchical morphology that serves of various bodily functions. Bone consists of at least six levels of structural hierarchy as shown in figure 2.1. It is a vital part of skeletal our system typically composed of a strong and dense external layer called cortical bone around an interior spongy cancellous bone, also known as trabecular bone. In addition to the structural role of supporting and protecting body organs, it also serves number of other functions such as production of red and white blood cells, and storage of minerals such as calcium and phosphorous. Bone is composed of the organic, mineral phase, and water. The relative proportions of organic, mineral phase, and water in bone is about 25%, 65%, and 10% respectively by weight [1-5], and around 32-44%, 33-43%, and 15-25% respectively by volume [5,6]. The organic phase in bone is mainly composed of Type I collagen, which are secreted by osteoblasts into the extracellular space. Collagen is the most abundant protein in our human body that constitute about 85-95% of the total bone protein [7]. The collagen molecules are fibrous structural proteins that serve as reinforcing members in bone and impart it with the necessary tensile strength and toughness. They are long and slender in shape about 300 nanometers in length and 1.23 nanometers in diameter [8]. The other constituents of organic phase include lipids and non-collageneous proteins such as phosphoproteins. The collagen molecules once secreted, self-assemble through entropy driven process to form a highly organized structure outside the cell, forming a framework where the hydroxyapatite ($Ca_{10}(PO_4)_6(OH)_2$) nanocrystals mineralize into a plate-like structures

approximately 50 nm by 25nm by 3 nm in size [9-12]. This highly organized structure is known as collagen fibril. The mineral component of bone imparts it with strength and rigidity. The hydroxyapatite found in bone is not pure and consists of various impurities such as carbonate that replaces the phosphate group in a mineral. The mineralization of hydroxyapatite in fibril is governed by various proteins such as biglycan and bone-sialoprotein[13]. In addition to the collagen and hydroxyapatite, which are the major components of bone, there are other organic and mineral phases in bone as well. The weight percentages of other constituents are shown in table 2.1. The ions such as fluoride, carbonate, sodium, potassium, and magnesium are responsible for various metabolic functions.

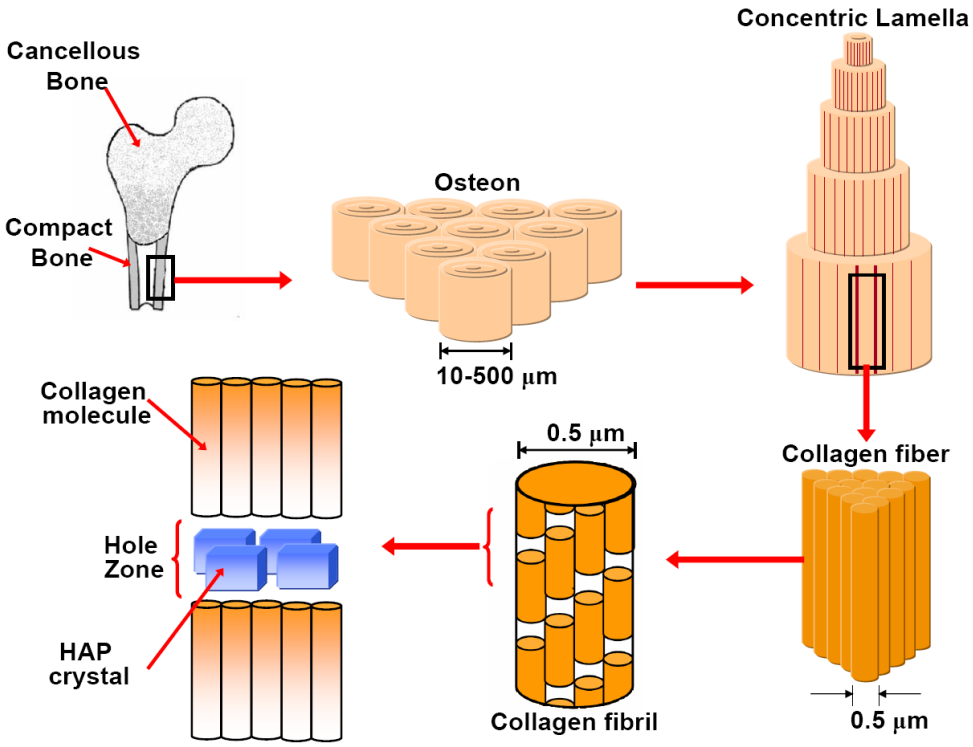

Figure 2.1. Structural hierarchy in bone (adapted from Bhowmik et al. [14]).

Table 2.1. Composition of bone [5,9,11,15]

Inorganic **wt%**	**Organic** **wt%**
Hydroxyapatite ~60 Carbonate ~4 Citrate ~0.9 Sodium ~0.7 Magnesium ~0.5 Other traces: Cl^-, F^-, K^+, Sr^{2+}, Pb^{2+}, Zn^{2+}, Cu^{2+}, Fe^{2+}	Collagen ~20 Non-collageneous proteins: osteocalcin, osteonectin, osteopontin, thrmbospodin, mmorphogenetic proteins, sailoprotein, serum proteins Other traces: Polysaccharides, lipids, cytokines Primary bone cells: osteoblasts, osteocytes, osteoclasts

Collagen fibril, the basic building block of bone material and collagen rich tissues [16], is about 50-250 nm in diameter and unknown length because they merge with neighboring fibrils [17]. In collagen fibril these molecules are packed parallel to each other along the longitudinal axis of bone as shown in figure 2.1. Each row of collagen molecules are axially staggered with respect to each other by 67 nanometers (D) resulting in a banded pattern along the length of collagen fibril [8,18]. The staggering also results in the overlap between the ends of adjacent collagen molecules that is 27 nanometers long. The covalent crosslinks develop between adjacent collagen molecules in the overlap zone, near the ends of collagen, with the maturation of tissues. This crosslinking between the adjacent ends of collagen molecule plays an important role in the mechanical property for fibril.

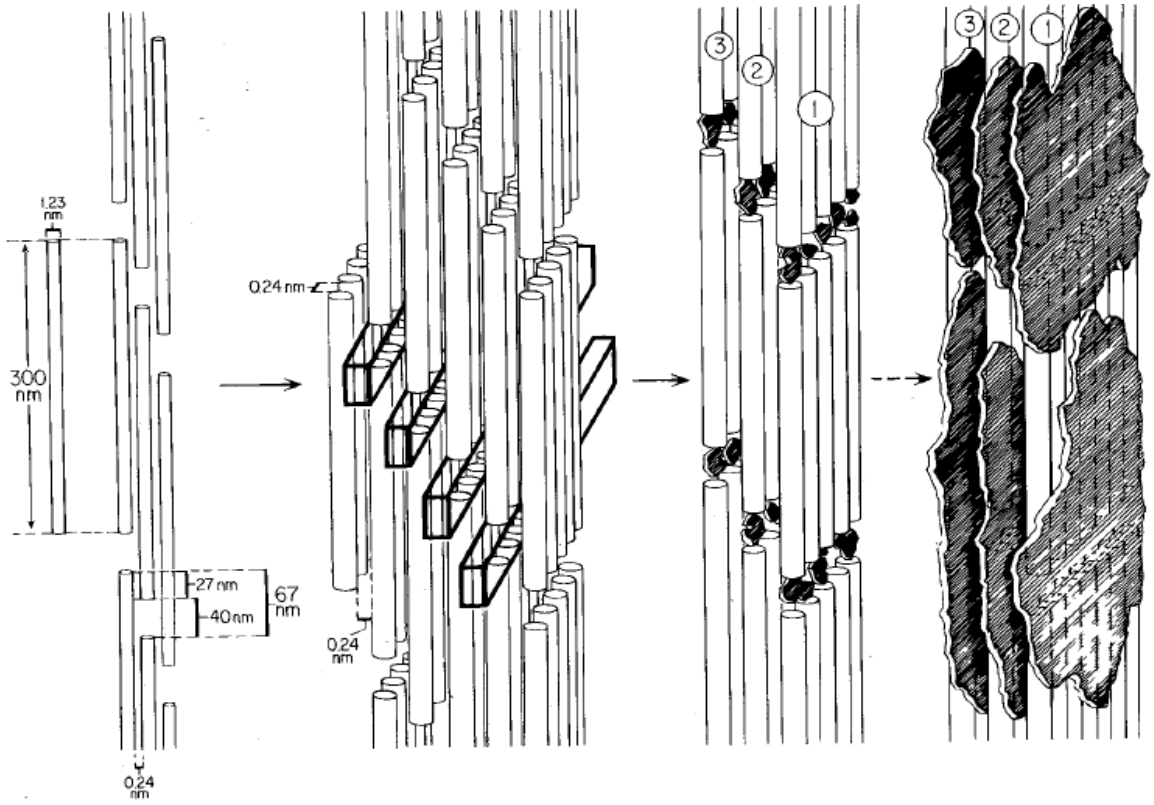

Figure 2.2. Organization of collagen molecules and mineral in a fibril (figure adapted from Landis et al. [8]).

There is a 40 nanometers wide gap between the collagen molecules aligned end to end along the longitudinal axis of collagen molecule. This region is known as gap- or hole-zone. The hole-zone corresponds to the region of low electron density in X-ray diffraction as compared to overlap zone resulting in the D-period of bands along collagen molecules [18]; the collagen molecules being approximately 300 nanometers corresponds to 4.4D. The hydroxyapatite crystals nucleate in the hole-zone, and these mineral places grow in size along the axial direction of collagen molecule and sideways along channels

[8,12,19,20]. As the bone matures the crystals outgrow the width of gap zone and enter the overlap zone squeezing in between the collagen molecules [21]. The crystals originating from the adjacent hole-zones join to form large and thick extended sheets that may occupy several hole-zones [8,12,17,22]. In collagen fibril the (0001) surface of hydroxyapatite present in the hole-zone is oriented perpendicular to the long axis of collagen. In addition to (0001) surface, the $(10\bar{1}0)$ face of HAP is also well developed, as seen from the electron diffraction study, and found to be oriented approximately parallel to each other [8,22,23]. In addition to intrafibrillar mineral, the surface of fibril is also coated by extrafibrillar mineral[24]. There are two different schools of thoughts in the research community as to where most of the minerals are located in bone. Some researchers believe that most of the minerals are located inside the collagen fibril [25-27], while others believe that most of the mineral are extrafibrillar [28-30]. The collagen fibrils in bone assemble together to form collagen fiber with the help of a hydrated matrix rich in proteoglycans. The diameter of fibrils show large variation and vary from 50 nanometers to several millimeters for thinner and very thicker fibrils. The collagen fibrils assemble to form circular lamellas which are further arranged to form osteons, which are the fundamental functional units of bone.

Bone is dynamic system capable of self-regeneration and reorganization that consists of three different types of cells serving various functions: osteoblast, osteocytes, and osteoclasts. The osteoblasts are oval shaped cells with a large eccentric nucleus that are created from osteoprogenitor cells. The osteoblast is responsible for synthesis of collagen fibers and formation of mineral deposits in the bone. The osteoblast cells get trapped in the bone matrix and turn into the mature bone cells knows as osteocytes, which

are responsible for maintenance of bond matrix. Osteoclasts are the largest bone cells responsible for resorption of bone. Bone tissue is sensitive to mechanical stimuli, a property known a mechanosensitivity, which creates biological response necessary for its adaptation and remodeling- a process that allows collagen rich tissues to repair damage [16,31]. Because of mechanosensitivity of bone in different parts of skeletal system exhibit distinct sets of mechanical property, as they all undergo different loading paths during out daily activities [32,33].

2.2. Mechanical Properties of Bone

Inorganic phase of bone provides the stiffness and rigidity whereas the organic phase provides the tensile strength and toughness. The mechanical properties of bone are shown in table 1.2. The mechanical property of bone is a great balance between the toughness and stiffness because with mineralization the toughness is decreased. This is evident by comparing the elastic modulus of bone (14-20 GPa) to the 1GPa of mouse of tail tendon [34].

Table 2.2. Mechanical properties of bone [9,15]

Properties	**Value**
Young's modulus (GPa)	14-20
Tensile strength (MPa)	50-150
Compressive strength (MPa)	170-193
Fracture toughness (MPa m1/2)	2-12
Strain to failure	1-3

2.3. Structure of Collagen and Microfibrils

Collagen is a long fibrous protein constituting more than quarter of all proteins in human body and present in various tissues such as bone, tendon, lungs, blood vessels, cartilage etc. There are at least 27 types of collagen in vertebrates [35], each denoted by roman numerals. The fibrillar collagens are of particular interest from the mechanical point of view as they are capable of assembling into collagen fibrils. The fibrillar collagen account for only seven of all the known collagen [36-39]: types I, II, III, V, XI, XXIV, and XXVII. Type I is the most abundant fibrillar collagen that is widely found in bone, skin, tendon, cornea, vasculature and lung etc. The nonfibrillar collagens "form networks (types IV, VIII, and X), associate with fibril surfaces (types IX, XII, and XIV), occur as transmembrane proteins (types XIII and XVII), or form 11-nm periodic beaded filaments (type VI) [36] ". The collagen molecules in nature can be of variable length ranging from 14 nanometers in nematocyst wall of hydra to 2400 nanometers in cuticle of annelids [40].

The molecular structure of collagen consists of three polypeptide chains, called α-chains, twisted in to a right-handed triple-helix and held together by inter-chain hydrogen bonds [35,41,42]. The structure of collagen is shown in figure 2.3. The individual α-chains are left-handed helical in structure, so the collagen molecule can be considered as a helix of helix. The α-chains consists of a repeating triplet of amino acids -Gly-X-Y- with the high percentage of proline and hydroxyproline residues respectively in the X and Y locations. The repetition of Glycine in every third residue is necessary for the close packing of polypeptide chains [42,43]. The collagen molecules consist of over 1014 amino acids along each polypeptide chains [44]. The collagen molecules consisting of three

identical α-chains are known as homotrimeric and the molecules consisting of two or three genetically different α-chains are known as heterotypic. For example, Type I collagen is heterotypic consisting of two α1-chains and one α2-chains and represented by $[\alpha1(I)]_2\alpha2(I)$; whereas, type II collagen is heterotypic consisting of three distinct α1-chains which is represented by $[\alpha1(I)]_3$.

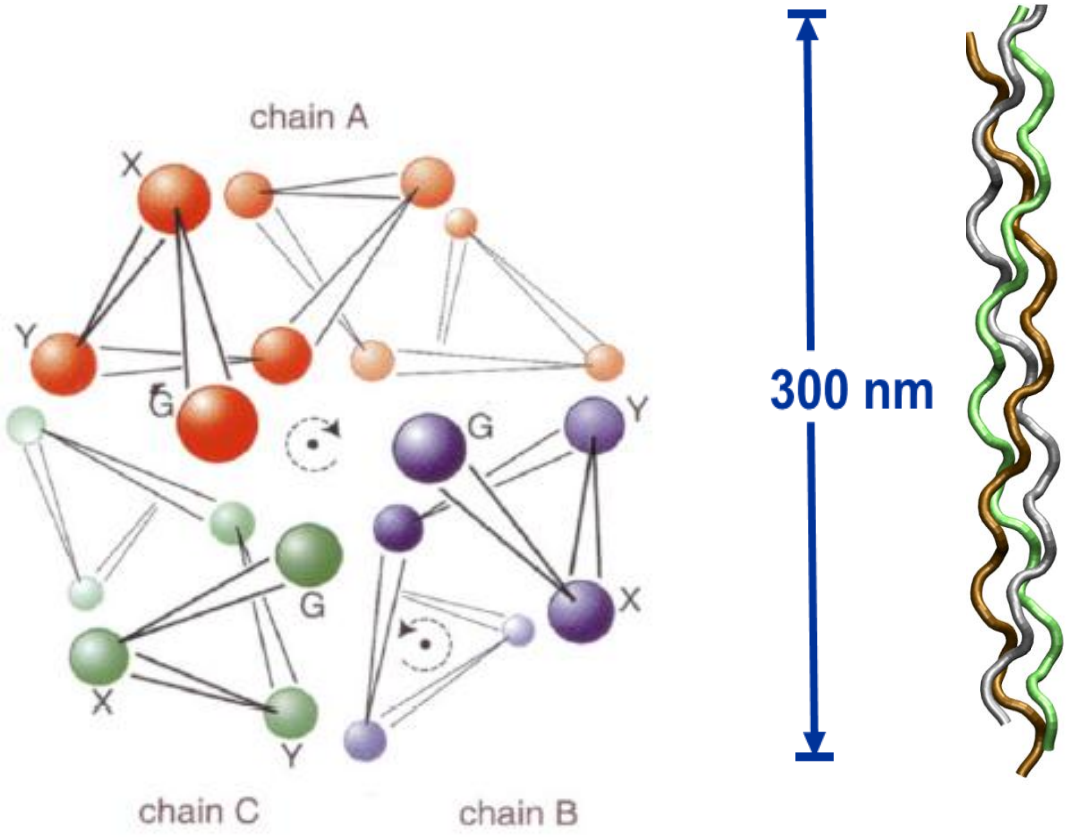

Figure 2.3. Left: The collagen structure consisting of three helical α-chains (adapted from Beck and Brodsky [45]). Right: The three chains of collagen wrapped into a triple helix.

The ends of collagen molecule, N- and C-termini, consist of non-helical structures known a telopeptides that are typically about 20 residues long; they are called N-telopeptides and C-telopeptides. The α-chains in telopeptides does not contain a repeating sequence of Gly-X-Y unlike in the middle domain. The sequence of N-terminal telopeptides type I collagen used in this work as follows [46,47]:

α1-GlnLeuSerTyrGlyTyrAspGluLysSerThrGlyIleSer-ValPro-helix (GlyProMet-)

α2-GlnPheAspAlaLysGlyGlyGlyPro-helix (GlyProMet-)

The evidence of the existence of subfibrillar structures called microfibrils, that links molecular level to fibrillar level, have been shown by number of studies such as the electron tomographic reconstruction in dry cornea [48,49] and AFM study of type I collagen [50]. The X-ray diffraction study by Orgel et al. [44] has determined crystallographic unit cell of type I collagen supermolecular structure using electron density maps. This study also shows that the quasihexagonal arrangement of collagen molecules existing in the overlap zone continues continue into and throughout the gap region. The quasihexagonal lattice of collagen molecules is shown in figure 2.4 (left). The study by Orgel et al has also revealed the presence of kinking of collagen molecules along the length of fibril as shown in figure 2.4 (right).

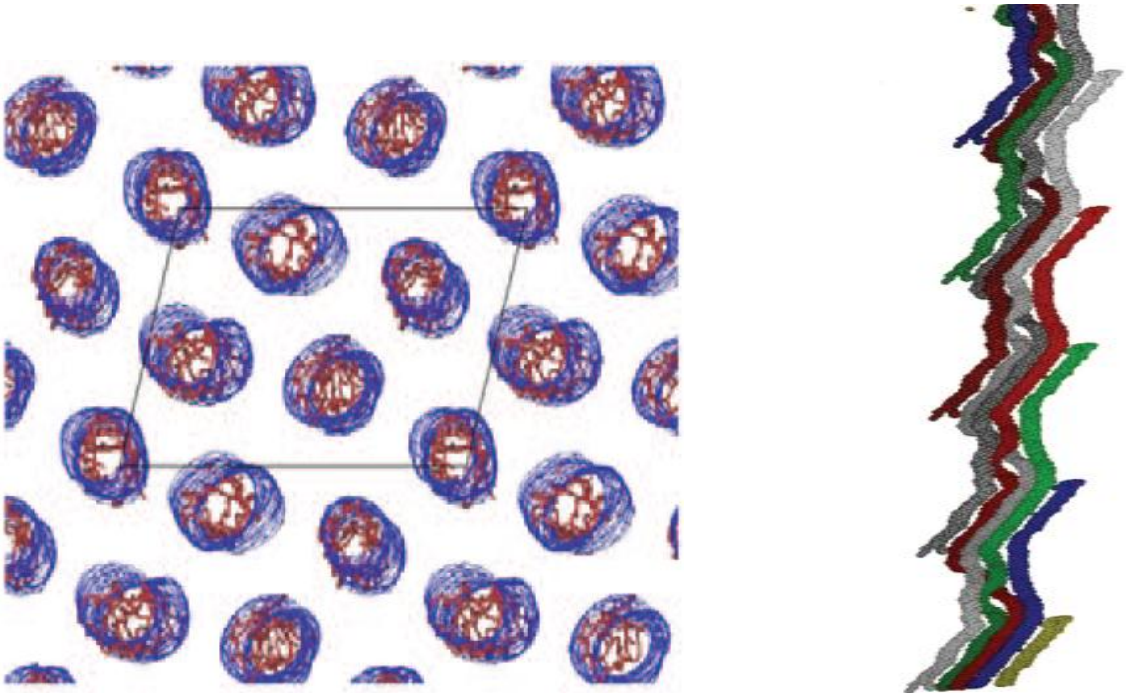

Figure 2.4. Left: The electron density of the quasihexagonal arrangement of collagen segements and the outline of the unit cell. Right: Microfibrillar structure of collagen. (adapted from Orgel et al. [44])

2.4. Theoretical and Experimental Studies of the Hierarchical Structures of Bone

The mechanical properties of bone and its hierarchical structure structures have been studied using various theoretical and experimental methods. Among various theoretical methods, one important approach is the utilization of continuum micromechanics formulation for modeling bone mechanics. This approach has been extensively used by Hellmich et al. and Ghanbari et al. [28,51-54]. The viscoelastic modeling of bone at fibrillar level using microstructural approach was carried out by Ciarletta et al.[55].

There are number of theoretical/computational studies investigating the mechanics of collagen fibril [56-61]. A molecular dynamics study of the nanomechanics of collagen microfibrils has been carried out by Gautieri et al.[56]. Buehler carried out the theoretical and molecular modeling study to explain the nanostructure of collagen fibrils [58] and the toughening of fibrils by mineralization [59]. Buehler's results show that Young's modulus (6.23 GPa vs. 4.59 GPa), yield strain (6.7% vs. 5%), and fracture stress (0.6GPa vs. 0.3 GPa) of mineralized fibril is higher compared to unmineralized fibril. The collagen crosslinks play an important role in the nanomechanics of collagen fibril. The mechanical properties of collagen fibril under varying crosslink densities is studied by Buehler [61] using atomistic and continuum methods and Tang et al.[57] using coarse grained molecular dynamics. The Young's modulus of unmineralized collagen microfibril estimated by Buehler [61], Tang et al. [57], and Gautieri et al. [56] from their modeling studies are 4.36 - 38 GPa, 5 - 35 GPa, and 0.3 – 1.2 GPa respectively for small-strain and large-strain. The experiments performed on collagen fibrils show following values of Young's modulus: 0.5-3.2 GPa [62], 0.86 ± 0.45 GPa [63], 0.2-0.8 GPa [64], 3.7-11.5 GPa [65]. The experimental moduli of collagen fibril are listed in table 2.3. Furthermore, type I collagen fibrils tested to strains as high as 100% by Shen et al. [63] demonstrated strain softening (yield stress = 0.22 ± 0.14 GPa; strain yield = 0.21 ± 0.13), strain hardening, and time dependent recoverable residual strain.

Table 2.3. Experimental studies of collagen fibril

Source	Modulus (GPa)	Comments
Gupta HS et al. [62]	0.5 – 3.2	• Synchrotron diffraction study • Modulus increasing with of mineral content • Type I collagen fibril
van der Rijt et al. [64]	2–7 (ambient conditions) 0.2–0.8 (aqueous media)	• AFM • Single collagen fibrils have been mechanically tested in ambient conditions and were found to behave reversibly up to stresses of 90 MPa.
Wenger et al. [65]	3.7 – 11.5	• Nanoindentation using AFM in air and at room temperature • Fibrils diameters: 50 to 200 nm. • Type I collagen fibril (rat tail tendon) • The fibrils assumed to possess isotropic mechanical properties
Shen et al. [63]	0.86 ± 0.45 (small strain) 0.72 ± 0.57 (large strain)	• Microelectromechanical systems (MEMS) technique • Small strain ($\varepsilon < 0.09$) • Fibrils diameters: 150–470 nm

There are number molecular dynamics studies investigating the mechanics of bone at the molecular scale [14,66-69]. Bhowmik et al [14,68] extensively studied deformation behavior of collagen in the proximity of mineral using steered molecular dynamics (SMD). Bhowmik et al.[14] found that the mechanics of collagen is significantly affected by the mineral proximity and that water plays a crucial in the interaction between collagen and mineral. Several steered molecular dynamics studies are also been carried out to evaluate mechanical properties of collagen (Gautieri et al. 2008; Lorenzo and Caffarena 2005; Buehler 2006a). An atomistic study of collagen proteins in collagen fibril is carried out by Streeter and de Leeuw [70,71] and Gautieri et al.[56]. Beside these studies, model structures of collagen molecules as well as collagen fibrils have been investigated using molecular dynamics methods[58,61,74-78]. There are also studies on the role of amino acid sequence on the mechanical property of collagen [83]. Besides molecular dynamics study, a coarse grained study of long collagen molecule has been carried out by Gautieri et al. [84].

2.5. References

1. Currey, J.D., Zioupos, P., Davies, P. & Casino, A. Mechanical properties of nacre and highly mineralized bone. *Proceedings. Biological sciences / The Royal Society* **268**, 107-11 (2001).
2. Fisher, L.W. & Termine, J.D. Noncollagenous proteins influencing the local mechanisms of calcification. *Clinical Orthopaedics and Related Research* **200**, 362-85 (1985).
3. Dorozhkin, S.V. & Epple, M. Biological and medical significance of calcium phosphates. *Angewandte Chemie, International Edition* **41**, 3130-3146 (2002).

4. Eastoe, J.E. & Eastoe, B. Organic constituents of mammalian compact bone. *Biochemical Journal* **57**, 453-9 (1954).

5. Olszta, M.J., Odom, D.J., Douglas, E.P. & Gower, L.B. A New Paradigm for Biomineral Formation: Mineralization via an Amorphous Liquid-Phase Precursor. *Connective Tissue Research* **44**, 326-334 (2003).

6. Currey, J.D. Biomechanics of mineralized skeletons. in *Skeletal Biomineralization :Patterns, processes, and evolutionary trends*, Vol. 1 (ed. Carter, J.G.) 11 (Van Nostrand, New York, 1990).

7. Termine, J.D. & G, R.P. Bone matrix proteins and the mineralization process. in *Primer on the Metabolic Bone Diseases and Disorders of Mineral Metabolism* (ed. Favus, M.J.) (The American Society for Bone and Mineral Research, Lippincott Williams & Wilkins, 1996).

8. Landis, W.J., Song, M.J., Leith, A., McEwen, L. & McEwen, B.F. Mineral and organic matrix interaction in normally calcifying tendon visualized in three dimensions by high-voltage electron microscopic tomography and graphic image reconstruction. *Journal of structural biology* **110**, 39-54 (1993).

9. Murugan, R. & Ramakrishna, S. Development of nanocomposites for bone grafting. *Composites Science and Technology* **65**, 2385-2406 (2005).

10. Rho, J.Y., Kuhn-Spearing, L. & Zioupos, P. Mechanical properties and the hierarchical structure of bone. *Medical engineering & physics* **20**, 92-102 (1998).

11. Ziv, V. & Weiner, S. Bone crystal sizes: a comparison of transmission electron microscopic and X-ray diffraction line width broadening techniques. *Connective tissue research* **30**, 165-75 (1994).

12. Landis, W.J. The strength of a calcified tissue depends in part on the molecular structure and organization of its constituent mineral crystals in their organic matrix. *Bone (New York, NY, United States)* **16**, 533-44 (1995).

13. Boskey, A.L. Biomineralization: An Overview. *Connective Tissue Research* **44**, 5-9 (2003).

14. Bhowmik, R., Katti, K.S. & Katti, D.R. Mechanics of molecular collagen is influenced by hydroxyapatite in natural bone. *Journal of Materials Science* **42**, 8795-8803 (2007).

15. Murugan, R. & Ramakrishna, S. Nanostructured biomaterials. *Encyclopedia of Nanoscience and Nanotechnology* **7**, 595-613 (2004).

16. Fratzl, P. & Weinkamer, R. Nature's hierarchical materials. *Progress in Materials Science* **52**, 1263-1334 (2007).

17. Weiner, S. & Wagner, H.D. The material bone: structure-mechanical function relations. *Annual Review of Materials Science* **28**, 271-298 (1998).

18. Hodge, A.J. & Petruska, J.A. Recent studies with the electron microscope on ordered aggregates of the tropocollagen molecule. 289-300 (1963).

19. Nylen, M.U., Scott, D.B. & Mosley, V.M. Mineralization of turkey leg tendon. II. Collagen-mineral relations revealed by electron and x-ray microscopy. **No. 64**, 129-42 (1960).

20. Traub, W., Arad, T. & Weiner, S. Three-dimensional ordered distribution of crystals in turkey tendon collagen fibers. *Proceedings of the National Academy of Sciences of the United States of America* **86**, 9822-6 (1989).

21. Arsenault, A.L. Image-analysis of collagen-associated mineral distribution in cryogenically prepared turkey leg tendons. *Calcified Tissue International* **48**, 56-62 (1991).

22. Landis, W.J. et al. Mineralization of collagen may occur on fibril surfaces: evidence from conventional and high-voltage electron microscopy and three-dimensional imaging. *Journal of Structural Biology* **117**, 24-35 (1996).

23. Moradianoldak, J., Weiner, S., Addadi, L., Landis, W.J. & Traub, W. Electron imaging and diffraction study of individual crystals of bone, mineralized tendon and synthetic carbonate apatite. *Connective Tissue Research* **25**, 219-228 (1991).

24. Rubin, M.A., Rubin, J. & Jasiuk, W. SEM and TEM study of the hierarchical structure of C57BL/6J and C3H/HeJ mice trabecular bone. *Bone* **35**, 11-20 (2004).

25. Weiner, S., Traub, W. & Wagner, H.D. Lamellar bone: structure-function relations. *Journal of structural biology* **126**, 241-55 (1999).

26. Jager, I. & Fratzl, P. Mineralized collagen fibrils: a mechanical model with a staggered arrangement of mineral particles. *Biophysical journal* **79**, 1737-46 (2000).

27. Gao, H., Ji, B., Jager, I.L., Arzt, E. & Fratzl, P. Materials become insensitive to flaws at nanoscale: Lessons from nature. *Proceedings of the National Academy of Sciences of the United States of America* **100**, 5597-5600 (2003).

28. Fritsch, A. & Hellmich, C. 'Universal' microstructural patterns in cortical and trabecular, extracellular and extravascular bone materials: micromechanics-based

prediction of anisotropic elasticity. *Journal of Theoretical Biology* **244**, 597-620 (2007).

29. Sasaki, N. et al. Atomic force microscopic studies on the structure of bovine femoral cortical bone at the collagen fibril-mineral level. *Journal of Materials Science-Materials in Medicine* **13**, 333-337 (2002).

30. Hellmich, C. & Ulm, F.J. Are mineralized tissues open crystal foams reinforced by crosslinked collagen?—some energy arguments. *Journal of biomechanics* **35**, 1199-1212 (2002).

31. Cowin, S.C. Bone stress adaptation models. *Journal of biomechanical engineering* **115**, 528-33 (1993).

32. Ramakrishna, S., Mayer, J., Wintermantel, E. & Leong, K.W. Biomedical applications of polymer-composite materials: a review. *Composites Science and Technology* **61**, 1189-1224 (2001).

33. Recum, A.F.v. *In Handbook Of Biomaterials Evaluation: Scientific, Technical And Clinical Testing Of Implant Materials*, (CRC Press, 1998).

34. Misof, K., Landis, W.J., Klaushofer, K. & Fratzl, P. Collagen from the osteogenesis imperfecta mouse model (oim) shows reduced resistance against tensile stress. *Journal of Clinical Investigation* **100**, 40-45 (1997).

35. Bhattacharjee, A. & Bansal, M. Collagen Structure: The Madras Triple Helix and the Current Scenario. *IUBMB Life* **57**, 161-172 (2005).

36. Hulmes, D.J.S. Building collagen molecules, fibrils, and suprafibrillar structures. *Journal of Structural Biology* **137**, 2-10 (2002).

37. Kadler, K.E., Holmes, D.F., Trotter, J.A. & Chapman, J.A. Collagen fibril formation. *Biochemical Journal* **316**, 1-11 (1996).

38. Koch, M. et al. Collagen XXIV, a Vertebrate Fibrillar Collagen with Structural Features of Invertebrate Collagens. *Journal of Biological Chemistry* **278**, 43236-43244 (2003).

39. Pace, J.M., Corrado, M., Missero, C. & Byers, P.H. Identification, characterization and expression analysis of a new fibrillar collagen gene, COL27A1. *Matrix Biology* **22**, 3-14 (2003).

40. Engel, J. Versatile Collagens in Invertebrates. *Science* **277**, 1785-1786 (1997).

41. Ramachandran, G.N. & Kartha, G. Structure of collagen. *Nature* **174**, 269-270 (1954).

42. Ramachandran, G.N. & Kartha, G. Structure of Collagen. **176**, 593-595 (1955).

43. Bella, J., Eaton, M., Brodsky, B. & Berman, H.M. Crystal and molecular structure of a collagen-like peptide at 1.9 A resolution. **266**, 75-81 (1994).

44. Orgel, J.P. et al. The in situ supermolecular structure of type I collagen. **9**, 1061-1069 (2001).

45. Beck, K. & Brodsky, B. Supercoiled protein motifs: the collagen triple-helix and the alpha -helical coiled coil. *Journal of Structural Biology* **122**, 17-29 (1998).

46. Jones, E.Y. & Miller, A. Structural models for the N- and C-terminal telopeptide regions of interstitial collagens. *Biopolymers* **26**, 463-80 (1987).

47. Otter, A., Kotovych, G. & Scott, P.G. Solution conformation of the type I collagen alpha-1 chain N-telopeptide studied by 1H NMR spectroscopy. *Biochemistry* **28**, 8003-10 (1989).

48. Holmes, D.F. et al. Corneal collagen fibril structure in three dimensions: Structural insights into fibril assembly, mechanical properties, and tissue organization. *Proceedings of the National Academy of Sciences of the United States of America* **98**, 7307-7312 (2001).

49. Holmes, D.F. & Kadler, K.E. The 10+4 microfibril structure of thin cartilage fibrils. *Proceedings of the National Academy of Sciences of the United States of America* **103**, 17249-17254 (2006).

50. Baselt, D.R., Revel, J.P. & Baldeschwieler, J.D. Subfibrillar structure of type I collagen observed by atomic force microscopy. *Biophysical journal* **65**, 2644-2655 (1993).

51. Hellmich, C., Celundova, D. & Ulm, F.J. Multiporoelasticity of Hierarchically Structured Materials: Micromechanical Foundations and Application to Bone. *Journal of Engineering Mechanics-Asce* **135**, 382-394 (2009).

52. Ghanbari, J. & Naghdabadi, R. Nonlinear hierarchical multiscale modeling of cortical bone considering its nanoscale microstructure. *Journal of Biomechanics* **42**, 1560-1565 (2009).

53. Hellmich, C., Barthelemy, J.F. & Dormieux, L. Mineral-collagen interactions in elasticity of bone ultrastructure - a continuum micromechanics approach. *European Journal of Mechanics a-Solids* **23**, 783-810 (2004).

54. Fritsch, A., Hellmich, C. & Dormieux, L. Ductile sliding between mineral crystals followed by rupture of collagen crosslinks: Experimentally supported micromechanical explanation of bone strength. *Journal of Theoretical Biology* **260**, 230-252 (2009).

55. Ciarletta, P., Micera, S., Accoto, D. & Dario, P. A novel microstructural approach in tendon viscoelastic modelling at the fibrillar level. *Journal of Biomechanics* **39**, 2034-2042 (2006).

56. Gautieri, A., Vesentini, S., Redaelli, A. & Buehler, M.J. Hierarchical Structure and Nanomechanics of Collagen Microfibrils from the Atomistic Scale Up. *Nano Letters* **11**, 757-766 (2011).

57. Tang, Y., Ballarini, R., Buehler, M.J. & Eppell, S.J. Deformation micromechanisms of collagen fibrils under uniaxial tension. *Journal of The Royal Society Interface* **7**, 839-850 (2010).

58. Buehler, M.J. Nature designs tough collagen: Explaining the nanostructure of collagen fibrils. *Proceedings of the National Academy of Sciences of the United States of America* **103**, 12285-12290 (2006).

59. Buehler, M.J. Molecular nanomechanics of nascent bone: fibrillar toughening by mineralization. *Nanotechnology* **18**(2007).

60. Buehler, M.J. Molecular architecture of collagen fibrils: A critical length scale for tough fibrils. *Current Applied Physics* **8**, 440-442 (2008).

61. Buehler, M.J. Nanomechanics of collagen fibrils under varying cross-link densities: Atomistic and continuum studies. *Journal of the Mechanical Behavior of Biomedical Materials* **1**, 59-67 (2008).

62. Gupta, H.S. et al. Synchrotron diffraction study of deformation mechanisms in mineralized tendon. *Physical Review Letters* **93**(2004).

63. Shen, Z.L., Dodge, M.R., Kahn, H., Ballarini, R. & Eppell, S.J. Stress-strain experiments on individual collagen fibrils. *Biophysical Journal* **95**, 3956-3963 (2008).

64. van der Rijt, J.A.J., van der Werf, K.O., Bennink, M.L., Dijkstra, P.J. & Feijen, J. Micromechanical testing of individual collagen fibrils. *Macromolecular Bioscience* **6**, 697-702 (2006).

65. Wenger, M.P.E., Bozec, L., Horton, M.A. & Mesquida, P. Mechanical properties of collagen fibrils. *Biophysical Journal* **93**, 1255-1263 (2007).

66. Dubey, D.K. & Tomar, V. Effect of changes in tropocollagen residue sequence and hydroxyapatite mineral texture on the strength of ideal nanoscale tropocollagen-hydroxyapatite biomaterials. *Journal of Materials Science-Materials in Medicine* **21**, 161-171 (2010).

67. Dubey, D.K. & Tomar, V. Role of the nanoscale interfacial arrangement in mechanical strength of tropocollagen-hydroxyapatite-based hard biomaterials. *Acta Biomaterialia* **5**, 2704-2716 (2009).

68. Bhowmik, R., Katti, K.S. & Katti, D.R. Mechanisms of Load-Deformation Behavior of Molecular Collagen in Hydroxyapatite-Tropocollagen Molecular System: Steered Molecular Dynamics Study. *Journal of Engineering Mechanics-Asce* **135**, 413-421 (2009).

69. Katti, D.R., Pradhan, S.M. & Katti, K.S. Directional dependence of hydroxyapatite-collagen interactions on mechanics of collagen. *Journal of Biomechanics* **43**, 1723-1730 (2010).

70. Streeter, I. & de Leeuw, N.H. Atomistic Modeling of Collagen Proteins in Their Fibrillar Environment. *Journal of Physical Chemistry B* **114**, 13263-13270 (2010).

71. Streeter, I. & de Leeuw, N.H. A molecular dynamics study of the interprotein interactions in collagen fibrils. *Soft Matter* **7**, 3373-3382 (2011).

72. Gautieri, A., Vesentini, S., Redaelli, A. & Buehler, M.J. Intermolecular slip mechanism in tropocollagen nanofibrils. *International Journal of Materials Research* **100**, 921-925 (2009).

73. Almora-Barrios, N. & de Leeuw, N.H. A Density Functional Theory Study of the Interaction of Collagen Peptides with Hydroxyapatite Surfaces. *Langmuir* **26**, 14535-14542 (2010).

74. Gautieri, A., Vesentini, S., Montevecchi, F.M. & Redaelli, A. Mechanical properties of physiological and pathological models of collagen peptides investigated via steered molecular dynamics simulations. *Journal of Biomechanics* **41**, 3073-3077 (2008).

75. Dubey, D.K. & Tomar, V. The effect of tensile and compressive loading on the hierarchical strength of idealized tropocollagen-hydroxyapatite biomaterials as a function of the chemical environment. *Journal of Physics-Condensed Matter* **21**(2009).

76. Dubey, D.K. & Tomar, V. Microstructure dependent dynamic fracture analyses of trabecular bone based on nascent bone atomistic simulations. *Mechanics Research Communications* **35**, 24-31 (2008).

77. Dubey, D.K. & Tomar, V. Role of the nanoscale interfacial arrangement in mechanical strength of tropocollagen-hydroxyapatite-based hard biomaterials. *Acta Biomaterialia* **5**, 2704-2716 (2009).

78. Dubey, D.K. & Tomar, V. Role of hydroxyapatite crystal shape in nanoscale mechanical behavior of model tropocollagen-hydroxyapatite hard biomaterials. *Materials Science and Engineering: C* **29**, 2133-2140 (2009).

79. Gautieri, A., Buehler, M.J. & Redaelli, A. Deformation rate controls elasticity and unfolding pathway of single tropocollagen molecules. *Journal of the Mechanical Behavior of Biomedical Materials* **2**, 130-137 (2009).

80. Katti, D.R., Pradhan, S.M. & Katti, K.S. Directional dependence of hydroxyapatite-collagen interactions on mechanics of collagen. *Journal of Biomechanics* **43**, 1723-1730 (2010).

81. Lorenzo, A.C. & Caffarena, E.R. Elastic properties, Young's modulus determination and structural stability of the tropocollagen molecule: a computational study by steered molecular dynamics. *Journal of Biomechanics* **38**, 1527-1533 (2005).

82. Pradhan, S.M., Katti, D.R. & Katti, K.S. Steered molecular dynamics study of mechanical response of full length and short collagen molecules. *ASCE Journal of Nanomechanics and Micromechanics* **1**,104-110 (2010).

83. Uzel, S.G.M. & Buehler, M.J. Nanomechanical sequencing of collagen: tropocollagen features heterogeneous elastic properties at the nanoscale. *Integrative Biology* **1**, 452-459 (2009).

84. Gautieri, A., Russo, A., Vesentini, S., Redaelli, A. & Buehler, M.J. Coarse-Grained Model of Collagen Molecules Using an Extended MARTINI Force Field. *Journal of Chemical Theory and Computation* **6**, 1210-1218 (2010).

85. Ghosh, P., Katti, D.R. & Katti, K.S. Mineral Proximity Influences Mechanical Response of Proteins in Biological Mineral-Protein Hybrid Systems. *Biomacromolecules* **8**, 851-856 (2007).

86. Bhowmik, R., Katti, K.S. & Katti, D.R. Influence of mineral on the load deformation behavior of polymer in hydroxyapatite-polyacrylic acid nanocomposite biomaterials: A steered molecular dynamics study. *Journal of Nanoscience and Nanotechnology* **8**, 2075-2084 (2008).

87. Sikdar, D., Pradhan, S.M., Katti, D.R., Katti, K.S. & Mohanty, B. Altered phase model for polymer clay nanocomposites. *Langmuir* **24**, 5599-5607 (2008).

CHAPTER 3. MOLECULAR DYNAMICS, STEERED MODLECULAR DYNAMICS, AND FINITE ELEMENT METHOD

3.1. Molecular Dynamics

Molecular dynamics is a computer simulation method that is used to model atomic scale dynamics of a system. Molecular dynamics was first used by Alder and Wainwright to study interactions of hard spheres [1,2]. It simulates the movement of atoms and molecules while they simultaneously interact with force fields due to all the other neighboring atoms and molecules. It can be used to study structural, dynamic, and thermodynamic properties of a system. Molecular dynamics uses classical mechanics to predict trajectory of a system as the positions and velocities of particles (constituting a system) evolve with time. In this method, each atom is moves in many-body potentials of all the other atoms and Newton's second law of motion is integrated to obtain the evolution of position and velocity of particles over time. The differential equation representing Newton's second law of motion is given by

$$\frac{d^2 r_i}{dt^2} = \frac{F_i}{m_i} \quad \text{.....(3.1.)}$$

where r_i is a position, m_i is mass and F_i is a force acting on particle i in the direction of r_i. The force F_i acting on a particle is obtained by computing gradient of potential energy function $U(r)$ as follows

$$F_i = -\nabla_i U(r) \quad \text{.....(3.2.)}$$

where $U(r)$ is a function of the position of a particle. The accelerations of a particles obtained from equation (1) can be used along with equations of motion to predict future

position and velocity of particles based on the initial positions and velocities. This is carried out in series of small time steps which must be chosen such that the steps are reasonably small compared to time period of the fastest motion (highest frequency motion) in a system. Typically, a time step of an order of $\tau/20$ is used as a thumb rule for a simulation, where τ is a time period of the fastest motion. As for example, the highest frequency motions of biomolecules such as protein is a stretching vibration of bond between hydrogen atom and a heavy atom, the time period of which is of an order of 10 fs; hence the time step of 0.5 fs may be may be used for the simulation. Such a small time step implies that it will require two million time steps to approach a nanosecond. Necessity of such a large number of time steps seriously limits our ability to carry out longer simulations. There are algorithms like SHAKE[3,4] and RATTLE[5] that can be used to constrain the fast moving atoms, and allow us to use bigger time steps for carrying out longer simulations.

The initial position of atoms and the molecular structure required for simulation is typically obtained from experimental techniques such as x-ray crystallography or NMR spectroscopy. The initial velocities of particles are usually assigned using a Maxwell-Boltzmann or Gaussian distribution corresponding to the required temperature so that the net momentum of a system is zero, i.e.

$$P = \sum_i^N m_i v_i = 0 \quad \text{.....(3.3.)}$$

where P is an overall momentum, N is the total number of atoms in a system, and v_i is a velocity. Maxwell-Boltzmann distribution at a given temperature T provides us the probability that an atom i is moving with velocity v_{ix} along the x direction.

$$p(v_{ix}) = \left(\frac{m_i}{2\pi k_B T} \right)^{1/2} e^{-\frac{m_i v_{ix}^2}{2\pi k_B T}} \quad \text{..... (3.4.)}$$

where $p(v_{ix})$ is the probability and k_B is the Boltzmann constant.

Due to complicated form of the potential energy function the differential equations representing Newton's equation of motion do not have an analytical solution. These equations are solved numerically by using various types of finite-difference integrations algorithms. These algorithms solve equations step by step while incrementing time by an interval Δt during each successive step. Thus, if the position and velocity of a particle is known at time t then the future positions and velocities at time t+Δt, t+2Δt, t+3Δt etc can be computed using this method. A good algorithm should be computationally efficient, minimize round off errors, and allow longer time steps while conserving energy and momentum. Number of finite-difference algorithms is available for integrating the equations of motion some of which are described below:

3.1.1. Verlet Algorithm

This algorithm uses forward $r(t+\partial t)$ and backward $r(t-\partial t)$ Taylor expansions as given in equations 5 and 6

$$r(t+\partial t) = r(t) + v(t)\partial t + \frac{1}{2}a(t)\partial t^2 \quad \text{..... (3.5.)}$$

$$r(t-\partial t) = r(t) - v(t)\partial t + \frac{1}{2}a(t)\partial t^2 \quad \text{..... (3.6.)}$$

Summing up above expressions we obtain

$$r(t+\partial t) = 2r(t) - r(t-\partial t) + a(t)\partial t^2 \quad \text{..... (3.7.)}$$

which is used to calculate the new positions at $t+\partial t$ and propagate position of a particle over time. This algorithm is a pretty straight forward implementation which is simplectic,

requires only a single force calculation per integration cycle, and conserves linear and angular momentum. Additionally, the position integration is simple which reduces storage requirements. The main disadvantage of this algorithm is that velocity propagation is prone to large errors.

3.1.2. Leap Frog Algorithm

This is a modification of Verlet algorithm in which the velocities are evaluated at a midpoint between position evaluations. The velocity at midpoint is then used to calculate the position ' r ' at time ($t + \partial t$).

$$r(t+\partial t) = r(t) + v(t+\frac{1}{2}\partial t)\partial t \quad \text{……..…..…..……} \quad (3.8.)$$

$$v(t+\frac{1}{2}\partial t) = v(t-\frac{1}{2}\partial t) + a(t)\partial t \quad \text{……..……} \quad (3.9.)$$

Advantage of this algorithm is that velocity evaluation is improved compared to Verlet algorithm. The disadvantage is that this algorithm is computationally more expensive and the evaluation of velocities is not carried out at the same time as the position.

3.1.3. Velocity Verlet Algorithm

This algorithm is a variant of Verlet integrator which is better at velocity propagation. Velocity verlet algorithm uses the following equations

$$r(t+\partial t) = r(t) + v(t)\partial t + \frac{1}{2}a(t)\partial t^2 \quad \text{……..……..} \quad (3.10.)$$

$$v(t+\partial t) = v(t) + \frac{1}{2}a(t)\partial t + \frac{1}{2}a(t+\partial t)\partial t \text{ …..……..…} \quad (3.11.)$$

The advantage of this algorithm is that it is simple and numerically stable providing better evaluation of velocities and better energy conservation. The main

disadvantage is that it is computationally expensive compared to Verlet and Leap-Frog algorithm.

Since molecular dynamics is based on laws of classical mechanics it is applicable only to cases where quantum effects are negligible. Hence, molecular dynamics is not suitable for reactions that involve electronic rearrangement, translation and rotation of light atoms or molecules such as He, H_2, and D_2, and for instances where frequencies (ν) of vibrational motion is such that $h\nu > k_BT$. MD cannot be used for capturing motions of high frequency and is unsuitable for low temperatures, where the thermal energy available to system is small compared to discrete quantum energy levels.

In general, molecular dynamics can be considered to be a computer simulation approach to statistical mechanics. It has wide ranges of applications that include study of a link between structure and function of various molectules, interactions between various molecular systems, and the structural and dynamic information of molecular system. It is an indispensable multiscale modeling tool for bridging a temporal and spatial gap between ab initio quantum models and microscopic models.

3.2. Steered Molecular Dynamics

Steered molecular dynamics (SMD) can be considered to be an extension of molecular dynamics in which an external force is applied to a molecule along certain degrees of freedom in order to guide a system from one state to another[6]. The applied force in SMD can be either constant or varying with time. SMD has various applications such as study of binding and dissociation of ligand, study of mechanism of unfolding of biopolymer, and simulation of AFM experiments. During processes such as binding and unbinding of ligand there is a transition from one equilibrium state to another, which

involves rare events like barrier crossing. Such events can be very difficult to reproduce in the MD time scales. SMD offers solution to this difficulty by allowing us to steer the system from one state to another while enhancing sampling along the pathway of interest[6]. Thus, SMD presents us with a tool to accelerate processes which are very slow to model using MD time scales and access molecular mechanisms that determine mechanical properties of molecules.

SMD is capable of simulating processes which involve major changes that deviate significantly from equilibrium such as extraction of ligand from enzyme and stretching termini of protein to initiate unfolding [7]. SMD simulations are similar to umbrella sampling when the change is minor, and the applied forces are small which vary slowly with time[7]. However, actual SMD simulations involve forces that change rapidly with time. As a result there is a large amount of irreversible work being performed that cause significant deviation of system from equilibrium. Therefore, it is necessary to discount irreversible work form SMD results to obtain equilibrium information and treat the results of SMD from the nonequilibrium viewpoint[6,8]. This is made possible by the work of Jarzynski [9] who showed that difference in equilibrium free energy between two states ΔF can be obtained from average of irreversible work $\langle W \rangle$ as given by the following equality

$$e^{-\beta \Delta F} = \langle e^{-\beta W} \rangle \quad \text{.....(3.12.)}$$

where $\beta = 1/(k_B T)$.

Constant-force SMD and constant velocity SMD are the two basic ways in which SMD can be carried out. However, SMD can also be done using other kinds of external potentials, complex forces that can change direction during the simulation process [10], or a

torque applied to parts of protein to cause rotational motion of domains [11,12]. In constant-force SMD the constant force is applied to atoms in a given direction. The forces applied are of an order of tens to a thousand picoNewtons (pN) [6,13]. In constant-force SMD the intermediaries are relatively clear and long surviving, which may be modeled using the theory of mean first passage time for barrier-crossing event[6,14,15]. In constant-velocity SMD the harmonic potential is used to restrain an atom of protein or center of mass of group of atom to a point in space. The restrained atoms are called SMD atoms and the restraint can be considered as a dummy atom. The restraint point is then moved with a constant velocity in a particular direction. The restrained atoms will experience a pull proportional to their separation from the restraint, which will cause them to follow the restraint. Assuming single reaction coordinate x, the external potential applied to SMD atoms is given by

$$U = K(x - x_o)^2 \quad \text{.....(3.13.)}$$

where K is the stiffness of restraint, x_o is the initial position of restraint, and x is a final position of restraint [6]. The force exerted on SMD atoms is given by

$$F = K(x_o + vt - x) \quad \text{.....(3.14.)}$$

where *v* is the constant velocity with the restraint is moving[11]. The constant velocity SMD simulates an Atomic Force Microscope (AFM) experimental technique used to pull biomolcules. The harmonic constraint used in SMD is analogous to stiffness of cantilever used in AFM. However, the spring constant k used in SMD simulation (k ~70 pN/Å) is very stiff compared to stiffness of cantilever (k ~1pN/A^o) used in AFM [6]. The stiffer spring in SMD allow us to achieve better spatial resolution and access detailed information about interaction energies. Additionally, higher velocity of puling on the

order of 1A/ps is used in SMD simulations, since the time scale of simulations are typically 10^5 times shorter than the AFM experiment due to present day computational limitations [6]. The longest time for which SMD simulations have been carried out is of an order of few nanoseconds. Higher velocity of pulling requires greater force for pulling and results in large amount of irreversible work that has to be discounted to obtain equilibrium information. Using SMD It is possible to apply more complex types of force compared to AFM for manipulating biomolecules. SMD is an invaluable simulation tool for probing nanomechanical properties of a molecules and to study biomolecular processes which are too slow to model. It is believed that most of the MD simulations in the future will include SMD.

3.3. Finite Element Method

Finite element method is a numerical technique used to solve physical problems in engineering analysis and design in various areas such as structural mechanics, thermal analysis, fluid mechanics, electromagnetics, and electric conduction. The development and use of finite element method to solve engineering problems was made possible by the advent of digital computers. In additional to the fields such as civil, mechanical, nuclear, and aerospace engineering finite element analysis is increasingly finding applications in relatively newer fields such as biomechanics and biomedical engineering for modeling biological soft and hard tissues. Finite element models can be used to simulate the response of complex structures before building the prototype, carry out complex tests which are very difficult or impossible to carry out in the laboratory, as well as, understand the mechanics of natural/synthetic materials such as bone and other nanocomposites.

The initial step in solving a physical problem is idealization into a mathematical model. The complex mathematical models often consist of differential equations for which the analytical solution may not be available. The numerical solution to complex differential equations can be obtained using finite element method. Finite element method is based on the idea of discretization of the structure, or region in to a large number of elements known as finite elements. These elements may be one, two, or three dimensional. The continuous system has infinite number of degrees of freedom and impossible to solve for all the field variables (e.g. displacement, temperature), unless the closed form analytical solution is available. In finite element method, the process of discretization is employed to limit the number of degree of freedom, and the value of field variable is computed at only a finite number of points known as node. The value of field variable at the nodes is then used to compute its variation over the domain of an element using interpolation function as follows:

$$u_i(x) = N_i(x)\tilde{u}_i \quad \text{.....(3.15.)}$$

Where $N_i(x)$ is an interpolation function (or shape function), $u_i(x)$ is a value of field variable at x, $\tilde{u}_i$ is the value of field variable at the node. The interpolation function can be linear, quadratic, cubic, hermitian, or special types. The interpolation function should be chosen such that its shape is approximately similar to the shape of the unknown field/solution in the domain of element.

There are different types of element used in finite element method which generally fall into following three catagories:

1) Continuum elements: truss, cable, plane stress, plane strain, generalized plane strain, axisymmetric elements, brick/hexahedral element

2) Structural elements: beam, plates, shells.
3) Special elements: gap-and-friction elements, pipe-bend element, curved-pipe element, shear panel element, cable element, rebar element, incompressible element, semi-infinite element etc.

In the formulation of continuum elements the displacements are interpolated in terms of nodal point displacement, whereas, in the formulation of structural elements the displacements are formulated in terms of midsurface displacements and rotations [16]. The continuum elements have displacement degree of freedom only, and hence not very appropriate for modeling thin structures dominated by bending.

Next step is to express the dependent flux field in terms of the nodal point unknowns. In the deformation problem the dependent flux field is strain, which is expressed in terms of nodal displacement,

$$\{\varepsilon(x)\} = [B]\{q\} \quad \text{(3.16.)}$$

where ε is a strain vector, [B] is a strain-displacement transformation matrix, and {q} is a nodal displacement vector. The strain field is then linked to stress field using the constitutive relations of a material,

$$\{\sigma(x)\} = [C]\{\varepsilon(x)\} \quad \text{(3.17.)}$$

where $\{\sigma(x)\}$ is the stress vector, and $[C]$ is the stress-strain matrix also known as elasticity matrix.

A crucial step in finite element method is to derive element equations, for which numbers of methods are available. Energy methods and residual methods are the two commonly used procedures used for deriving element equations. Element equations ensure equilibrium of an element with its surrounding and relate the nodal displacements

to the load. The element equations lump the physical significance of element at its nodes as shown by equation below:

$$[K]\{q\} - \{Q\} = 0 \quad \text{.....(3.18.)}$$

where **[K]** is an element property matrix (e.g. stiffness matrix for deformation problems and conductivity for thermal problems), **{q}** is a nodal vector (nodal displacement vector for deformation problem) and **{Q}** is a nodal load vector that consists of nodal forces, body force (e.g. due to gravity) traction etc. The element property matrix is given by

$$[K] = \int_v [B]^T [C][B] dV \quad \text{.....(3.19.)}$$

The individual element equations are assembled to achieve equilibrium of an entire structure, as well as, the continuity of nodal point unknowns. The continuity requirements depend on type of element chosen and problem type, e.g. for in plane deformation problems using continuum elements it is sufficient for displacement to be continuous, however, in bending problems using structural elements the higher derivatives of displacement should be continuous as well. Finally the boundary conditions are applied and the resulting global equations are solved using numerical methods to obtain primary unknowns. The secondary quantities or dependent flux fields like stress and strain are then derived from primary quantities.

3.4. References

1. Alder, B.J. & Wainwright, T.E. Phase transition for a hard sphere system. *Journal of Chemical Physics* **27**, 1208-1209 (1957).
2. Alder, B.J. & Wainwright, T.E. Studies in molecular dynamics .1. General method. *Journal of Chemical Physics* **31**, 459-466 (1959).

3. Vangunsteren, W.F. & Berendsen, H.J.C. Algorithms for macromolecular dynamics and constraint dynamics. *Molecular Physics* **34**, 1311-1327 (1977).

4. Ryckaert, J.P., Ciccotti, G. & Berendsen, H.J.C. Numerical-integration of cartesian equations of motion of a system with constraints - molecular-dynamics of n-alkanes. *Journal of Computational Physics* **23**, 327-341 (1977).

5. Andersen, H.C. Rattle - a velocity version of the shake algorithm for molecular-dynamics calculations. *Journal of Computational Physics* **52**, 24-34 (1983).

6. Phillips, J.C. et al. Scalable molecular dynamics with NAMD. *Journal of Computational Chemistry* **26**, 1781-1802 (2005).

7. Isralewitz, B., Gao, M. & Schulten, K. Steered molecular dynamics and mechanical functions of proteins. *Current Opinion in Structural Biology* **11**, 224-230 (2001).

8. Gullingsrud, J.R., Braun, R. & Schulten, K. Reconstructing potentials of mean force through time series analysis of steered molecular dynamics simulations. *Journal of Computational Physics* **151**, 190-211 (1999).

9. Jarzynski, C. Nonequilibrium equality for free energy differences. *Physical Review Letters* **78**, 2690-2693 (1997).

10. Isralewitz, B., Izrailev, S. & Schulten, K. Binding pathway of retinal to bacterio-opsin: a prediction by molecular dynamics simulations. *Biophysical Journal* **73**, 2972-2979 (1997).

11. Izrailev, S., Stepaniants, S. & Schulten, K. Applications of steered molecular dynamics to protein-ligand/membrane binding. *Biophysical Journal* **74**, A177-A177 (1998).

12. Wriggers, W. & Schulten, K. Protein domain movements: Detection of rigid domains and visualization of hinges in comparisons of atomic coordinates. *Proteins-Structure Function and Genetics* **29**, 1-14 (1997).

13. Lu, H. & Schulten, K. The key event in force-induced unfolding of titin's immunoglobulin domains. *Biophysical Journal* **79**, 51-65 (2000).

14. Schulten, K., Schulten, Z. & Szabo, A. Dynamics of reactions involving diffusive barrier crossing. *Journal of Chemical Physics* **74**, 4426-32 (1981).

15. Lu, H., Krammer, A., Isralewitz, B., Vogel, V. & Schulten, K. Computer modeling of force-induced titin domain unfolding. *Advances in Experimental Medicine and Biology* **481**, 143-162 (2000).

16. Klaus-Jürgen, B. *Finite Element Procedures*, (Prentice-Hall Inc., 1996).

CHAPTER 4. DIRECTIONAL DEPENDANCE OF HYDROXYAPATITE-COLLAGEN INTERACTIONS ON MECHANICS OF COLLAGEN

This chapter presents study of the directional dependence of mineral-collagen interactions on the mechanics of collagen. The content of this study has been published in Katti, D. R., Pradhan, S. M., and Katti, K. S. (2010). "Directional dependence of hydroxyapatite-collagen interactions on mechanics of collagen." *Journal of Biomechanics*, 43(9), 1723-1730.

4.1. Introduction

Bone is a biological nanocomposite that exhibits a highly optimized and complex multi-level hierarchical structure. It is an integral part of skeletal system, most of which are generally composed of a strong and dense external layer called cortical bone around an interior spongy cancellous bone (also called trabecular bone). It's remarkable mechanical properties lend itself to the structural role within the body by providing strength necessary to support and protect softer tissues and organs. Additionally, it also serves other functions such as production of red and white blood cells, and storage of minerals such as calcium and phosphorous. Bone is composed of the organic, mineral phase, and water. The relative proportions of organic, mineral phase, and water is about 25%, 65%, and 10% respectively by weight[1-5], and around 32-44%, 33-43%, and 15-25% respectively by volume[5,6]. Mechanical properties of bone have been extensively experimentally studied by the Cowin group who has also modeled the poromechanics behavior of bone. [7-11]. Notable experiments and modeling efforts are also carried out by Lakes and Katz on viscoelastic behavior of bone [12-18]. The organic phase in bone is

mainly composed of Type I collagen, which are secreted by osteoblasts into the extracellular space. The collagen molecules self-assemble to from a structure known as fibril that comprises about 85-95% of the total bone protein[19]. The mineralized fibril, the basic building blocks of bone material[20], is about 80-100 nm in diameter and unknown length because they merge with neighboring fibrils[21]. The other constituents of organic phase include lipids and non-collageneous proteins such as phosphoproteins.

Within the fibril, the collagen molecules are aggregated parallel to each other and staggered along the axial direction by 67 nm resulting from the presence of a hole zone with 40 nm length and overlap zone with 27 nm length[22,23]. The individual cylindrical collagen molecules are about 300 nm in length and 1.23 nm in width[22]. The collagen molecule consists of three polypeptide chains (called α chains) folded in a triple helical fashion. The mineral component of bone is made of hydroxyapatite (HAP) which is oriented such that its c-axis is roughly parallel to the long axis of collagen[21,24]. The $(10\ \bar{1}\ 0)$ face of HAP is found to be well developed from electron diffraction study and approximately parallel to each other[22,25,26]. The HAP crystal platelets nucleate in hole zones, and grow in length along collagen long axis and width along channels[22,27-29]. The crystals continue to grow, outgrowing the width of gap zone, into the overlap zone squeezing in between the collagen molecules[30]. The growing crystals join to form large and thick extended sheets that may occupy several hole zones[21,22,25,28]. In addition to intrafibrillar mineral, the surface of fibril is coated by extrafibrillar mineral[31].

The study of bone hierarchy in relation to its mechanical properties has been carried out using various modeling approaches. The modeling of bone was carried out by Hellmich et al. and Naghdabadi et al. using micromechanics formulation [32-34]. Ciarletta et

al. carried out viscoelastic modeling of bone at fibrillar level using microstructural approach [35]. Beside these studies, model structures of collagen molecules as well as collagen fibrils have been investigated individually using molecular dynamics methods[36-42].

The organization of collagen and mineral in the fibril point to a fact that there is substantial interfacial interaction area between them. The interface between collagen and HAP have important bearing on the mechanical properties of bone. However, the interface between collagen and HAP is not very well understood. Our previous studies using molecular dynamics have elucidated the nature of mineral-organic interface and the role of mineral proximity on the mechanical behavior of protein [43-47]. Also, the molecular dynamics study of collagen-mineral interface was carried out to understand mechanics of collagen in the proximity of mineral[48-50]. All of these studies have shown that the mechanics of protein is substantially influenced by the presence of mineral in the proximity.

The location of mineral along collagen length (i.e. at the side or next to the end of collagen) result in relative orientations of collagen with respect to these mineral surfaces which allow for different types of interaction between these two constituents. The relative orientation of collagen with respect to mineral corresponds to different interfacial configurations/locations within the fibril, which is where the directional dependence of hydroxyapatite-mineral interactions comes into picture. We have considered two possible cases of the relative orientations between collagen and mineral: (i) collagen normal to the hydroxyapatite surface, and (ii) collagen parallel to the mineral surface. The collagen pulled normal to the mineral surface provides us with an understanding of the mechanics

of interaction between the end of collagen and the mineral located in the hole zone; whereas, the collagen pulled parallel to the mineral surface elucidates the interaction between the collagen and the mineral situated on the side of collagen within the fibril as well as in the interfibrillar space. This study is important, especially since a good proportion of mineral in bone is within the fibril, amounting to 23%, while the remaining 77% is in the interfibrillar space [51]- both of these mineral masses interfacing with the substantial portions of collagen. In this study, we have investigated the directional dependence of the mechanics of collagen when stretched normal and parallel to the HAP surface. We have also studied role of $(10\ \bar{1}\ 0)$ and (0001) crystallographic surfaces of HAP on the deformation behavior of collagen using molecular dynamics.

All of the MD and SMD simulations were carried out using NAMD[52] simulation software developed by Theoretical Biophysics Group (TBG) in the Beckman Institute at the University of Illinois at Urbana-Champaign. The CHARMm[53] (Chemistry at Harvard Macromolecular Mechanics) force field is used in simulations and VMD [54] is used for graphical visualization and analysis of results.

4.2. Model Building

The interfacial interactions between collagen and hydroxyapatite were studied using molecular dynamics. The molecular model consists of a collagen molecule placed near the surface of HAP. Collagen is composed of a three polypeptide chains, called α chains, each folded into a left-handed helix and winded about common axis to form a right-handed triple helical structure [55,56]. These chains are held together by interchain hydrogen bonds. The Protein Data Bank-ID of the $(GPP)_n$ model of collagen used is 1k6f[57]. The solvated collagen molecules consisting of N-terminal telopeptide and without

telopeptide were used for our simulations. The structure of collagen with N-terminal telopeptide, consisting of two α1 chains and one α2 chain, used in our model was obtained from literature[58]. The sequence of N-terminal telopeptide used in our simulation is as follows[59,60]:

α1-GlnLeuSerTyrGlyTyrAspGluLysSerThrGlyIleSer-ValPro-helix (GlyProMet-)

α2-GlnPheAspAlaLysGlyGlyGlyPro-helix (GlyProMet-)

The CHARMm[53] force field is used to geometrically optimize collagen molecule by energy minimization. The minimized collagen is then solvated with TIP3P water molecules and minimized again. The temperature of solvated collagen is increased gradually from 0 K to 300 K in steps of 100 K. Then the pressure is increased in steps of 0.25 bar from 0 bar to 1.01 bar. This model is used for studying collagen in absence of HAP using steered molecular dynamics SMD.

The HAP in bone has a hexagonal structure with space group $P6_3/m$[61] and unit cell parameters a = 9.424 Å, b = 9.424 Å, c = 6.879, α = 90°, β = 90°, γ = 120°. The (10 $\bar{1}$ 0) and (0001) surfaces are developed from this unit cell, the detailed description of which is presented in our previous work [50]. The dimension of HAP model with (0001) surface are a = 75.392 Å, b = 75.392 Å, c = 20.639 Å. It consists of 192 unit cells of HAP, i.e., 8 unit cells along a-axis, 8 unit cells along b-axis, 3 unit cells along c-axis. Another model of HAP with (10 $\bar{1}$ 0) surface has a size a = 18.848 Å, b = 37.696 Å, c = 151.338 Å corresponding to 176 unit cells of HAP (2 unit cells along a-axis, 4 unit cells along b-axis, 22 unit cells along c-axis). The HAP is geometrically optimized and the temperature and pressure are raised using a procedure similar to that used for collagen as described above. The model is again geometrically optimized using energy minimization.

This model is used to create surface with no dipole moment perpendicular to the surface. This is done because the surface energy diverges and becomes infinite, rendering surface unstable, when there is a dipole moment perpendicular to the surface as shown by Bertaut[62]. The non-dipolar surface was created using the reconstruction described by Taskar et al.[63]. The surface was rendered non-dipolar by transferring half of the surface ions (calcium ions) from the surface to the opposite surface. The HAP with non-dipolar surface is geometrically optimized through energy minimization, and the temperature and pressure are incrementally raised to 300 K and 1.01 bar respectively. Furthermore, the model is minimized to achieve global minimum and used for constructing HAP-Collagen model.

The minimized structures of solvated collagen and HAP surface constructed above are brought in close proximity of each other. This HAP-collagen model is geometrically optimized through energy minimization. The temperature is raised to 300 K in steps of 100 K and the pressure is raised to 1.01 bar in steps of 0.25 bar. This is a model used for our steered molecular dynamics (SMD) simulations (Fig. 4.1).

4.3. Simulation Details

The models constructed above were considered in our study. For minimization of structures the conjugate gradient method is used. Periodic boundary conditions are employed for all of the MD and SMD simulations. Isothermal and isobaric ensemble (NPT) is considered for all of the simulations. NPT ensemble is simulated using combination of Langevin piston Nose-Hoover [64,65] method (for maintaining pressure) and Langevin dynamics (for maintaining temperature). Particle Mesh Ewald (PME) method is used to compute full electrostatics for a system. The van der Waals cut off distance of 9

Å is used for all the simulations and Verlet algorithm is used for integrating Newton's laws of motion.

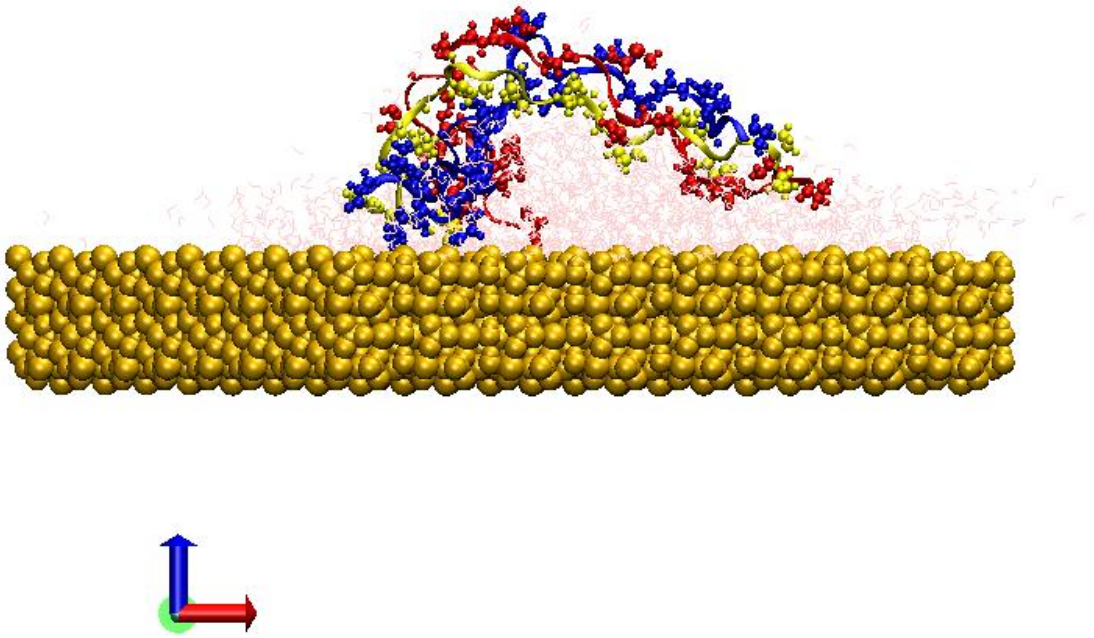

Figure 4.1. Solvated N-collagen pulled parallel to the surface to HAP. The left end of collagen is fixed and its center of mass pulled towards the right.

The SMD simulations are carried out on models at 300 K and 1.01 bar. During SMD simulations, each of the three chains of collagen is fixed at one end and the center of mass of molecule is harmonically constrained to a reference point which is moved with a constant velocity. As for N-collagen the ends of all the three telopeptide chains are fixed at carbonyl atoms of pyroglutamic acid residues. The different velocities used in our simulations are 0.25 Å/ps, 0.5 Å/ps, 0.75 Å/ps, and 1.0 Å/ps. The force constant of

spring (harmonic constraint) is considered to be 4.0 kcal mol^{-1} $Å^{-2}$, which corresponds to a spatial (thermal) fluctuation[66] of center of mass $\delta x = \sqrt{k_B T/k}$ = 0.77 Å at T = 300 K. SMD was carried out to study mechanical behavior of collagen and its deformation mechanism in presence and absence of HAP. The SMD was carried out by pulling center of mass of collagen normal to the HAP surface and parallel to the HAP surface (Fig. 4.2). The deformation mechanism of collagen pulled normal to HAP surface is described in our previous work [50], and used in this work for the purpose of comparison with pulling in parallel direction.

4.4. Results and Discussion

When collagen is stretched, the load-displacement response is strongly influenced by non-bonded interactions between water, collagen, and HAP, which alter the deformation behavior of collagen. Among these three components, water appears to have a very strong attractive interaction with both the collagen and HAP, the interaction being strongest with HAP as evident from a typical plot shown in figure 4.2. Because of this reason the water molecules are very strongly bound and densely clustered around HAP surface. Speaking of water, our previous study has shown that the deformation behavior of collagen is substantially altered by the solvation of collagen molecule, and even more so in the proximity of HAP [50]. Furthermore, HAP is seen to entail greater influence on collagen in association with water than on its own. Here, we compare deformation response of solvated collagen molecule when pulled perpendicular and parallel to the HAP surface.

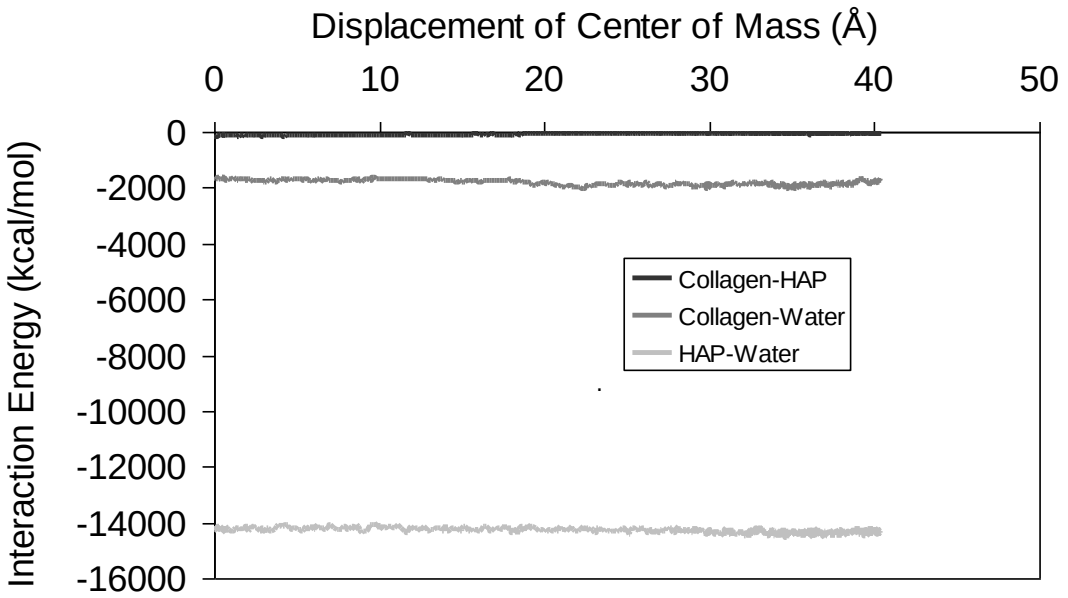

Figure 4.2. Interaction energy between collagen-HAP, collagen-water, and HAP-water when collagen is pulled in x-direction at 1 Å/ps on (0001) surface of HAP.

The load-deformation response of N-collagen pulled normal and parallel to the HAP (0001) surface is shown in figures 4.3 and 4.4 respectively. When collagen is pulled perpendicular to the HAP surface it has to overcome the attraction of the water molecules which are very strongly bound to the HAP surface. This event dominates initial portion of load displacement curve when the collagen molecule is closer to the HAP, and attenuates at large displacement. This effect is captured by regions A1A2 and A2A3 (Fig. 4.3) of load-displacement curve. The attractive interaction energy between collagen and water generally diminish with increasing displacement (region A2A3) as shown in figure 4.5(a) due to separation of large segment of collagen from water molecules that are strongly bound to the HAP. This effect on the load-displacement response of collagen due to the

water molecules tightly bound to the HAP is lower when the collagen is pulled parallel to the HAP surface This is observed in the lower stiffness of the load-displacement curve in the regions B1B2 and B2B3 (Fig. 4.4) of the collagen pulled parallel to the HAP surface compared to the normal direction as shown in figure 4.6. This is possibly because it is easier for collagen to shear past the layers of water tightly bound to HAP in the direction parallel to the HAP surface than in the normal direction.

The hydrogen bonds between three polypeptide chains of collagen and between the side-chains of same strand continuously break and form throughout the unfolding process of collagen. This fluctuation in number of hydrogen bonds with displacement of center of mass as shown in figure 4.7, in which there is a gradual depletion in number of hydrogen bonds as the collagen molecule is stretched. In case of collagen pulled parallel to the HAP surface, the rate of breaking of hydrogen bond is very rapid at small displacement in region B1B2 compared to the collagen pulled normal to the HAP in the region A1A2 (Fig. 4.7). In the regions A2A3 and B2B3 the rate of breaking of hydrogen bond is moderate for both parallel and normal directions of pulling. However, in the regions A3A4 (Fig. 4.3) and B3B4 (Fig. 4.4) the breaking of hydrogen bonds becomes prominent, for collagen pulled along HAP surface as well as normal to HAP surface, as shown in figure 4.7. The rapid breaking of hydrogen bond is due to polypeptide chains unwinding against each other. In these regions, the rapid breaking of hydrogen bonds is accompanied by the increase in stiffness of load displacement curve. This increase in stiffness may be attributed to the combined effect of rapid breaking of hydrogen bond and increasing contribution of very stiff backbone chain. The breaking of hydrogen bonds within collagen molecule is succeeded by creation of new hydrogen bond between

collagen and water molecules in the vicinity. This results in the increase in attractive interaction energy between collagen and water in the region A3A4 and B3B4 as seen in figure 4.5. Following the breaking of most of the hydrogen bonds, the influence of backbone becomes prominent as seen in region A4A5 (Fig. 4.3) and B4B5 (Fig 4.4). The stretching of carbon backbone of collagen molecule in these regions results in a very stiff load-displacement response. The slope of these regions of load-displacement curve is similar for simulations in both perpendicular and parallel directions.

The area under the load-displacement curve represents the energy expended in deformation of collagen. Figure 4.8 shows load-displacement response for different velocities: 1 Å/ps, 0.75 Å/ps, 0.5 Å/ps, and 0.25 Å/ps. It is clear from these plots that there is a velocity dependence of load-displacement response. Greater force and energy is required to stretch collagen when rate of pulling is increased, which is true for collagen pulled parallel to HAP surface as well as perpendicular direction. Furthermore, from figures 4.6 and 4.8 it is seen that response is stiffer requiring more energy at small displacements when pulled in perpendicular direction, while at large displacement more energy is required to pull in a parallel direction. The above observations elucidate the deformation behavior of N-collagen in the proximity of HAP (0001) surface. It is seen that the proximity of mineral surface alters mechanical behavior of collagen which is dependent on direction of stretching of collagen.

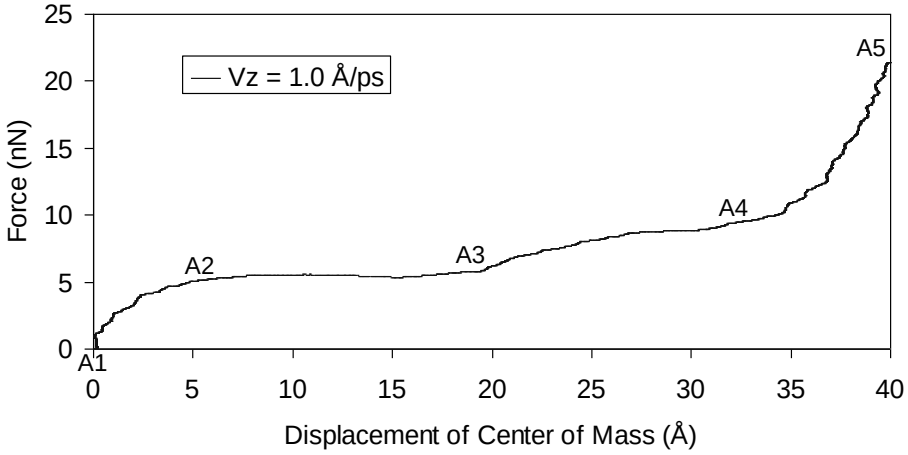

Figure 4.3. Typical Load-deformation behavior of solvated collagen pulled normal to HAP (0001) surface.

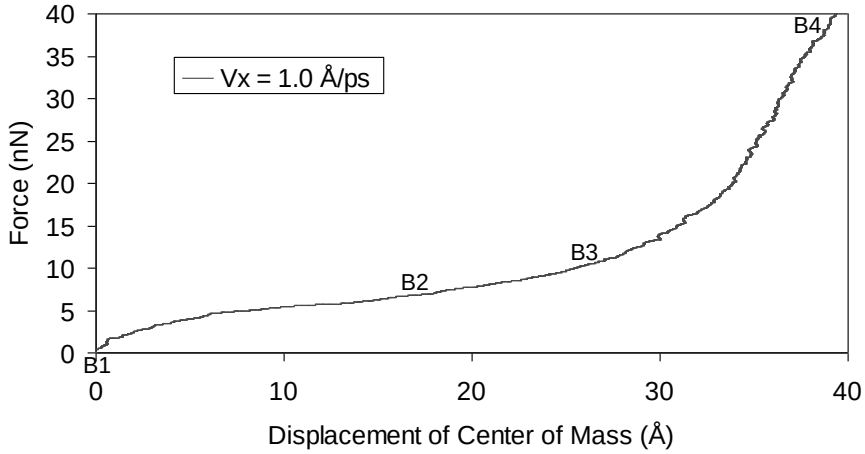

Figure 4.4. Typical Load-deformation behavior of solvated collagen pulled parallel to HAP (0001) surface.

(a)

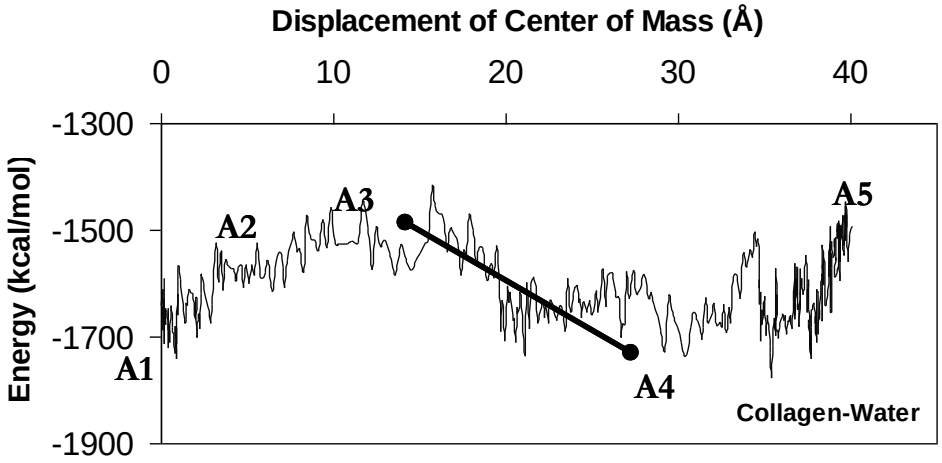

(b)

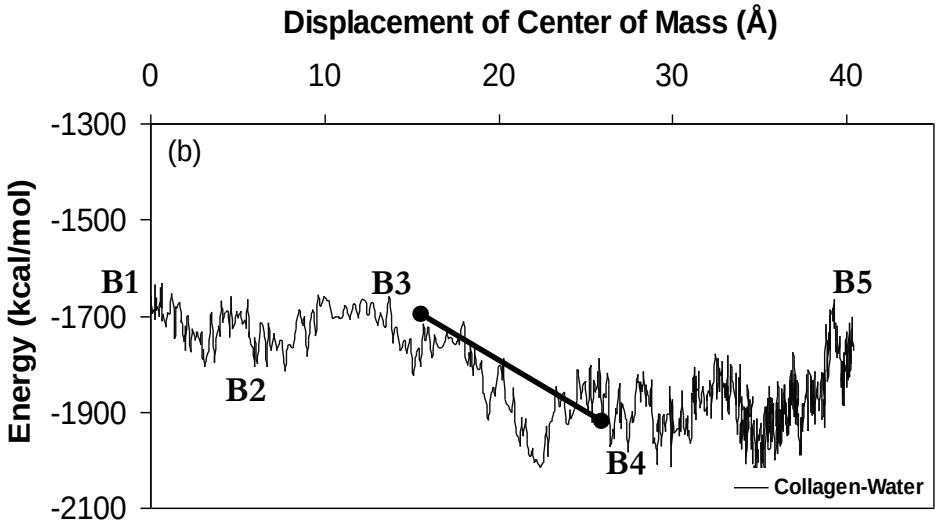

Figure 4.5. Interaction energy between collagen and water: (a) pulled perpendicular to HAP surface, (b) pulled parallel to HAP (0001) surface.

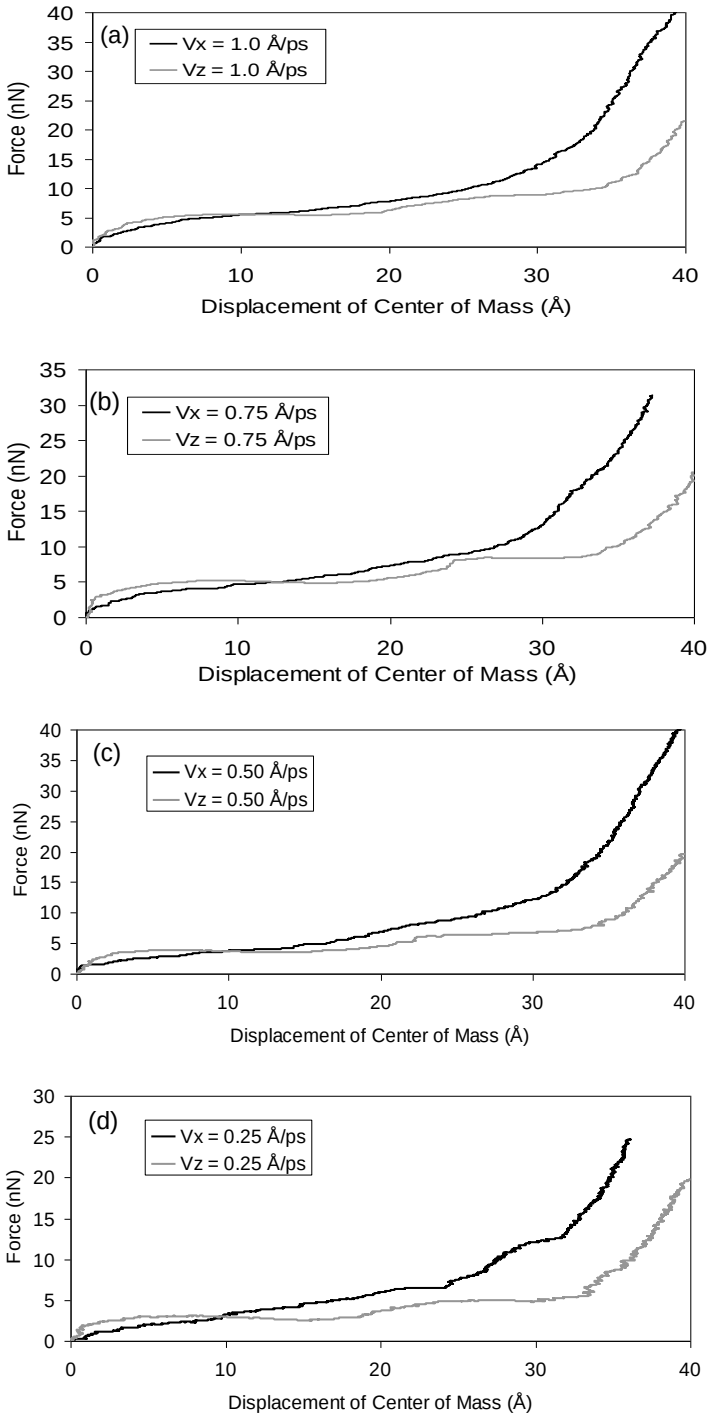

Figure 4.6. Comparison of Load-deformation behavior of solvated collagen pulled parallel (x-direction) and normal (z-direction) to HAP (0001) surface at different velocities: (a) 1 Å/ps, (b) 0.75 Å/ps, (c) 0.5 Å/ps, (d) 0.25 Å/ps.

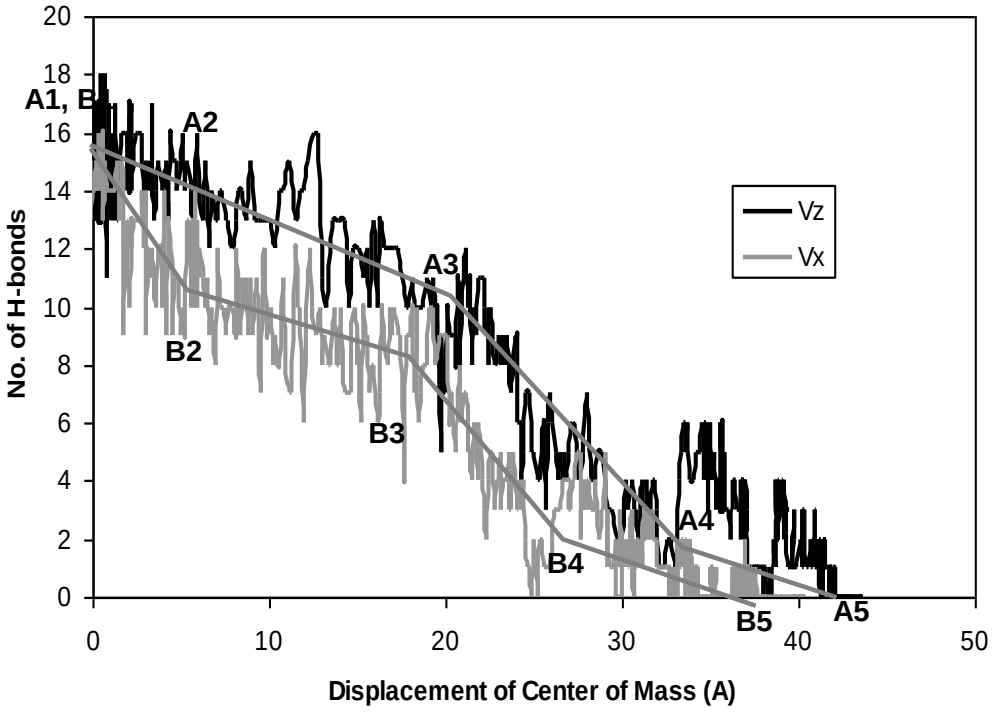

Figure 4.7. Number of hydrogen bonds between polypeptide chains of collagen when center of mass is pulled normal (Vz) and parallel (Vx) to the HAP (0001) surface.

It is evident that a good length of collagen molecule is in the proximity of (10 $\bar{1}$ 0) surface of HAP. Hence, the interaction between collagen and HAP (10 $\bar{1}$ 0) surface is of importance in determining the overall mechanical response of collagen in bone. For this simulation the collagen molecule without telopeptide was used as it is present only at the end of collagen. Figure 4.9 shows the load-displacement response of the collagen pulled parallel to the HAP (10 $\bar{1}$ 0) surface and the absence of HAP. It is seen that the proximity of HAP alters the stiffness of collagen, enhancing it to a great extent. Comparing areas under the load-displacement curves for collagen in presence and absence of HAP, it is evident that the relatively large amount of energy must be expended to stretch collagen in

the proximity of HAP. Evaluated at 15 Å displacement, it is seen that approximately 5 times more energy is necessary to pull collagen in proximity of HAP compared to absence of HAP. Also, as it can be inferred from figure 4.9(a), the ratio of energy expended in presence of HAP to absence of HAP increases up to an extension of about 22 Å and decreases at larger displacement where the load-displacement curves are nearly parallel to each other due to stretching of backbone. The magnified view of load-displacement response for small displacement is shown in figure 4.9(b). At small displacement the effect of rate of pulling on the stiffness of collagen is more prominent, though this effect is also present at larger displacement. It is seen that higher the velocity of pulling, stiffer is the response for both the collagen pulled in the proximity of HAP and the absence of HAP.

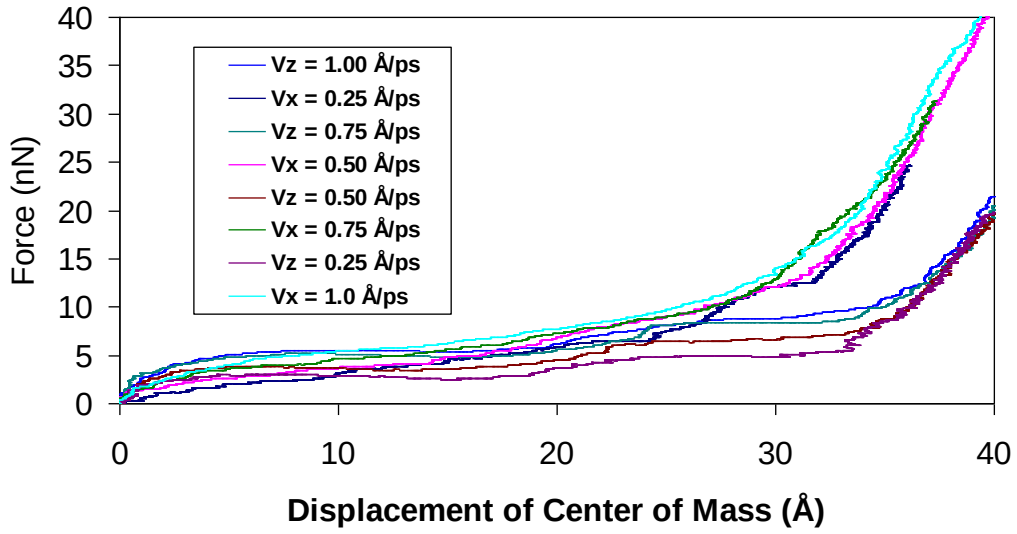

Figure 4.8. Comparison of load-deformation behavior of solvated collagen pulled in normal (z-direction) and parallel (x-direction) to HAP (0001) surface at different velocities.

The results of simulations in presence and absence of HAP show that the deformation behavior of collagen is greatly influenced by the proximity of mineral. Having observed an influence of mineral on the deformation behavior collagen it would be interesting to see the effect of proximity of different crystal surfaces of HAP. The comparison of load displacement response of collagen in the proximity of HAP (10 $\bar{1}$ 0) and HAP (0001) surfaces at different velocities are shown in figure 4.11. The collagen pulled parallel to (0001) surface is stiffer at small displacement (~7 Å) while at large displacement the stiffness is comparable for both the surfaces. At small displacement the relative difference in stiffness for (0001) and (10 $\bar{1}$ 0) surfaces is large for small velocity (0.25 and 0.5 Å/ps) compared to greater velocities (0.75 and 1.0 Å/ps). Also, the load-displacement response of collagen in the proximity of (0001) surface appears to have more steps like features compared to (10 $\bar{1}$ 0) surface which suggests that the deformation mechanisms of collagen for these surfaces could be quite different.

These findings point to the fact that in addition to the proximity of mineral, the mechanics of collagen is greatly influenced by the nature of interface with the mineral. The nature of interface in this study, implies both the relative orientations between collagen and mineral and the type of hydroxyapatite surface in proximity. Hence, although all the collagen molecules bear similar molecular structure, all of them (or different segments of them, to be precise) will not behave the same way during deformation depending on the nature of its interface with hydroxyapatite. Thus the mechanics of fibril cannot be accurately predicted, unless the mechanics of these individual collagens-mineral interfaces are taken into account. This is the primary motivation for studying a single collagen molecule along with hydroxyapatite in the

proximity because this provides a fundamental starting point as well as the correct approach towards understanding the role of collagen in the mechanics of fibril.

(a)

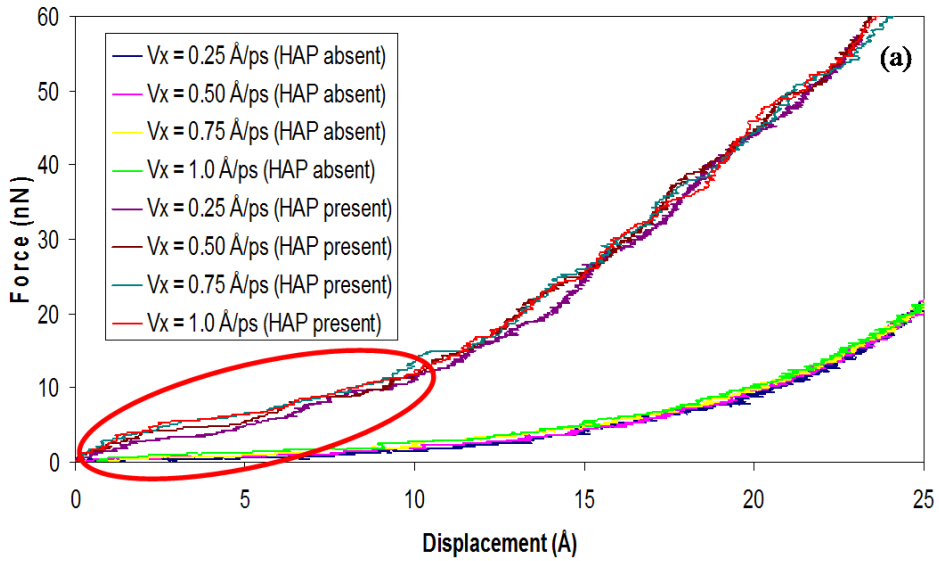

(b)

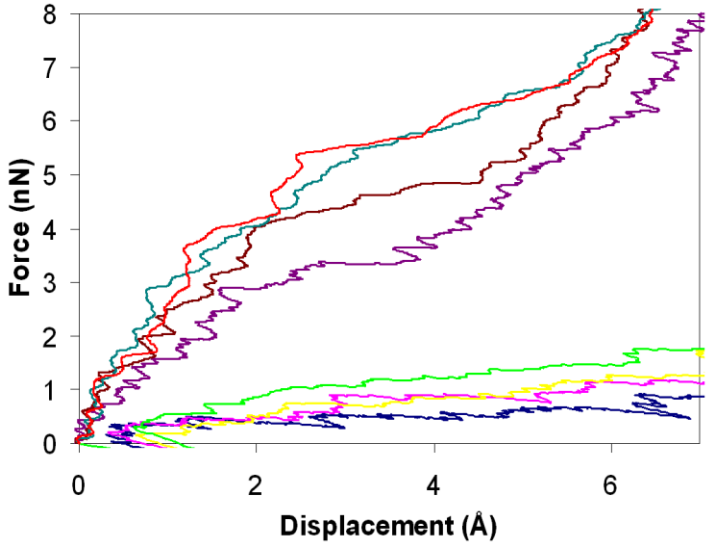

Figure 4.9. (a) Load deformation behavior of collagen in absence and presence of the HAP (10 0) surface pulled parallel to the surface at different velocities, (b) magnified view showing effect of velocity of pulling on stiffness.

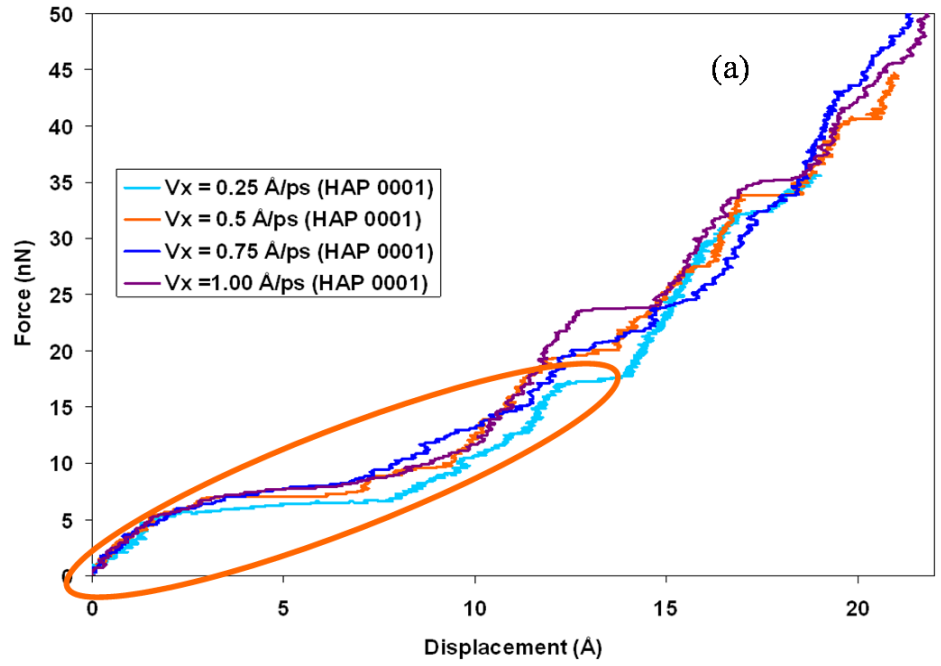

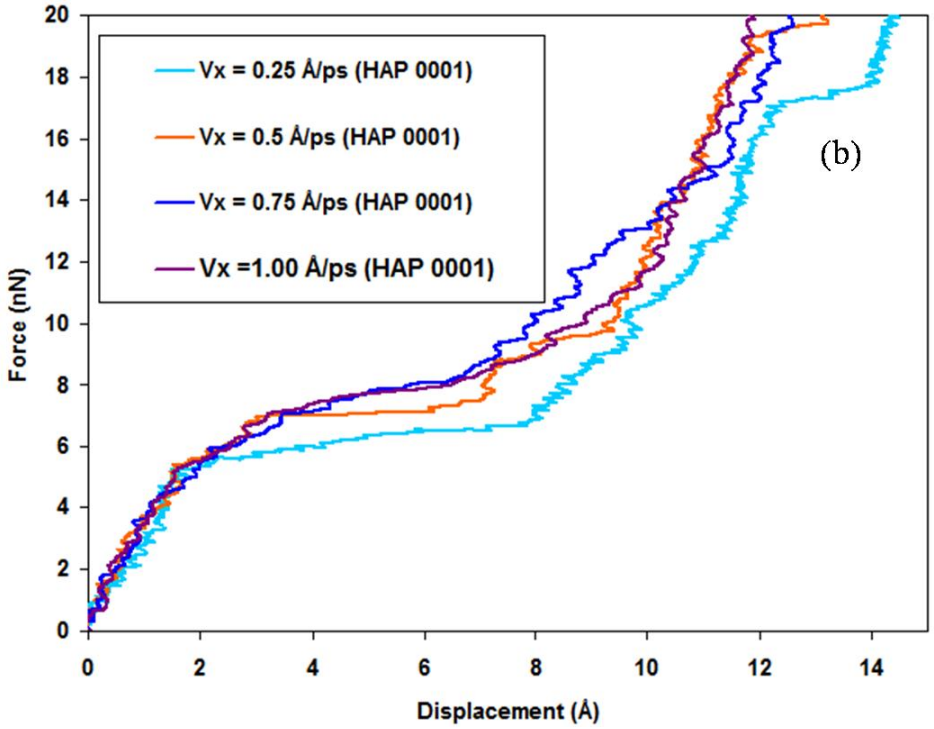

Figure 4.10. (a) Load-displacement response of collagen pulled parallel to HAP (0001) surface, (b) magnified view showing effect of velocity of pulling on stiffness.

(a)

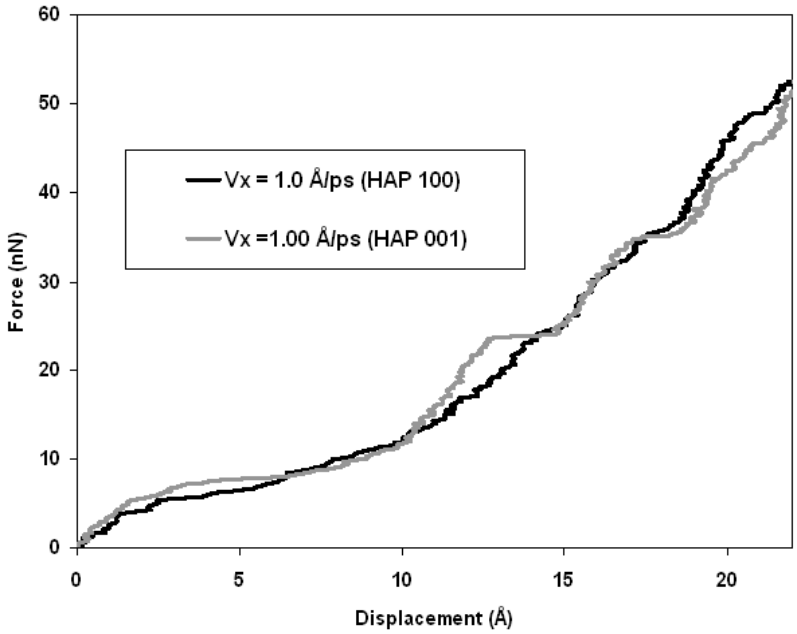

(b)

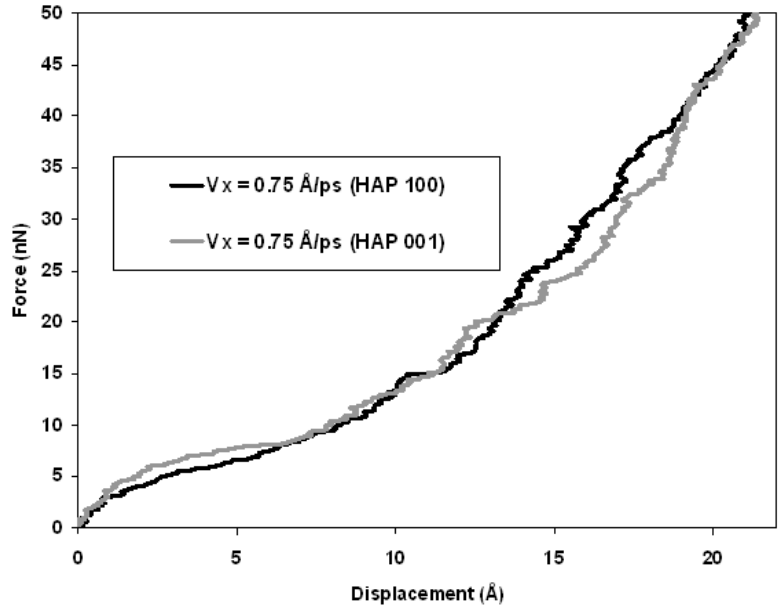

Figure 4.11. Comparison of load-displacement response of collagen pulled parallel to (10 $\bar{1}$ 0) and (0001) surface of HAP at different velocities: (a) 1 Å/ps, (b) 0.75 Å/ps, (c) 0.5 Å/ps, (d) 0.25 Å/ps.

(c)

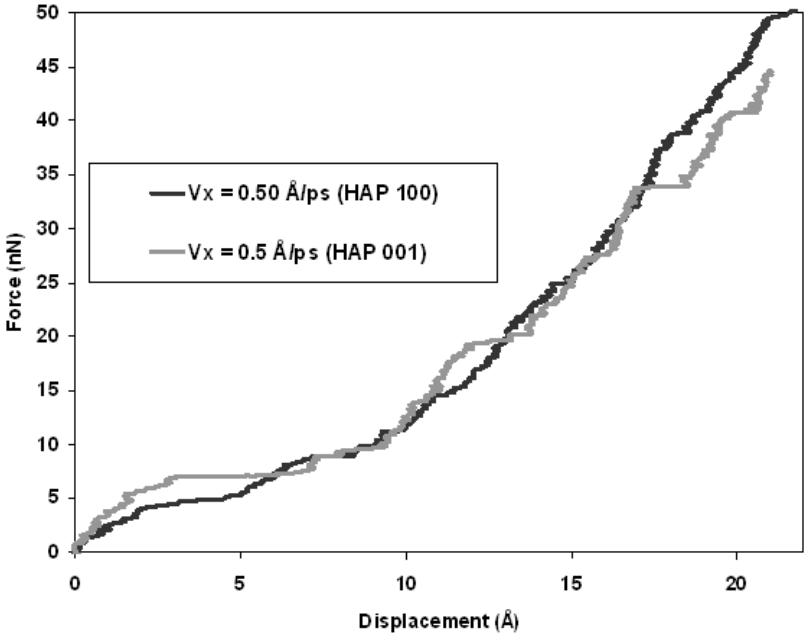

(d)

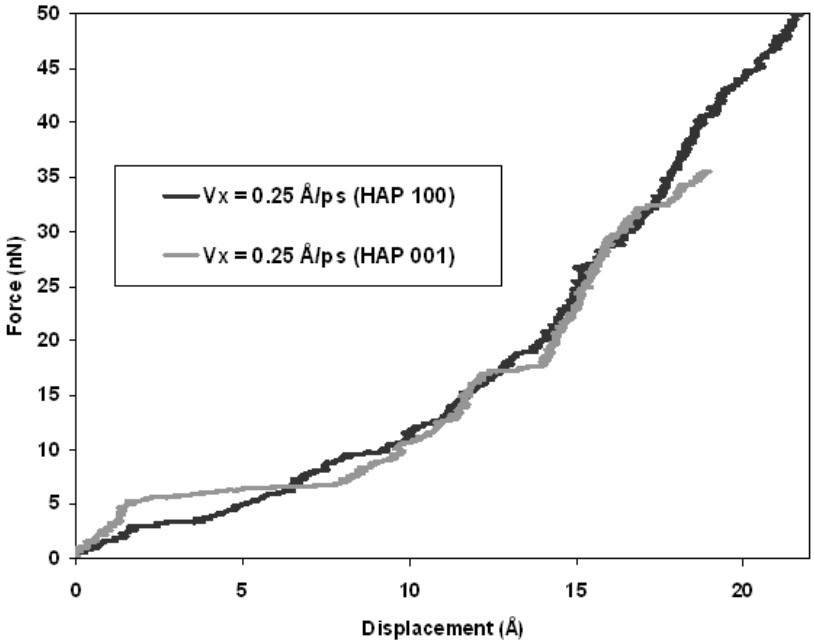

Figure 4.11. Comparison of load-displacement response of collagen pulled parallel to (10 0) and (0001) surface of HAP at different velocities: (a) 1 Å/ps, (b) 0.75 Å/ps, (c) 0.5 Å/ps, (d) 0.25 Å/ps. (Continued)

4.5. Summary and Conclusions

Models of hexagonal HAP ($10\bar{1}0$) and (0001) surface, and collagen with and without telopeptides were built to investigate the mechanical behavior of collagen in the proximity of mineral. Steered Molecular Dynamics was performed where the center of mass of collagen molecule was pulled at different velocities in presence and absence of HAP. In the proximity of HAP, collagen was pulled normal and parallel to the (0001) surface. Load-deformation behaviors of collagen pulled perpendicular and parallel to HAP showed four regions. Water molecules were found have important impact on deformation behavior of collagen in the proximity of HAP due to high interaction energy of water with both collagen and HAP. Water acts as an intermediary between collagen and HAP, which allows HAP to influence mechanical behavior of collagen despite the relatively low interaction energy between them. The effect of water is especially prominent in the initial portion of load-displacement curve of collagen pulled in normal direction, where collagen has to overcome attractive interaction of water strongly bound to HAP. Due to this reason, collagen is stiffer at small displacement when pulled normal to HAP surface. At large displacement, collagen pulled parallel to HAP surface is stiffer. This difference in mechanical response of collagen pulled in parallel and perpendicular direction is due to difference in deformation mechanism of collagen which is evident from the difference in pattern and rate of breaking of inter-chain hydrogen bonds that stabilize collagen molecule. This type of behavior was observed for all the rates of pulling of collagen.

The collagen molecule pulled in the proximity of HAP, parallel to surface, showed marked improvement in stiffness compared to absence of HAP. This is a

response shown by collagen pulled at all the velocities. Higher stiffness of load-displacement response implies that greater amount of energy must be expended to achieve same displacement. Measured at 15 Å displacements of center of mass, it was found that approximately five times more energy must be expended in presence of HAP compared to absence of HAP. This is remarkable from the perspective of energy absorption/dissipation by collagen since it is the only major component of bone capable of large displacement, which is important for toughness of bone. Furthermore, the deformation behavior of collagen not only depends on the presence or absence of HAP and direction of pulling, but also on the type of mineral surface in the proximity. The collagen pulled parallel to $(10\,\bar{1}\,0)$ and (0001) showed characteristically different types of load-displacement response. This has its roots in different deformation mechanisms, which are indicated by the distinct shapes of load-displacement curves.

In conclusion, the deformation response of collagen is substantially influenced by mineral proximity. In addition, the direction and orientation of the mineral-collagen interaction has significant influence on mechanics of the collagen. These orientation dependent properties of collagen are very important to consider for proper modeling of bone.

4.6. Acknowledgements

The computational resources are provided by National Center for Supercomputing Applications (NCSA) through Teragrid, and Center for High Performance Computing (CHPC) at NDSU. Author SMP would like to acknowledge support from North Dakota State University (NDSU) Presidential Fellowship. Financial support from ND EPSCoR is also acknowledged.

4.7. References

1. Currey, J.D., Zioupos, P., Davies, P. & Casino, A. Mechanical properties of nacre and highly mineralized bone. *Proceedings. Biological sciences / The Royal Society* **268**, 107-11 (2001).
2. Fisher, L.W. & Termine, J.D. Noncollagenous proteins influencing the local mechanisms of calcification. *Clinical Orthopaedics and Related Research* **200**, 362-85 (1985).
3. Dorozhkin, S.V. & Epple, M. Biological and medical significance of calcium phosphates. *Angewandte Chemie, International Edition* **41**, 3130-3146 (2002).
4. Eastoe, J.E. & Eastoe, B. Organic constituents of mammalian compact bone. *Biochemical Journal* **57**, 453-9 (1954).
5. Olszta, M.J., Odom, D.J., Douglas, E.P. & Gower, L.B. A New Paradigm for Biomineral Formation: Mineralization via an Amorphous Liquid-Phase Precursor. *Connective Tissue Research* **44**, 326-334 (2003).
6. Currey, J.D. Biomechanics of mineralized skeletons. in *Skeletal Biomineralization :Patterns, processes, and evolutionary trends*, Vol. 1 (ed. Carter, J.G.) 11 (Van Nostrand, New York, 1990).
7. Cowin, S.C. The anisotropic elastic constants of cancellous bone. Vol. 198-1 (eds Katsube, N., Soboyejo, W.O. & Sacks, M.) 231-253 (2001).
8. Cowin, S.C. Bone poroelasticity. *Journal of Biomechanics* **32**, 217-238 (1999).
9. Cowin, S.C. The significance of bone microstructure in mechanotransduction. Vol. 40 S105-S109 (2007).

10. Cowin, S.C. & He, Q.C. Tensile and compressive stress yield criteria for cancellous bone. *Journal of Biomechanics* **38**, 141-144 (2005).

11. Zhang, D.J., Weinbaum, S. & Cowin, S.C. On the calculation of bone pore water pressure due to mechanical loading. *International Journal of Solids and Structures* **35**, 4981-4997 (1998).

12. Lakes, R.S., Katz, J.L. & Sternstein, S.S. Biaxial stress relaxation and dynamic properties of human cortical bone. *Journal of Bone and Joint Surgery-American Volume* **A 57**, 578-578 (1975).

13. Katz, J.L., Lakes, R.S. & Sternstein, S.S. Shear viscoelastic response in human and bovine cortical bone. *Journal of Bone and Joint Surgery-American Volume* **A 57**, 578-578 (1975).

14. Lakes, R., Yoon, H.S. & Katz, J.L. Slow compressional wave-propagation in wet human and bovine cortical bone. *Science* **220**, 513-515 (1983).

15. Lakes, R., Yoon, H.S. & Katz, J.L. Ultrasonic wave-propagation and attenuation in wet bone. *Journal of Biomedical Engineering* **8**, 143-148 (1986).

16. Lakes, R.S., Katz, J.L. & Sternstein, S.S. Viscoelastic properties of wet cortical bone .1. Torsional and biaxial studies. *Journal of Biomechanics* **12**, 657-& (1979).

17. Lakes, R.S. & Katz, J.L. Viscoelastic properties of wet cortical bone .2. Relaxation mechanisms. *Journal of Biomechanics* **12**, 679-687 (1979).

18. Lakes, R.S. & Katz, J.L. Viscoelastic properties of wet cortical bone .3. Nonlinear constitutive equation. *Journal of Biomechanics* **12**, 689-698 (1979).

19. Termine, J.D. & G, R.P. Bone matrix proteins and the mineralization process. in *Primer on the Metabolic Bone Diseases and Disorders of Mineral Metabolism*

(ed. Favus, M.J.) (The American Society for Bone and Mineral Research, Lippincott Williams & Wilkins, 1996).

20. Fratzl, P. & Weinkamer, R. Nature's hierarchical materials. *Progress in Materials Science* **52**, 1263-1334 (2007).

21. Weiner, S. & Wagner, H.D. The material bone: structure-mechanical function relations. *Annual Review of Materials Science* **28**, 271-298 (1998).

22. Landis, W.J., Song, M.J., Leith, A., McEwen, L. & McEwen, B.F. Mineral and organic matrix interaction in normally calcifying tendon visualized in three dimensions by high-voltage electron microscopic tomography and graphic image reconstruction. *Journal of structural biology* **110**, 39-54 (1993).

23. Hodge, A.J. & Petruska, J.A. Recent studies with the electron microscope on ordered aggregates of the tropocollagen molecule. 289-300 (1963).

24. Schmidt, W.J. Uber die Kristallorientierung im Zahnschmelz. *Naturwissenschaften* **24**, 361 (1936).

25. Landis, W.J. et al. Mineralization of collagen may occur on fibril surfaces: evidence from conventional and high-voltage electron microscopy and three-dimensional imaging. *Journal of Structural Biology* **117**, 24-35 (1996).

26. Moradianoldak, J., Weiner, S., Addadi, L., Landis, W.J. & Traub, W. Electron imaging and diffraction study of individual crystals of bone, mineralized tendon and synthetic carbonate apatite. *Connective Tissue Research* **25**, 219-228 (1991).

27. Nylen, M.U., Scott, D.B. & Mosley, V.M. Mineralization of turkey leg tendon. II. Collagen-mineral relations revealed by electron and x-ray microscopy. **No. 64**, 129-42 (1960).

28. Landis, W.J. The strength of a calcified tissue depends in part on the molecular structure and organization of its constituent mineral crystals in their organic matrix. *Bone (New York, NY, United States)* **16**, 533-44 (1995).

29. Traub, W., Arad, T. & Weiner, S. Three-dimensional ordered distribution of crystals in turkey tendon collagen fibers. *Proceedings of the National Academy of Sciences of the United States of America* **86**, 9822-6 (1989).

30. Arsenault, A.L. Image-analysis of collagen-associated mineral distribution in cryogenically prepared turkey leg tendons. *Calcified Tissue International* **48**, 56-62 (1991).

31. Rubin, M.A., Rubin, J. & Jasiuk, W. SEM and TEM study of the hierarchical structure of C57BL/6J and C3H/HeJ mice trabecular bone. *Bone* **35**, 11-20 (2004).

32. Fritsch, A. & Hellmich, C. 'Universal' microstructural patterns in cortical and trabecular, extracellular and extravascular bone materials: micromechanics-based prediction of anisotropic elasticity. *Journal of Theoretical Biology* **244**, 597-620 (2007).

33. Hellmich, C., Celundova, D. & Ulm, F.J. Multiporoelasticity of Hierarchically Structured Materials: Micromechanical Foundations and Application to Bone. *Journal of Engineering Mechanics-Asce* **135**, 382-394 (2009).

34. Ghanbari, J. & Naghdabadi, R. Nonlinear hierarchical multiscale modeling of cortical bone considering its nanoscale microstructure. *Journal of Biomechanics* **42**, 1560-1565 (2009).

35. Ciarletta, P., Micera, S., Accoto, D. & Dario, P. A novel microstructural approach in tendon viscoelastic modelling at the fibrillar level. *Journal of Biomechanics* **39**, 2034-2042 (2006).

36. Gautieri, A., Vesentini, S., Montevecchi, F.M. & Redaelli, A. Mechanical properties of physiological and pathological models of collagen peptides investigated via steered molecular dynamics simulations. *Journal of Biomechanics* **41**, 3073-3077 (2008).

37. Buehler, M.J. Nanomechanics of collagen fibrils under varying cross-link densities: Atomistic and continuum studies. *Journal of the Mechanical Behavior of Biomedical Materials* **1**, 59-67 (2008).

38. Buehler, M.J. Nature designs tough collagen: Explaining the nanostructure of collagen fibrils. *Proceedings of the National Academy of Sciences of the United States of America* **103**, 12285-12290 (2006).

39. Dubey, D.K. & Tomar, V. The effect of tensile and compressive loading on the hierarchical strength of idealized tropocollagen-hydroxyapatite biomaterials as a function of the chemical environment. *Journal of Physics-Condensed Matter* **21**(2009).

40. Dubey, D.K. & Tomar, V. Microstructure dependent dynamic fracture analyses of trabecular bone based on nascent bone atomistic simulations. *Mechanics Research Communications* **35**, 24-31 (2008).

41. Dubey, D.K. & Tomar, V. Role of the nanoscale interfacial arrangement in mechanical strength of tropocollagen-hydroxyapatite-based hard biomaterials. *Acta Biomaterialia* **5**, 2704-2716 (2009).

42. Dubey, D.K. & Tomar, V. Role of hydroxyapatite crystal shape in nanoscale mechanical behavior of model tropocollagen-hydroxyapatite hard biomaterials. *Materials Science and Engineering: C* **29**, 2133-2140 (2009).

43. Ghosh, P., Katti, D.R. & Katti, K.S. Mineral Proximity Influences Mechanical Response of Proteins in Biological Mineral-Protein Hybrid Systems. *Biomacromolecules* **8**, 851-856 (2007).

44. Ghosh, P., Katti, D.R. & Katti, K.S. Mineral and protein-bound water and latching action control mechanical behavior at protein-mineral interfaces in biological nanocomposites. *Journal of Nanomaterials*, 8 (2008).

45. Ghosh, P., Katti, D.R. & Katti, K.S. Impact of beta-sheet conformations on the mechanical response of protein in biocomposites. *Materials and Manufacturing Processes* **21**, 676-682 (2006).

46. Bhowmik, R., Katti, K.S. & Katti, D.R. Influence of mineral on the load deformation behavior of polymer in hydroxyapatite-polyacrylic acid nanocomposite biomaterials: A steered molecular dynamics study. *Journal of Nanoscience and Nanotechnology* **8**, 2075-2084 (2008).

47. Katti, D.R., Ghosh, P., Schmidt, S. & Katti, K.S. Mechanical Properties of the Sodium Montmorillonite Interlayer Intercalated with Amino Acids. *Biomacromolecules* **6**, 3276-3282 (2005).

48. Bhowmik, R., Katti, K.S. & Katti, D.R. Mechanisms of Load-Deformation Behavior of Molecular Collagen in Hydroxyapatite-Tropocollagen Molecular System: Steered Molecular Dynamics Study. *Journal of Engineering Mechanics-Asce* **135**, 413-421 (2009).

49. Bhowmik, R., Katti, K.S., Venna, D. & Katti, D.R. Probing molecular interactions in bone biomaterials: Through molecular dynamics and Fourier transform infrared spectroscopy. *Materials Science & Engineering C-Biomimetic and Supramolecular Systems* **27**, 352-371 (2007).

50. Bhowmik, R., Katti, K.S. & Katti, D.R. Mechanics of molecular collagen is influenced by hydroxyapatite in natural bone. *Journal of Materials Science* **42**, 8795-8803 (2007).

51. Sasaki, N. et al. Atomic force microscopic studies on the structure of bovine femoral cortical bone at the collagen fibril-mineral level. *Journal of Materials Science-Materials in Medicine* **13**, 333-337 (2002).

52. Kale, L. et al. NAMD2: Greater Scalability for Parallel Molecular Dynamics. *Journal of Computational Physics* **151**, 283-312 (1999).

53. Brooks, B.R. et al. CHARMM: a program for macromolecular energy, minimization, and dynamics calculations. *Journal of Computational Chemistry* **4**, 187-217 (1983).

54. Humphrey, W., Dalke, A. & Schulten, K. VDM: visual molecular dynamics. *Journal of Molecular Graphics* **14**, 33-8, plates, 27-28 (1996).

55. Beck, K. & Brodsky, B. Supercoiled protein motifs: the collagen triple-helix and the alpha -helical coiled coil. *Journal of Structural Biology* **122**, 17-29 (1998).

56. Brodsky, B. & Persikov, A.V. Molecular structure of the collagen triple helix. in *Fibrous Proteins: Coiled-Coils, Collagen and Elastomers*, Vol. 70 301-+ (2005).

57. Berisio, R., Vitagliano, L., Mazzarella, L. & Zagari, A. Crystal structure of the collagen triple helix model [(Pro-Pro-Gly)10]3. *Protein Science* **11**, 262-270 (2002).

58. Malone, J.P., George, A. & Veis, A. Type I collagen N-telopeptides adopt an ordered structure when docked to their helix receptor during fibrillogenesis. *Proteins-Structure Function and Genetics* **54**, 206-215 (2004).

59. Jones, E.Y. & Miller, A. Structural models for the N- and C-terminal telopeptide regions of interstitial collagens. *Biopolymers* **26**, 463-80 (1987).

60. Otter, A., Kotovych, G. & Scott, P.G. Solution conformation of the type I collagen alpha-1 chain N-telopeptide studied by 1H NMR spectroscopy. *Biochemistry* **28**, 8003-10 (1989).

61. Sudarsanan, K. & Young, R.A. Significant precision in crystal structural details: Holly Springs hydroxyapatite. *Acta Crystallographica, Section B Structural Crystallography and Crystal Chemistry* **25**, 1534-43 (1969).

62. Bertaut, F. The electrostatic term of the surface energy. **246**, 3447-50 (1958).

63. Tasker, P.W. The stability of ionic crystal surfaces. *Journal of Physics C Solid State Physics* **12**, 4977-84 (1979).

64. Feller, S.E., Zhang, Y., Pastor, R.W. & Brooks, B.R. Constant pressure molecular dynamics simulation: the Langevin piston method. *Journal of Chemical Physics* **103**, 4613-21 (1995).

65. Martyna, G.J., Tobias, D.J. & Klein, M.L. Constant pressure molecular dynamics algorithms. *Journal of Chemical Physics* **101**, 4177-89 (1994).

66. Balsera, M., Stepaniants, S., Izrailev, S., Oono, Y. & Schulten, K. Reconstructing potential energy functions from simulated force-induced unbinding processes. *Biophysical Journal* **73**, 1281-1287 (1997).

CHAPTER 5. STEERED MOLECULAR DYNAMICS STUDY OF MECHANICAL RESPONSE OF FULL LENGTH AND SHORT COLLAGEN MOLECULES

In this chapter the steered molecular dynamics study of full length and short collagen are presented. The role of collagen length in the deformation behavior, as well as the similarities and differences in the mechanics of short and full length collagen are discussed in this chapter. The contents of the chapter have been published in Pradhan, S. M., Katti, D. R., and Katti, K. S. (2011). "Steered Molecular Dynamics Study of Mechanical Response of Full Length and Short Collagen Molecules." Journal of Nanomechanics and Micromechanics, 1(3), 104-110.

5.1. Introduction

Collagen is the most abundant fibrous protein that makes up more than quarter of the total proteins in human body, and forms an integral part of various connective tissues. At least 27 different types of collagen (i.e. type I to XXVII) are found in vertebrates [1]. Of these collagen types, the type I is the most abundant and found in tissues such as bone, skin, tendon, and cornea. Collagen provides structural integrity to these tissues. In bone, collagen molecules are packed in a staggered fashion and organized into hierarchical structures called mineralized fibrils, which are the basic building blocks of bone material [2]. Bone is primarily composed of three components: mineral, organic, and water comprising about 65%, 25%, and 10% respectively by weight [3-7] and 33-43%, 32-44%, and 15-25% respectively by volume[7, 8]. The collagen constitutes major fraction of total bone protein that range from 85-95% [9].

Collagen is a long rod-like molecule composed of three polypeptide chains, known as α chains, wound together into a right-handed triple helical structure and stabilized by interchain hydrogen bonds [10]. The individual polypeptide chains are coiled structures of left-hand helix. The polypeptide chains are composed of a repeating sequence of three amino acids $(Glycine\text{-}X\text{-}Y)_n$, where X and Y positions are mostly occupied by Proline and Hydroxyproline. The repetition of Glycine in every third residue is a strict requirement dictated by close packing of polypeptide chains [10, 11]. The collagen molecules consists of over 1000 amino acids along each polypeptide chains [12] and are about 300 nm in length and 1.23 nm in diameter [13].

There are number of studies carried out to investigate mechanical properties of various hierarchical structures of bone. The various methods that are used include micromechanical approaches [14, 14-18] and molecular mechanics [19-23]. The deformation behavior of collagen has important role on the mechanical properties of bone due to its hierarchical structure. Understating the deformation mechanism of collagen is critical to understanding mechanical properties of fibril, which is the building block of bone. In our previous work, [22] and Katti et. al;[24] we have extensively studied deformation behavior of collagen in the proximity of mineral using steered molecular dynamics (SMD). Several SMD studies are also been carried out to evaluate mechanical properties of collagen[25-28]. In additions to these SMD studies, the coarse grained modeling of collagen molecule has been recently carried out to simulate 300 nm long collagen molecule [29].

The current molecular dynamics studies on collagen utilize a short segment of collagen about 8.5 nm in length, which is very short compared to the full length of collagen molecule (~300nm). The use of short segment of collagen may not be able to

completely capture the deformation mechanism and mechanical response exhibited by the collagen molecule of full length. Hence, in this study we have modeled a collagen of 300nm length using steered molecular dynamics in order to investigate the role of collagen length on its deformation behavior. From this study we are able to evaluate similarities and differences in mechanisms and conformational changes when the short and full length collagen (referred to in this paper as long collagen) molecules are deformed under varying loading conditions.

5.2. Model Building and Simulations Procedure

Glycine-Proline-Proline (GPP) model collagen is used in our simulations. GPP is a commonly used model of collagen and has been used by number of researchers including docking study of type-1 collagen N-telopeptide with collagen during fibrillogenesis (Malone et al 2003). There are many types of collagen and GPP would be a good model for modeling the mechanics of triple helix collagen molecule in general. The authors have also used GPP model of collagen extensively in their previous studies, which include their studies on deformation behavior of collagen in the mineral proximity [28, 30, 31]. The amino acid sequence for different collagen types would be different and would affect mechanical properties [32] and stability [33] of collagen molecule.

The solvated collagen models of two different lengths of collagen are built, which will be referred to as short and long collagen model. The length of long collagen model is about 300 nm, which is of an order of the length of actual collagen molecule. The short collagen molecule was directly obtained from Protein Data Bank (PDB ID: 1k6f). The short collagen molecule consists of 29 residues in each of the individual chains that constitute the triple helix and measures about 85 Å in length. The short

collagen molecule is solvated with 1317 water molecules. The long collagen molecule is constructed by replicating short molecules along the longitudinal axis. The long collagen used in our studies consists of 1014 residues along each of the polypeptide chains and is about 2900 Å in length. The long collagen molecule is solvated with a total of 19417 water molecules distributed along its length. TIP3P model of water was used in all our simulations[34].

Molecular dynamics (MD) and steered molecular dynamics (SMD) simulations were carried out using NAMD [35] simulation package developed by Theoretical and Computational Biophysics Group (TCB) at the University of Illinois at Urbana-Champaign. CHARMM [36] force field parameters for proteins were used for all our simulations, whereas for solvent TIP3P model of water was used. Minimization was carried out using conjugate gradient method. The temperature and pressure were increased to 300 K and 1.01 bar respectively in steps. Temperature was increased in steps of 100 K and pressure was increased in steps of 0.25 bar. Langevin dynamics was used to control temperature and Nose-Hoover piston method was used to control pressure [37, 38]. All molecular dynamics simulations were carried out using isothermal-isobaric (NPT) ensemble using periodic boundary conditions. Particle Mesh Ewald (PME) method was used for calculation of electrostatic interaction energy [35]. The cutoff distance of 10 Å was used for all non-bonded energy calculations.

Steered molecular dynamics simulations were carried out by pulling the center of mass of collagen molecules at wide range of velocities using a harmonic spring of varying spring constants. The effect of spring constant on mechanical properties of tropocollagen molecules have been investigated by Lorenzo and Caffarena [26]. It was

shown that the stiffness of spring needs to be sufficiently high compared to the stiffness of molecule, and that the elastic modulus of short collagen converges above the spring constant of 3.6 kcal/mol/Å^2. Furthermore, it was also shown that the uncertainty in collected data increases if the chosen spring stiffness is very large compared to stiffness of molecule. Based on this finding, we have used lower values of spring constants for long collagen compared to short collagen because it has a significantly lower stiffness compared to short collagen. In our simulations, the short collagen is pulled using spring constants (k) of 1, 4, and 9 kcal/mol/Å^2 respectively, while the long collagen is pulled using spring constants of 0.1 and 1 kcal/mol/Å^2 respectively.

Steered molecular dynamics (SMD) was used to study deformation behavior of long and short collagen using wide range of pulling rates. The collagen molecules were pulled with velocities corresponding to strain rates of 0.0003 ps^{-1}, 0.003 ps^{-1}, 0.006 ps^{-1}, 0.009 ps^{-1}, and 0.003 ps^{-1} respectively. The velocities corresponding to these pulling rates are 0.026 Å/ps, 0.25 Å/ps, 0.5 Å/ps, and 1.0 Å/ps respectively for the short collagen; and 0.975 Å/ps, 9.375 Å/ps, 18.75 Å/ps, 28.125 Å/ps, and 37.5 Å/ps for the full-length collagen. When pulling molecules of different lengths, the utilization of same strain rates ensures that their loading conditions are similar, thereby allowing us to carry out reasonable comparison of their deformation response. It has been reported that the mechanical properties of collagen is independent of loading rate (i.e. strain rate) at lower rates of pulling [39]. Based on this result, the effect of loading rate on mechanical properties appears to be minimal at strain rates as low as 0.0003 ps^{-1}. Hence, we have limited the lowest strain rate for pulling long collagen to 0.0003 ps^{-1} because the computational cost of pulling collagen at very low strain rates encountered in experimental studies is

enormous. The load-displacement response of short collagen molecule in different orientations in the proximity of different surfaces of hydroxyapatite have been described in detail in our previous work [22, 24, 28].

5.3. Results and Discussion

The snapshots of short and long collagen molecules equilibrated at room temperature and pressure (i.e. 300 K and 1.01 bar) before carrying out SMD simulation are shown in figure 5.1(a) and (b). The short molecule appears to be slightly bent, similar to previously reported in the literature [24, 40]. The snapshot for long collagen molecule as shown in figure 5.1 shows an interesting feature consisting of series of helical turns along the length. The close visual observations of these helical turns reveal to us that the helices which are well defined are mostly left handed, which are opposite in sense compared to the right handed triple helix. This is a first time such a structural conformation of collagen has been reported to our knowledge. One of the reasons this conformation was not observed in previous studies using short collagen is because the length of short collagen is of an order of the pitch of collagen triple helix (~8.5 nm) and not long-enough for the formation of a such structure. The presence of this structure may have important implications on the mechanical behavior of collagen.

The deformation response of short and long collagen molecule under different pulling rates are shown in figure 5.2. The load-displacement plots show an initial nonlinear region of low stiffness followed by a fairly linear region of very high stiffness. The linear stiff region of load displacement curve corresponds to stretching of collagen backbone. In case of short collagen, a larger spread in load-displacement curves for different rates of pulling are seen at small displacement compared to large displacement

regime. However, in case of long collagen the spread in load-displacement curves is seen throughout the displacement range, the spread increasing at larger displacement. The displacement (of center of mass) has been normalized using its original length (i.e. the ratio of displacement to original length of collagen expressed in percentage) to facilitate comparison of deformation response between short and long collagen molecules; we refer to this ratio as reduced-displacement. In the initial region of load displacement curve, we observe straightening of a slightly bent short collagen molecule under applied tensile forces. In case of long collagen, the coils along the length of collagen stretch when the collagen is extended. The visual observation of long collagen during pulling shows that these coiled features can be quite resilient, and may exist up to a significant strain of about 15-25%. When collagen is stretched the straining is accompanied by a conformational change and the consequent rotation of its end. The observed rotation of the end of collagen upon pulling is the combined response of the straightening of coiled structure and the unwinding of the triple helix.

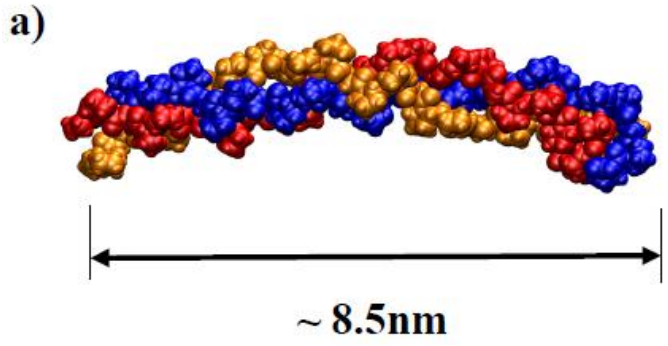

Figure 5.1. Snapshot of short and full-length collagen at the beginning of the steered molecular dynamics simulation: (a) short collagen; (b) full-length collagen (partial magnified view).

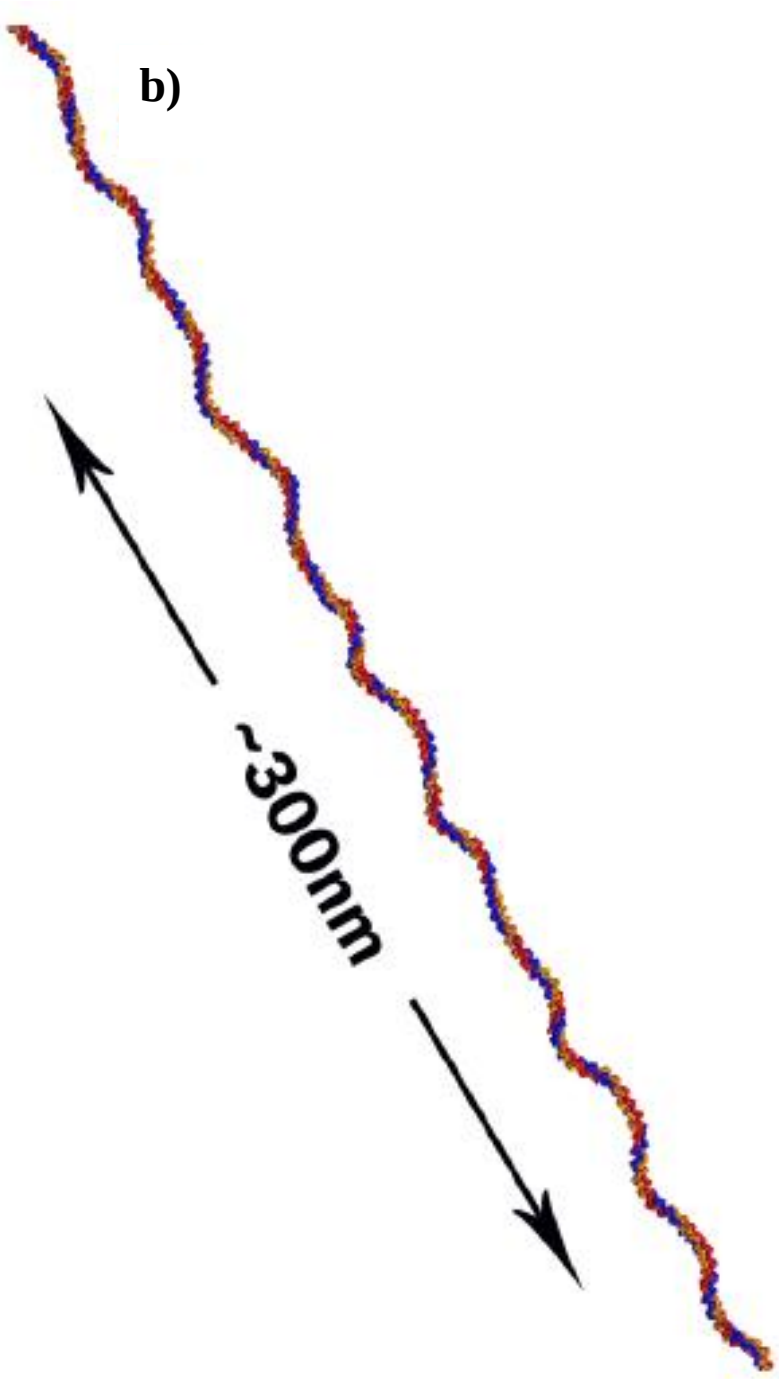

Figure 5.1. Snapshot of short and full-length collagen at the beginning of the steered molecular dynamics simulation: (a) short collagen; (b) full-length collagen (partial magnified view). (Continued)

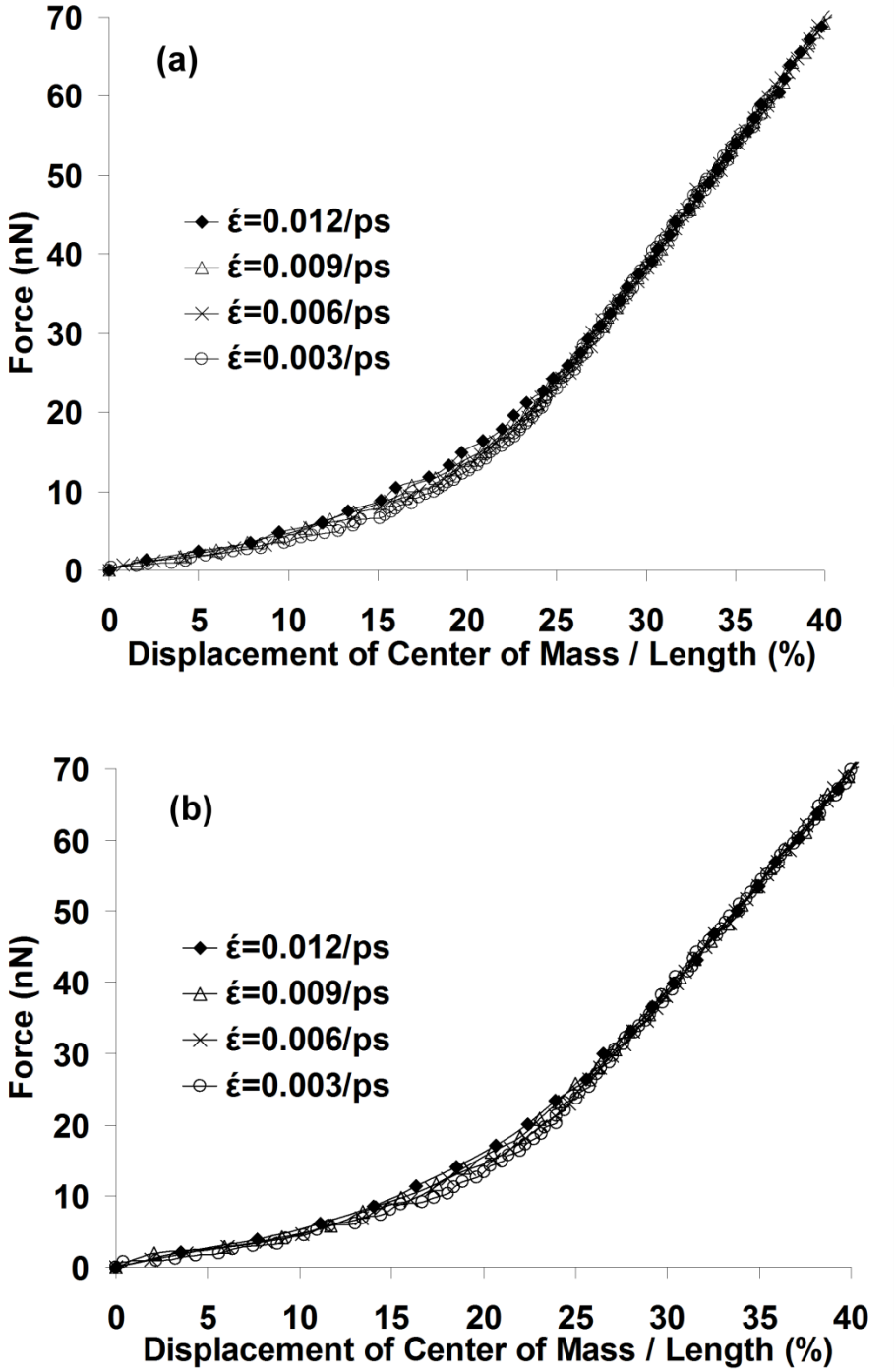

Figure 5.2. Force-displacement response of short and long collagen using different spring constants: (a) short (k = 4.0 kcal/mol/Å^2), (b) short (k = 9.0 kcal/mol/Å2), (c) long (k = 0.1 kcal/mol/Å^2), and (d) long (k = l.0 kcal/mol/Å^2).

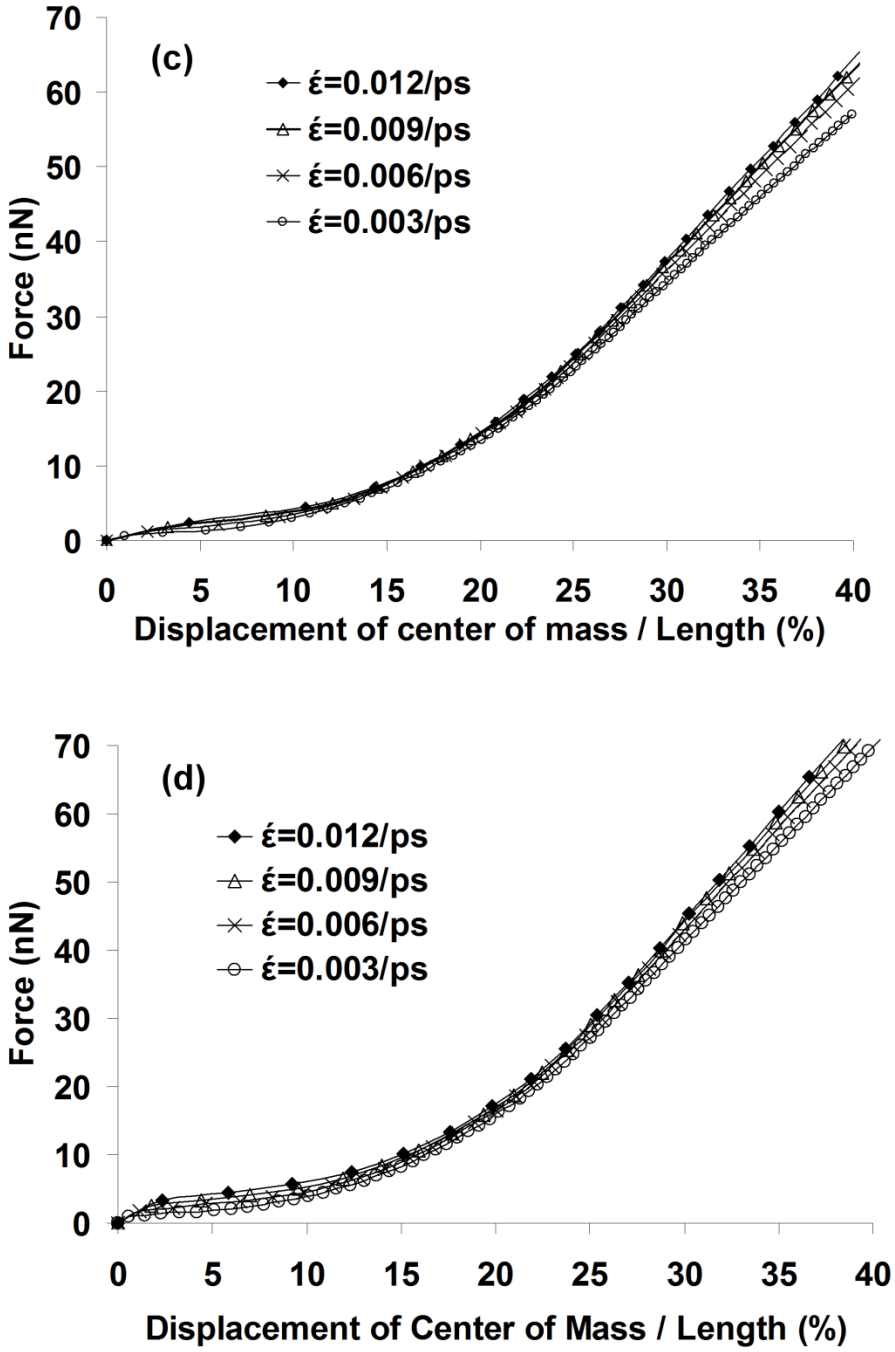

Figure 5.2. Force-displacement response of short and long collagen using different spring constants: (a) short (k = 4.0 kcal/mol/Å2), (b) short (k = 9.0 kcal/mol/Å2), (c) long (k = 0.1 kcal/mol/Å2), and (d) long (k = l.0 kcal/mol/Å2). (Continued)

Figure 5.3 shows load-deformation response of short and long collagen for up to 7% reduced displacement when pulled using different pulling rates and spring constants. When the short and long collagen molecules are pulled at different rates, they display strain rate effects (i.e. at higher strain rates the response of molecule is stiffer). This behavior has been reported in number of studies related to collagen and other biomolecules [28, 41, 42]. The consequence of this effect is less prominent at higher displacement (Fig. 5.2), while it can quite significant at smaller elongations as shown in figure 5.3. In addition to the rate of pulling, the stiffness of the spring used to pull collagen also has an important effect on the mechanical response of collagen. This can be observed in figure 5.4, where comparison of load-displacement response between different spring constants is shown for short and long collagen structures. As shown in the figure, in our simulations collagen appears to display stiffer response when pulled with a spring of higher spring constant; though to a certain degree, the result using higher spring constant is subject to greater uncertainty in collected data [26], which is inherent to SMD. As for short collagen, the load-displacement response for spring constant of 9 kcal/mol/Å^2 is somewhat stiffer than for 4 kcal/mol/Å^2. This is seen in figures 5.2, 5.3, and 5.4. In case of long collagen, the response of molecule is found to be quite stiff, at spring constant of 1 kcal/mol/Å^2 compared to 0.1 kcal/mol/Å^2 at both small and large displacements (Figs. 5.2, 5.3, and 5.4). This difference in stiffness is quite significant for small displacement in case of long collagen (Fig. 5.3).

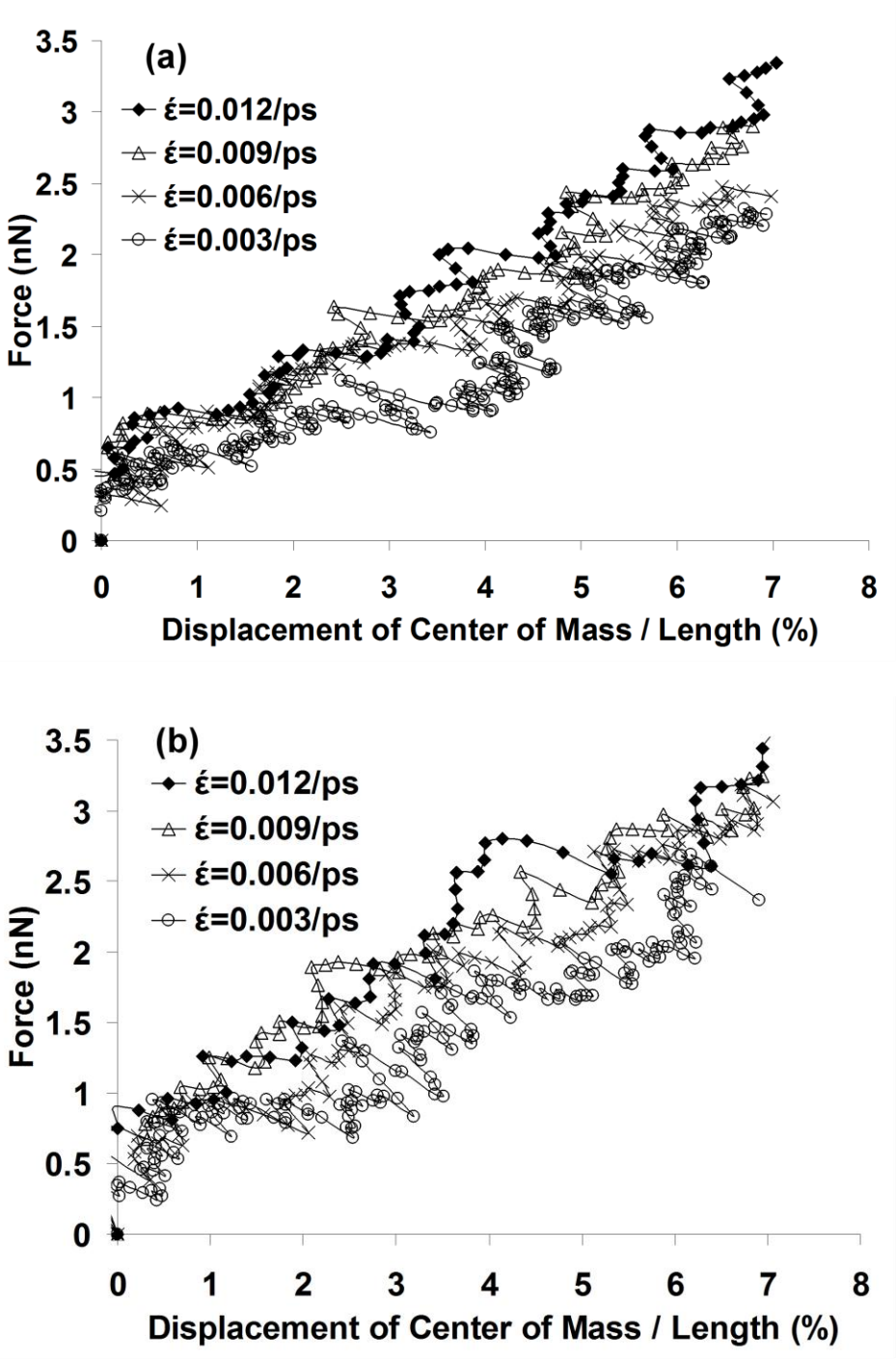

Figure 5.3. Force-displacement of response of short and long collagen in the elastic range using different spring constants: (a) short (k = 4.0 kcal/mol/Å^2), (b) short (k = 9.0 kcal/mol/Å^2), (c) long (k = 0.1 kcal/mol/Å^2), and (d) long (k = 1.0 kcal/mol/Å^2).

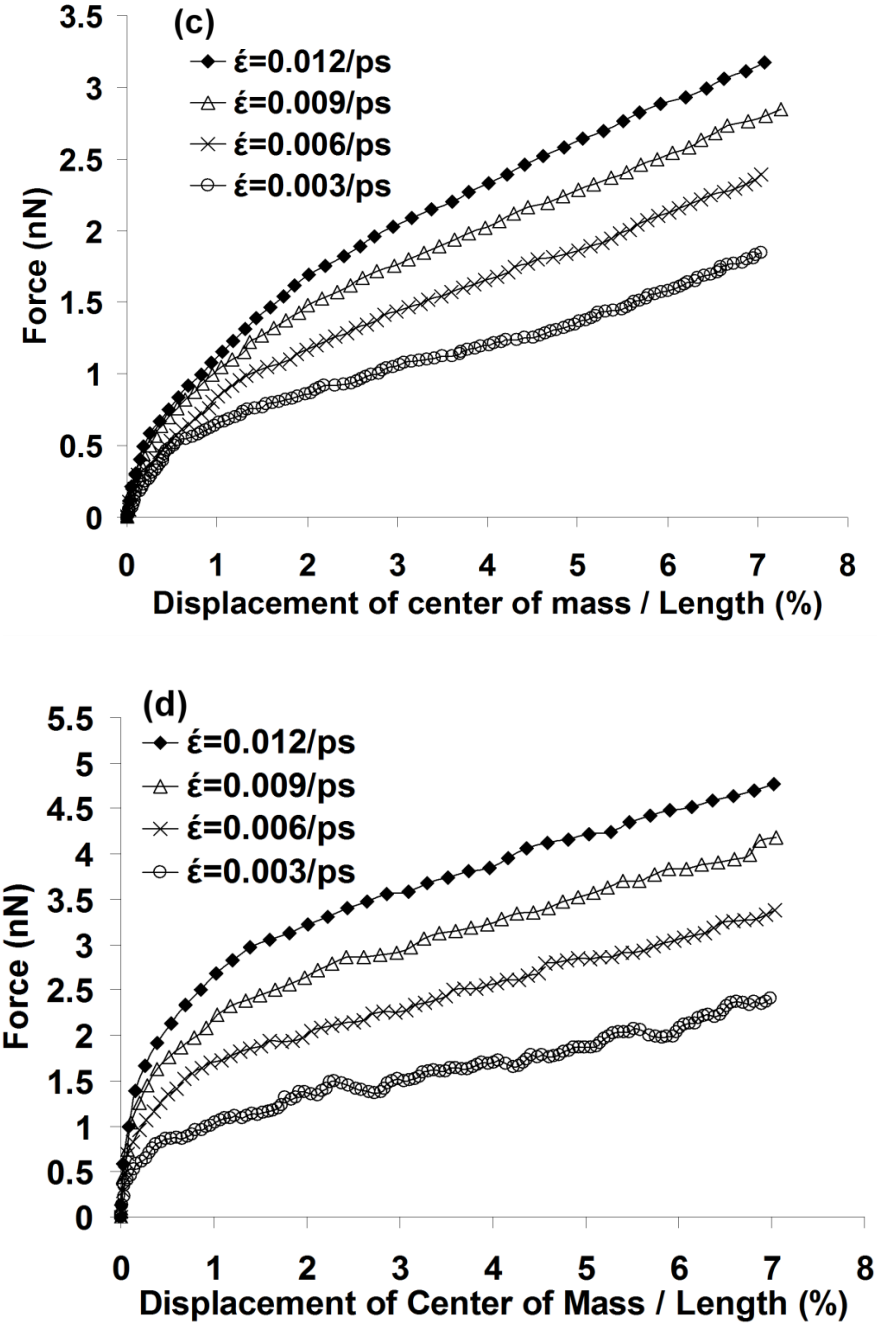

Figure 5.3. Force-displacement of response of short and long collagen in the elastic range using different spring constants: (a) short (k = 4.0 kcal/mol/Å^2), (b) short (k = 9.0 kcal/mol/Å^2), (c) long (k = 0.1 kcal/mol/Å^2), and (d) long (k = 1.0 kcal/mol/Å^2). (Continued)

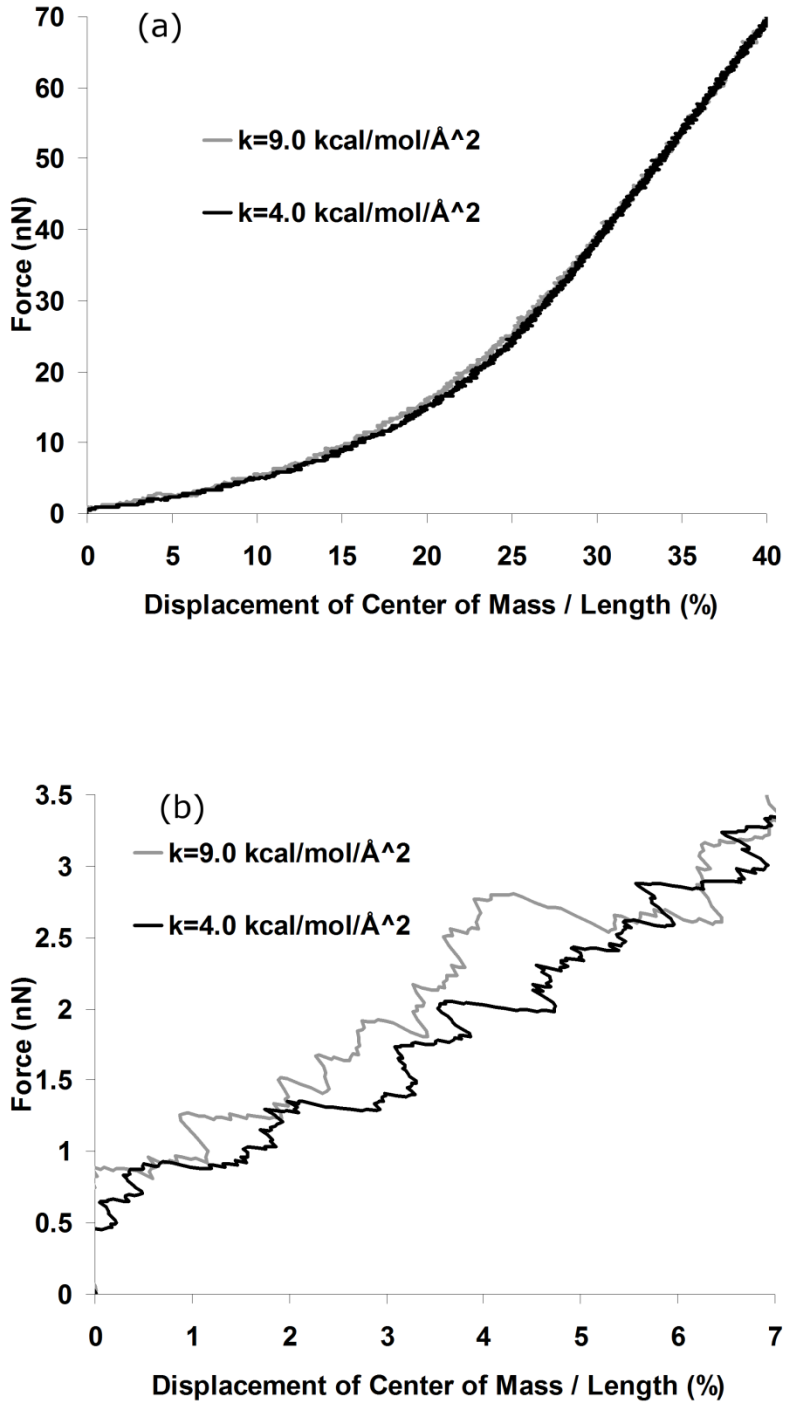

Figure 5.4. Comparison of force-displacement response using different spring constants for (a) short collagen, (b) short collagen in small displacement range, (c) long collagen, (d) long collagen in small displacement range.

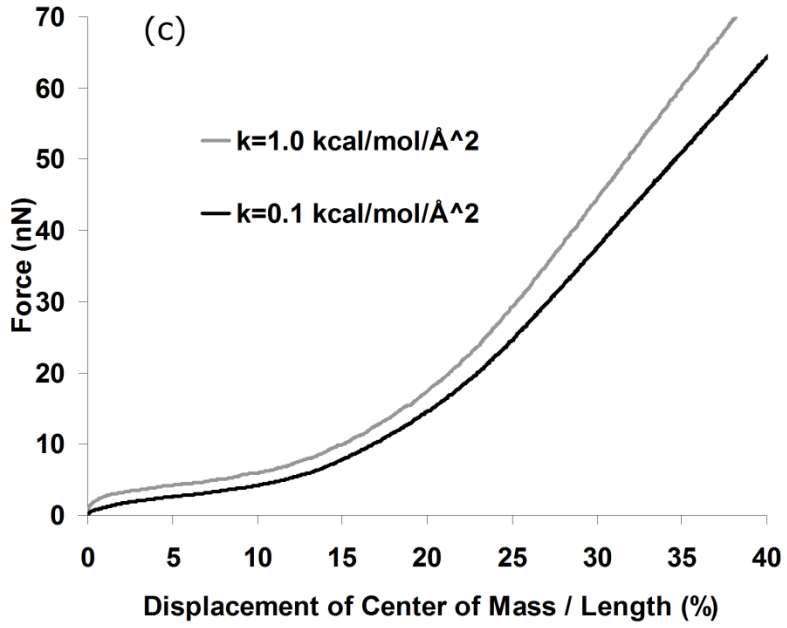

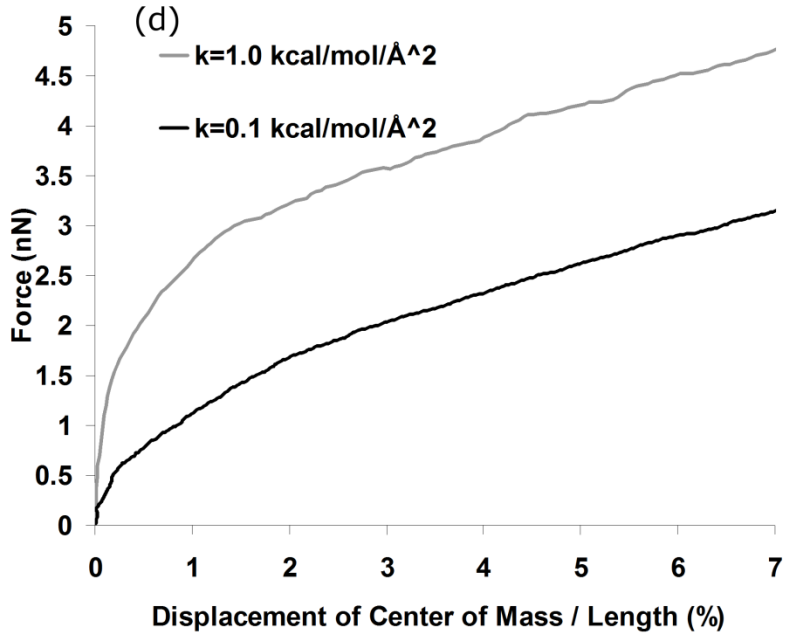

Figure 5.4. Comparison of force-displacement response using different spring constants for (a) short collagen, (b) short collagen in small displacement range, (c) long collagen, (d) long collagen in small displacement range. (Continued)

One of the interesting features that are apparent when comparing load-displacement plot of short and long collagen are the saw tooth-like appearance of curve in case of short collagen (Fig. 5.3). The response of short collagen is seen to have large fluctuations in force and displacement, which is readily observed in the small displacement regime. The mechanical response of long collagen is seen to not have these features and minimal fluctuations in force and displacement are observed. The large fluctuations in force and displacement observed in case of short collagen are possibly the result of the short length and the very large amplitude fluctuations in number of hydrogen bonds during breaking and forming, which will be discussed in the subsequent paragraphs. The elastic modulus of short and long collagen molecules evaluated from SMD simulations are shown in tables 5.1 and 5.2. The table contains elastic modulus of collagen pulled using springs of different spring constants and various strain rates. Elastic modulus is calculated by using an approach similar to Lorenzo and Caffarena [26], where Young's modulus, $Y = k_{collagen} \times L_0 / A$. In this equation L_0 is initial collagen length and A is the cross-sectional area. The cross-sectional area of 143.14 $Å^2$ was estimated by considering the cylinder bounding Van der Waals surface of molecule. The stiffness of collagen, $k_{collagen}$ is estimated by carrying out least square linear fit of load-displacement plot up to 7% reduced displacement. The straight line is fitted such that it passes through the origin. Observation of the load-displacement response of collagen shows a region of very high stiffness within the 1% reduced displacement (Fig. 5.3), followed by a less stiff region. Hence, the tangent modulus computed in this low strain region (<1% reduced displacement) would be very large, while at higher strains (1-7% reduced displacement) it would be relatively small. Therefore a linear fit of an entire curve to obtain reasonable

and average estimate of an elastic modulus is used. From table 5.1 it is observed that the elastic modulus is very much dependent on the rate of pulling and stiffness of spring used to pull collagen. The elastic modulus appears to increase with increasing rate of pulling as well as stiffness of spring. The elastic modulus of short collagen is lower at k = 1 kcal/mol/Å^2 compared to k = 4 kcal/mol/Å^2 and k = 9 kcal/mol/Å^2, as softer response is expected for smaller spring constant. For long collagen, the elastic modulus is relatively large at k = 1.0 kcal/mol/Å^2 compared to k = 0.1 kcal/mol/Å^2. The elastic modulus of short collagen is found to vary from 6.2 to 13.79 GPa depending on the choice of various strain rates and spring constants. As for long collagen the larger spread in elastic modulus values ranging from 4.5 to 22.15 GPa were observed. At smaller pulling rates of 0.0003 /ps and 0.003/ps, the elastic modulus computed for short and long collagen structures are comparable. However, at larger pulling rates the modulus calculated for long collagen is significantly larger than computed using short collagen.

It is appropriate to use similar loading conditions when carrying out reasonable comparison between mechanical response of short and long collagen. In our case, we simulate equivalent loading conditions by using similar strain rate and relative spring constant (i.e. we define relative spring constant as the ratio of stiffness of spring to that of molecule). Hence, for comparison purpose we consider elastic modulus corresponding to k = 4.0 kcal/mol/Å^2 and k = 0.1 kcal/mol/Å^2 respectively for short and long collagen. The comparison of elastic modulus values for short and long collagen at different rates of pulling is shown in table 5.3 and figure 5.5. It is seen from the figure that for long collagen higher modulus is obtained at higher rates pulling, where as at lower rates of pulling, the modulus values are close.

Table 5.1. Elastic modulus of short collagen corresponding to various pulling rates and spring constants

έ (ps^{-1}) >>>	**0.0003**	**0.003**	**0.006**	**0.009**	**0.012**
k (kcal/mol/$Å^2$)	**E (GPa)**	**E (GPa)**	**E (GPa)**	**E (GPa)**	**E (GPa)**
1	-	8.36	7.92	9.9	9.59
4	6.2	8.46	10.17	11.63	12.46
9	6.5	10.02	12.27	13.54	13.79

Table 5.2. Elastic modulus of full length collagen corresponding to various pulling rates and spring constants

έ (ps^{-1}) >>>	**0.0003**	**0.003**	**0.006**	**0.009**	**0.012**
k (kcal/mol/$Å^2$)	**E (GPa)**	**E (GPa)**	**E (GPa)**	**E (GPa)**	**E (GPa)**
0.1	3.98	7.45	10.1	12.41	14.23
1	4.5	9.99	14.81	18.58	22.15

Table 5.3. Comparisons of elastic modulus of full length collagen (using k = 0.1 kcal/mol/$Å^2$) and short collagen (using k = 4.0 kcal/mol/$Å^2$)

έ (ps^{-1}) >>>	**0.0003**	**0.003**	**0.006**	**0.009**	**0.012**
	E (GPa)	**E (GPa)**	**E (Gpa)**	**E (GPa)**	**E (GPa)**
Long	3.98	7.45	10.1	12.41	14.23
Short	6.2	8.46	10.17	11.63	12.46

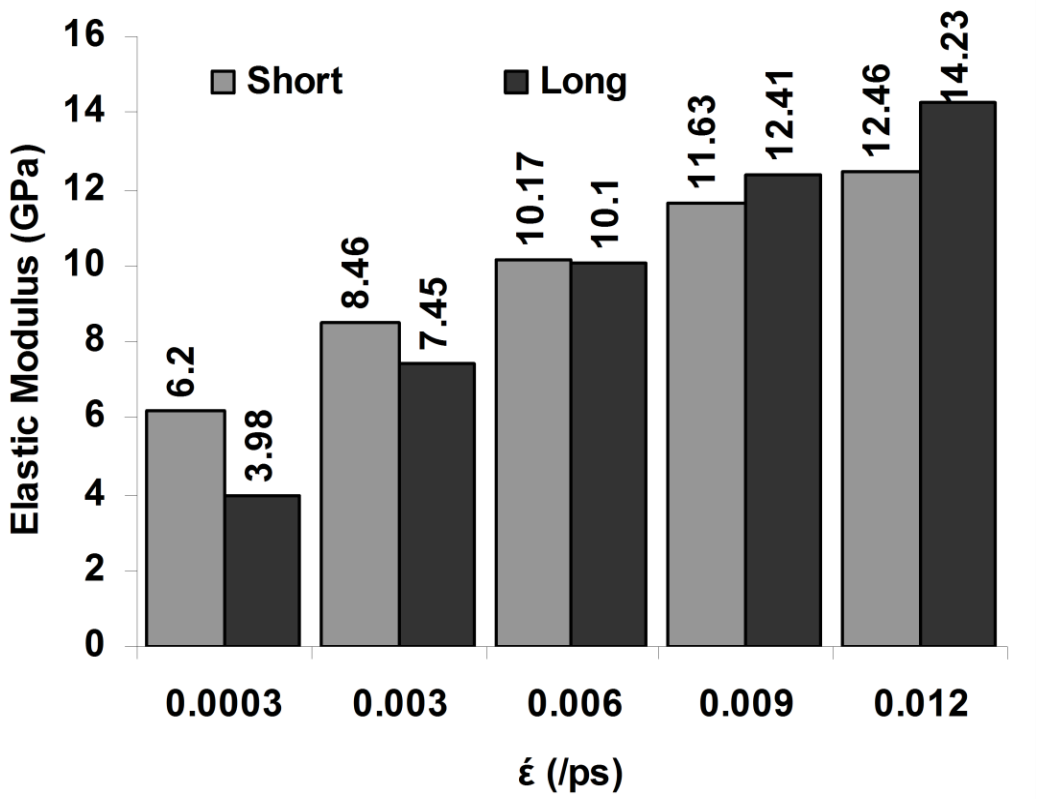

Figure 5.5. Comparison of elastic modulus for short and long collagen corresponding to spring constants k = 4.0 kcal/mol/Å^2 for short collagen and k = 0.1 kcal/mol/Å^2 for long collagen.

The load-displacement response of collagen shows a very stiff and relatively linear response at large displacement due to the stretching of the backbone (Fig. 5.2). The tangent modulus of collagen computed at large displacement is shown in table 5.4. The modulus of full-length collagen is seen to vary from 59.25 to 76.51 GPa, while in case of short collagen modulus values are very close to 65.5 GPa. In case of the full-length collagen the modulus is higher when stiffer spring and larger pulling rate are used but such variation is not seen in case of short collagen.

Table 5.4. Tangent modulus of short collagen and full length collagen at various pulling rates and spring constants

	k (kcal/mol/Å^2)				
	Long		**Short**		
Strain rate (/ps)	**0.1**	**1.0**	**1.0**	**4.0**	**9.0**
0.003	59.26	70.40	65.08	65.56	65.60
0.006	63.96	73.79	65.08	65.56	65.60
0.009	66.08	75.52	65.08	65.56	65.60
0.012	67.62	76.51	65.08	65.56	65.60

The hydrogen bonds between polypeptide chains of collagen are responsible for the integrity of the triple helical structure of collagen. Figure 5.6 shows the evolution in number of hydrogen bonds between polypeptide chains when the short and long collagen are pulled at different rates. For calculation of number of hydrogen bond, we have used a geometric criterion that requires donor-acceptor distance ≤ 3.5 Å and donor-hydrogen-acceptor angle $\leq 60^{\circ}$. The hydrogen bonds between chains of collagen molecule are strained during deformation of collagen, causing them to break and form again at various locations. As a result we observe a local fluctuation in number of hydrogen bonds between the chains during deformation of collagen as seen in figure 5.6. The amplitude of fluctuation of hydrogen bond is found to be larger in case of short collagen compared to long collagen. As we continue to stretch the collagen, the rate of breaking dominates the rate of formation of hydrogen bonds; since the hydrogen bond donor and acceptor groups on opposite chains face less favorable conditions for the formation of hydrogen bond as the triple helix is strained or water molecules interacting at these sites. However, interestingly in the case of long collagen, the formation of hydrogen bonds appear to dominate between 18 to 28% reduced displacements.

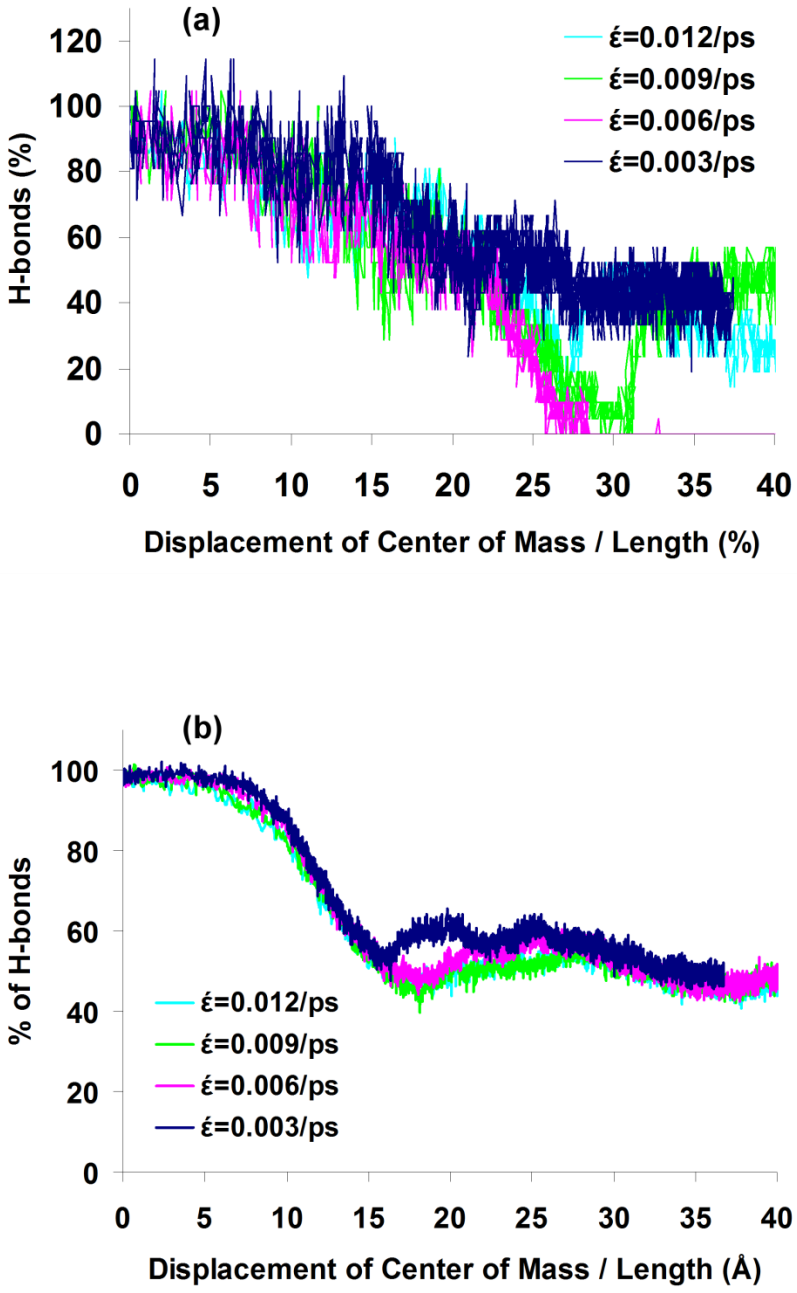

Figure 5.6. Percentage of hydrogen bonds between polypeptide chains of collagen it is stretched: (a) short collagen (k = 4.0 kcal/mol/Å^2), (b) long collagen k = 0.1 kcal/mol/Å^2.

At displacements up to about 7-8% there is no appreciable drop in number of hydrogen bonds both in cases of short and long collagen as shown in figures 5.6 and 5.7, although breaking and formation of hydrogen bonds is significantly lower for short collagen. The range of hydrogen bonds is between 70% to 110% of the original bonds for short collagen in this region. However, in case of long collagen the breaking and formation is significantly smaller ranging from 100 to 95% up to 4% reduced displacement and 98% to 85% for 4% to 7%. As described before, in this displacement range the molecule is coiled and the unwinding of triple helical chains is negligible. The short collagen in this region displays very large amplitude of fluctuations in number hydrogen bonds compared to long collagen (Fig. 5.7). Additionally, hydrogen bonds appear to break more rapidly in case of short collagen compared to long collagen. Both in cases of short and long collagen the rate of breaking of hydrogen bonds is found to be faster at higher rates of pulling, though it is hard to observe in case of short collagen due to large fluctuation in number of bonds. Beyond about 8% reduced displacement, the hydrogen bonds break very rapidly up to about 18% reduced displacement. The breaking of hydrogen bonds corresponds to increase in stiffness of load-displacement curve in this region (Fig. 5.2). With further stretching of collagen, the backbone begins to stretch and the number of hydrogen bonds remains fairly steady amid some small variations.

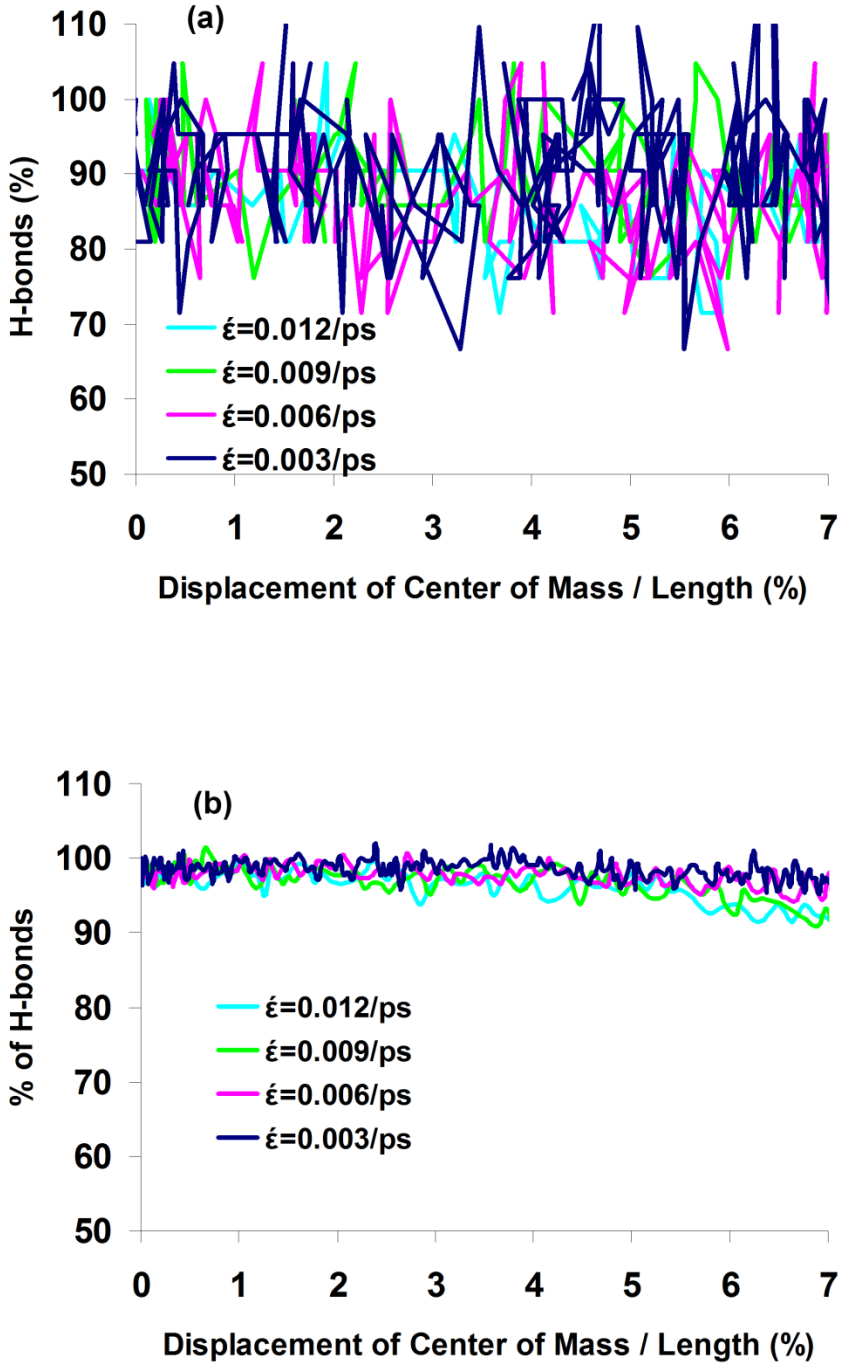

Figure 5.7. Percentage of hydrogen bonds between polypeptide chains of collagen in the elastic range: (a) short collagen (k = 4.0 kcal/mol/Å^2), (b) long collagen k = 0.1 kcal/mol/Å^2.

5.4. Conclusions

Steered molecular dynamics study of short and long collagen was carried out to investigate deformation behavior of collagen. It has been found that the length of collagen used in the molecular dynamics study has a significant impact on the mechanical response of collagen. The elastic modulus was evaluated for short and long collagen by carrying out SMD simulations using various pulling rates and spring constants. The elastic modulus was found to be higher when the larger spring constants and higher rates of pulling are used. At lower pulling rates the elastic modulus for short and long collagen are found to be comparable. However, at higher pulling rates the moduli of long collagen are found to be higher. Additionally, the load-displacement plots and hydrogen bond plots for short collagen exhibited large saw tooth-like features (variations) in case of short collagen. Such large fluctuations were not observed in case of long collagen. At a very low pulling rate of 0.0003/ps (at which the effect of pulling rate on modulus is minimal), the elastic moduli of short and long collagen were found to be about 6.2 GPa and 4.5 GPa respectively. The difference in elastic modulus may likely be due to the presence of coiled features in long collagen which are not present in short collagen. These coiled features, which have been observed for the first time, appear to be quite resilient during deformation of long collagen and may have an important influence on the elastic properties of the collagen. In addition to the differences in the mechanical behavior between short and long molecule, it appears that the deformation mechanisms between short and full length collagen molecules are significantly different as a result of differences in hydrogen bond breaking and forming and differences in conformational changes.

5.5. Acknowledgements

The authors acknowledge TeraGrid for computational resources at the NCSA Supercomputing Center. The computational resources at NDSU center for high performance computing (CHPC) are acknowledged. The authors thank Dr. Greg Wettstein for hardware and software support. Author SMP acknowledges support from ND EPSCOR.

5.6. References

1. Bhattacharjee,A. & Bansal,M. Collagen Structure: The Madras Triple Helix and the Current Scenario. *IUBMB Life* **57**, 161-172 (2005).
2. Fratzl,P. & Weinkamer,R. Nature's hierarchical materials. *Prog. Mater. Sci.* **52**, 1263-1334 (2007).
3. Currey,J.D., Zioupos,P., Davies,P., & Casino,A. Mechanical properties of nacre and highly mineralized bone. *Proc Biol Sci* **268**, 107-111 (2001).
4. Dorozhkin,S.V. & Epple,M. Biological and medical significance of calcium phosphates. *Angew. Chem. , Int. Ed.* **41**, 3130-3146 (2002).
5. Eastoe,J.E. & Eastoe,B. Organic constituents of mammalian compact bone. *Biochem. J.* **57**, 453-459 (1954).
6. Fisher,L.W. & Termine,J.D. Noncollagenous proteins influencing the local mechanisms of calcification. *Clin. Orthop. Relat. Res.* **200**, 362-385 (1985).
7. Olszta,M.J., Odom,D.J., Douglas,E.P., & Gower,L.B. A New Paradigm for Biomineral Formation: Mineralization via an Amorphous Liquid-Phase Precursor. *Connect. Tissue Res.* **44**, 326-334 (2003).

8. Currey,J.D. Biomechanics of mineralized skeletons in *Skeletal Biomineralization :Patterns, processes, and evolutionary trends* (ed. Carter,J.G.) 11 (Van Nostrand, New York, 1990).

9. Termine,J.D., Wuthier,R.E., & Posner,A.S. Amorphous-crystalline mineral changes during endochondral and periosteal bone formation. *Proc. Soc. Exp. Biol. Med.* **125**, 4-9 (1967).

10. Ramachandran,G.N. & Kartha,G. Structure of Collagen. *Nature* **176**, 593-595 (1955).

11. Bella,J., Eaton,M., Brodsky,B., & Berman,H.M. Crystal and molecular structure of a collagen-like peptide at 1.9 A resolution. *Science* **266**, 75-81 (1994).

12. Orgel J.P. *et al.* The in situ supermolecular structure of type I collagen. *Structure* **9**, 1061-1069 (2001).

13. Landis,W.J., Song,M.J., Leith,A., McEwen,L., & McEwen,B.F. Mineral and organic matrix interaction in normally calcifying tendon visualized in three dimensions by high-voltage electron microscopic tomography and graphic image reconstruction. *J Struct Biol* **110**, 39-54 (1993).

14. Hellmich,C., Celundova,D., & Ulm,F.J. Multiporoelasticity of Hierarchically Structured Materials: Micromechanical Foundations and Application to Bone. *J. Eng. Mech. -ASCE* **135**, 382-394 (2009).

15. Hamed,E., Lee,Y., & Jasiuk,I. Multiscale modeling of elastic properties of cortical bone. *Acta Mechanica* **213**, 131-154 (2010).

16. Fritsch,A., Hellmich,C., & Dormieux,L. Ductile sliding between mineral crystals followed by rupture of collagen crosslinks: experimentally supported

micromechanical explanation of bone strength. *Journal of theoretical biology* **260**, 230-252 (2009).

17. Ghanbari,J. & Naghdabadi,R. Nonlinear hierarchical multiscale modeling of cortical bone considering its nanoscale microstructure. *J. Biomech.* **42**, 1560-1565 (2009).

18. Fritsch,A. & Hellmich,C. 'Universal' microstructural patterns in cortical and trabecular, extracellular and extravascular bone materials: micromechanics-based prediction of anisotropic elasticity. *J. Theor. Biol.* **244**, 597-620 (2007).

19. Dubey,D.K. & Tomar,V. Microstructure dependent dynamic fracture analyses of trabecular bone based on nascent bone atomistic simulations. **35**, 24-31 (2008).

20. Buehler,M.J. Nanomechanics of collagen fibrils under varying cross-link densities: Atomistic and continuum studies. *J. Mech. Behav. Biomed. Mater.* **1**, 59-67 (2008).

21. Buehler,M.J. Nature designs tough collagen: Explaining the nanostructure of collagen fibrils. *Proc. Natl. Acad. Sci. U. S. A.* **103**, 12285-12290 (2006).

22. Bhowmik,R., Katti,K.S., & Katti,D.R. Mechanics of molecular collagen is influenced by hydroxyapatite in natural bone. *J. Mater. Sci.* **42**, 8795-8803 (2007).

23. Bhowmik,R., Katti,K.S., Venna,D., & Katti,D.R. Probing molecular interactions in bone biomaterials: Through molecular dynamics and Fourier transform infrared spectroscopy. *Mater. Sci. Eng. C-Biomimetic Supramol. Syst.* **27**, 352-371 (2007).

24. Katti,D.R., Pradhan,S.M., & Katti,K.S. Directional dependence of hydroxyapatite-collagen interactions on mechanics of collagen. *Journal of Biomechanics*(2010).

25. Gautieri,A., Vesentini,S., Montevecchi,F.M., & Redaelli,A. Mechanical properties of physiological and pathological models of collagen peptides investigated via steered molecular dynamics simulations. *J. Biomech.* **41**, 3073-3077 (2008).

26. Lorenzo,A.C. & Caffarena,E.R. Elastic properties, Young's modulus determination and structural stability of the tropocollagen molecule: a computational study by steered molecular dynamics. *Journal of Biomechanics* **38**, 1527-1533 (2005).

27. Buehler,M.J. Atomistic and continuum modeling of mechanical properties of collagen: elasticity, fracture, and self-assembly. *J. Mater. Res.* **21**, 1947-1961 (2006).

28. Bhowmik,R., Katti,K.S., & Katti,D.R. Mechanisms of Load-Deformation Behavior of Molecular Collagen in Hydroxyapatite-Tropocollagen Molecular System: Steered Molecular Dynamics Study. *Journal of Engineering Mechanics* **135**, 413-421 (2009).

29. Gautieri,A., Russo,A., Vesentini,S., Redaelli,A., & Buehler,M.J. Coarse-Grained Model of Collagen Molecules Using an Extended MARTINI Force Field. *Journal of Chemical Theory and Computation* **6**, 1210-1218 (2010).

30. Katti,D.R., Pradhan,S.M., & Katti,K.S. Directional dependence of hydroxyapatite-collagen interactions on mechanics of collagen. *Journal of Biomechanics* **43**, 1723-1730 (2010).

31. Bhowmik,R., Katti,K.S., & Katti,D.R. Mechanics of molecular collagen is influenced by hydroxyapatite in natural bone. *J. Mater. Sci.* **42**, 8795-8803 (2007).

32. Uzel,S.G.M. & Buehler,M.J. Nanomechanical sequencing of collagen: tropocollagen features heterogeneous elastic properties at the nanoscale. *Integrative Biology* **1**, 452-459 (2009).

33. Persikov,A.V., Ramshaw,J.A.M., & Brodsky,B. Prediction of collagen stability from amino acid sequence. *Journal of Biological Chemistry* **280**, 19343-19349 (2005).

34. Jorgensen,W.L., Chandrasekhar,J., Madura,J.D., Impey,R.W., & Klein,M.L. Comparison of simple potential functions for simulating liquid water. *J. Chem. Phys* **79**, 926-935 (1983).

35. Kale,L. *et al.* NAMD2: Greater Scalability for Parallel Molecular Dynamics. *J. Comput. Phys.* **151**, 283-312 (1999).

36. MacKerell,A.D. *et al.* All-atom empirical potential for molecular modeling and dynamics studies of proteins. *J. Phys. Chem. B* **102**, 3586-3616 (1998).

37. Feller,S.E., Zhang,Y., Pastor,R.W., & Brooks,B.R. Constant pressure molecular dynamics simulation: the Langevin piston method. *J. Chem. Phys.* **103**, 4613-4621 (1995).

38. Martyna,G.J., Tobias,D.J., & Klein,M.L. Constant pressure molecular dynamics algorithms. *J. Chem. Phys.* **101**, 4177-4189 (1994).

39. Gautieri,A., Buehler,M.J., & Redaelli,A. Deformation rate controls elasticity and unfolding pathway of single tropocollagen molecules. *Journal of the Mechanical Behavior of Biomedical Materials* **2**, 130-137 (2009).

40. Gautieri,A., Buehler,M.J., & Redaelli,A. Deformation rate controls elasticity and unfolding pathway of single tropocollagen molecules. *Journal of the Mechanical Behavior of Biomedical Materials* **2**, 130-137 (2009).

41. Gautieri,A., Buehler,M.J., & Redaelli,A. Deformation rate controls elasticity and unfolding pathway of single tropocollagen molecules. *Journal of the Mechanical Behavior of Biomedical Materials* **2**, 130-137 (2009).

42. Lu,H. & Schulten,K. Steered molecular dynamics simulation of conformational changes of immunoglobulin domain I27 interprets atomic force microscopy observations. *Chem. Phys.* **247**, 141-153 (1999).

CHAPTER 6. STRUCTURAL HIERARCHY CONTROLS DEFORMATION BEHAVIOR OF COLLAGEN

This chapter discusses the role of structural hierarchy in the mechanics of collagen. The contents of the chapter are published in Pradhan, S. M., Katti, K. S., and Katti, D. R. (2012). "Structural Hierarchy Controls Deformation Behavior of Collagen." *Biomacromolecules*, 13(8), 2562-2569.

6.1. Introduction

The molecular structures of biological materials have a significant impact on mineralization as well as the mechanics of these structures [1-4]. Collagen is an abundant fibrous protein in mammals that is an integral part of various connective tissues. It is an important building material that fulfills different kinds of mechanical roles in various tissues. There are at least 27 types of collagen structures found in vertebrates (i.e. type I to XXVII) of these types, the type I is the most abundant protein found in tissues such as bone, skin, tendon, and cornea [5]. Fibrillar collagens, such as Type I collagen found in bone, form structures known as collagen fibrils which consist of a staggered arrangement of collagen molecules with a periodicity of 67 nm [6, 7]. In this structure, minerals are present in the hole-zone between collagen molecules, mainly in the form of flat plates, and on the outside fibril region as extrafibrillar mineral [8-12]. The behavior of collagen-mineral system has been extensively studied using molecular dynamics [13-16], density functional theory [17] and continuum micromechanics theory [18, 19]. The atomistic study of collagen proteins in their fibrillar environment has also been carried out [20]. Interestingly,

a relationship between organic concentration and mineral concentration in bone over numerous species, organs and age groups leading to potential 'universal' mass density-elasticity relationships has also been recently reported [21].

Collagen is a long slender molecule about 290 nm in length and 1.5 nm in width. It consists of 1014 residues. It is composed of three polypeptide chains, also known as alpha chains, folded about each other into a right handed triple helix[22]. Each of the polypeptide chains consist of more than 1000 amino acids [23]. The collagen molecule consisting of three identical alpha chains is known as homotrimeric (e.g. type II & III), while molecules not consisting of three identical alpha chains are known as hetrotypic (e.g. type I & XI). Each polypeptide chain is a left hand helix composed of a repeating triplet of amino acids (Gly-X-Y), where X and Y may be any amino acid, but most often they are proline and hydroxyproline. The repetition of Glycine as every third residue is shown to be necessary for close packing of the three polypeptide chains [22, 24]. The sterically small Glycine is situated near the center axis of collagen and the residues X and Y are on the surface. The three polypeptide chains of collagen are held together by inter-chain hydrogen bonds.

Prior studies on the deformation behavior of collagen in literature consist mainly of steered molecular dynamics of 8.5 nm length short collagen molecule [13-15, 25-27]. Recently, we have carried out steered molecular dynamics study of full length collagen to investigate similarities and differences in deformation under various loading conditions [28]. Micromechanics studies have included relationships of hydroxyapatite crystals sliding on rupture of crosslinks in collagen during deformation [19]. Studies have also been carried out to investigate the role of the amino acid sequence on the mechanical property of

collagen [29]. In addition to molecular dynamics studies, coarse grained study of long collagen molecule has been carried out by Gautieri et al. [30]. Although providing some useful results, coarse graining may not describe detailed molecular mechanisms and their specific contributions to mechanics. Here, we present the results of steered molecular dynamics study of full length collagen to investigate molecular mechanisms governing deformation response of collagen. We explore the conformational evolution of different helical hierarchies of collagen to elucidate different mechanisms responsible for the mechanical response of collagen when collagen is deformed.

6.2. Collagen Model Construction

The Glycine-Proline-Proline (GPP) structure (~8.5nm) of collagen used in this study was obtained from Protein Data Bank (PDB ID 1k6f). GPP is a the first and most widely used sequence in the structural studies of collagen model compounds[31]. The full length molecule was built by connecting these short structures end-to-end, along the longitudinal axis following appropriate translational and rotational transformations. The resulting molecule is about 290 nm long and consists of 1014 residues along each alpha chain. This molecule is used as a "model collagen system" to study the role of structural hierarchy on the deformation of collagen molecules. The molecule was solvated in a box with 19417 water molecules distributed along its length. The TIP3P model of water was used in all the simulations [32].

6.2.1. Molecular Dynamics and Steered Molecular Dynamics Simulation Details

Molecular Dynamics (MD) and Steered Molecular Dynamics (SMD) simulations were carried out using NAMD [33], and the molecular visualizations and analysis were carried out using VMD [34]. Energy minimization was carried out using the conjugate

gradient method. The temperature and pressure of the molecule were raised to 300 K and 1.01 bars in gradual steps of 100 K and 0.25 bar respectively. Langevin dynamics and Nose-Hoover piston methods were used to control temperature and pressure [35, 36]. A cutoff distance of 10 Å was used for all nonbonded calculations. The Particle Mesh Ewald (PME) method was used for the calculation of Coulombic interactions. Steered molecular dynamics (SMD) simulations were carried out by fixing one end and pulling the center of mass of the collagen molecule at various pulling rates using a harmonic spring. Our previous work showed that a spring stiffness of 0.1 kcal/mol/$Å^2$ was appropriate for pulling the collagen molecule . In our simulations, pulling rates of 0.00003 ps^{-1}, 0.0003 ps^{-1}, 0.003 ps^{-1}, 0.006 ps^{-1}, 0.009 ps^{-1}, and 0.012 ps^{-1} were used. It is to be noted that the lowest two pulling rates used are in the range where the mechanical response of collagen converges, as shown in literature [26]. All the simulations were carried out using a time step of 0.5 fs except for the pulling rate of 0.00003 ps^{-1}. In the case of a pulling rate of 0.00003 ps^{-1}, the time step of 2 fs is used along with ShakeH and SETTLE algorithms to constrain covalent bond lengths involving hydrogen atoms in case of protein and water respectively.

For carrying out conformational analysis of polypeptide chains, the helical parameters were calculated according to the methods developed by Sugeta and Miyazawa [37] and Bansal et al [5]. The evolution of hydrogen bonds during pulling was studied using a combination of geometric criteria, (i.e. donor-hydrogen distance $\leq$ 3.5 Å and donor-hydrogen-acceptor angle $\leq 60^o$) and interaction energy criteria (the hydrogen bond pairs with positive magnitude of interaction energy between them are excluded from the

calculations). The total inter-chain hydrogen bond energy was calculated by summation of interaction energy between individual hydrogen bonding pairs.

6.3. Results and Discussion

6.3.1. Deformation Response of Hierarchies of Collagen

The structure of collagen is comprised of an interesting hierarchy of helices: it is the triple-helix of three polypeptide chains called alpha chains that are also helical. The individual polypeptide chains of collagen are left-handed helices, three of which are twisted about each other into a right hand helix through the mediation of hydrogen bonds. The stretching of collagen comes at the cost of deformation of these helices subject to the lateral restraint, provided by the series of hydrogen bonds distributed along the length. The helices of individual polypeptide chains and the triple-helix will be referred in this paper as the level-1 and the level-2 helix respectively (Figs. 6.1a, 6.1b). The presence of the level-2 helix is a due to the non-integral "number of residues per turn" of the level-1 helix, i.e. the level-2 helix will not exist if the level-1 helix has integral number of residues per turn [22, 38-40]. The conformation of the level-1 helix allows for the three polypeptide chains to be hydrogen bonded, and form the level-2 helix. Thus, the level-2 helix is a consequence of the geometric conformity of polypeptide chains, which satisfy the stringent requirements of the formation of inter-chain hydrogen bonds. In line with this argument, the authors point out the possibility that the effect of the geometric conformity (of the level-1 helix) may extend beyond the level-2 helix, to give rise to the helix of higher order. This can possibly help explain crimping of a short collagen molecule that has been reported in number of studies [26, 28]. In case of the short collagen molecule it difficult to see coiling because the length is too short for observing the

helicity. Figure 6.1(c) shows the crimped structure of a full-length collagen at the beginning of SMD simulation. This observation is comparable to the experimental study of microfibrillar structure that suggests the presence of the molecular crimped structure of collagen[41, 42] and the macroscopic crimp observed in fibril structures[42-44]. The observation of this full-length structure shows that the majority of the crimps are in fact helical in shape and not just random planar curves as described earlier. These higher level helical structures formed by collagen are referred to here as the level-3 helix.

6.3.2. Evolution of the Level 1 Hierarchy of Collagen over the Deformation Range

The study of conformational evolution of the collagen helices during stretching is necessary for understanding deformation mechanisms of the collagen. Figures 6.2 and 6.3 show changes in the average radius and pitch of the level-1 helices respectively when the collagen molecule is stretched. The level-1 helices show decrease in radius (Fig. 6.2) and increase in pitch (Fig. 6.3) when the collagen is extended. This is similar to the behavior of a typical helical spring, which shrinks in radius with the corresponding increase in pitch during stretching. The rate of change in pitch and radius are initially small at small displacement and more prominent for higher rates of pulling (Figs. 6.2a, 6.2b, 6.3a, 6.3b). The rate of change of pitch and radius increase at displacements beyond ~ 7%, which coincides with the rapid breaking of inter-chain hydrogen bonds (more details will be described in the following paragraphs). The increase in pitch at various rates of pulling is significant at small as well as large displacement regimes: found to be about 4-8% at 7% displacement, and about 50% at 40% displacement. This increase in pitch leads to the increase in the overall length of level 1.

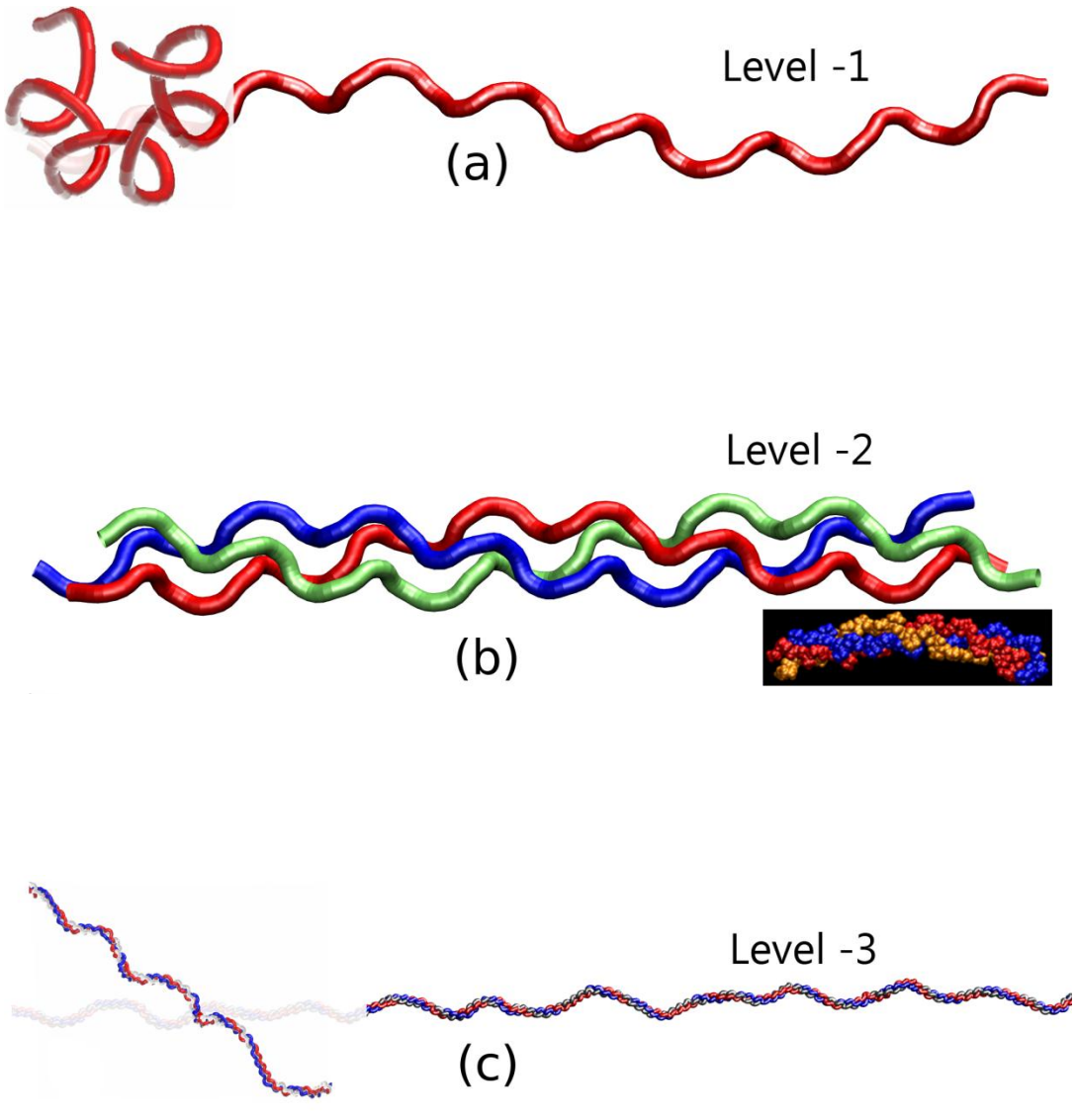

Figure 6.1. Figure showing (a) level-1 helix, (b) level-2 helix, and (c) snapshot of full length collagen at the beginning of SMD simulation showing helical features along the length.

.

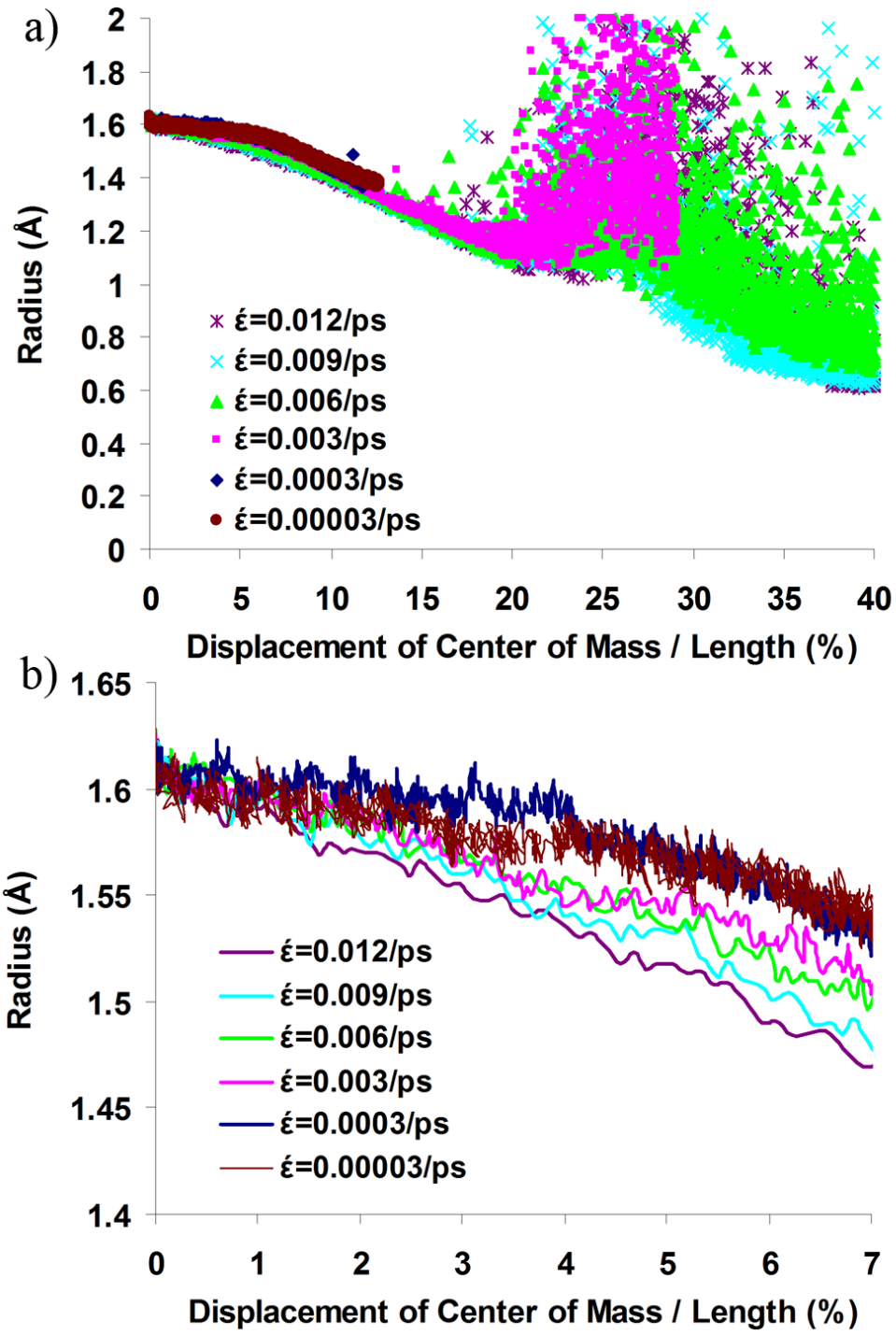

Figure 6.2. Average radius of the level-1 helix (i.e. alpha chain) during extension of collagen at various pulling rates: (a) large displacement, (b) small displacement.

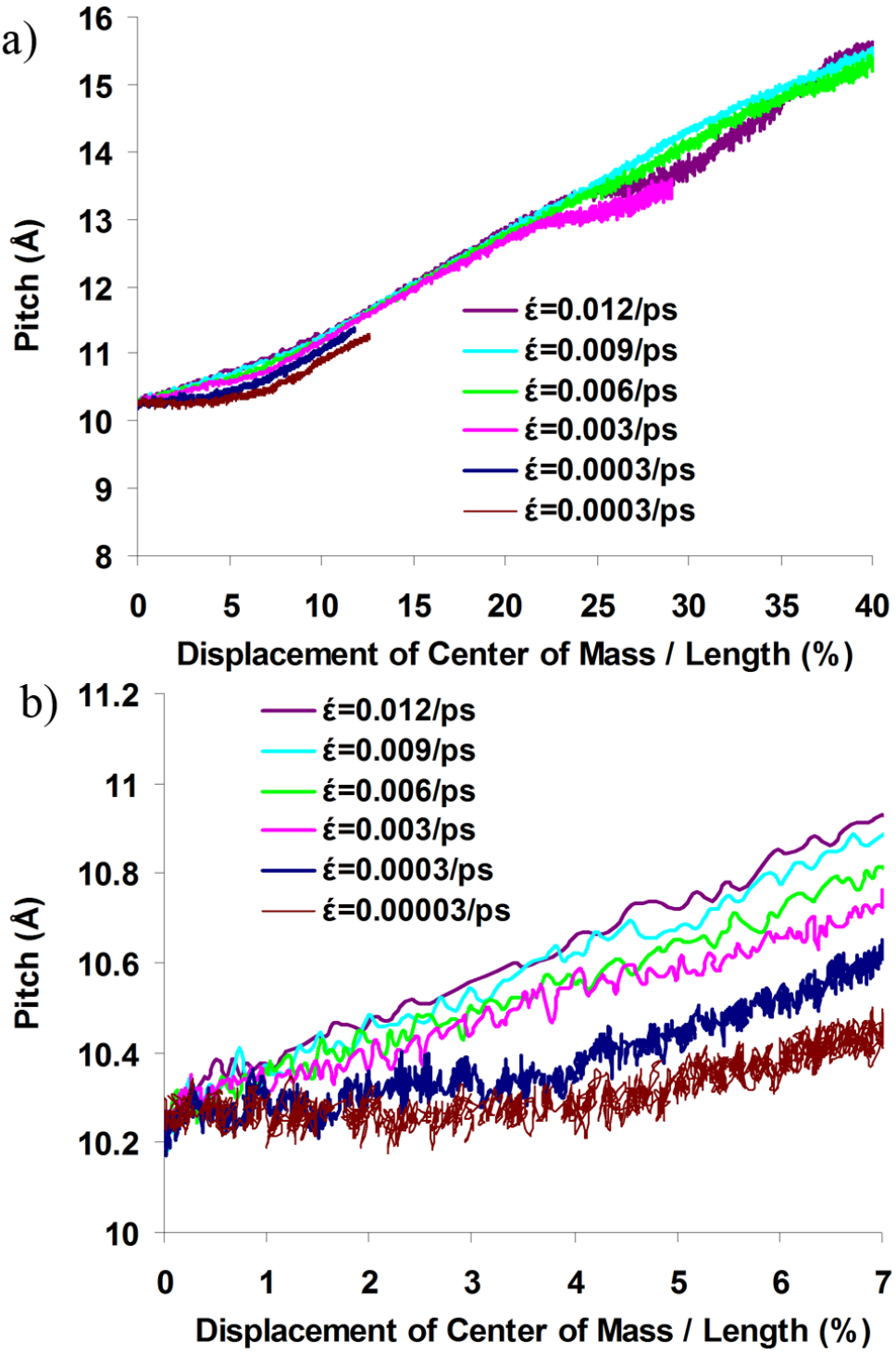

Figure 6.3. Average pitch of the level-1 helix (i.e. alpha chain) during extension of collagen at various pulling rates: (a) large displacement, (b) small displacement.

The variation in the total number of turns of the level-1 helix with stretching is shown in figure 6.4. The plot shows overall decrease in number of turns with displacement. However, in the small displacement range of 0 to 7%, a slight increase in number of turns with displacement is observed. The decrease in number of turns even under 40% stretching is about 1% or less than the total number of level-1 turns. In the small deformation regime, for a pulling rate of 0.00003/ps, an increment of about 3 turns is observed. The level-1 helix is restrained from unwinding by the series of inter-chain hydrogen bonds along the chain length. This prevents large variation in the total number of turns, and hence the number of residues per turn, during stretching (Fig. 6.4). In a deformation regime from 7% to 15%, only a small drop of about 3 turns out of the initial total of about 295 turns is observed (i.e. there is only a slight increase in the average number of residues per turn from 3.424 to 3.462). Figure 6.5 shows a plot of the number of inter chain hydrogen bonds, hydrogen bond energy, and interaction energy between the three alpha chains during deformation. A significant decrease in the number of hydrogen bonds is observed with the largest decrease from 700 to 200 bonds within the first 15% of the deformation (Fig. 6.5a). Corresponding to the decrease in the number of hydrogen bonds, we see a decrease in hydrogen bond energy and drop in interaction energy between the chains (Fig. 6.5b) with deformation. It is interesting that the drop in the number of turns, albeit small, corresponds to the regime of rapid drop in the number of hydrogen bonds during stretching. Furthermore, it is worth pointing out that we would have expected a larger variation in the total number of turns if the single isolated polypeptide chain was pulled instead of the collagen triple helix. This '***stabilizing effect'*** due to triple helical structure that preserves the level-1 helix can be visualized using an

analogy of interlocking gears as shown in figure 6.6a. In the collagen molecule, each of the polypeptide chains form hydrogen bonds with both the adjacent chains, one to its right and the other to its left (figure 6.6b). The three gears can be considered to be polypeptide chains of collagen, and the meshing between teeth on the adjacent gears can be thought of as an inter-chain hydrogen bond (figure 6.6c). In this interlocked configuration, each of the gears is restrained against any kind of axial rotation by the two adjacent gears. Thus, the interlocking mechanism introduced by the inter-chain hydrogen bonds can prevent unfolding of the level 1 helix, which would otherwise unfold with relative ease. This deformation mechanism during stretching is a likely explanation of why the collagen molecule is composed of three helical chains held in place by hydrogen bonds that facilitate interlocking mechanism.

6.3.3. Evolution of the Level 2 Hierarchy of Collagen over the Deformation Range

The variation in total number of turns of the level-2 helix during deformation of collagen is shown in figure 6.7a. The geometry of the level-2 helix facilitates conditions necessary for the formation of inter-chain hydrogen bonds and hence is crucial for the integrity of collagen structure. The number of turns of the level-2 helix, shows a small variation (< approximately 2 turns) and remains fairly constant up to 40% displacement. This observation is remarkable, because the full-length collagen does not show much unwinding of triple helix, unlike that exhibited by short collagen [13, 14, 26]. If the full length collagen is to unwind at the rate comparable to the short collagen, we would expect a significant unwinding that is at least seven times greater than that observed in simulations for short collagen at similar pulling rate by Gautieri etal. [26].

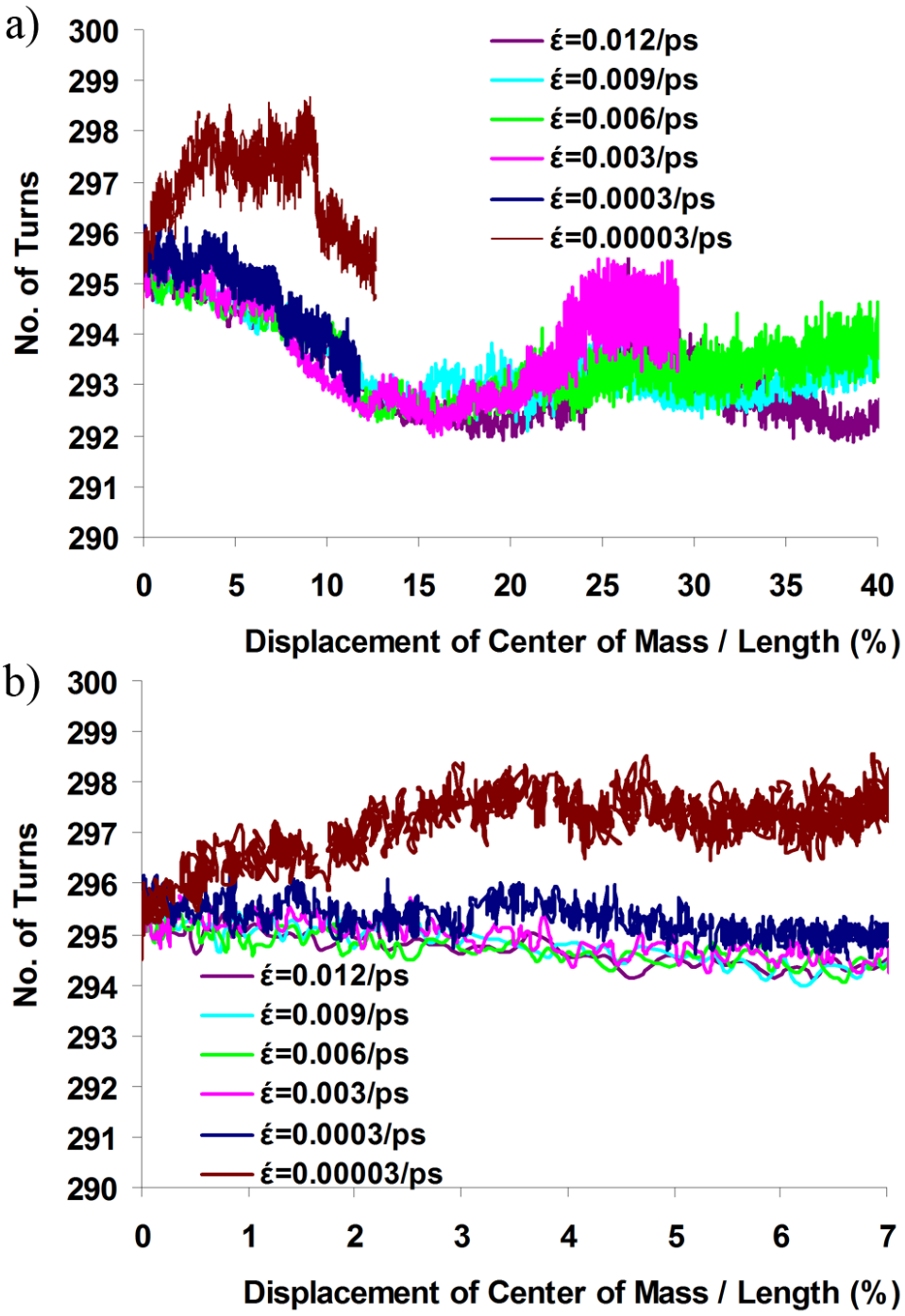

Figure 6.4. Variation of the total number of turns along the length of the level-1 helix (i.e. alpha chain) during loading: (a) large displacement, (b) small displacement.

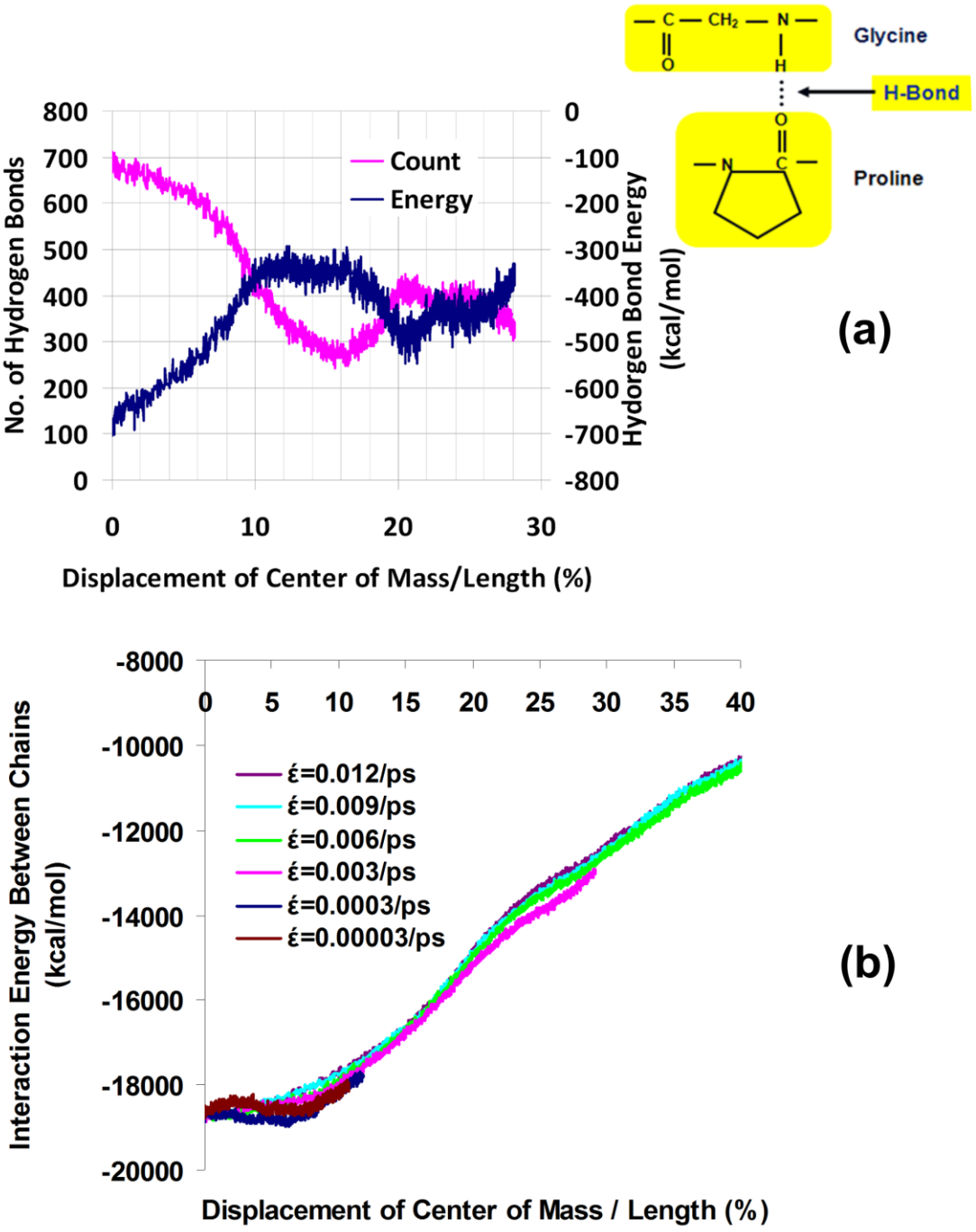

Figure 6.5. Figure showing (a) the variation in number of hydrogen bonds and the total interaction energy between the hydrogen bonding pairs during the deformation of collagen, (b) the interaction energy between three alpha chains of collagen when stretched at different pulling rates.

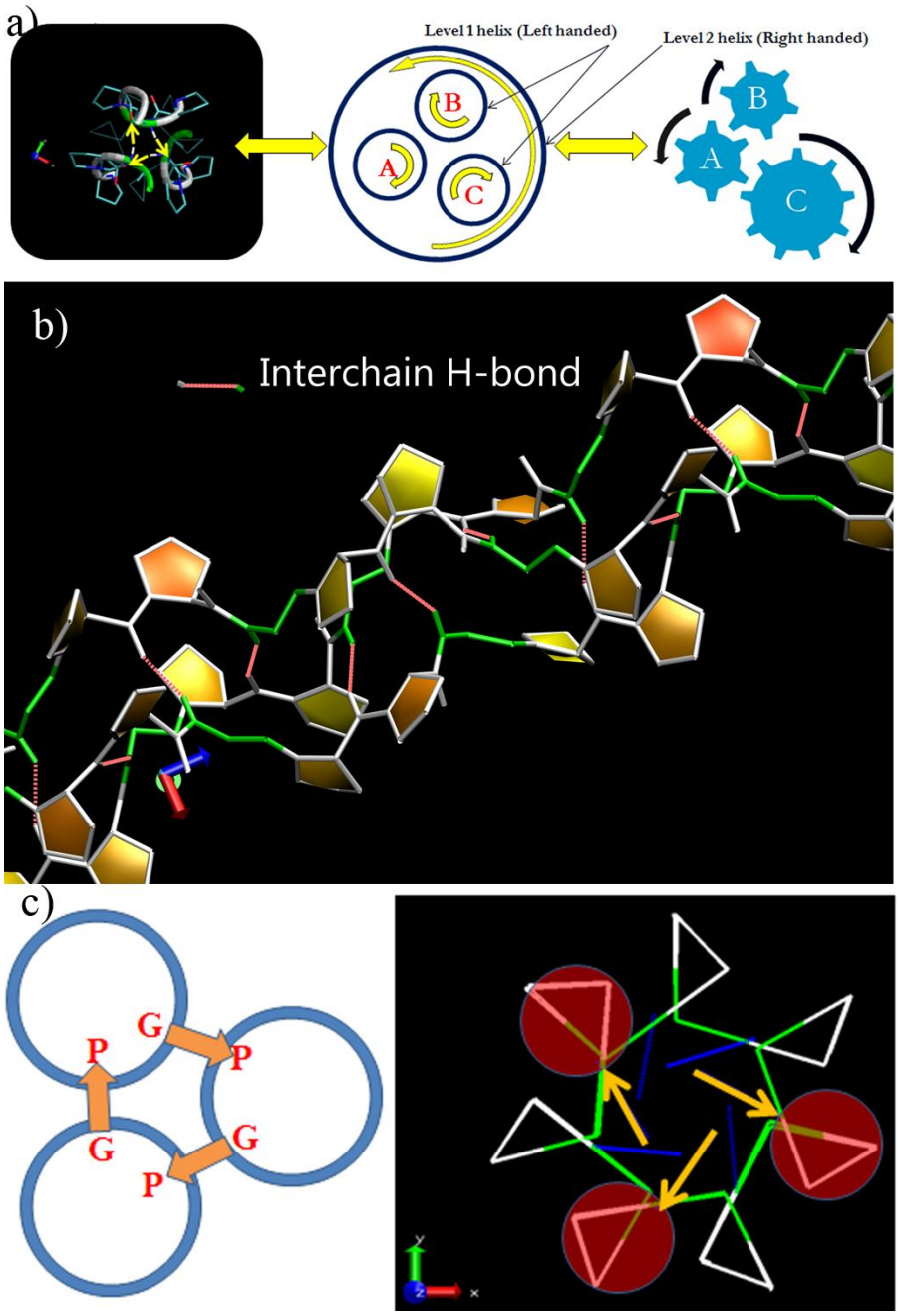

Figure 6.6. Schematic of interlocking gear analogy: (a) the gears represent alpha chains and the meshing between teeth on adjacent gears represents inter-chain hydrogen bonds, (b) Interchain hydrogen bonds along a portion of the length of the collagen molecule, c) location of hydrogen bonds at a representative cross-section of the molecule.

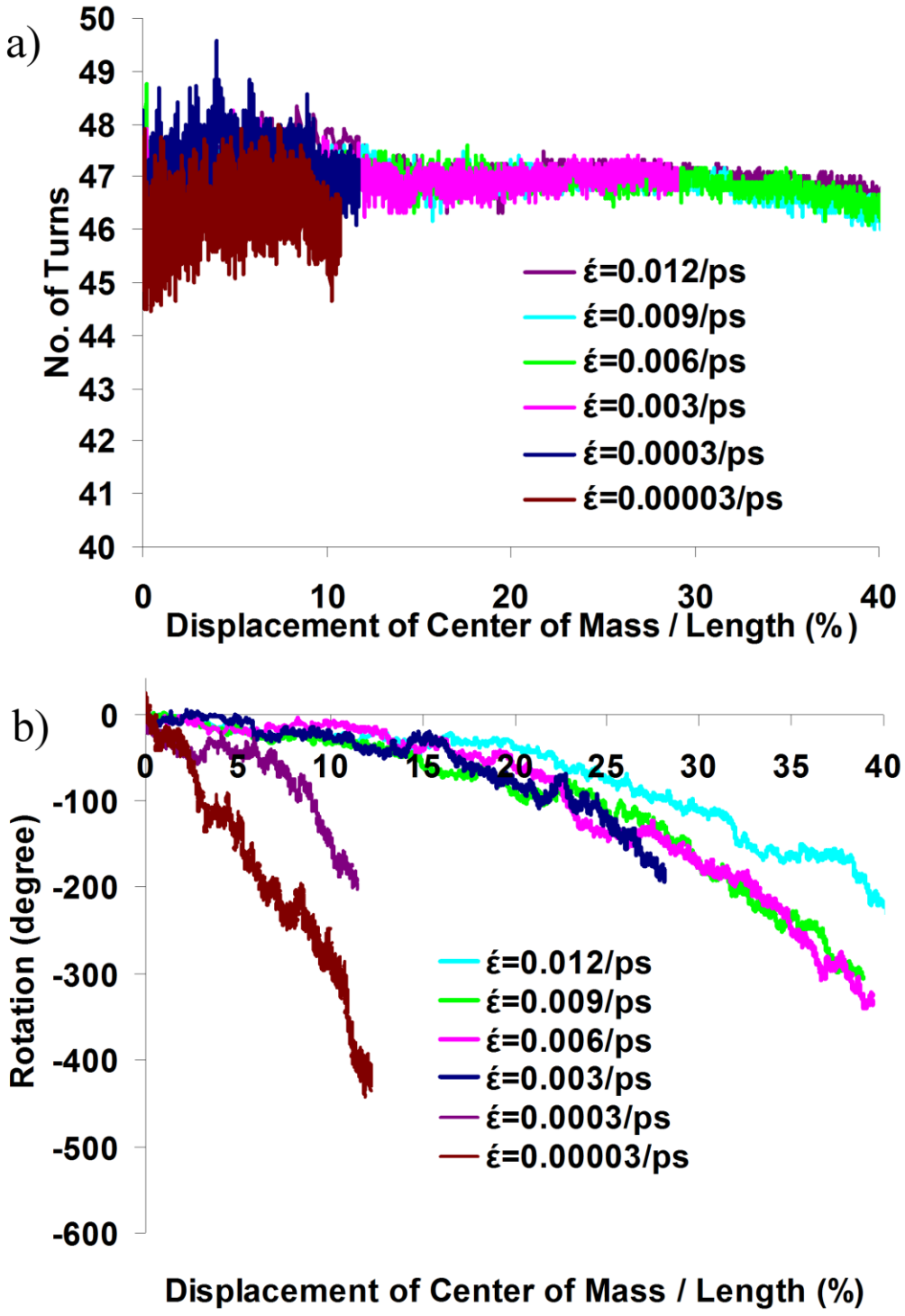

Figure 6.7. Figure showing (a) total number of turns of turns of the level-2 helix (i.e. triple helix) at different rates of pulling, (b) the rotation of the free end of collagen during extension of collagen at various pulling rates.

The rotation of the free end of the collagen during pulling is shown in figure 6.7b, where negative rotation implies unraveling of right handed triple helix. It is seen that the collagen does not unwind significantly in both small and large deformation range to cause significant unfolding of collagen. This is in agreement with the small variation in the total number of turns of the level-2 helix as discussed above.

6.3.4. Interplay of the Level 1 and Level 2 Hierarchies through Hydrogen Bonding

It is pertinent to discuss hydrogen bonds at this point, as they are the vital links between the level-1 and level-2 helices. The variation in the number of hydrogen bonds and the interaction energies between hydrogen bonding pairs are shown in figure 6.5. The hydrogen bond number shows a slower decline (700 to 550), in the smaller displacement regime of up to about 7%. This is followed by a regime of rapid drop in number of hydrogen bonds (550 to approximately 200), between 7 to 15% displacement. The rapid drop in the number of hydrogen bonds coincides with the increase in the rate of change of pitch and radius, and the drop in number of turns of the level-1 helix as discussed above. Additionally, the rapid drop in hydrogen bonds is also correlated with the increase in stiffness of collagen [14, 26]. However, the rapid drop in number of hydrogen bonds is not seen to have huge consequence for unfolding of the level-2 helix. Therefore, this leads us to infer that the rapid drop in hydrogen bonds is primarily due to changes in conformation of the level-1 helix.

The interaction energy between three polypeptide chains during collagen deformation is shown in figure 6.5b. The interaction energy is fairly steady in the small displacement regime. This is followed by the a rapid decline in attractive energy beyond about 7% displacement, which interestingly coincides with the beginning of rapid drop in

number of hydrogen bonds (Fig. 6.5a). However, unlike the hydrogen bonds which partially recover after 15% displacement, the interaction energy between chains continues to decline progressively.

The comparison of interaction energies between three alpha chains (Fig. 6.5b) and total interaction energy between hydrogen bonding pairs (Fig. 6.5a) leads us to an interesting insight about the conformational stability of collagen. We find that the total hydrogen bond energy (~700 kcal/mol) is significantly smaller (~25 times) than the interaction energy between the chains (~18,000 kcal/mol) in collagen. This implies that the three chains have strong attractive interactions among themselves to stay intact albeit the absence of inter-chain hydrogen bonds. This may sound antithetical to the number of studies giving credence to the hydrogen bonds as an important stabilizing feature of collagen. However, the simulations presented here on full length collagen indicate that the high attractive energy between the chains does not diminish the important role hydrogen bonds play in collagen structure. The hydrogen bonds, due to their highly directional nature, are essential for preserving the conformation of the level-1 and level-2 helix, and therefore that of collagen. The level-1 and level-2 helices, are in fact very intimately related through mediation of hydrogen bonds. The non-integral numbers of residues per turn of the level-1 helix are indeed the reason for the existence of the level-2 helix. For an ideal collagen structure with uniform sequence, it is possible to derive the following simple relationship between the number of residues per turn of the level-1 helix (n), and the level-2 triple helix (N), based on geometric compatibility: $N=3n/(n-3) = 3[1+(3/n)^1 + (3/n)^2 + (3/n)^2 + (3/n)^3 +\ldots]$, where n=(3, 4). This equation indicates an inverse relation between the level-1 and level-2 helices, which would not be possible in

the absence of the hydrogen bonds. In simple terms, hydrogen bonds help with conformational stability of collagen, by allowing interaction between these competing helices during deformation of collagen. Such interactions between the level-1 and level-2 helices help preserve the conformational integrity/stability of each other, by preventing each other from unfolding during deformation of collagen. This mechanism of enhancement of conformational stability of collagen is a result of an interesting alliance between the level-1 helix, hydrogen bonds, and the level-2 helix.

6.3.5. Evolution of the Level-3 Hierarchy of Collagen and Impact of Deformation of Level 1 and 2 on Level 3 Helix

The deformation of collagen under tensile loading results from the composite response of the level-1, level-2, and level-3 helices. The variation in the length of the level-1 and level-2 helix during the extension of collagen is measured along the center line of the respective helices. The extension of both the level-1 helix and the level-2 helix, are found to be gradual in the small displacement regime, and relatively rapid after 7% displacement (again coinciding with the rapid breaking of hydrogen bonds). Since the length of the level-2 helix is same as the contour length of collagen, the level-1 helix is initially longer than the level-2 helix. The length of the level-2 helix increases somewhat faster than the level-1 helix, and consequently at a large displacement of about 20%, these two helices become nearly equal in length.

Extension of the level-2 helix can originate from three sources: extension of the level-1 helix, the unraveling of the level-2 helix (i.e. triple helical chains itself), and shrinking of collagen radius. However, the triple helix does not unravel much even at large displacement (Fig. 6.2) and no significant shrinking of collagen radius was

observed during pulling. This indicates that the extension of the level-2 helix results primarily from the extension of the level-1 helix and not from the unfolding of triple helical chains. As shown in figure 6.3, the change in pitch leads to the increase in the overall length of level 1, which subsequently translates into the change in length of the level-2 helix (i.e. contour length of collagen). These observations suggest that the level-1 helix is an important contributor to the deformation response of collagen in both small as well as large deformation regimes (although at very large displacements the stretching of backbone has a dominant effect on force response [13, 26]. Furthermore, in a hypothetical case even if the triple-helix somehow unfolded completely, the maximum achievable extension of collagen is less than 5%. This is because the alpha chains (i.e. the level-1 helix) of collagen in the unstrained state are about 5% longer, than the contour length of collagen. However, albeit level-2 helix exhibits limited extensibility, the triple helical structure of collagen has important implications for the mechanical response of collagen. The improved stiffness of triple helix compared to three isolated chains has been shown in the literature [25]. The answer to enhancement in conformational stability and mechanical response possibly resides in the mechanisms that help preserve conformation of the level-1 and level-2 helix. These mechanisms have been described previously in this work in terms of "interlocking gear analogy" and the "interactions between the level-1 and level-2 helices", both of which depend on the mediation of inter-chain hydrogen bonds that function like lateral braces. Also, it important at to point out that the hydrogen bonds are not aligned exactly perpendicular to the axis of collagen. Therefore, some of the contribution to enhanced stiffness may also be attributed to tensile force on hydrogen bond, though it is difficult to quantify the level of its contribution.

The displacement of the free-end of collagen during pulling is the combined result of the extension of the level-2 helix (i.e. change in contour length of collagen) and level-3 helix. The displacement contribution of the level-3 helix at various rates of pulling is shown in figure 6.8. When collagen is pulled, the level-3 helix extends fairly linearly until it is completely extended, as shown by initial steep slope, followed by a rapid transition to the flat slope in the figure. The flat slope corresponds to the regime in which the helical crimps have been stretched out and the collagen is completely stretched as shown in figure 6.9. It is seen that the level-3 helix deforms slower at higher rates of pulling compared to lower rates of pulling (Fig. 6.8). The deformation up to which the level-3 helix remains resilient before being stretched as predicted by figure 6.8 agrees well with the visual observation of simulation trajectory (figure 6.9). The deformations at which the level-3 helical crimps are stretched out are at 9%, 10%, 11%, 12%, 15%, and 18% displacements for the pulling rates of 0.00003 ps^{-1}, 0.0003 ps^{-1}, 0.003 ps^{-1}, 0.006 ps^{-1}, 0.009 ps^{-1}, and 0.012 ps^{-1} respectively. Thus, the level-3 helix significantly influences the mechanics of collagen molecule. The deformation behavior of the level-3 helix appears to be dependent on the rate of pulling as well as the stiffness of spring used to pull the collagen molecule.

The understanding of the deformation mechanism of collagen is not complete without knowing the relative contributions of each of the helical levels towards total displacement. As discussed previously, the extension of the level-1 helix translates directly to the change in the length of the level-2 helix. The level-1 helix is a principal source of extension of the level-2 helix, since there is no significant unfolding of the level-2 helix (i.e. triple helix does not unfold much). The relative contributions of the

level-2 and level-3 helices towards total extension of collagen are shown in figure 6.10. It is observed that at up to a certain displacement there is a contribution of both the level-2 and level-3 helix. The contribution of the level-3 helix disappears at large displacement when it becomes completely straight (Fig. 6.9). The joint contribution of the level-2 (which is a result of the level-1 deformation) and 3 helices towards total extension of collagen in the small displacement regime indicates that the level-3 helix is capable of exhibiting a significant deformation and force resistance, to be considered important for the mechanical behavior of collagen.

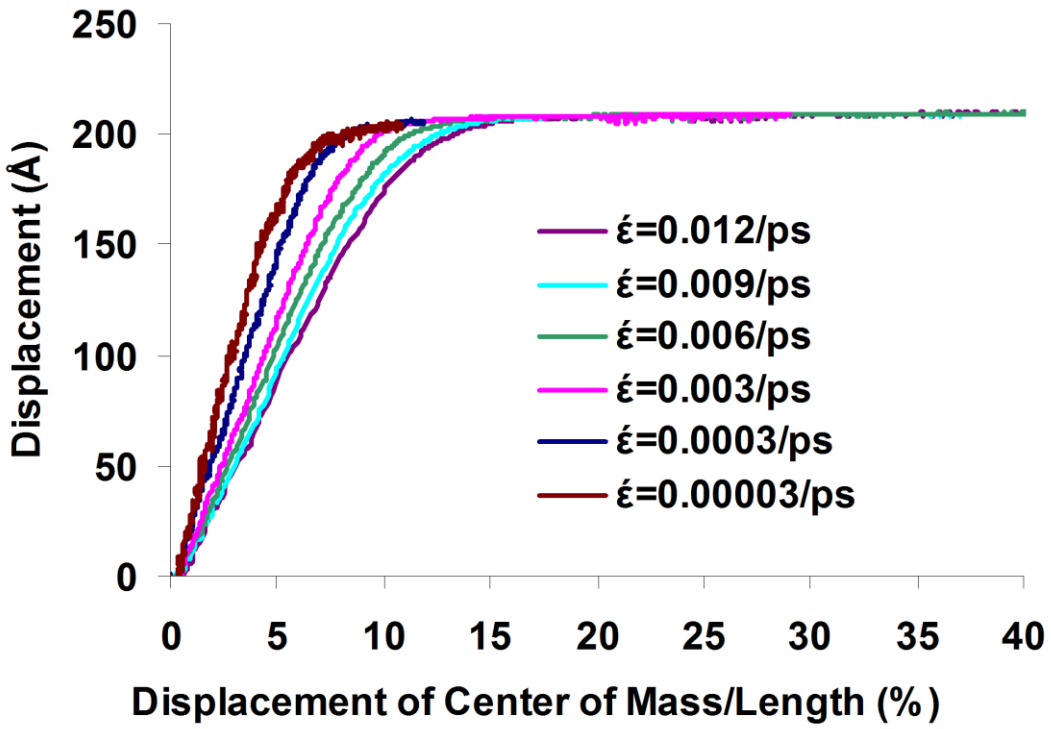

Figure 6.8. The contribution of the level-3 helix to the total displacement of free end of collagen when pulled at different rates.

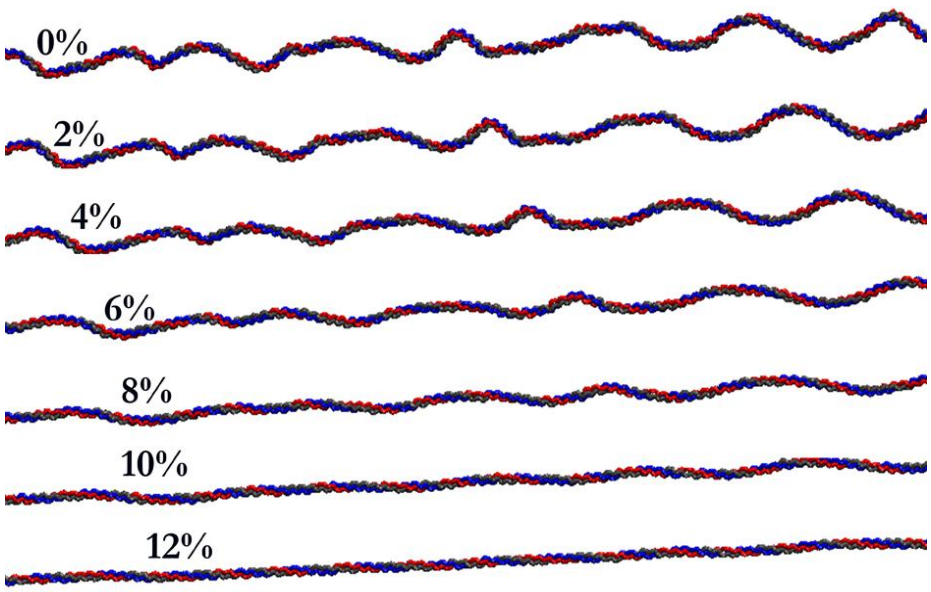

Figure 6.9. Snapshots showing the evolution of the level-3 helices when collagen is stretched. The helical features along the collagen length disappear after certain displacement.

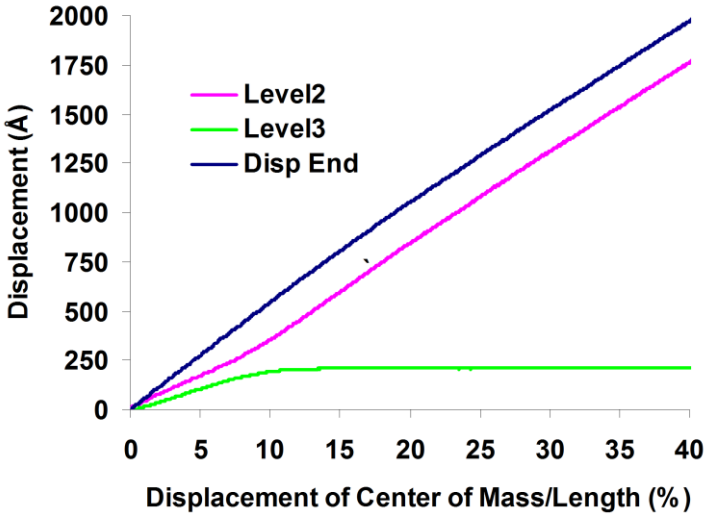

Figure 6.10. The plot showing displacement contributions of the level-2 and level-3 helix. The end-to-end displacement, which is a sum of the level-2 and level-3 contributions are also shown.

6.4. Conclusions

This work elucidates molecular mechanisms governing the deformation behavior of the full length collagen molecule through the detailed study of its multi-level helical hierarchies (conformations), when the collagen is extended. An observation of a third level of helical structure is also presented here, which can only be observed in the full length collagen structure. We observe that the deformation of collagen originates from the collective extension of left-handed alpha chain helices (the level-1 helix), and the helical turns observed along the length of collagen (level-3 helix). The extension of the level-3 helix, and therefore its stiffness show dependency on pulling rate. The level-3 helix is found to be quite resilient, and is seen to exist up to a very significant deformation of the collagen molecule. Additionally, the triple helix (level-2) is found to be much more stable against unfolding, as it does not show significant unfolding even at large deformation, unlike that reported in the literature, where simulations were conducted on short collagen molecule models. The relative stability of triple helix over large deformation plays a vital role in the conformational stability of collagen during extension. The presence of the level-2 helix allows collagen to possess higher stiffness (compared to three isolated alpha chains) and stability, while retaining ability to undergo large deformation through extension of alpha chains. The mechanisms responsible for deformation response and the conformational stability of collagen during straining are elucidated in this work with the help of "interlocking gear" analogy, that describes the interactions between three alpha chains, and the interactions between the level-1 and level-2 helices. The inter-chain hydrogen bonds play an integral role in both instances. Another important result reported here, is that the interchain hydrogen bond energy in the

full length collagen is significantly smaller than the overall interchain nonbonded interaction energies, suggesting that the nonbonded interactions have far more important role than hydrogen bonds in the mechanics of collagen. However, hydrogen bonding is essential for the triple helical conformation of the collagen. Hence, the mechanics of collagen is controlled by nonbonded interchain interaction energies while the confirmation is attributed to the interchain hydrogen bonding.

6.5. Acknowledgements

The authors acknowledge NCSA Teragrid and NDSU Center for High Performance Computing (CHPC) for computational resource. The authors thank Dr. Greg Wettstein for hardware and software support at CHPC. Author SMP acknowledges support from ND EPSCOR.

6.6. References

1. Weiner, S.; Wagner, H. D., The material bone: structure-mechanical function relations. *Annual Review of Materials Science* **1998,** 28, 271-298.
2. Weiner, S.; Addadi, L., Acidic macromolecules of mineralized tissues: the controllers of crystal formation. *Trends in biochemical sciences* **1991,** 16, (7), 252-6.
3. Ghosh, P.; Katti, D. R.; Katti, K. S., Mineral Proximity Influences Mechanical Response of Proteins in Biological Mineral-Protein Hybrid Systems. *Biomacromolecules* **2007,** 8, (3), 851-856.
4. Ghosh, P.; Katti, D. R.; Katti, K. S., Mineral and protein-bound water and latching action control mechanical behavior at protein-mineral interfaces in biological nanocomposites. *Journal of Nanomaterials* **2008**.

5. Bhattacharjee, A.; Bansal, M., Collagen Structure: The Madras Triple Helix and the Current Scenario. *IUBMB Life* **2005,** 57, (3), 161-172.

6. Fratzl, P.; Weinkamer, R., Nature's hierarchical materials. *Progress in Materials Science* **2007,** 52, (8), 1263-1334.

7. Hodge, A. J.; Petruska, J. A., Recent studies with the electron microscope on ordered aggregates of the tropocollagen molecule. In *Aspects of Protein Structure*, Ramachandran, G. N., Ed. Academic Press: New York, 1963; pp 289-300.

8. Rubin, M. A.; Rubin, J.; Jasiuk, W., SEM and TEM study of the hierarchical structure of C57BL/6J and C3H/HeJ mice trabecular bone. *Bone* **2004,** 35, (1), 11-20.

9. Landis, W. J.; Hodgens, K. J.; Arena, J.; Song, M. J.; McEwen, B. F., Structural relations between collagen and mineral in bone as determined by high voltage electron microscopic tomography. *Microscopy research and technique* **1996,** 33, (2), 192-202.

10. Landis, W. J.; Hodgens, K. J.; Song, M. J.; Arena, J.; Kiyonaga, S.; Marko, M.; Owen, C.; McEwen, B. F., Mineralization of collagen may occur on fibril surfaces: evidence from conventional and high-voltage electron microscopy and three-dimensional imaging. *Journal of structural biology* **1996,** 117, (1), 24-35.

11. Landis, W. J.; Song, M. J.; Leith, A.; McEwen, L.; McEwen, B. F., Mineral and organic matrix interaction in normally calcifying tendon visualized in three dimensions by high-voltage electron microscopic tomography and graphic image reconstruction. *Journal of structural biology* **1993,** 110, (1), 39-54.

12. Weiner, S.; Traub, W.; Wagner, H. D., Lamellar bone: structure-function relations. *Journal of structural biology* **1999,** 126, (3), 241-55.

13. Katti, D. R.; Pradhan, S. M.; Katti, K. S., Directional dependence of hydroxyapatite-collagen interactions on mechanics of collagen. *Journal of Biomechanics* **2010,** 43, (9), 1723-1730.

14. Bhowmik, R.; Katti, K. S.; Katti, D. R., Mechanics of molecular collagen is influenced by hydroxyapatite in natural bone. *Journal of Materials Science* **2007,** 42, (21), 8795-8803.

15. Bhowmik, R.; Katti, K. S.; Katti, D. R., Mechanisms of Load-Deformation Behavior of Molecular Collagen in Hydroxyapatite-Tropocollagen Molecular System: Steered Molecular Dynamics Study. *Journal of Engineering Mechanics-Asce* **2009,** 135, (5), 413-421.

16. Dubey, D. K.; Tomar, V., Effect of changes in tropocollagen residue sequence and hydroxyapatite mineral texture on the strength of ideal nanoscale tropocollagen-hydroxyapatite biomaterials. *Journal of Materials Science-Materials in Medicine* **2010,** 21, (1), 161-171.

17. Almora-Barrios, N.; de Leeuw, N. H., A Density Functional Theory Study of the Interaction of Collagen Peptides with Hydroxyapatite Surfaces. *Langmuir* **2010,** 26, (18), 14535-14542.

18. Hellmich, C.; Barthelemy, J. F.; Dormieux, L., Mineral-collagen interactions in elasticity of bone ultrastructure - a continuum micromechanics approach. *European Journal of Mechanics a-Solids* **2004,** 23, (5), 783-810.

19. Fritsch, A.; Hellmich, C.; Dormieux, L., Ductile sliding between mineral crystals followed by rupture of collagen crosslinks: Experimentally supported micromechanical explanation of bone strength. *Journal of Theoretical Biology* **2009,** 260, (2), 230-252.

20. Streeter, I.; de Leeuw, N. H., Atomistic Modeling of Collagen Proteins in Their Fibrillar Environment. *Journal of Physical Chemistry B* **2010,** 114, (41), 13263-13270.

21. Vuong, J.; Hellmich, C., Bone fibrillogenesis and mineralization: Quantitative analysis and implications for tissue elasticity. *Journal of Theoretical Biology* **2011,** 287, 115-130.

22. Ramachandran, G. N.; Kartha, G., Structure of collagen. *Nature* **1955,** 176, (4482), 593-595.

23. Orgel, J. P.; Miller, A.; Irving, T. C.; Fischetti, R. F.; Hammersley, A. P.; Wess, T. J., The in situ supermolecular structure of type I collagen. *Structure* **2001,** 9, (11), 1061-1069.

24. Bella, J.; Eaton, M.; Brodsky, B.; Berman, H. M., Crystal and molecular structure of a collagen-like peptide at 1.9 A resolution. *Science* **1994,** 266, (5182), 75-81.

25. Gautieri, A.; Vesentini, S.; Montevecchi, F. M.; Redaelli, A., Mechanical properties of physiological and pathological models of collagen peptides investigated via steered molecular dynamics simulations. *Journal of Biomechanics* **2008,** 41, (14), 3073-3077.

26. Gautieri, A.; Buehler, M. J.; Redaelli, A., Deformation rate controls elasticity and unfolding pathway of single tropocollagen molecules. *Journal of the Mechanical Behavior of Biomedical Materials* **2009,** 2, (2), 130-137.

27. Lorenzo, A. C.; Caffarena, E. R., Elastic properties, Young's modulus determination and structural stability of the tropocollagen molecule: a computational study by steered molecular dynamics. *Journal of Biomechanics* **2005,** 38, (7), 1527-1533.

28. Pradhan, S., M.; Katti, D. R.; Katti, K. S., Steered Molecular Dynamics Study of Mechanical Response of Full Length and Short Collagen Molecules. *Journal of Nanomechanics and Micromechanics* **2011,** 1, (3), 104-110.

29. Uzel, S. G. M.; Buehler, M. J., Nanomechanical sequencing of collagen: tropocollagen features heterogeneous elastic properties at the nanoscale. *Integrative Biology* **2009,** 1, (7), 452-459.

30. Gautieri, A.; Russo, A.; Vesentini, S.; Redaelli, A.; Buehler, M. J., Coarse-Grained Model of Collagen Molecules Using an Extended MARTINI Force Field. *Journal of Chemical Theory and Computation* **2010,** 6, (4), 1210-1218.

31. Berisio, R.; Vitagliano, L.; Mazzarella, L.; Zagari, A., Crystal structure of the collagen triple helix model [(Pro-Pro-Gly)10]3. *Protein Science* **2002,** 11, (2), 262-270.

32. Jorgensen, W. L.; Chandrasekhar, J.; Madura, J. D.; Impey, R. W.; Klein, M. L., Comparison of simple potential functions for simulating liquid water. *J.Chem.Phys* **1983,** 79, 926-935.

33. Kale, L.; Skeel, R.; Bhandarkar, M.; Brunner, R.; Gursoy, A.; Krawetz, N.; Phillips, J.; Shinozaki, A.; Varadarajan, K.; Schulten, K., NAMD2: Greater Scalability for Parallel Molecular Dynamics. *Journal of Computational Physics* **1999,** 151, (1), 283-312.

34. Humphrey, W.; Dalke, A.; Schulten, K., VMD: Visual molecular dynamics. *Journal of Molecular Graphics* **1996,** 14, (1), 33-&.

35. Feller, S. E.; Zhang, Y. H.; Pastor, R. W.; Brooks, B. R., Constant-pressure molecular-dynamics simulation - the langevin piston method. *Journal of Chemical Physics* **1995,** 103, (11), 4613-4621.

36. Martyna, G. J.; Tobias, D. J.; Klein, M. L., Constant-pressure molecular-dynamics algorithms. *Journal of Chemical Physics* **1994,** 101, (5), 4177-4189.

37. Sugeta, H.; Miyazawa, T., General method for calculating helical parameters of polymer chains from bond lengths bond angles and internal-rotation angles. *Biopolymers* **1967,** 5, (7), 673-&.

38. Ramachandran, G. N., Structure of collagen. *Nature* **1956,** 177, (4511), 710-711.

39. Ramachandran, G. N.; Bansal, M.; Ramakrishnan, C., Hydroxyproline stabilizes both intrafibrillar structure as well as inter-protofibrillar linkages in collagen. *Current Science* **1975,** 44, (1), 1-3.

40. Ramachandran, G. N.; Chandrasekharan, R., Interchain hydrogen bonds via bound water molecules in the collagen triple helix. *Biopolymers* **1968,** 6, (11), 1649-1658.

41. Orgel, J. P. R. O.; Irving, T. C.; Miller, A.; Wess, T. J., Microfibrillar structure of type I collagen in situ. *Proceedings of the National Academy of Sciences* **2006,** 103, (24), 9001-9005.

42. Wess, T. J., Collagen fibrillar structure and hierarchies. In *Collagen Structure and Mechanics*, Fratzl, P., Ed. Springer US: 2008; pp 40-80.

43. Fratzl, P.; Misof, K.; Zizak, I.; Rapp, G.; Amenitsch, H.; Bernstorff, S., Fibrillar Structure and Mechanical Properties of Collagen. *Journal of Structural Biology* **1998,** 122, (1–2), 119-122.

44. Diamant, J.; Keller, A.; Baer, E.; Litt, M.; Arridge, R. G. C., Collagen; Ultrastructure and Its Relation to Mechanical Properties as a Function of Ageing. *Proceedings of the Royal Society of London. Series B, Biological Sciences* **1972,** 180, (1060), 293-315.

CHAPTER 7. A MULTISCALE MODEL OF COLLAGEN FIBRIL IN BONE: ELASTIC RESPONSE

This chapter discussed multiscale modeling of collagen fibril that bridges molecular model with the finite element model of fibril. The effect of mineral proximity on the elastic response of collagen fibril has also been elucidated in this study. The content of the chapter is in print in Pradhan, S., Katti, K., and Katti, D. (2012). "A Multiscale Model of Collagen Fibril in Bone: Elastic Response." Journal of Engineering Mechanics.

7.1. Introduction

The collagen molecule and mineral are the fundamental constituents of bone at the molecular scale, which are organized into the structure known as collagen fibril. The collagen fibrils assemble into collagen fiber, which further organize to form concentric lamella followed by higher hierarchical structure, the osteon until we get to the scale of the functional bone. Thus, bone is a biological nanocomposites with a highly organized hierarchical morphology spanning multiple length scales, which makes it a complicated material for investigating deformation mechanism under mechanical load. Bone is a part of skeletal system which has the structural roles of protecting and supporting softer tissues and organs. The non-structural functions of bone include production of red and white blood cells, and storage of minerals such as calcium and phosphorous. Morphologically bone is generally comprised of a dense and strong external layer known as cortical bone around an interior spongy cancellous bone. The mineral phase and organic phase, are the two major constituents of bone- 65% and 25% respectively by

weight [1-5], and 33-43% and 32-44% respectively by volume [1,6], while the remaining weight/volume fraction is occupied by water. Collagen constitutes majority of the organic phase that can be up to 85-95% of the total bone protein [7]. The other organic materials include lipids and non-collageneous proteins such as phosphoproteins.

The collagen molecules in bone are organized into parallel arrays along the longitudinal axis of bone, and staggered with respect to each other by 67 nanometers as shown in figure 1. The molecules assemble into long and cylindrical structural units known as collagen fibril, which are the building blocks of bone [8]. The staggering between collagen molecules result in a 40 nm hole zone between the opposite ends of collagen molecule (i.e. N-terminus and C-terminus) and the 27 nm overlap-zone between the ends of overlapping collagen molecules [9,10]. The overlap and hole zone are visible as consecutive stripes along the length of fibril in electron micrographs. Collagen fibrils are long and cylindrical structures typically 50 to 200 nanometers in diameter [11,12] and unknown length because they merge with neighboring fibrils [13]. The mineralized collagen fibril consists of hydroxyapatite in the hole zone with its c-axis aligned parallel to the long axis of collagen. The hydroxyapatite nucleating in the hole zone grow in size along c-axis and width along channel, and also squeeze between the collagen in overlap zone often forming large extended sheets [9,14-17]. In addition to the intrafibrillar mineral found in the hole zone, an appreciable amount of the mineral is found outside of fibril [18,19].

There are number of modeling studies on the deformation mechanisms of collagen fibril [20-23]. The Young's modulus of collagen fibril estimated by Buehler [24], Tang et al. [23], and Gautieri et al. [25] from their modeling studies for small-strain are 4.36 GPa, 5 GPa, and 0.3 Gpa respectively. The experiments performed on different collagen

fibrils show following values of Young's modulus: 0.5-3.2 GPa [26], 0.86 ± 0.45 GPa [27], 0.2-0.8 GPa [28], 3.7-11.5 GPa [29]. In addition to these modeling and experimental studies, there are number of studies based on molecular dynamics [30-34], density functional theory [35] and continuum micromechanics theory [36,37] that have explored collagen-hydroxyapatite interactions or inclusions in bone. An atomistic study of collagen proteins in collagen fibril is carried out by Streeter and de Leeuw [38,39].

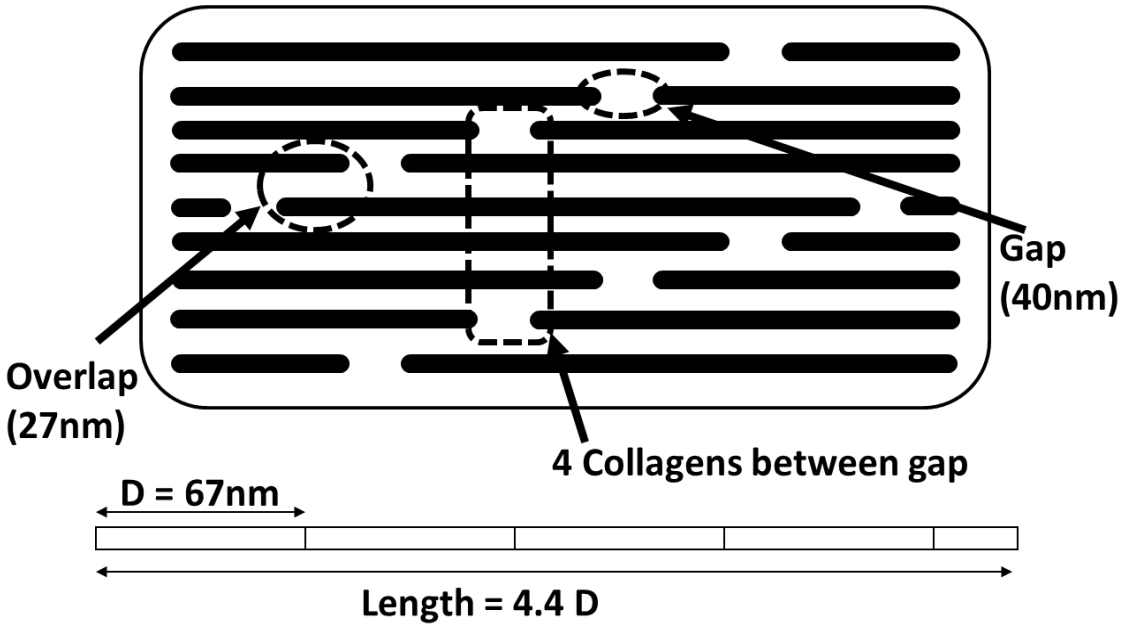

Figure 7.1. Organization of collagen molecules in collagen fibril showing stagger of 67 nanometers and hole zone.

The organization of collagen and mineral within collagen fibril gives rise to the significant interfaces between the constituents at the molecular scale. The interfaces between organic and mineral at molecular scale have been shown to have a significant effect on the deformation behavior of organic as seen in number of our previous studies

involving various biological and synthetic materials [40-42]. Similar behavior has been observed in our molecular dynamics studies of collagen-hydroxyapatite interface, wherein the mechanical response of collagen was found to be significantly enhanced in the proximity of mineral [32-34]. The study of the directional dependence of collagen deformation in mineral proximity and the influence of different (100) and (001) surfaces of hydroxyapatite are discussed in Katti et al. [34]. The molecular studies discussed above indicate the possibility that the properties of collagen-mineral interface and the altered mechanical behavior of collagen in the mineral proximity significantly affect the deformation characteristics of collagen fibril and higher levels of hierarchy in bone. Hence, the mechanical properties at the molecular scale must be passed on to the finite element model of collagen-fibril to correctly model its mechanical behavior. This can be achieved by multiscale modeling of collagen fibril that links the interactions at the molecular scale to the mechanical response of collagen fibril. This bottom-up approach used in this study is known as hierarchical multiscale modeling.

In this study we show that it is important to incorporate the effect of molecular interactions between hydroxyapatite and collagen on the mechanics of collagen into the multiscale model that aims to bridge the deformation behavior of collagen molecule with that of fibril. Here we develop the multiscale model of collagen fibril based on a hierarchical scheme by exporting the molecular-scale mechanical properties, obtained from the steered molecular dynamics simulations, into the finite element model of fibril. Our multiscale model bridges the molecular properties of collagen with the continuum model of fibril, and for the first time allows us to understand the role of collagen-mineral interactions in the deformation response of collagen fibril. We believe such an approach

can be very useful for modeling the behavior of host of other biomaterials, tissues, and nanocomposites and shed light on how the molecular interactions affect the material properties at higher length scales [40,42-45].

7.2. Model Construction and Simulation Details

The development of hierarchical multiscale model of collagen fibril involves bridging the molecular properties of collagen to the continuum model of collagen fibril. At the molecular scale the behavior of collagen is simulated using molecular dynamics. Steered molecular dynamics is used to stretch the collagen molecule and evaluate its elastic properties in the presence and absence of mineral proximity under different pulling conditions that simulate the environment of collagen molecule within the collagen fibril. The three dimensional model of collagen fibril is built using finite element method. The finite element model of collagen fibril makes use of the material properties of the collagen molecules evaluated from molecular simulations.

7.2.1. Molecular Model

The glycine-proline-proline model of collagen is obtained from Brookhaven Protein Date Bank (PDB ID: 1k6f). This structure is used to build a full-length collagen approximately 300 Å long and consisting of 1024 residues along each chain. The structure is minimized using CHARMM [46] force field using the conjugate gradient method. The molecule is solvated with TIP3P water molecules and is minimized again. The temperature of the minimized molecule was raised using the steps of 100 K to 300K and the pressure was raised using the steps of 0.25 bar to 1.01 bar. The equilibrated collagen molecule is fixed at one end and extended with the pulling rate of 0.00003 ps^{-1} (i.e. pulling velocity of 0.0975 Å/ps, or 9.75 m/s) using steered molecular dynamics for

estimating the elastic modulus of collagen. The utilization of the same pulling rate (expressed in the unit of strain rate), rather than same pulling velocity, ensures that the loading conditions are similar when collagen molecules of different lengths are pulled as shown by Pradhan et al. [47]. The harmonic spring of spring constant 0.1 kcal/mol/Å^2 was used for pulling the full-length collagen molecule.

The hydroxyapatite used in the study has a hexagonal structure with the space group $P6_3/m$ [48] and unit cell parameters a = 9.424 A˚ , b = 9.424 A˚ , c = 6.879 A˚, α = 90˚, β = 90˚, and γ = 120˚. The details of the development of hydroxyapatite model and the non-dipolar surfaces using reconstruction method described by Taskar [49] is discussed in Bhowmik et al. [32,50]. The CHARMM force field parameters of HAP was obtained from Bhowmik et al [50], which are given in table 7.1 and 7.2. Two surfaces of hydroxyapatite are used in this study: (100) and (001). For the construction of collagen-hydroxyapatite models, the minimized structure of solvated collagen is brought in the proximity of mineral surface. This collagen-hydroxyapatite model is geometrically optimized by energy minimization. The temperature and pressure are then raised to 300 K and 1.01 bar using steps of 100 K and 0.25 bar respectively. In bone the collagen molecules are aligned along the c-axis of hydroxyapatite [51,52]. Therefore the (001) hydroxyapatite surface is used for investigating the deformation response of collagen molecule pulled perpendicular the mineral surface. The (100) surface of hydroxyapatite is used for evaluating deformation response of collagen pulled parallel to the mineral surface. Further information on the steered dynamics study of collagen in the proximity of different mineral surfaces and pulled in different directions can be found in our previous

work [32,34]. The models of collagen pulled under different conditions are shown in figure 7.2.

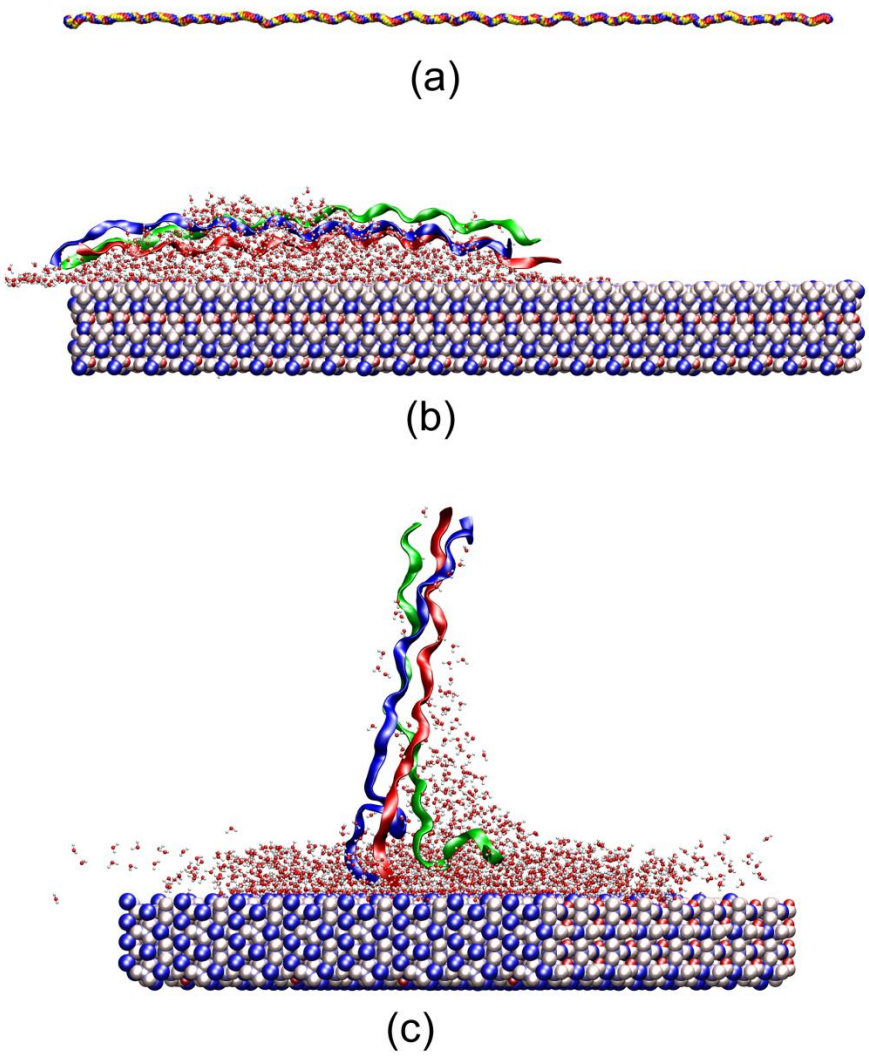

Figure 7.2. Molecular models of collagen pulled under different conditions: (a) full-length collagen molecule pulled under no influence of mineral, (b) collagen molecule pulled parallel to the hydroxyapatite (100) surface, (c) collagen molecule pulled normal to hydroxyapatite (001) surface.

Table 7.1. Van der Waals parameters of hydroxyapatite [50]

	ε_{ii}	r_{ii}^*
Ca	0.118630403	3.301533011
H	0.000012146	1.55
O(H)	0.11703	3.471655906
O(P)	0.25201	3.40391668
P	0.97406	3.91251096

Table 7.2. Bonded parameters of hydroxyapatite [50]

Bonded atoms	Bonded parameters
P-O	K_b = 254.00 kcal $mol^{-1}Å^{-2}$, b_0= 1.53 Å
O-P-O	K_b = 6.83 kcal $mol^{-1}deg^{-2}$, θ_0= 109.5º
O-H	K_b = 524.34 kcal $mol^{-1}Å^{-2}$, b_0= 0.96 A° Å

Elastic parameters of collagen are determined from the steered molecular dynamics study of collagen extended using a pulling rate of 0.00003 ps^{-1} (i.e. pulling velocity of 0.0026 Å/ps, or 0.26 m/s). The steered molecular dynamics is carried out by fixing one end of a molecule and pulling the molecule at constant velocity using a harmonic spring of spring constant 4 kcal/mol/$Å^2$. The approximate diameter of collagen was determined based on the cylinder enclosing Van der Waals radius of molecule, similar to the method used by other researchers [53,54]. This diameter is used to compute the average stress over the cross-sectional area of the collagen molecule for the computation of elastic modulus. Elastic modulus was computed from the force-displacement response of collagen by considering the small displacement regime of up to

7% by using the relation $E = k \times L/A$, where 'k' is the stiffness of load-displacement response, 'L' is the length of collagen molecule, 'A' is the cross sectional area of collagen. This method was employed for collagen in the proximity of mineral, as well as the collagen by itself.

For determining shear parameters, the region between collagen molecules and between collagen and mineral is termed "interlayer". The interlayer is responsible for the transfer of shear between the molecules. The thickness of interlayer necessary for the calculation of shear modulus is estimated from the molecular dynamics study by approximating the distance between Van der Waals surfaces of two molecules. This thickness is used for calculation of shear strain. The shear modulus is computed from the region of load-displacement curve before slipping/failure occurs between collagen molecules or between collagen and mineral. The shear modulus was calculated using a simplistic approach. The relation for shear modulus used is $G = k \times d/A$, where 'k' is the stiffness of load displacement response before the sliding event, 'd' the average distance between the collagen and mineral surface, 'A' is the contact area between the molecules. For the calculation of shear force between the collagen molecules, the molecule to be pulled is surrounded by six other collagen molecules to mimic quasihexagonal packing of collagen molecules [55], as shown in figure 7.3. The average distance between the collagen molecule at the center and surrounding molecules estimated from our molecular model is 15.75 Å. The backbone of surrounding molecules is fixed and the center molecule is pulled at the constant rate of 0.00003/ps. The area of cylinder midway between the center collagen molecule and surrounding collagen molecule was used for estimation of average shear stress. As for the evaluation of shear modulus between the collagen and mineral,

the collagen was pulled parallel to the surface of mineral using steered molecular dynamics. When pulling collagen molecule next to the mineral surface one of the ends of collagen molecule is not fixed unlike during the evaluation of elastic modulus. As for the estimation of the interfacial surface area between collagen and mineral, the collagen is enclosed in a cylinder that passes through the midpoint of the gap between collagen and mineral Van der Waals surfaces. The interfacial area for calculation of shear stress is assumed to be one-fourth of the surface area of the cylinder.

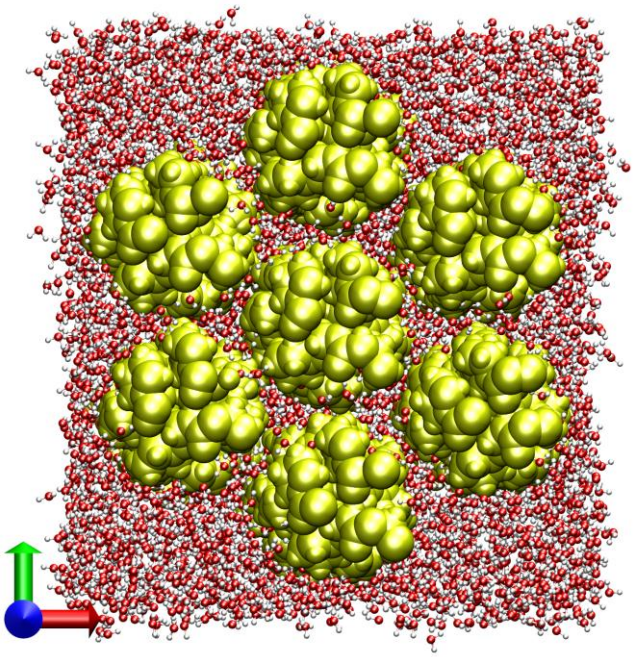

Figure 7.3. Molecular model of collagen molecules arranged in a quasihexagonal fashion, where the center molecule is pulled with respect to the surrounding molecules.

7.2.2. Finite Element Model

The finite element model of collagen fibril was carried out using MSC Mentat 2008, preprocessor/postprocessor of MSC Marc. The construction of finite element model of fibril starts with a single collagen molecule of 294.8 nanometers length, which is assumed to have a square cross section. Apart from the length of collagen, the other dimensions used to construct this model were obtained from Landis et al. [9]. The collagen molecule is built using the eight noded isoparametric elements and meshed manually so that the adjacent nodes fall in the same location when the collagen is duplicated and staggered by 67 nanometers. The duplicate nodes formed due to overlapping of nodes are swept away routinely. The initial collagen is encapsulated by the elements representing an interlayer, and the mineral is attached to the end of collagen. This unit is duplicated 33 times in the x-direction to obtain an array of collagen molecules. This array of collagen is duplicated in the y-direction 33 times with the stagger of 67 nanometers along z-direction. The entire block is then duplicated 13 times in the z-direction. After this step, the fibril of length 1.005 micron is selected and the remaining elements are deleted. Furthermore, the additional collagen molecules are removed so that the cross-section is circular in shape. This results in a model of fibril with 34 × 34 collagen molecules along the diameter as shown in figure 7.4. The banded pattern due to stagger between collagen molecules is also seen in the model. The resulting finite element model of fibril model consists of 4,325,922 elements. This model consists of mineral layers aligned parallel to each other over the circular cross section. This arrangement is similar to the to the parallel crystal layers of hydroxyapatite seen in mineralized turkey tendon and some bones [9,13,16,56]. The mineral plates located in the hole zone are 40 nm wide and 1.23 nm

thick. The gap between collagen molecules in our model is 2.4 Å, which is taken from Landis et al (Landis, et al., 1993). The gap "between collagen molecules" and "between collagen and mineral" in our finite element model are assigned the shear properties obtained from steered molecular dynamics. Similarly, the elastic modulus of collagen for finite element model is obtained from steered molecular dynamics simulations discussed above. The elastic modulus of hydroxyapatite, determined from nanoindentation test, obtained from literature is 150.38 GPa [57]. For carrying out finite element simulation of collagen fibril the symmetry of the model was exploited to reduce computational resources. The simulations were carried out using half of the circular cross-section by restraining the displacement of nodes in the plane of symmetry (i.e central yz-plane) in the x-direction.

Two separate finite element models of collagen fibril were constructed. In the first model the collagen is assigned the same elastic modulus throughout its length. The elastic modulus of collagen for this model is determined from the steered molecular dynamics simulation of a collagen not in the proximity of mineral. This model does not take into account the enhancement in the elastic properties of collagen in the mineral proximity. However, in the second model the portions of collagen molecule in the proximity of mineral is assigned the elastic modulus of collagen pulled normal and parallel to mineral surface as shown in figure 7.5. All simulations were carried out in the small displacement regime. For finite element simulation, the bottom nodes of the model are fixed and the maximum stress of 2 pN/Å^2 (i.e. 200 MPa) is applied to the top surface of collagen fibril in 10 increments.

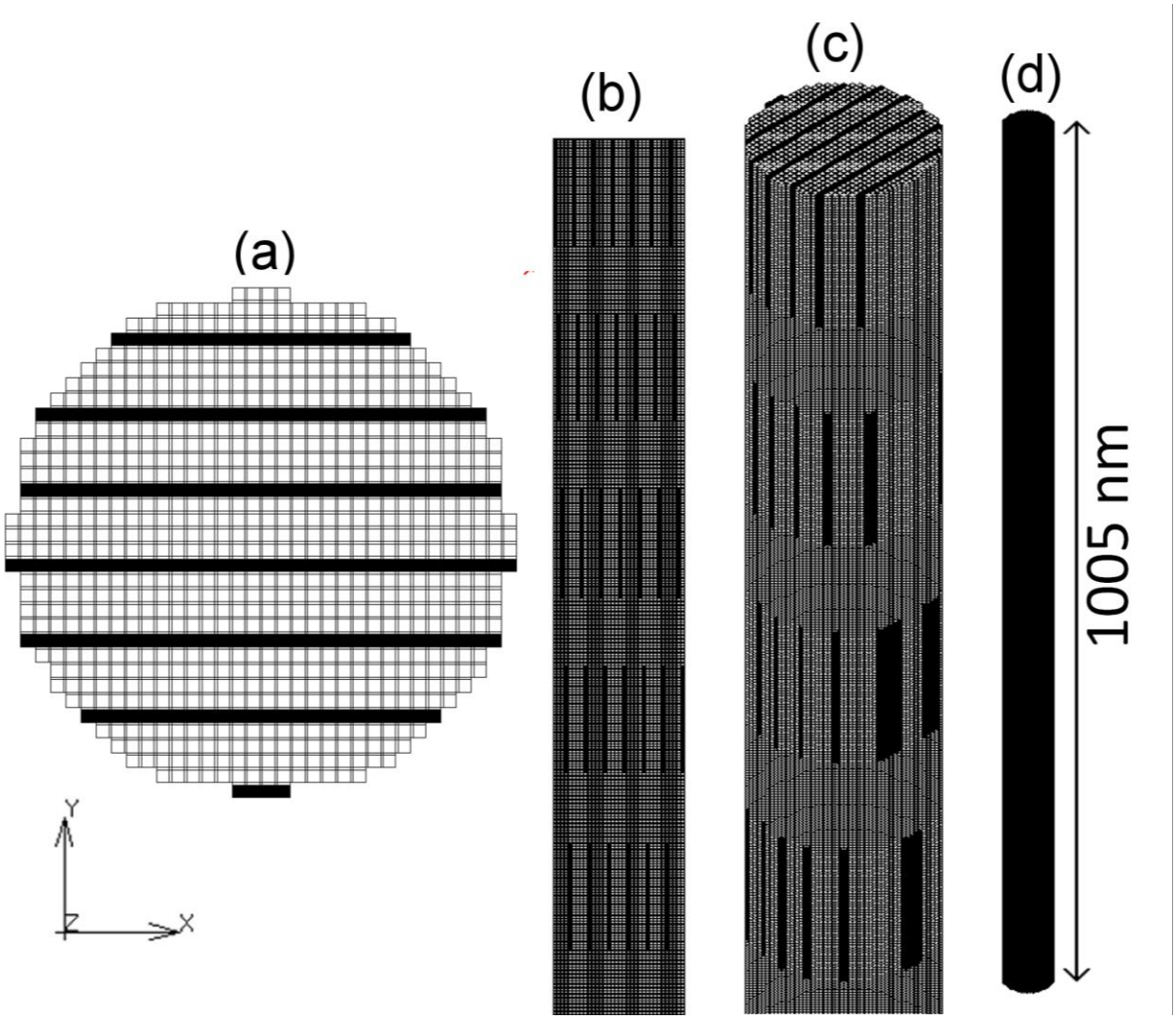

Figure 7.4. Finite element model of collagen fibril: (a) cross sectional view showing collagen molecules and mineral plates (in black), (b) section through the center of collagen fibril showing a banded pattern due to gap and overlap regions, (c) isometric view, (d) entire collagen fibril model (mesh not visible due to large number of elements).

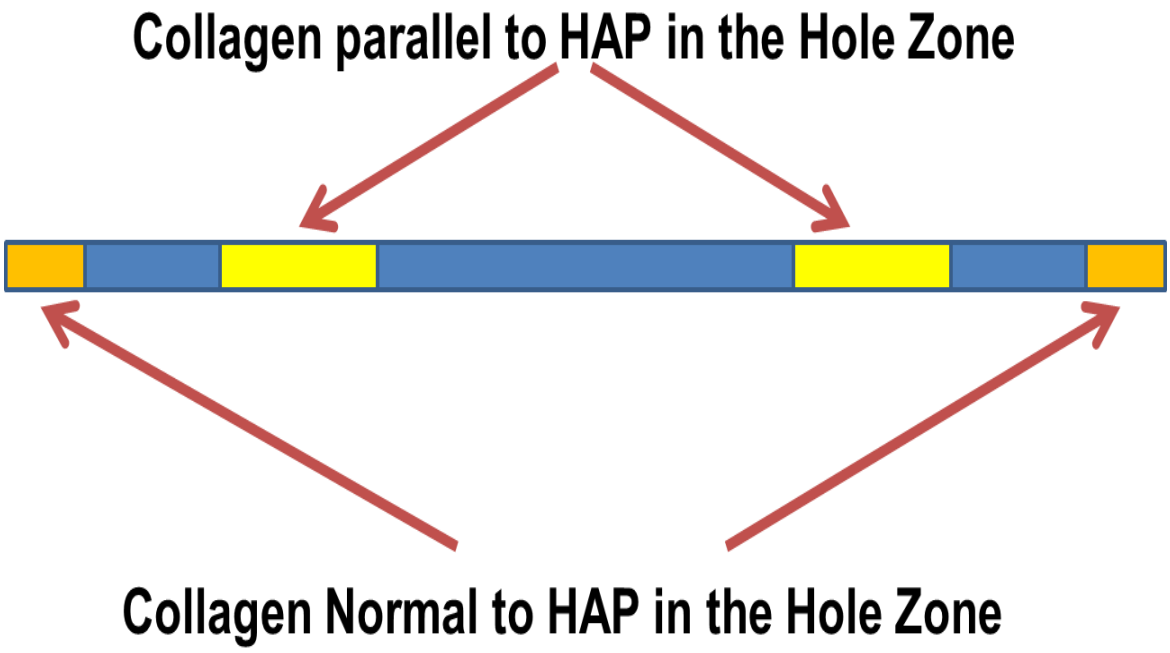

Figure 7.5. The figure showing strips of collagen molecule in the proximity of hydroxyapatite.

7.3. Results and Discussion

Steered molecular dynamics simulations are used to simulate deformation response of collagen molecules in the proximity of mineral and in the absence of mineral. In the proximity of mineral the collagen is the pulled next to (100) and (001) surfaces of hydroxyapatite.The elastic modulus is evaluated from load-displacement response obtained from steered molecular dynamics by considering a small displacement regime of up to 7%. The elastic modulus of collagen for different pulling conditions is presented in table 7.3. The elastic modulus values suggest that the mineral proximity has a significant influence on the deformation mechanism of collagen [34]. The collagen pulled parallel to the mineral (100) surface is found to have the highest elastic modulus of 13.17 GPa,

followed by the collagen pulled perpendicular to (001) mineral surface with elastic modulus of 6.26 GPa; whereas, the collagen not in the proximity of mineral has an elastic modulus of 2.95 GPa. This shows that the elastic modulus of collagen is significantly higher in the proximity of mineral. This has important implications for modeling the mechanical response of the bone, as it has substantial interfacial area between collagen and hydroxyapatite. In the case of collagen fibril, the collagen molecules interface with intrafibrilar minerals present in the hole zone which are 40 nanometers wide (Fig. 7.1). It is observed that at least 27% of the lengths of collagen molecules are in the proximity of mineral within the collagen fibril. This suggests that the effect of mineral proximity on the mechanical response of collagen cannot be overlooked, and must be included in the multiscale model of collagen fibril.

Table 7.3. Elastic Modulus of collagen estimated from steered molecular dynamics at various pulling conditions

Pulling Conditions of Collagen	**Elastic Modulus (GPa)**
Collagen	2.95
Collagen in the proximity of hydroxyapatite (100) surface (pulled parallel to surface)	13.17
Collagen in the proximity of hydroxyapatite (001) surface (pulled normal to surface)	6.26

The load-displacement response of the shearing between collagen molecules is shown in figure 7.6. The load displacement response shows an initial region where there is no sliding between collagen molecules followed by the region where the molecules start to slide with respect to each other. The shear property of interlayer is estimated from

the steered molecular dynamics by considering the initial region of load-displacement response before the sliding occurs. Similar load-displacement response was observed when collagen was pulled parallel to the mineral surface. The shear modulus of interlayer between collagen molecules and between collagen and mineral (100) surface, estimated using a method described in the previous section, is shown is Table 7.4. It is observed that the shearing resistance between the collagen and mineral is significantly higher than between collagen molecules.

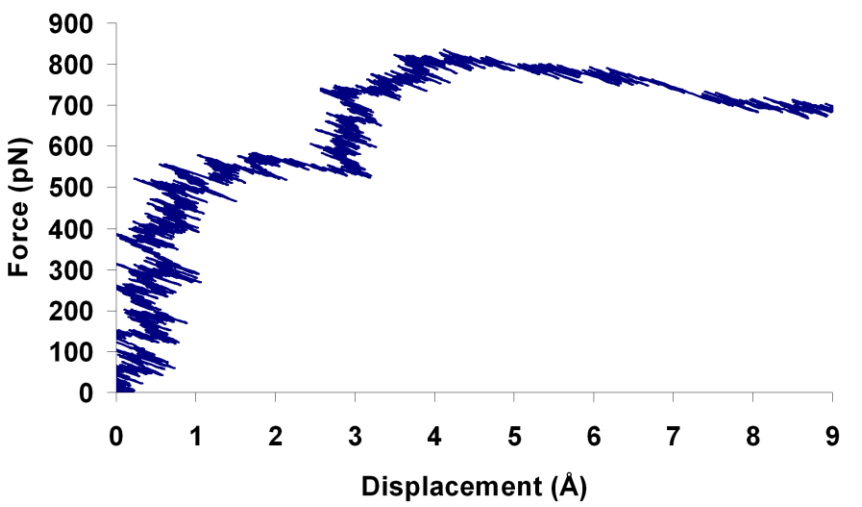

Figure 7.6. Force-displacement response of the shearing between collagen molecules.

Table 7.4. Shear properties of the interlayer between collagen molecules and between collagen and mineral

Interlayer	**Shear Modulus (GPa)**
Between Collagen Molecules	0.007
Between Collagen and Mineral	0.094

The load displacement responses of finite element models of collagen fibril are shown in figure 7.7. The second model of collagen fibril that incorporates the enhanced elastic modulus of collagen due to mineral proximity is found to show stiffer response compared to the first model that does not take into account the effect of mineral proximity. The axial strain at the maximum load of 2 pN/Å^2 and the elastic modulus of the collagen fibril models are shown in Table 7.5. The first model shows the higher maximum axial strain of 0.049 compared to 0.041 exhibited by the second model. Furthermore, the second fibril model shows an approximately 20% higher elastic modulus of 4.81 GPa compared to 4.01 GPa for the first fibril model, i.e. the elastic modulus of fibril is substantially greater when we take into account the effect of mineral proximity on collagen modulus. This shows that the molecular interaction between collagen and mineral significantly alters the mechanical response of collagen fibril in bone. The elastic modulus values for small strain obtained from our simulations are close to the experimental results of mineralized collagen fibril: 0.5 (low mineral content) to 3.2 GPa (high mineral content) [26]. It is also close to the small-strain elastic modulus of 4.36 GPa [24], 6.23 GPa for mineralized fibril [21] estimated from the modeling study.

Table 7.5. Strain at the applied load of 2 pN/Å^2 and the elastic modulus of collagen fibril from finite element simulations, when the influence of mineral on collagen molecule is considered and not considered

Finite Element Analysis	**Strain @ 2 pN/Å^2**	**Elastic Modulus (GPa)**
No influence of HAP on Collagen	0.049	4.01
Influence of HAP on Collagen	0.041	4.81

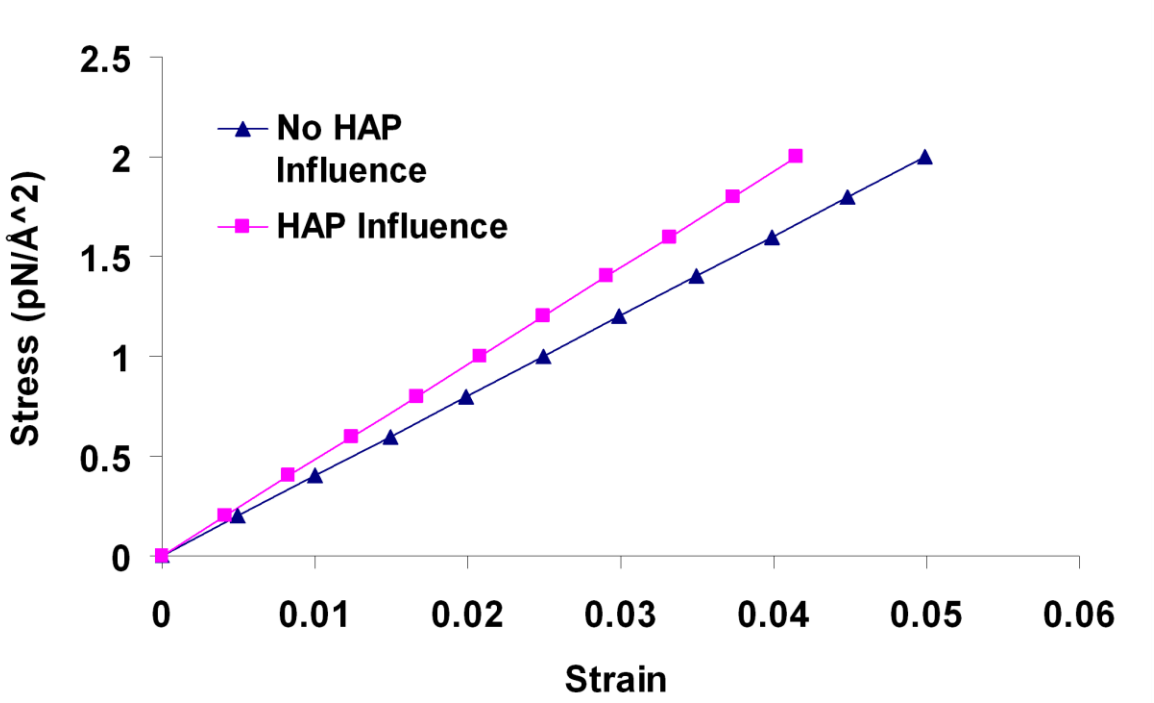

Figure 7.7. Stress-strain response of the finite element models collagen fibril when the influence of mineral proximity on collagen modulus is (i) not taken into consideration, and (ii) is considered.

The strain contour in the longitudinal section passing through center of collagen fibril under the tensile load of 2 pN/Å^2 is shown in figure 7.8. It is observed that the strain distribution imitates the characteristic banded appearance of collagen fibril. The strain in the overlap region is found to be greater compared to the mineral rich gap region. Higher strain energy density is also found in the overlap region as shown in figure 7.9. Strain energy density also follows a periodic pattern exhibited by strain contour. The larger strain and strain energy density in the overlap zone indicates that this region is plays an important role in the deformation mechanism of collagen fibril in the small displacement regime.

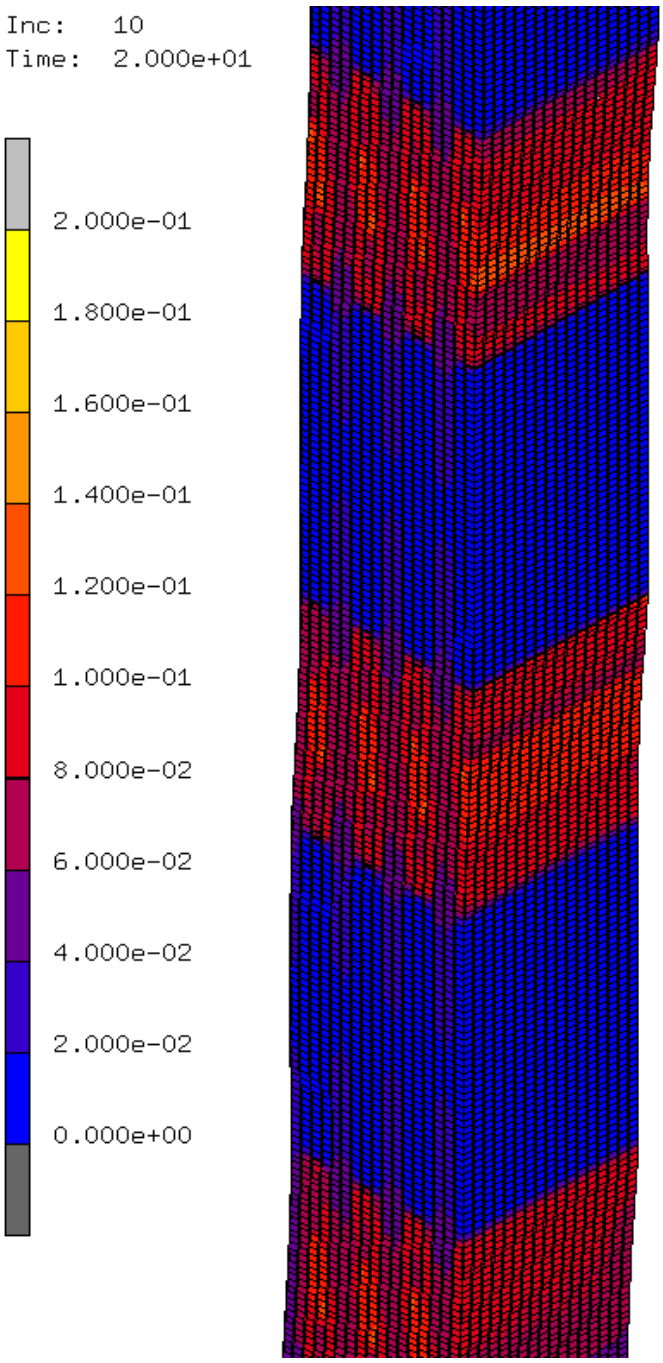

Figure 7.8. Strain contour (units: Å/Å).at the central section of collagen fibril.

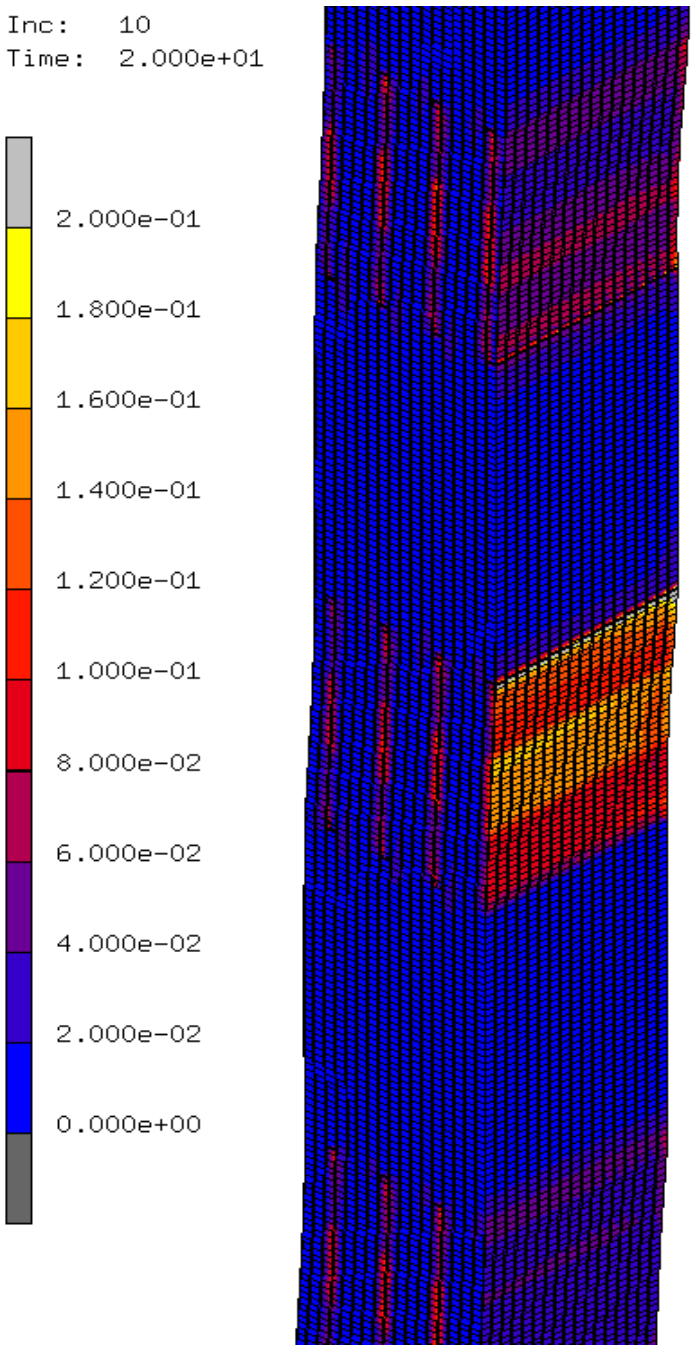

Figure 7.9. Strain energy density contour (units: pN/Å^2).at the central section of collagen fibril.

7.4. Summary and Conclusions

We have carried out hierarchical multiscale modeling of collagen fibril by combining molecular dynamics and finite element methods. The molecular models of collagen and hydroxyapatite systems are constructed and the deformation response of collagen is studied using steered molecular dynamics by employing a low pulling rate of 0.00003/ps. Our steered molecular dynamics study show that the elastic modulus of collagen is significantly enhanced in the proximity of mineral. The elastic modulus of collagen not in the proximity of mineral is found to be 2.95 GPa, whereas the collagen molecule pulled normal to hydroxyapatite (001) surface, and pulled parallel to hydroxyapatite (100) surface are found to be 6.26 GPa, and 13.17 GPa respectively. Series of steered molecular dynamics studies were also carried out to investigate the shear properties of the interface between the collagen molecules and between the collagen and mineral. The shearing resistance of the interlayer between the collagen molecule and mineral is found to be higher than between the collagen molecules. The finite element models of collagen fibril measuring a micrometer in length and 50 nanometers in diameter are built. The properties of collagen molecules and interfaces determined from steered molecular dynamics are incorporated in this model. The simulation results show greater strain and strain energy density in the overlap region compared to the gap region during fibril deformation. Two separate finite element models of the fibril are constructed to investigate the influence of interaction between the collagen and mineral at the molecular scale on the mechanical response of collagen fibril. The first collagen fibril model with uniform elastic modulus of 2.95 GPa along the length of collagen resulted in an elastic modulus of 4.01 GPa, whereas the second fibril model

with altered elastic modulus along length of collagen, at the regions of mineral proximity, resulted in the elastic modulus of 4.81 GPa. The enhancement in the elastic modulus of fibril is nearly 20% when the effect of mineral proximity in the stiffness of collagen is taken into consideration. Hence, our multiscale model of collagen fibril predicts that the elastic behavior of fibril is significantly influenced by the molecular interaction of mineral present in the hole zone. This work shows that it is important to consider the molecular interactions between collagen and mineral phase when carrying our multiscale modeling of collagen fibril in bone. In addition to bone, the insights provided by this multiscale modeling study are highly pertinent to wide ranges of biological and synthetic nanocomposites, wherein their properties may be strongly influenced by the interactions between constituents at the molecular scale.

7.5. Acknowledgements

The authors acknowledge TeraGrid for computational resources at the NCSA. The computational resources at NDSU Center for Computationally Assisted Science & Technology (CCAST) are acknowledged. The authors thank Dr. Greg Wettstein for hardware and software support. Author SMP acknowledges support from ND EPSCOR.

7.6. References

1. Olszta, M.J., Odom, D.J., Douglas, E.P. & Gower, L.B. A New Paradigm for Biomineral Formation: Mineralization via an Amorphous Liquid-Phase Precursor. *Connective Tissue Research* **44**, 326-334 (2003).
2. Currey, J.D., Zioupos, P., Davies, P. & Casinos, A. Mechanical properties of nacre and highly mineralized bone. *Proceedings of the Royal Society of London Series B-Biological Sciences* **268**, 107-111 (2001).

3. Dorozhkin, S.V. & Epple, M. Biological and medical significance of calcium phosphates. *Angewandte Chemie, International Edition* **41**, 3130-3146 (2002).

4. Eastoe, J.E. & Eastoe, B. Organic constituents of mammalian compact bone. *Biochemical Journal* **57**, 453-9 (1954).

5. Fisher, L.W. & Termine, J.D. Noncollagenous proteins influencing the local mechanisms of calcification. *Clinical Orthopaedics and Related Research* **200**, 362-85 (1985).

6. Currey, J.D. Biomechanics of mineralized skeletons. in *Skeletal Biomineralization :Patterns, processes, and evolutionary trends*, Vol. 1 (ed. Carter, J.G.) 11 (Van Nostrand, New York, 1990).

7. Termine, J.D. & Robey, P.G. Bone matrix proteins and the mineralization process. in *Primer on the Metabolic Bone Diseases and Disorders of Mineral Metabolism*, Vol. 4 (ed. Favus, M.J.) (The American Society for Bone and Mineral Research, Lippincott Williams & Wilkins, 1996).

8. Fratzl, P. & Weinkamer, R. Nature's hierarchical materials. *Progress in Materials Science* **52**, 1263-1334 (2007).

9. Landis, W.J., Song, M.J., Leith, A., McEwen, L. & McEwen, B.F. Mineral and organic matrix interaction in normally calcifying tendon visualized in three dimensions by high-voltage electron microscopic tomography and graphic image reconstruction. *Journal of structural biology* **110**, 39-54 (1993).

10. Hodge, A.J. & Petruska, J.A. Recent studies with the electron microscope on ordered aggregates of the tropocollagen molecule. 289-300 (1963).

11. Gupta, H.S. et al. Fibrillar level fracture in bone beyond the yield point. *International Journal of Fracture* **139**, 425-436 (2006).

12. Nanci, A. Content and distribution of noncollagenous matrix proteins in bone and cementum: relationship to speed of formation and collagen packing density. *Journal of structural biology* **126**, 256-69 (1999).

13. Weiner, S. & Wagner, H.D. The material bone: structure-mechanical function relations. *Annual Review of Materials Science* **28**, 271-298 (1998).

14. Nylen, M.U., Scott, D.B. & Mosley, V.M. Mineralization of turkey leg tendon. II. Collagen-mineral relations revealed by electron and x-ray microscopy. **No. 64**, 129-42 (1960).

15. Landis, W.J. The strength of a calcified tissue depends in part on the molecular structure and organization of its constituent mineral crystals in their organic matrix. *Bone (New York, NY, United States)* **16**, 533-44 (1995).

16. Traub, W., Arad, T. & Weiner, S. Three-dimensional ordered distribution of crystals in turkey tendon collagen fibers. *Proceedings of the National Academy of Sciences of the United States of America* **86**, 9822-6 (1989).

17. Arsenault, A.L. Image-analysis of collagen-associated mineral distribution in cryogenically prepared turkey leg tendons. *Calcified Tissue International* **48**, 56-62 (1991).

18. Rubin, M.A., Rubin, J. & Jasiuk, W. SEM and TEM study of the hierarchical structure of C57BL/6J and C3H/HeJ mice trabecular bone. *Bone* **35**, 11-20 (2004).

19. Bonar, L.C., Lees, S. & Mook, H.A. Neutron diffraction studies of collagen in fully mineralized bone. *Journal of molecular biology* **181**, 265-70 (1985).

20. Buehler, M.J. Nature designs tough collagen: Explaining the nanostructure of collagen fibrils. *Proceedings of the National Academy of Sciences of the United States of America* **103**, 12285-12290 (2006).

21. Buehler, M.J. Molecular nanomechanics of nascent bone: fibrillar toughening by mineralization. *Nanotechnology* **18**(2007).

22. Gautieri, A., Vesentini, S., Redaelli, A. & Buehler, M.J. Intermolecular slip mechanism in tropocollagen nanofibrils. *International Journal of Materials Research* **100**, 921-925 (2009).

23. Tang, Y., Ballarini, R., Buehler, M.J. & Eppell, S.J. Deformation micromechanisms of collagen fibrils under uniaxial tension. *Journal of The Royal Society Interface* **7**, 839-850 (2010).

24. Buehler, M.J. Nanomechanics of collagen fibrils under varying cross-link densities: Atomistic and continuum studies. *Journal of the Mechanical Behavior of Biomedical Materials* **1**, 59-67 (2008).

25. Gautieri, A., Vesentini, S., Redaelli, A. & Buehler, M.J. Hierarchical Structure and Nanomechanics of Collagen Microfibrils from the Atomistic Scale Up. *Nano Letters* **11**, 757-766 (2011).

26. Gupta, H.S. et al. Synchrotron diffraction study of deformation mechanisms in mineralized tendon. *Physical Review Letters* **93**(2004).

27. Shen, Z.L., Dodge, M.R., Kahn, H., Ballarini, R. & Eppell, S.J. Stress-strain experiments on individual collagen fibrils. *Biophysical Journal* **95**, 3956-3963 (2008).

28. van der Rijt, J.A.J., van der Werf, K.O., Bennink, M.L., Dijkstra, P.J. & Feijen, J. Micromechanical testing of individual collagen fibrils. *Macromolecular Bioscience* **6**, 697-702 (2006).

29. Wenger, M.P.E., Bozec, L., Horton, M.A. & Mesquida, P. Mechanical properties of collagen fibrils. *Biophysical Journal* **93**, 1255-1263 (2007).

30. Dubey, D.K. & Tomar, V. Effect of changes in tropocollagen residue sequence and hydroxyapatite mineral texture on the strength of ideal nanoscale tropocollagen-hydroxyapatite biomaterials. *Journal of Materials Science-Materials in Medicine* **21**, 161-171 (2010).

31. Dubey, D.K. & Tomar, V. Role of the nanoscale interfacial arrangement in mechanical strength of tropocollagen-hydroxyapatite-based hard biomaterials. *Acta Biomaterialia* **5**, 2704-2716 (2009).

32. Bhowmik, R., Katti, K.S. & Katti, D.R. Mechanics of molecular collagen is influenced by hydroxyapatite in natural bone. *Journal of Materials Science* **42**, 8795-8803 (2007).

33. Bhowmik, R., Katti, K.S. & Katti, D.R. Mechanisms of Load-Deformation Behavior of Molecular Collagen in Hydroxyapatite-Tropocollagen Molecular System: Steered Molecular Dynamics Study. *Journal of Engineering Mechanics-Asce* **135**, 413-421 (2009).

34. Katti, D.R., Pradhan, S.M. & Katti, K.S. Directional dependence of hydroxyapatite-collagen interactions on mechanics of collagen. *Journal of Biomechanics* **43**, 1723-1730 (2010).

35. Almora-Barrios, N. & de Leeuw, N.H. A Density Functional Theory Study of the Interaction of Collagen Peptides with Hydroxyapatite Surfaces. *Langmuir* **26**, 14535-14542 (2010).

36. Hellmich, C., Barthelemy, J.F. & Dormieux, L. Mineral-collagen interactions in elasticity of bone ultrastructure - a continuum micromechanics approach. *European Journal of Mechanics a-Solids* **23**, 783-810 (2004).

37. Fritsch, A., Hellmich, C. & Dormieux, L. Ductile sliding between mineral crystals followed by rupture of collagen crosslinks: Experimentally supported micromechanical explanation of bone strength. *Journal of Theoretical Biology* **260**, 230-252 (2009).

38. Streeter, I. & de Leeuw, N.H. Atomistic Modeling of Collagen Proteins in Their Fibrillar Environment. *Journal of Physical Chemistry B* **114**, 13263-13270 (2010).

39. Streeter, I. & de Leeuw, N.H. A molecular dynamics study of the interprotein interactions in collagen fibrils. *Soft Matter* **7**, 3373-3382 (2011).

40. Ghosh, P., Katti, D.R. & Katti, K.S. Mineral Proximity Influences Mechanical Response of Proteins in Biological Mineral-Protein Hybrid Systems. *Biomacromolecules* **8**, 851-856 (2007).

41. Bhowmik, R., Katti, K.S. & Katti, D.R. Influence of mineral on the load deformation behavior of polymer in hydroxyapatite-polyacrylic acid

nanocomposite biomaterials: A steered molecular dynamics study. *Journal of Nanoscience and Nanotechnology* **8**, 2075-2084 (2008).

42. Sikdar, D., Pradhan, S.M., Katti, D.R., Katti, K.S. & Mohanty, B. Altered phase model for polymer clay nanocomposites. *Langmuir* **24**, 5599-5607 (2008).

43. Ghosh, P., Katti, D.R. & Katti, K.S. Mineral and protein-bound water and latching action control mechanical behavior at protein-mineral interfaces in biological nanocomposites. *Journal of Nanomaterials* (2008).

44. Katti, D.R. & Katti, K.S. Modeling microarchitecture and mechanical behavior of nacre using 3D finite element techniques - Part I - Elastic properties. *Journal of Materials Science* **36**, 1411-1417 (2001).

45. Katti, K.S., Katti, D.R., Pradhan, S.M. & Bhosle, A. Platelet interlocks are the key to toughness and strength in nacre. *Journal of Materials Research* **20**, 1097-1100 (2005).

46. Brooks, B.R. et al. CHARMM: a program for macromolecular energy, minimization, and dynamics calculations. *Journal of Computational Chemistry* **4**, 187-217 (1983).

47. Pradhan, S.M., Katti, D.R. & Katti, K.S. Steered molecular dynamics study of mechanical response of full length and short collagen molecules. *ASCE Journal of Nanomechanics and Micromechanics* **1**, 104-110 (2010).

48. Sudarsanan, K. & Young, R.A. Significant precision in crystal structural details: Holly Springs hydroxyapatite. *Acta Crystallographica, Section B Structural Crystallography and Crystal Chemistry* **25**, 1534-43 (1969).

49. Tasker, P.W. The stability of ionic crystal surfaces. *Journal of Physics C Solid State Physics* **12**, 4977-84 (1979).

50. Bhowmik, R., Katti, K.S. & Katti, D. Molecular dynamics simulation of hydroxyapatite-polyacrylic acid interfaces. *Polymer* **48**, 664-674 (2007).

51. Landis, W.J., Hodgens, K.J., Arena, J., Song, M.J. & McEwen, B.F. Structural relations between collagen and mineral in bone as determined by high voltage electron microscopic tomography. *Microscopy research and technique* **33**, 192-202 (1996).

52. Wenk, H.R. & Heidelbach, F. Crystal alignment of carbonated apatite in bone and calcified tendon: results from quantitative texture analysis. *Bone* **24**, 361-369 (1999).

53. Lorenzo, A.C. & Caffarena, E.R. Elastic properties, Young's modulus determination and structural stability of the tropocollagen molecule: a computational study by steered molecular dynamics. *Journal of Biomechanics* **38**, 1527-1533 (2005).

54. Gautieri, A., Buehler, M.J. & Redaelli, A. Deformation rate controls elasticity and unfolding pathway of single tropocollagen molecules. *Journal of the Mechanical Behavior of Biomedical Materials* **2**, 130-137 (2009).

55. Orgel, J.P. et al. The in situ supermolecular structure of type I collagen. **9**, 1061-1069 (2001).

56. Landis, W.J. et al. Mineralization of collagen may occur on fibril surfaces: evidence from conventional and high-voltage electron microscopy and three-dimensional imaging. *Journal of structural biology* **117**, 24-35 (1996).

57. Saber-Samandari, S. & Gross, K.A. Micromechanical properties of single crystal hydroxyapatite by nanoindentation. *Acta Biomaterialia* **5**, 2206-2212 (2009).

CHAPTER 8. MULTISCALE MODELING OF COLLAGEN FIBRIL IN BONE AT VARIOUS CROSSLINK DENSITIES: AN INSIGHT INTO ITS DEFORMATION MECHANISM IN THE SMALL AND LARGE DISPLACEMENT REGIME

This chapter discusses the multiscale model of collagen fibril to elucidate its deformation mechanism and the role of crosslinks in the mechanics of collagen fibril. The content of this chapter is being submitted for publication.

8.1. Introduction

The collagen molecules are fibrous structural proteins found in abundance in our human body, constituting 85-95% of body proteins[1], and known for its superior mechanical properties[2, 3]. The collagen molecules assemble to form a highly organized structure known as collagen fibril, which are the basic building units of bone material and collagen rich tissues[4]. The collagen molecules are long and cylindrical structures composed of a triple-helix formed by three polypeptide chains[5], also known as α-chains, and measuring about 300 nanometers in length and 1.23 nanometers in diameter[6]. There are at least 27 different types of collagen molecules found in vertebrates[7] and fibrillar collagen account for only seven of all the known collagen types [8-11]. Type I is the most abundant fibrillar collagen that is widely found in bone, skin, tendon, cornea, vasculature and lung etc. The diameter of collagen fibrils range from fifty to several-hundred nanometers[12, 13], while their length is unknown because they merge with neighboring fibrils [14]. The collagen fibril consists of an array of collagen molecules arranged parallel to each other and staggered by 67 nm (i.e. D period) with respect to each other along the

longitudinal axis[15]. The staggering of collagen molecules result in a banded pattern of along the length of fibril consisting of an alternating overlap- and hole-zones, which corresponds to the regions of high and low electron densities respectively in X-ray diffraction[15] and visible as consecutive stripes in the electron micrograph. Hole-zone is a region separating the ends of two collagen molecules (i.e. N-terminus and C-terminus) aligned along the longitudinal axis of collagen. The sizes of hole-zone and overlap zone are 27 and 40 nanometers respectively[6, 15]. The covalent crosslinks develop between adjacent collagen molecules in the overlap zone, near the ends of collagen, with the maturation of tissues. This crosslinking between the adjacent ends of collagen molecule plays an important role in the mechanical property for fibril. In bone the hydroxyapatite ($Ca_{10}(PO_4)_6(OH)_2$) mineralizes in the hole zone into a plate-like structures, which grow in size along the axial direction of collagen molecule and sideways along channels[6, 16-18]. The mineral in bone consists of various impurities such as carbonate, and constitutes a significant portion of bone- 65% by weight[19-23] and 33-43% by volume[23, 24]. In bone the mineral component is responsible for imparting the necessary stiffness, strength, and rigidity to bone.

In the mineralized collagen fibril the (0001) surface of hydroxyapatite is oriented normal to the collagen molecule. In addition to (0001) surface, the electron diffraction studies show that the $(10\,\bar{1}\,0)$ surfaces of HAP are also well developed and are oriented approximately parallel to each other [6, 25, 26]. The molecular dynamics study of collagen-hydroxyapatite interface was first carried out by Bhowmik et. al[27, 28] showing the presence of strong interactions at the interface which significantly affects the mechanics of collagen molecule. Bhowmik et al. also showed the important role played by water in

mediating the interactions between collagen and mineral[27]. Similar behavior has also been shown in a number of other nanocomposites such as nacre and polymer clay nanocomposite, in which the mechanical behavior of organic material is enhanced by the mineral proximity[29-31]. The mineral surface shares a significant interfacial area with collagen molecules within the collagen fibril leading to the substantial hydroxyapatite-collagen interactions. The mechanics collagen in the proximity of (0001) and $(10\bar{1}0)$ surfaces of hydroxyapatite and directional dependence of mineral-collagen interactions have been studied in detail by Katti et al. using molecular dynamics [32]. The results of this study indicate that the mechanics of collagen pulled in different directions with respect to hydroxyapatite is significantly different. The role of the thickness of mineral on the mechanical properties of the collagen-hydroxyapatite interface has been carried out by Qin et al. which show that the tensile modulus of biomineral surface converges around 2 nanometer thickness of mineral[33]. Other studies of collagen hydroxyapatite system include molecular dynamics study [34-36], density functional study[37], and continuum micromechanics study[38, 39]. In addition to collagen-hydroxyapatite systems, there are number of molecular dynamics studies investigating the mechanical properties of single collagen molecules[40-43] that show wide variation of elastic modulus. The steered molecular dynamics study of full-length collagen molecule that investigates the mechanical response of the entire 300 nanometers length is carried out for the first time by Pradhan et al.[40].

The molecular molecular modeling study of collagen microfibrils has been carried out by number of researchers[44-47]. The two dimensional coarse grain study of unmineralized and mineralized collagen mifrofibril has been carried out by Buehler [48, 49].

Most of the studies found in the current literature are limited to the investigation of microfibril and the study of a collagen fibril is very scarce. While the collagen fibrils in bone are mineralized, majority of these microfibril models are either unmineralized or do not include the effect of minerals proximity in the mechanics of collagen molecules, as evident from the number of molecular dynamics studies[27, 32]. Recently the Pradhan et al. has carried out a multiscale modeling of mineralized collagen fibril by combining molecular modeling with the continuum description of the fibril microstructure[50]. In this study the mechanical response of collagen in the mineral proximity is evaluated using steered molecular dynamics and incorporated into the three-dimensional finite element model of collagen fibril. This study is limited to the mechanics of collagen fibril in the small displacement regime. In this paper we present the results of our simulation in a larger displacement regime as well as the deformation response of collagen fibril under various crosslink densities.

8.2. Model Construction and Simulation Details

The key feature of this model is the multiscale model of collagen fibril that bridges molecular level properties with the continuum model of fibril. Molecular dynamics is used to simulate collagen-hydroxyapatite interactions at the molecular scale, and finite element method is used to model the mechanical response of fibril. At the molecular scale, the collagen is pulled in the proximity of mineral and in the absence of mineral proximity using steered molecular dynamics. These conditions correspond to the different mineral environments of collagen inside the collagen fibril. The two mineral surfaces used in this study include (0001), and $(10\bar{1}0)$ surface. For the construction of collagen-hydroxyapatite models the solvated collagen molecule (PDB ID: 1k6f) is

brought in the proximity of mineral surface and geometrically optimized by energy minimization using conjugate gradient method. The temperature and pressure are brought to 300 K and 1.01 bar respectively in the steps of 100 K and 0.25 bar. The langevin dynamics and Nose-Hoover piston method are used to maintain temperature and pressure[51]. The simulations are carried out using a NAMD[52] package and CHARMM[53] force field. The force field parameters for hydroxyapatite are obtained from Bhowmik et al. [54]. For evaluating load-displacement response, the collagen molecules is fixed at one end and extended using a harmonic spring at the pulling rate of 0.00003 ps^{-1} using steered molecular dynamics. The spring constants of 4 kcal/mol/$Å^2$ and 0.1 kcal/mol/$Å^2$ were used for short (~8.5 nm long) and full-length (~290 nm long) molecules respectively. In the proximity of mineral, the short collagen molecule is pulled parallel and perpendicular to the hydroxyapatite $(10\bar{1}0)$ and (0001) surfaces respectively. Steered molecular dynamics is also used to estimate the breaking stress between the end of collagen and mineral (0001) surface. The center of mass of collagen with N-telopeptide at the end is pulled perpendicular to the mineral surface using a pulling rate of 0.00003 ps^{-1} until the collagen and mineral are completely detached. The breaking stress of 24.2 pN/$Å^2$ is estimated from the peak force during the detachment of collagen and mineral.

The elastic modulus of collagen is estimated for the small displacement regime of 7%. The deformation of collagen beyond 7% displacement is considered be inelastic and represented using a piecewise linear description for finite element modeling. For the collagen molecule the elastic modulus is computed for a small displacement of 7% using a relation $E = k \times L/A$, where 'k' is the stiffness of load-displacement response, 'L' is the length of collagen molecule, 'A' is the cross-sectional area of collagen. The cross-

sectional area of collagen is estimated by enclosing the Van der Waals surface of collagen with a cylinder, similar to the method used by other researchers[41, 42]. The modulus of collagen not in the mineral proximity is 2.95 GPa, whereas the collagen molecule pulled parallel to $(10\bar{1}0)$ and perpendicular to mineral (0001) surfaces are 13.17 and 6.26 GPa respectively[50].

The collagen-collagen interface and collagen-mineral interface are assumed to consist of thin region called "interlayer" that is responsible for the transfer of shear between the constituents. The thickness of interlayer is estimated from molecular dynamics study by approximating the distance between Van der Waals surfaces of two molecules. The details of steered molecular dynamics study in which the central collagen molecule is sheared with respect to the surrounding six other molecules, arranged in a quasihexagonal manner, can be found in our previous work [40]. From the load-displacement response the shear modulus and sliding/yield stress of the interlayer between collagen molecules are estimated to be 0.027 pN/Å^2 and 0.166 pN/Å^2 respectively. The shearing characteristics of collagen-mineral interface is studied by pulling collagen parallel to the mineral $(10\bar{1}0)$ surface using steered molecular dynamics. The load-displacement response obtained from steered molecular dynamics is utilized to estimate shear modulus of interlayer using finite element method. This method allows us to separate the deformation of interlayer from those of collagen and mineral during shearing. The finite element model of collagen pulled on the surface of mineral is shown in figure 8.1. This model consists of a collagen and mineral separated by a 0.24 nm thick interlayer. The finite element simulation is carried out by fixing the bottom surface of the mineral and applying tensile load to the right end of collagen. Series of

simulations was carried out by varying the shear modulus of interlayer until the stiffness response obtained matches to the value obtained from steered molecular dynamics. The shear modulus of interlayer obtained from this iteration is 1.51 pN/Å^2. The maximum stress on the interlayer when the collagen begins to slide over mineral is estimated to be 1.42 pN/Å^2. The elastic modulus of hydroxyapatite, determined from nanoindentation test, obtained from literature is 150.38 GPa [55].

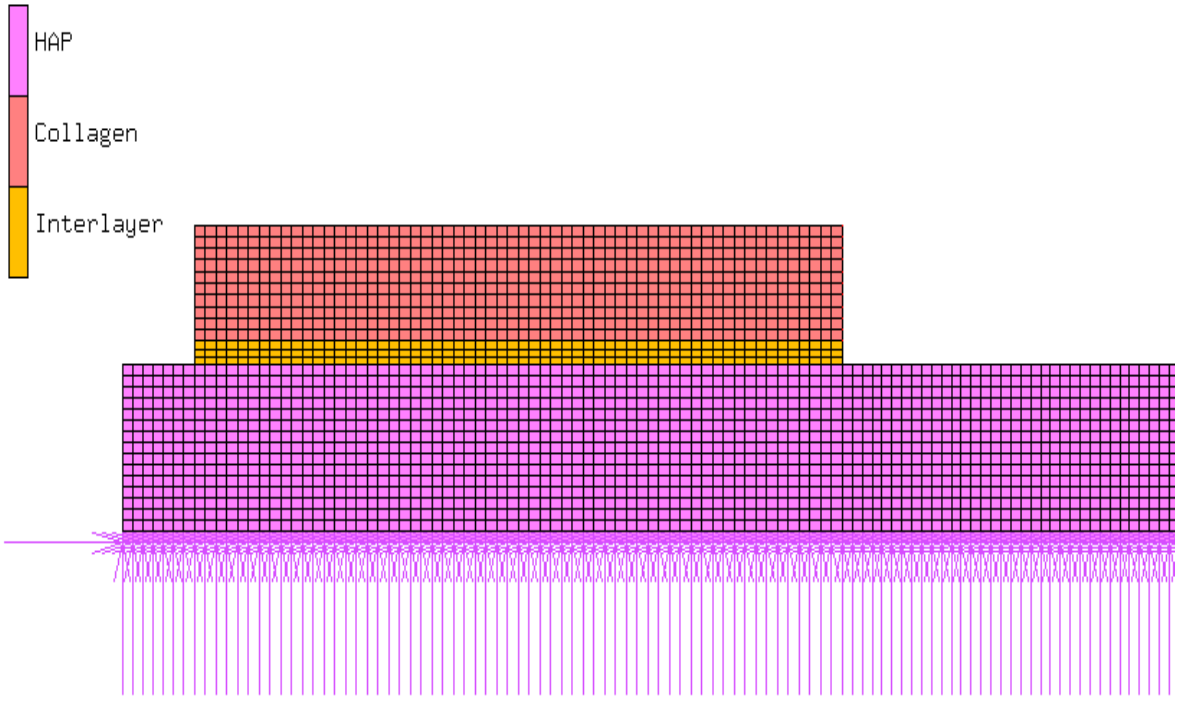

Figure 8.1. Finite element model of collagen pulled on the mineral surface.

The material properties of collagen and interlayers estimated from steered molecular dynamics are passed over the finite element model of collagen fibril. The finite element model of collagen fibril is constructed using MSC Mentat as described in detail in our previous work[50]. This model of fibril is cylindrical in shape 1005 nm in length, approximately 50 nm in diameter, and consists of 34 molecules across the cross-sectional width. The total number of elements in this model is 4,325,922, while only the symmetric half of the model is used for simulation. The collagen molecules in this model are 294.8 nm long corresponding to 4.4D, where D is the longitudinal stagger of 67 nm. The staggering of collagen molecules with respect to each other in this model results in a banded pattern along the fibril length as shown in figure 8.2. The ends of collagen molecules consist of a region known a hole-zone that consists of a plate shaped hydroxyapatite 40 nm wide and 1.23 nm thick. The mineral plates in this model are aligned parallel to each other, with an arrangement similar to the parallel layers of hydroxyapatite seen in mineralized turkey tendon and some bones [6, 14, 18, 25]. The separation between adjacent collagen molecules in our model is 2.4 Å, which is taken from Landis et al [6]. The crosslinks are modeled as the elements bridging the adjacent collagen molecules spanning 6 nm from the end of collagen molecules. In our simulations, the stiffness of crosslink obtained from Buehler's work[48] is 1181.143 pN/Å., while the bond strength of covalent crosslink is considered to be 2.1 nN [56-58]. The simulations of collagen fibril were carried out for zero, one, two, there, four, and five crosslinks. The finite element simulations were carried out by fixing nodes on the bottom face and applying the fixed-displacement tensile loadings to the nodes on the top face of the fibril model. The mineral component of bone is strong in compression but not in

tension. The collagen molecules function as reinforcing structural members that impart bone with the adequate tensile and bending strength (in conjunction with mineral). However, majority of mineral is interfibrillar in nature, which makes it highly likely that the collagen fibril is predominantly a tensile member. The true nature of load in collagen fibril can be determined only from the modeling of collagen fiber and higher bone structures and the study of deformation under various loading scenarios, which is beyond the scope of this study. For this study we have utilized a tensile load on collagen fibril, applied in small increments.

8.3. Results and Discussion

The constituents of collagen fibril, collagen molecule, mineral, and water, are known to have significant non-bonded interactions among themselves. The steered molecular dynamics studies show that the mechanical property of collagen molecule is significantly affected by the mineral proximity. It has been shown in our previous work that the elastic modulus of the mineralized collagen fibril is significantly altered by the molecular interactions at the collagen-mineral interface [50]. Here we look that the effect of crosslink in the enhancement of mechanical property of collagen fibril due to the presence of mineral. The finite element simulations are carried out for crosslink densities varying form zero crosslink to five crosslinks per end of a collagen molecule. The elastic modulus of collagen fibril estimated at the small strain of 4% at various crosslink densities are shown in table 8.1. The table shows that the elastic modulus of collagen fibril at various crosslink densities is significantly higher when the influence of mineral on collagen mechanics is taken into consideration as compared to the case when the influence of mineral on collagen is not taken into account. The interesting thing of this

finding it that the enhancement in the elastic modulus of fibril due to collagen-mineral interaction is found to exist irrespective of the presence of crosslink and at all crosslink densities.

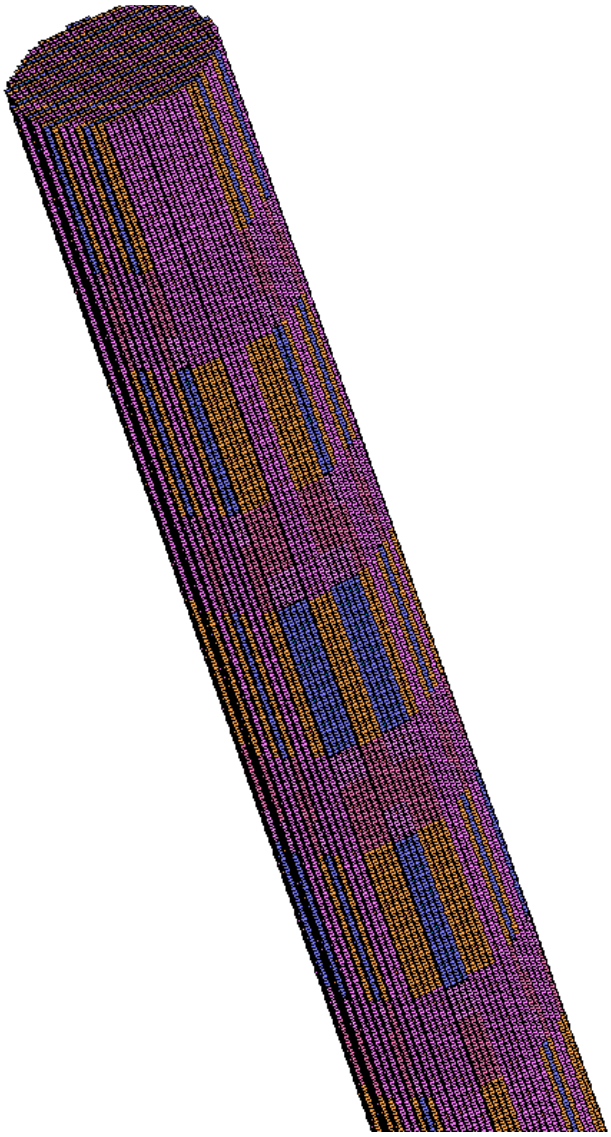

Figure 8.2. Section of the the finite element model of collagen fibril showing banded pattern along the length formed by alternating gap and overlap zones.

The typical stress-strain response of collagen fibril obtained from finite element simulation is shown in figure 8.3. We see that in addition to the small displacement regime, the deformation response of collagen fibril is significantly stiffer in the large displacement regime when the effect of mineral proximity on collagen is taken into consideration. Our simulations show that there is significant enhancement in the stiffness response of collagen fibril in the large displacement regime at all the crosslink densities.

Table 8.1. Elastic modulus of collagen fibril at various crosslink densities when the influence of hydroxyapatite on collagen mechanics is (i) taken into consideration, and (ii) not taken into consideration

Number of Crosslinks	Elastic Modulus of Collagen Fibril (GPa)	
	Mineral Influence	No Mineral Influence
0	3.99	3.52
3	4.33	3.79
5	4.43	3.89

The elastic modulus of collagen fibril corresponding to 4% strain at various crosslink densities is shown in figure 8.4. It is seen in figure that the fibril exhibit higher elastic modulus at high crosslink densities. Furthermore, it is to be noted that there is a larger increment in elastic modulus between zero crosslink and one crosslink compared to between one, two, there, four- , and five crosslinks. The enhancement in the elastic modulus due to presence of crosslinks is seen to vary from 5% to 11% compared to the collagen fibril with no crosslink. This shows that the crosslinks plays an important role in collagen fibril by imparting with higher elastic modulus.

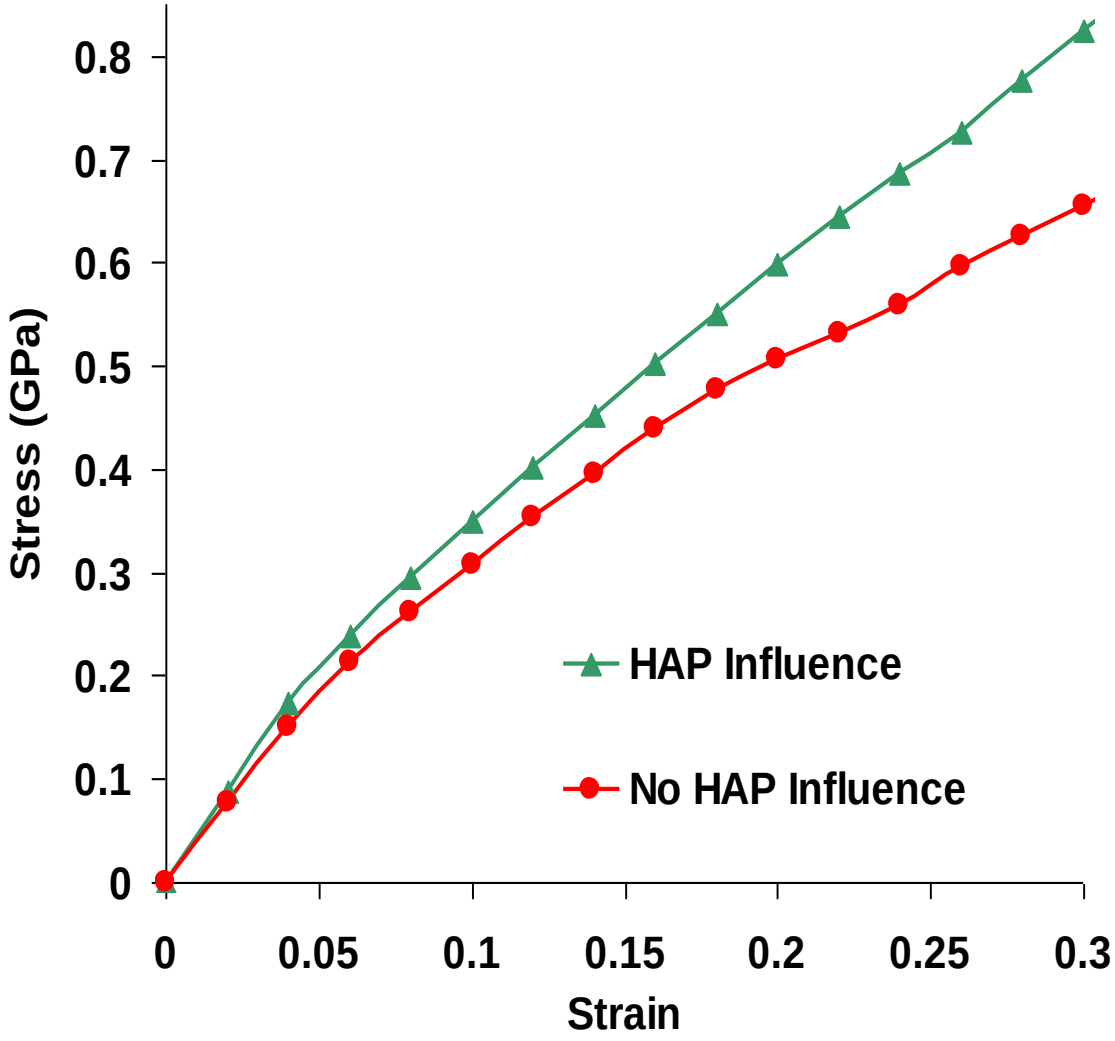

Figure 8.3. Stress-strain response of collagen fibril when the influence of mineral proximity is taken into account and not taken into account.

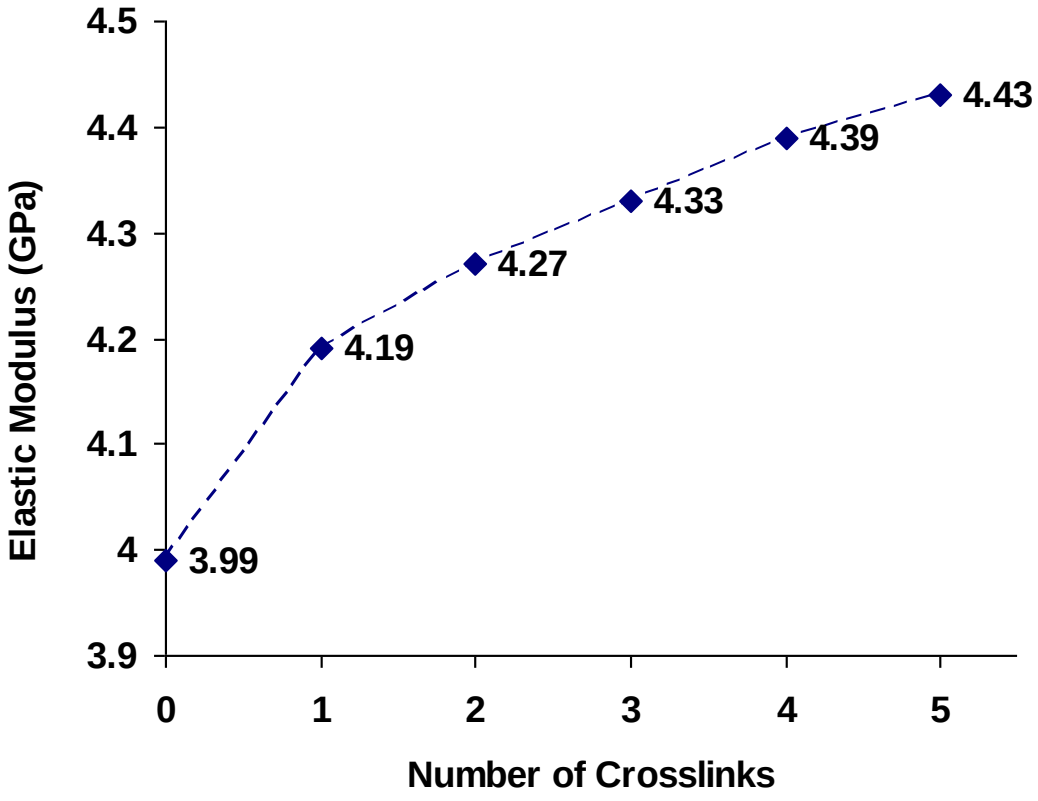

Figure 8.4. Elastic modulus of collagen fibril at various crosslink densities.

The deformation response of collagen fibril at crosslink densities varying from zero crosslink to five crosslinks is shown in figure 8.5. It is seen from the plot that the larger number of crosslinks results in the higher stiffness of collagen fibril. A very interesting observation from this stress strain response is that the yielding or failure of collagen fibril due to the breaking of crosslink is not observed for any of the crosslink densities throughout the entire deformation range. A more striking observation from this plot is that the fibril model with no crosslink is also able to sustain the applied load without yielding or failure even at a large strain of 30%. To explain this observation it is necessary to look closely at the arrangement of collagen molecules in a fibril. The

schematic of the longitudinal section of collagen fibril approximately 1 micrometer in length and 50 nanometers in diameter, consisting of 34 collagen molecules across the width, is shown in figure 8.6. The adjacent molecules are longitudinally staggered with respect to each other by 67 nanometers resulting in a gap- and overlap- zone of length 40 nanometers and 27 nanometers respectively along the length. Overlap zone is a region where the transfer of tensile force occurs between the adjacent collagen molecules with the help of crosslinks and shearing between molecules. Therefore, the pullout between the ends of collagen molecules in the overlap zone can be considered one of the important mechanisms of collagen fibril failure. As shown by the dotted lines in the figure the adjacent overlap zones in collagen fibril is inclined at an angle of about 1.25 degrees relative the longitudinal direction of fibril. The inclination of this line can be estimated using a relation $Tan^{-1}(d/D)$, where d is a center to center lateral distance between collagen molecules and D is the D-spacing of 67 nanometers. Thus the dotted lines represent the region where the collagen fibril fails due to the pullout between the overlapping ends of two molecules. While the pullout between the overlapping ends of two molecules is an important mechanism of fibril failure, it is essential to understand its dependency on the length and diameter of collagen fibril. We can do this by referring back to the schematics of collagen fibril shown in figure 8.6 and asking a question if it is possible to cause it to fail by pullout in the overlapping zone (i.e. along the dotted lines), when the opposite ends of fibril are pulled. Let's consider a parallelogram shaped region of fibril bounded two of the inclined dotted lines and red arrows on the left and right end of fibril section. Evidently there is no overlapping between the ends of collagen in this region, so the failure due to pullout and breaking of crosslinks is not possible. The

deformation mechanism of this region is purely governed by the shearing between the adjacent collagen molecules. For the failure of collagen by pullout in the overlap zone to be possible at least one of the dotted lines should intersect the opposite edges of fibril (i.e. top and bottom edges). This gives rise to an idea of characteristic length (L_c) of fibril that governs its deformation mechanism. The characteristic length is given by the relation, $L_c = \phi \times D/d$, where ϕ is the diameter of fibril, D is the D-spacing of 67 nanometers, and d is a center to center lateral distance between collagen molecules. The deformation will be governed by intermolecular shear if the fibril length (L) is shorter than L_c, whereas it will be governed by the pullout between the pullout between collagen ends and breaking of crosslinks if L is longer than L_c. The diameter of collagen fibril model is 50 micrometers and it corresponding characteristic length is 2.3 micrometers, which is much longer the length of our model (i.e. 1 micrometers). Because of this reason we do not see the yielding/failure of collagen fibril due to pullout between ends of collagen even when no crosslink is present (Fig. 8.5). The fact that mechanical response of collagen fibril is dependent on the size of fibril has also been shown experimentally. The experimental study by Shen et al.[59] show that the post yield behavior of collagen fibril is dependent on the fibril volume, and as result of which the collagen fibril cannot be considered representative volume elements.

In bone the exact mechanism of load transfer to fibrils are not very clear as there are currently two opposing viewpoints: (i) load transfer to fibril occurs through proteoglycan bridges between fibrils[60, 61], and (ii) "force transmission within the tissues occurs along spanning collagen fibrils themselves, long intertwined fibrils, and bifurcating/fusing fibrils[62]". Hence, the true nature and distribution of the stress acting

along the length of collagen fibril when the bone is strained is largely unknown. In bone the load is most likely transferred to the collagen fibril as distributed stress acting along its length due to neighboring fibrils or interfibrillar mineral and proteoglycan bridges in different proportions that is not clear at this point. As a result, variable tensile stress is developed along the length of fibril with the presence of regions that are stressed and unstressed, i.e. every section along the length of fibril may not be under equal tensile strain and that there may be regions without any straining. Hence, we define the continuous length over which fibril experiences the tensile stress/strain due to the applied distributed load as "effective length" for that particular loading condition, i.e. it is defined as the distance between two successive points of zero tension. The deformation mechanism of fibril depends on whether the effective length is greater or smaller than the characteristic length. If the effective length is greater than the characteristic length the deformation mechanism will be governed by the overlap zone and the breaking of crosslinks. However, if the effective length is less than the characteristic length the deformation mechanism of fibril will be governed by the intermolecular shear between collagen molecules. The finding that the deformation mechanism of collagen fibril is dependent on the characteristic length has an interesting an implication for the bone mechanics. As the characteristic length is directly proportional to the fibril diameter as discussed above, it can vary from the few microns for a fibril of small diameter to the tens of microns for a fibril of larger diameter. Because of this reason the fibrils of different diameter will exhibit different deformation response for similar loading conditions due to the differences in deformation mechanisms.

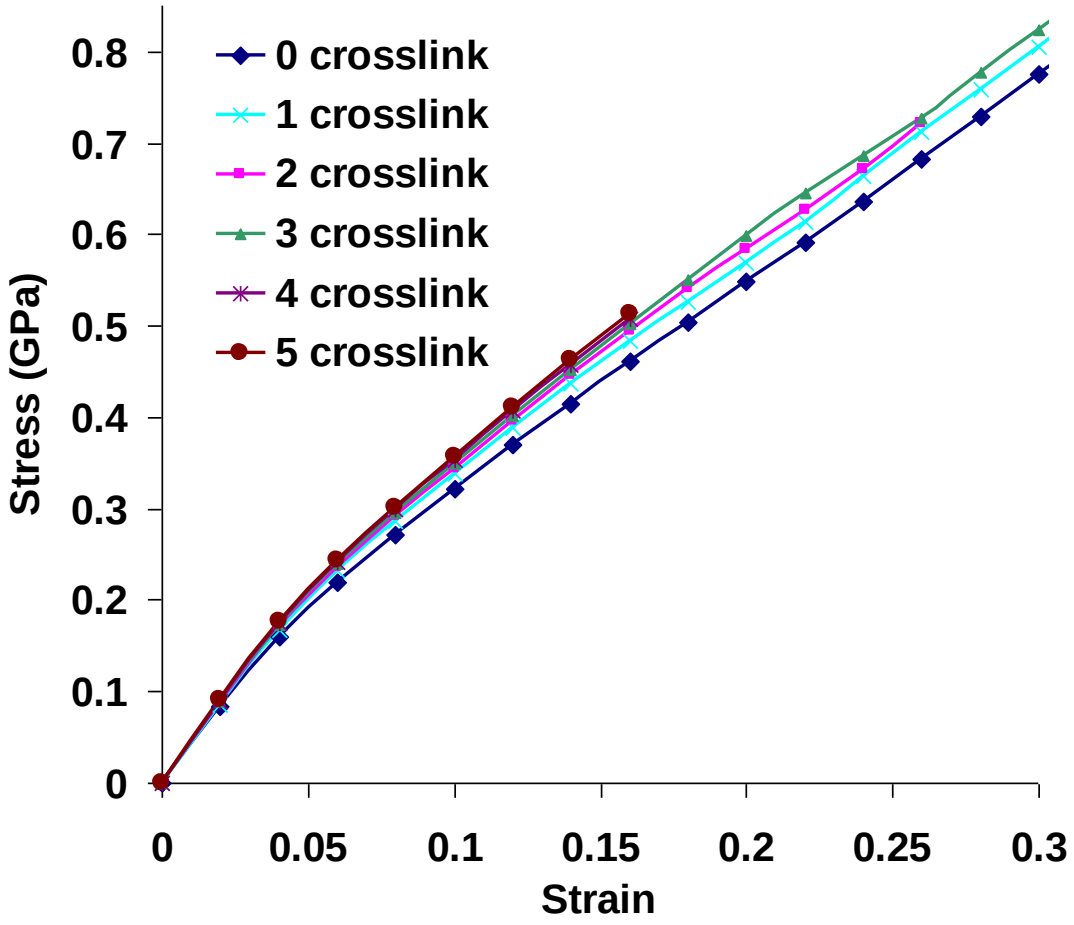

Figure 8.5. Stress-strain response of collagen fibril at crosslink densities varying from zero crosslink to five crosslinks per collagen end.

When the collagen fibril is stretched the overlap and gap zone undergo different amounts of strain. The longitudinal strain along the collagen fibril in tension is shown in figure 8.7. The gap zone undergoes significantly lesser strain compared to the overlap zone, as its deformation originates from the pure stretching of collagen molecules, nearly 50% of which are stiffened by the nonbonded interaction with hydroxyapatite due to the close proximity. Due to this reason the collagen molecules in the overlap zone which are

closer to the mineral show lesser strain compared to the others. However, in case of overlap zone the deformation is achieved by shearing between the overlapping collagen molecules and the extension of crosslinks. In the overlap zone the ends of collagen show lesser strain compared to remaining length. The longitudinal stress along collagen fibril under tension is shown in figure 8.8. The mineral component of fibril being very stiff experiences the highest magnitude of stress followed by the overlap zone. In overlap zone the region consisting of crosslinks experiences higher stress compared to the part that do not contain crosslinks. The strain energy per unit volume stored in collagen fibril when it is stretched is shown in figure 8.9. Overlap zone is the region of collagen that undergoes the highest strain, as a result of which the strain energy density is highest in this region.

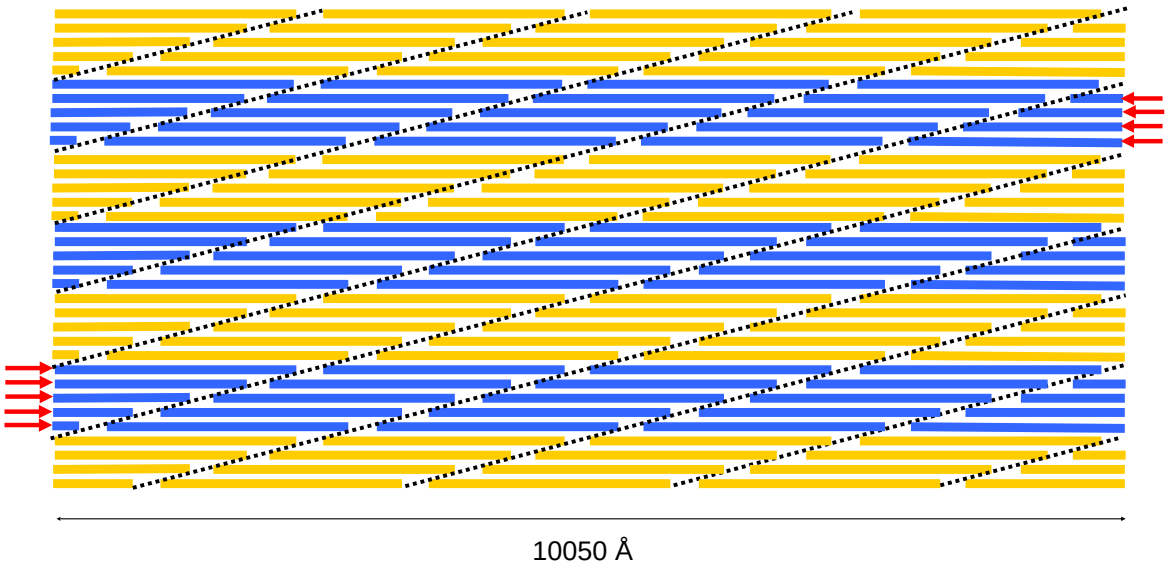

Figure 8.6. The schematic of the longitudinal section of collagen fibril in our model showing the arrangement of collagen molecules staggered with respect to each other by 67 nanometers. The dotted lines represent the location of overlap zone where the crosslinks are formed near the end of collagen molecule.

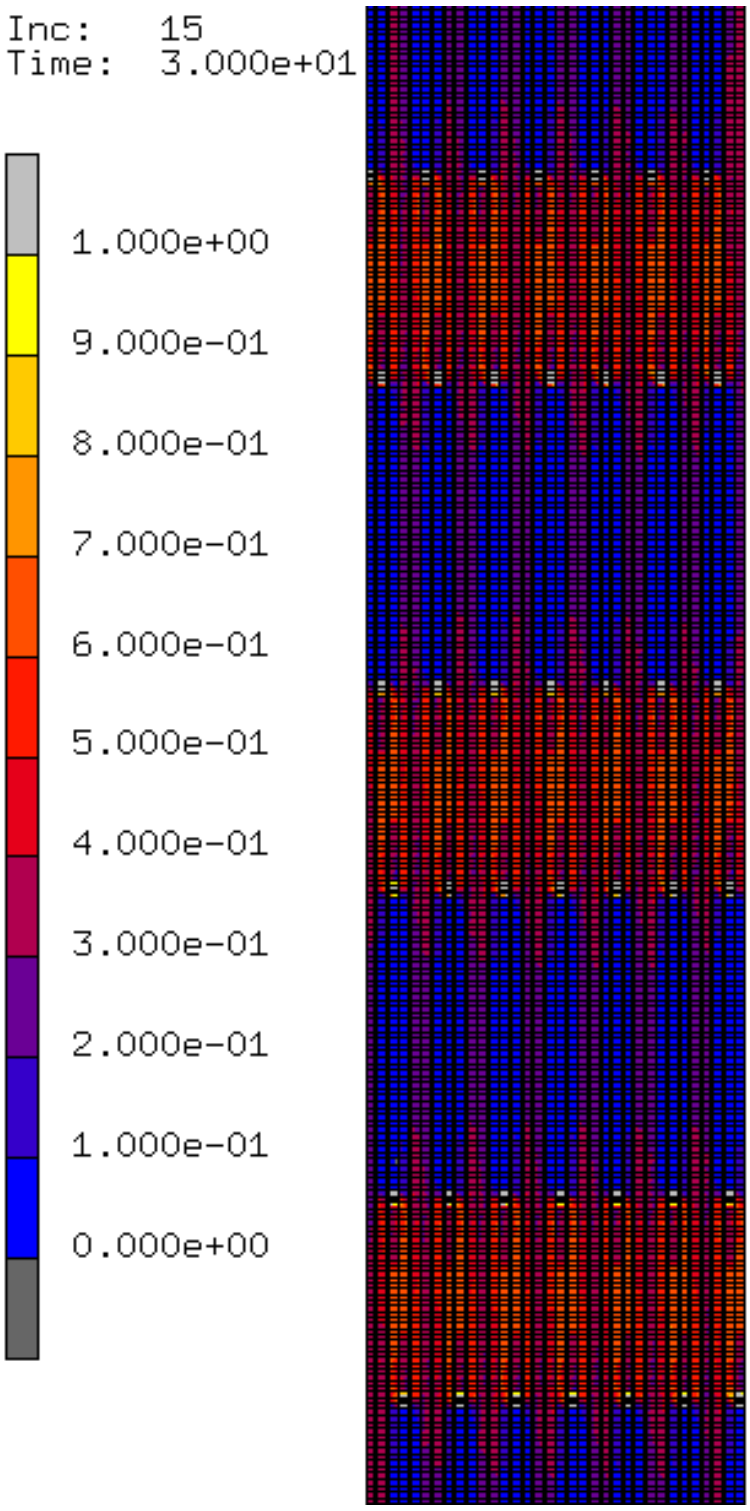

Figure 8.7. Strain along collagen fibril in tension.

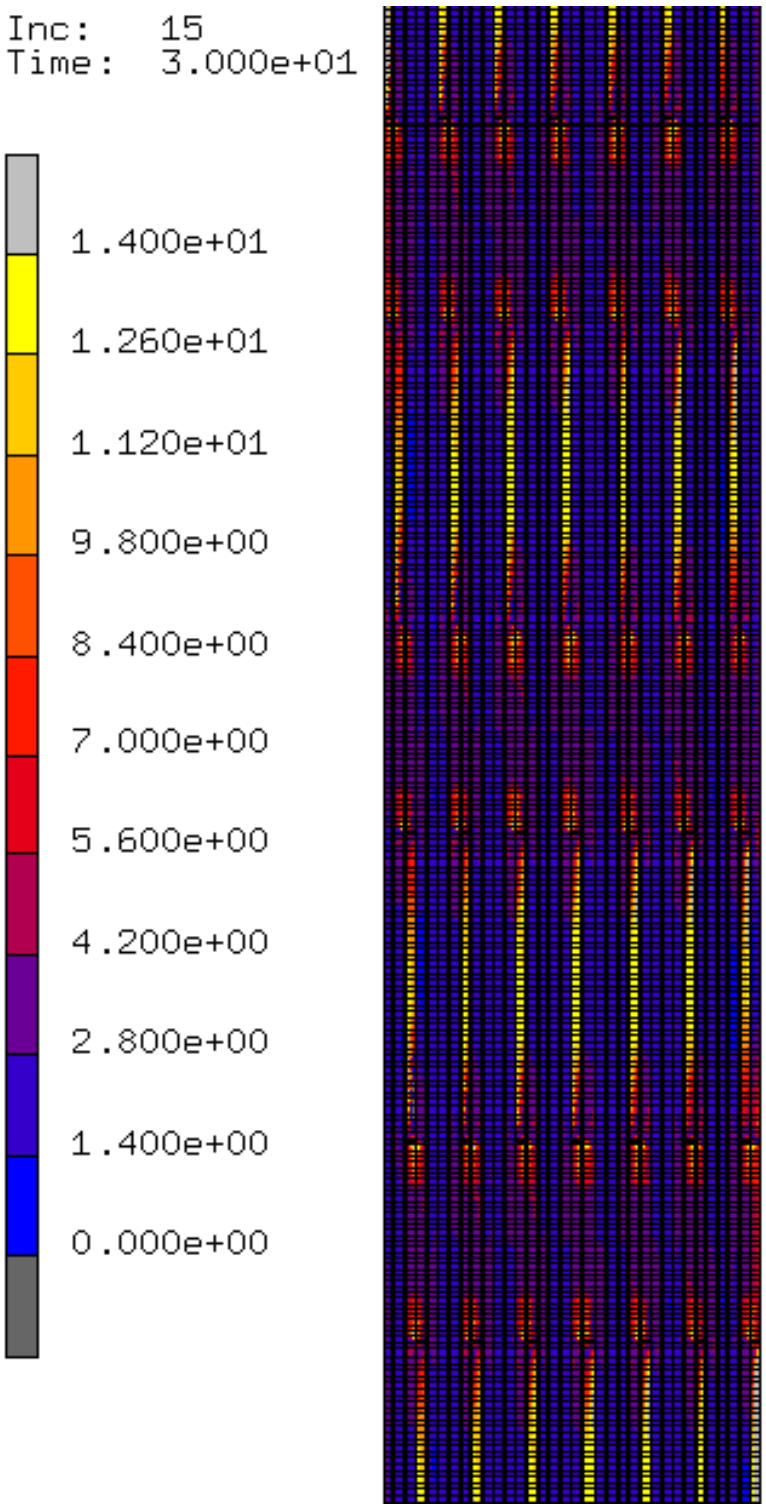

Figure 8.8. Stress along collagen fibril in tension.

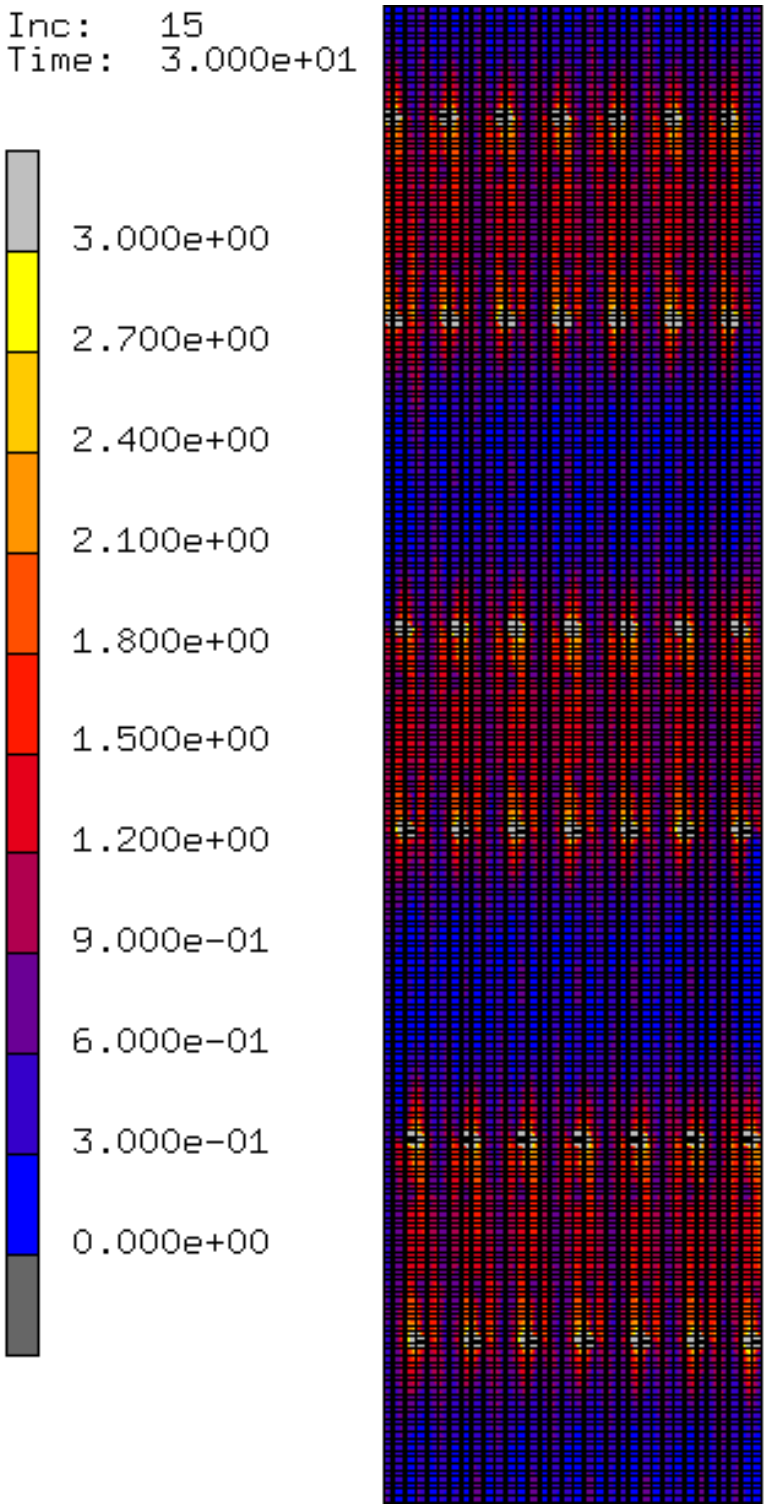

Figure 8.9. Strain energy density along collagen fibril in tension.

8.4 Summary and Conclusions

Multiscale modeling of collagen fibril is carried out by incorporating the material properties of collagen obtained from steered molecular dynamics into the finite element model of collagen fibril. The collagen fibril is extended using displacement control to study its deformation response and the underlying mechanisms at various crosslink densities. The simulations show that the nonbonded interactions between collagen and mineral contribute to the significant enhancement of the elastic modulus of collagen fibril at all the crosslink densities, establishing the importance of taking into account these molecular interactions for modeling the mechanical response of collagen fibril. In addition to the small displacement regime, the stiffening of collagen fibril due to molecular interactions between collagen and mineral is also observed in the large displacement regime of 30% strain. The crosslinks are found to play important role in the mechanical response of collagen fibril, the enhancement in elastic modulus ranging from 5-11% for various crosslink densities compared to the collagen fibril with no crosslink. This stiffening behavior due to crosslinks is found to be true for small as well as large strain regimes, with the higher crosslink densities typically resulting in stiffer response of collagen fibril.

In this study we have elucidated two different mechanisms of fibril deformation depending on the characteristic length of collagen fibril. The stress distribution within the collagen fibril affects the effective length for fibril deformation. The effective length is defined as the length of collagen fibril between two consecutive points of zero tension. The deformation mechanism is governed by the pullout between the ends of collagen molecules in the overlap zone, following the breaking of crosslinks, if the effective length

is greater than the characteristic length. However, if the effective length is less than the characteristic length the deformation mechanism is dictated by the shearing between the staggered collagen molecules which are adjacent to each other. In this study deformation response is found to be governed by the shearing between adjacent collagen molecules, as opposed to pullout in the overlap region, since the effective length of our model is smaller than the characteristic length of fibril. The study of the deformation response of the longer collagen fibril using finite element method is a topic of next study, which at present is infeasible due to the computational limitation.

The overlap zone is seen to undergo the higher strain compared to the gap zone. This is a result of the continuous length of collagen molecule present in the gap zone, enhancement of mechanical response of collagen due to nonbonded interactions with hydroxyapatite, as well as, the additional stiffness provided by the mineral. The highest magnitude of stress is found in the mineral due to its high stiffness, followed by the overlap zone. In the overlap zone the end regions consisting of crosslinks are found to experience higher stress compared to the non-crosslinked section. Furthermore, the overlap zone due to its ability to undergo larger strain is found to have the higher concentration of strain energy compared to other regions of collagen fibril.

8.5. References

1. Termine, J. D.; Robey, P. G., Bone matrix proteins and the mineralization process. In *Primer on the Metabolic Bone Diseases and Disorders of Mineral Metabolism*, Favus, M. J., Ed. The American Society for Bone and Mineral Research, Lippincott Williams & Wilkins: 1996; Vol. 4.

2. Hulmes, D. J.; Wess, T. J.; Prockop, D. J.; Fratzl, P., Radial packing, order, and disorder in collagen fibrils. *Biophysical Journal* **1995,** 68, (5), 1661-70.

3. Bozec, L.; Horton, M., Topography and mechanical properties of single molecules of type I collagen using atomic force microscopy. *Biophysical Journal* **2005,** 88, (6), 4223-4231.

4. Fratzl, P.; Weinkamer, R., Nature's hierarchical materials. *Progress in Materials Science* **2007,** 52, (8), 1263-1334.

5. Ramachandran, G. N.; Kartha, G., Structure of Collagen. *Nature* **1955,** 176, (4482), 593-595.

6. Landis, W. J.; Song, M. J.; Leith, A.; McEwen, L.; McEwen, B. F., Mineral and organic matrix interaction in normally calcifying tendon visualized in three dimensions by high-voltage electron microscopic tomography and graphic image reconstruction. *Journal of structural biology* **1993,** 110, (1), 39-54.

7. Bhattacharjee, A.; Bansal, M., Collagen Structure: The Madras Triple Helix and the Current Scenario. *IUBMB Life* **2005,** 57, (3), 161-172.

8. Hulmes, D. J. S., Building collagen molecules, fibrils, and suprafibrillar structures. *Journal of Structural Biology* **2002,** 137, (1-2), 2-10.

9. Kadler, K. E.; Holmes, D. F.; Trotter, J. A.; Chapman, J. A., Collagen fibril formation. *Biochemical Journal* **1996,** 316, (1), 1-11.

10. Koch, M.; Laub, F.; Zhou, P.; Hahn, R. A.; Tanaka, S.; Burgeson, R. E.; Gerecke, D. R.; Ramirez, F.; Gordon, M. K., Collagen XXIV, a Vertebrate Fibrillar Collagen with Structural Features of Invertebrate Collagens. *Journal of Biological Chemistry* **2003,** 278, (44), 43236-43244.

11. Pace, J. M.; Corrado, M.; Missero, C.; Byers, P. H., Identification, characterization and expression analysis of a new fibrillar collagen gene, COL27A1. *Matrix Biology* **2003,** 22, (1), 3-14.

12. Gupta, H. S.; Wagermaier, W.; Zickler, G. A.; Hartmann, J.; Funari, S. S.; Roschger, P.; Wagner, H. D.; Fratzl, P., Fibrillar level fracture in bone beyond the yield point. *International Journal of Fracture* **2006,** 139, (3-4), 425-436.

13. Nanci, A., Content and distribution of noncollagenous matrix proteins in bone and cementum: relationship to speed of formation and collagen packing density. *Journal of structural biology* **1999,** 126, (3), 256-69.

14. Weiner, S.; Wagner, H. D., The material bone: structure-mechanical function relations. *Annual Review of Materials Science* **1998,** 28, 271-298.

15. Hodge, A. J.; Petruska, J. A., Recent studies with the electron microscope on ordered aggregates of the tropocollagen molecule. In *Aspects of Protein Structure*, Ramachandran, G. N., Ed. Academic Press: New York, 1963; pp 289-300.

16. Nylen, M. U.; Scott, D. B.; Mosley, V. M., Mineralization of turkey leg tendon. II. Collagen-mineral relations revealed by electron and x-ray microscopy. **1960,** No. 64, 129-42.

17. Landis, W. J., The strength of a calcified tissue depends in part on the molecular structure and organization of its constituent mineral crystals in their organic matrix. *Bone (New York, NY, United States)* **1995,** 16, (5), 533-44.

18. Traub, W.; Arad, T.; Weiner, S., Three-dimensional ordered distribution of crystals in turkey tendon collagen fibers. *Proceedings of the National Academy of Sciences of the United States of America* **1989,** 86, (24), 9822-6.

19. Currey, J. D.; Zioupos, P.; Davies, P.; Casinos, A., Mechanical properties of nacre and highly mineralized bone. *Proceedings of the Royal Society of London Series B-Biological Sciences* **2001,** 268, (1462), 107-111.

20. Dorozhkin, S. V.; Epple, M., Biological and medical significance of calcium phosphates. *Angewandte Chemie, International Edition* **2002,** 41, (17), 3130-3146.

21. Eastoe, J. E.; Eastoe, B., Organic constituents of mammalian compact bone. *Biochemical Journal* **1954,** 57, 453-9.

22. Fisher, L. W.; Termine, J. D., Noncollagenous proteins influencing the local mechanisms of calcification. *Clinical Orthopaedics and Related Research* **1985,** 200, 362-85.

23. Olszta, M. J.; Odom, D. J.; Douglas, E. P.; Gower, L. B., A New Paradigm for Biomineral Formation: Mineralization via an Amorphous Liquid-Phase Precursor. *Connective Tissue Research* **2003,** 44, (Suppl. 1), 326-334.

24. Currey, J. D., Biomechanics of mineralized skeletons. In *Skeletal Biomineralization :Patterns, processes, and evolutionary trends*, 1 ed.; Carter, J. G., Ed. Van Nostrand: New York, 1990; Vol. 1, p 11.

25. Landis, W. J.; Hodgens, K. J.; Song, M. J.; Arena, J.; Kiyonaga, S.; Marko, M.; Owen, C.; McEwen, B. F., Mineralization of collagen may occur on fibril surfaces: evidence from conventional and high-voltage electron microscopy and three-dimensional imaging. *Journal of structural biology* **1996,** 117, (1), 24-35.

26. Moradianoldak, J.; Weiner, S.; Addadi, L.; Landis, W. J.; Traub, W., Electron imaging and diffraction study of individual crystals of bone, mineralized tendon

and synthetic carbonate apatite. *Connective Tissue Research* **1991,** 25, (3-4), 219-228.

27. Bhowmik, R.; Katti, K. S.; Katti, D. R., Mechanics of molecular collagen is influenced by hydroxyapatite in natural bone. *Journal of Materials Science* **2007,** 42, (21), 8795-8803.

28. Bhowmik, R.; Katti, K. S.; Katti, D. R., Mechanisms of Load-Deformation Behavior of Molecular Collagen in Hydroxyapatite-Tropocollagen Molecular System: Steered Molecular Dynamics Study. *Journal of Engineering Mechanics-Asce* **2009,** 135, (5), 413-421.

29. Sikdar, D.; Pradhan, S. M.; Katti, D. R.; Katti, K. S.; Mohanty, B., Altered phase model for polymer clay nanocomposites. *Langmuir* **2008,** 24, (10), 5599-5607.

30. Ghosh, P.; Katti, D. R.; Katti, K. S., Mineral Proximity Influences Mechanical Response of Proteins in Biological Mineral-Protein Hybrid Systems. *Biomacromolecules* **2007,** 8, (3), 851-856.

31. Katti, K.; Katti, D. R.; Tang, J.; Pradhan, S.; Sarikaya, M., Modeling mechanical responses in a laminated biocomposite - Part II - Nonlinear responses and nuances of nanostructure. *Journal of Materials Science* **2005,** 40, (7), 1749-1755.

32. Katti, D. R.; Pradhan, S. M.; Katti, K. S., Directional dependence of hydroxyapatite-collagen interactions on mechanics of collagen. *Journal of Biomechanics* **2010,** 43, (9), 1723-1730.

33. Qin, Z.; Gautieri, A.; Nair, A. K.; Inbar, H.; Buehler, M. J., Thickness of Hydroxyapatite Nanocrystal Controls Mechanical Properties of the Collagen-Hydroxyapatite Interface. *Langmuir* **2012,** 28, (4), 1982-1992.

34. Dubey, D. K.; Tomar, V., Role of hydroxyapatite crystal shape in nanoscale mechanical behavior of model tropocollagen-hydroxyapatite hard biomaterials. *Materials Science and Engineering: C* **2009,** 29, (7), 2133-2140.

35. Dubey, D. K.; Tomar, V., Effect of changes in tropocollagen residue sequence and hydroxyapatite mineral texture on the strength of ideal nanoscale tropocollagen-hydroxyapatite biomaterials. *Journal of Materials Science-Materials in Medicine* **2010,** 21, (1), 161-171.

36. Dubey, D. K.; Tomar, V., Role of the nanoscale interfacial arrangement in mechanical strength of tropocollagen-hydroxyapatite-based hard biomaterials. *Acta Biomaterialia* **2009,** 5, (7), 2704-2716.

37. Almora-Barrios, N.; de Leeuw, N. H., A Density Functional Theory Study of the Interaction of Collagen Peptides with Hydroxyapatite Surfaces. *Langmuir* **2010,** 26, (18), 14535-14542.

38. Hellmich, C.; Barthelemy, J. F.; Dormieux, L., Mineral-collagen interactions in elasticity of bone ultrastructure - a continuum micromechanics approach. *European Journal of Mechanics a-Solids* **2004,** 23, (5), 783-810.

39. Fritsch, A.; Hellmich, C.; Dormieux, L., Ductile sliding between mineral crystals followed by rupture of collagen crosslinks: Experimentally supported micromechanical explanation of bone strength. *Journal of Theoretical Biology* **2009,** 260, (2), 230-252.

40. Pradhan, S. M.; Katti, D. R.; Katti, K. S., Steered Molecular Dynamics Study of Mechanical Response of Full Length and Short Collagen Molecules. *Journal of Nanomechanics and Micromechanics* **2011,** 1, (3), 104-110.

41. Gautieri, A.; Buehler, M. J.; Redaelli, A., Deformation rate controls elasticity and unfolding pathway of single tropocollagen molecules. *Journal of the Mechanical Behavior of Biomedical Materials* **2009,** 2, (2), 130-137.

42. Lorenzo, A. C.; Caffarena, E. R., Elastic properties, Young's modulus determination and structural stability of the tropocollagen molecule: a computational study by steered molecular dynamics. *Journal of Biomechanics* **2005,** 38, (7), 1527-1533.

43. Buehler, M. J., Atomistic and continuum modeling of mechanical properties of collagen: elasticity, fracture, and self-assembly. *Journal of Materials Research* **2006,** 21, (8), 1947-1961.

44. Gautieri, A.; Vesentini, S.; Redaelli, A.; Buehler, M. J., Hierarchical Structure and Nanomechanics of Collagen Microfibrils from the Atomistic Scale Up. *Nano Letters* **2011,** 11, (2), 757-766.

45. Streeter, I.; de Leeuw, N. H., A molecular dynamics study of the interprotein interactions in collagen fibrils. *Soft Matter* **2011,** 7, (7), 3373-3382.

46. Streeter, I.; de Leeuw, N. H., Atomistic Modeling of Collagen Proteins in Their Fibrillar Environment. *Journal of Physical Chemistry B* **2010,** 114, (41), 13263-13270.

47. Tang, Y.; Ballarini, R.; Buehler, M. J.; Eppell, S. J., Deformation micromechanisms of collagen fibrils under uniaxial tension. *Journal of The Royal Society Interface* **2010,** 7, (46), 839-850.

48. Buehler, M. J., Nanomechanics of collagen fibrils under varying cross-link densities: Atomistic and continuum studies. *Journal of the Mechanical Behavior of Biomedical Materials* **2008,** 1, (1), 59-67.

49. Buehler, M. J., Molecular nanomechanics of nascent bone: fibrillar toughening by mineralization. *Nanotechnology* **2007,** 18, (29).

50. Pradhan, S.; Katti, K.; Katti, D., A Multiscale Model of Collagen Fibril in Bone: Elastic Response. *Journal of Engineering Mechanics* **2012**.

51. Feller, S. E.; Zhang, Y. H.; Pastor, R. W.; Brooks, B. R., CONSTANT-PRESSURE MOLECULAR-DYNAMICS SIMULATION - THE LANGEVIN PISTON METHOD. *Journal of Chemical Physics* **1995,** 103, (11), 4613-4621.

52. Phillips, J. C.; Braun, R.; Wang, W.; Gumbart, J.; Tajkhorshid, E.; Villa, E.; Chipot, C.; Skeel, R. D.; Kale, L.; Schulten, K., Scalable molecular dynamics with NAMD. *Journal of Computational Chemistry* **2005,** 26, (16), 1781-1802.

53. MacKerell, A. D.; Bashford, D.; Bellott, M.; Dunbrack, R. L.; Evanseck, J. D.; Field, M. J.; Fischer, S.; Gao, J.; Guo, H.; Ha, S.; Joseph-McCarthy, D.; Kuchnir, L.; Kuczera, K.; Lau, F. T. K.; Mattos, C.; Michnick, S.; Ngo, T.; Nguyen, D. T.; Prodhom, B.; Reiher, W. E.; Roux, B.; Schlenkrich, M.; Smith, J. C.; Stote, R.; Straub, J.; Watanabe, M.; Wiorkiewicz-Kuczera, J.; Yin, D.; Karplus, M., All-atom empirical potential for molecular modeling and dynamics studies of proteins. *Journal of Physical Chemistry B* **1998,** 102, (18), 3586-3616.

54. Bhowmik, R.; Katti, K. S.; Katti, D., Molecular dynamics simulation of hydroxyapatite-polyacrylic acid interfaces. *Polymer* **2007,** 48, (2), 664-674.

55. Saber-Samandari, S.; Gross, K. A., Micromechanical properties of single crystal hydroxyapatite by nanoindentation. *Acta Biomaterialia* **2009,** 5, (6), 2206-2212.

56. Grandbois, M.; Beyer, M.; Rief, M.; Clausen-Schaumann, H.; Gaub, H. E., How Strong Is a Covalent Bond? *Science* **1999,** 283, (5408), 1727.

57. Lantz, M. A.; Hug, H. J.; Hoffmann, R.; van Schendel, P. J. A.; Kappenberger, P.; Martin, S.; Baratoff, A.; Güntherodt, H. J., Quantitative Measurement of Short-Range Chemical Bonding Forces. *Science* **2001,** 291, (5513), 2580-2583.

58. Buehler, M. J., Nature designs tough collagen: Explaining the nanostructure of collagen fibrils. *Proceedings of the National Academy of Sciences of the United States of America* **2006,** 103, (33), 12285-12290.

59. Shen, Z. L.; Dodge, M. R.; Kahn, H.; Ballarini, R.; Eppell, S. J., Stress-strain experiments on individual collagen fibrils. *Biophysical Journal* **2008,** 95, (8), 3956-3963.

60. Cribb, A. M.; Scott, J. E., Tendon response to tensile stress: an ultrastructural investigation of collagen: proteoglycan interactions in stressed tendon. *Journal of anatomy* **1995,** 187.

61. Redaelli, A.; Vesentini, S.; Soncini, M.; Vena, P.; Mantero, S.; Montevecchi, F. M., Possible role of decorin glycosaminoglycans in fibril to fibril force transfer in relative mature tendons—a computational study from molecular to microstructural level. *Journal of Biomechanics* **2003,** 36, (10), 1555-1569.

62. Provenzano, P. P.; Vanderby Jr, R., Collagen fibril morphology and organization: Implications for force transmission in ligament and tendon. *Matrix Biology* **2006,** 25, (2), 71-84.

CHAPTER 9. EVOLUTION OF MOLECULAR INTERACTIONS IN THE INTERLAYER OF NA-MONTMORILLONITE SWELLING CLAY WITH INCREASING HYDRATION

This chapter seeks to understand the swelling behavior of clay by exploring the evolution of molecular interaction in the Na-montmorillonite clay with increasing degrees of interlayer hydration. The content of this chapter has been submitted for publication.

9.1. Introduction

The swelling behavior of smectite clays are widely known for its detrimental effect on the civil infrastructures, resulting in millions of dollars in damage every year throughout the world. However, smectite clays are not without the number of useful applications such as in case of the borehole stabilization during drilling, drug delivery systems and in polymer-clay-nanocomposite for the enhancement of material properties. The expansive nature of these clays when exposed to water resulting in the large change in its volume, or alternatively the large build up in swelling pressure when the volume is confined continues to be the topic of extensive research. The theory of Stern and Guoy, known as diffuse double layer theory, is one of the earlier models that attempts to explain interactions between clay and water in the interlayer (1). Another theory called DLVO (Derjaguin, Landau, Verwey and Overbeek) theory (2, 3) is able to describe stability of clay colloidal suspension fairly well for larger spacing, but is not satisfactory for spacing smaller than 20Å. However, despite the wide prevalence of these theories, they fail at smaller layer spacings and are unable to describe swelling behavior.

In addition to the theoretical studies described above there are numbers of computational studies on swelling behavior of hydrated smectite clays using molecular

dynamics (MD) and Monte Carlo (MC) methods (4-11). Skipper et al. (4) carried out Monte Carlo and molecular dynamics computer simulation of interlayer water in 2:1 clays. Delville (11, 12) conducted Monte Carlo simulation to quantify swelling and showed that solvation of the interlayer cations have important role on the swelling properties of clay. Karaborni et al. (7) used both MC and MD simulations to study the mechanism of swelling. Tambach et al. (8) did molecular simulations of swelling clay minerals to study different types of clay, water models and cations. Smith et al. (9, 10, 13, 14) devised grand canonical molecular dynamics and Monte Carlo simulation and showed the dependencies of clay swelling on pressure, temperature and chemical potential. Katti et al (15) carried out first steered molecular dynamics (SMD) studies to investigate the mechanical response of clay mineral pyrophyllite interlayer. Similar studies were carried out on sodium montmorillonite to study its mechanical response under different amounts of hydration (16, 17). In addition to these computational studies the experimental investigations have been carried out by Katti et al to investigate evolution of clay microstructure during swelling using scanning electron microscopy (17, 18). It was shown that during swelling the clay particles successively break down resulting in smaller particle size. This finding was incorporated into a separate computational study using discrete element method (DEM) to investigate the effect of particle breakdown on the swelling and swelling pressure (19).

In this study we carry out molecular modeling of montmorillonite with increasing amounts of water in the interlayer, up to ten layers of water, using molecular dynamics. This study of focused on investigating the molecular mechanisms involved in different levels of hydration through the detailed study of interactions between clay layers,

interlayer water and cations. In addition, the evolution of interlayer spacing and conformation of water molecules in the interlayer are also explored.

9.2. Construction of Clay Model

The sodium montmorillonite (Na-Mt) used in this study has a chemical formula $NaSi_{16}(Al_6FeMg)O_{20}(OH)_4$, which is a simplified model of the clay sample (Swy-2) acquired from The Clay Minerals Society source clays repository for our previous study (16, 17, 20). The montmorillonite has a tetrahedral-octaheral-tetrahedral structure. The octahedral sheet of Na-Mt is substituted by a cation of lesser charge resulting in a layer charge of 0.5|e| per unit cell, which is counterbalanced by 0.5Na cations per unit cell in the clay interlayer.

The molecular model of clay we have constructed is shown in figure 9.1. The initial unit cell dimensions are 5.28 Å × 9.14 Å × 6.56 Å (10^{-10}m; 1 Å = 0.1 nm). Each of the clay layers consist of four unit cells in the X direction and two unit cells in Y direction, resulting in an overall dimension of 21.12 Å × 18.28 Å × 6.56 Å. The initial basal spacing of 10 Å was used. Basal spacing is defined as a distance from the top of first clay layer to the top of second clay layer. The detailed description of the construction of montmorillonite structure can be found in our previous work (16).

The hydrated models of clay consisting of two, four, six, eight, and ten monolayers of water were constructed by introducing water between clay layers as shown in figure 9.2. The level of hydration in these models corresponds to interlayer moisture of 20%, 40%, 60%, 80%, and 100% respectively. The total numbers of water molecules used in our model corresponding to the different levels of hydration are 64, 128, 192, 256, and 320 respectively. The water model used in the MD studies is TIP3P (21).

We have carried out molecular modeling of clay using Molecular Dynamics (MD). Molecular dynamics (MD) is a molecular modeling technique used to simulate behavior of molecules and molecular systems.

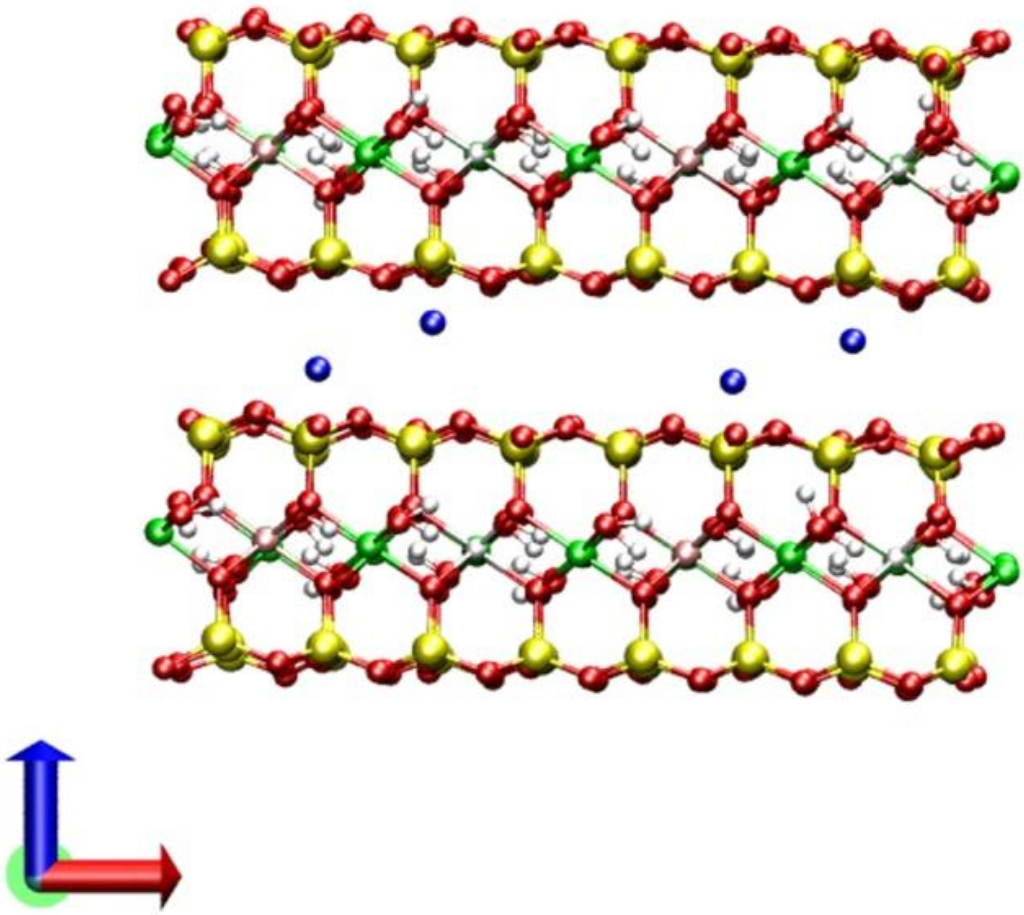

Figure 9.1. Molecular model of Na-montmorillonite showing clay layers and sodium ions.

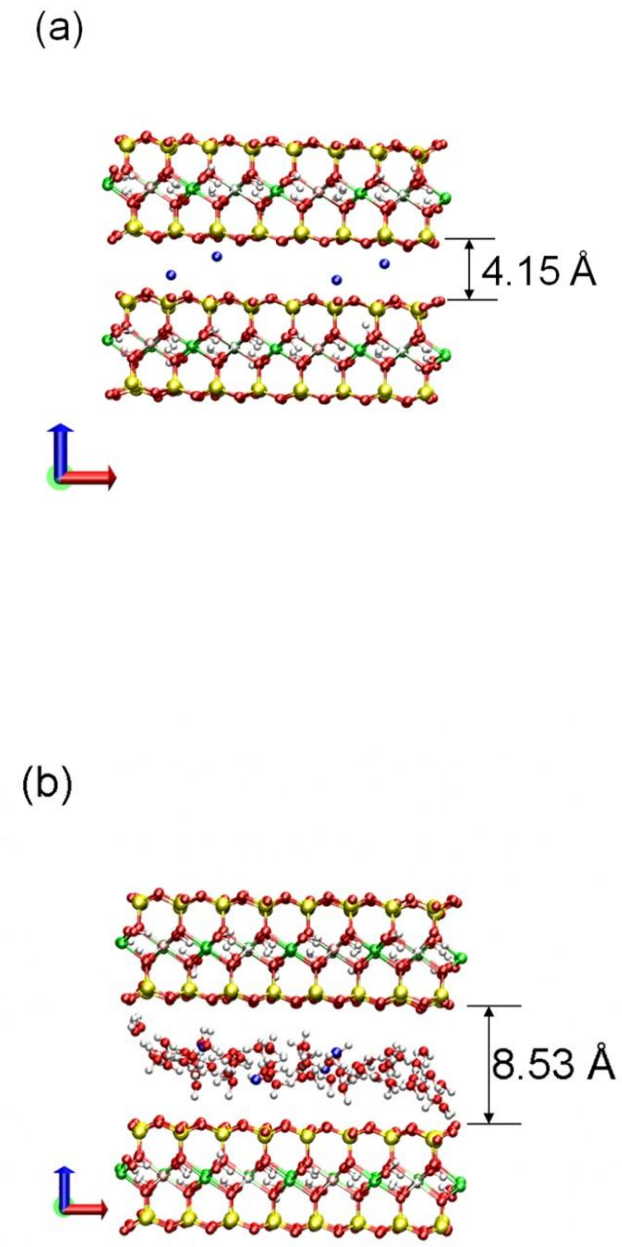

Figure 9.2. Montmorillonite models with different levels of interlayer hydration consisting of, (a) dry clay, (b) two layers, (c) four layers, (d) six layers, (e) eight layers, (f) ten layers of water.

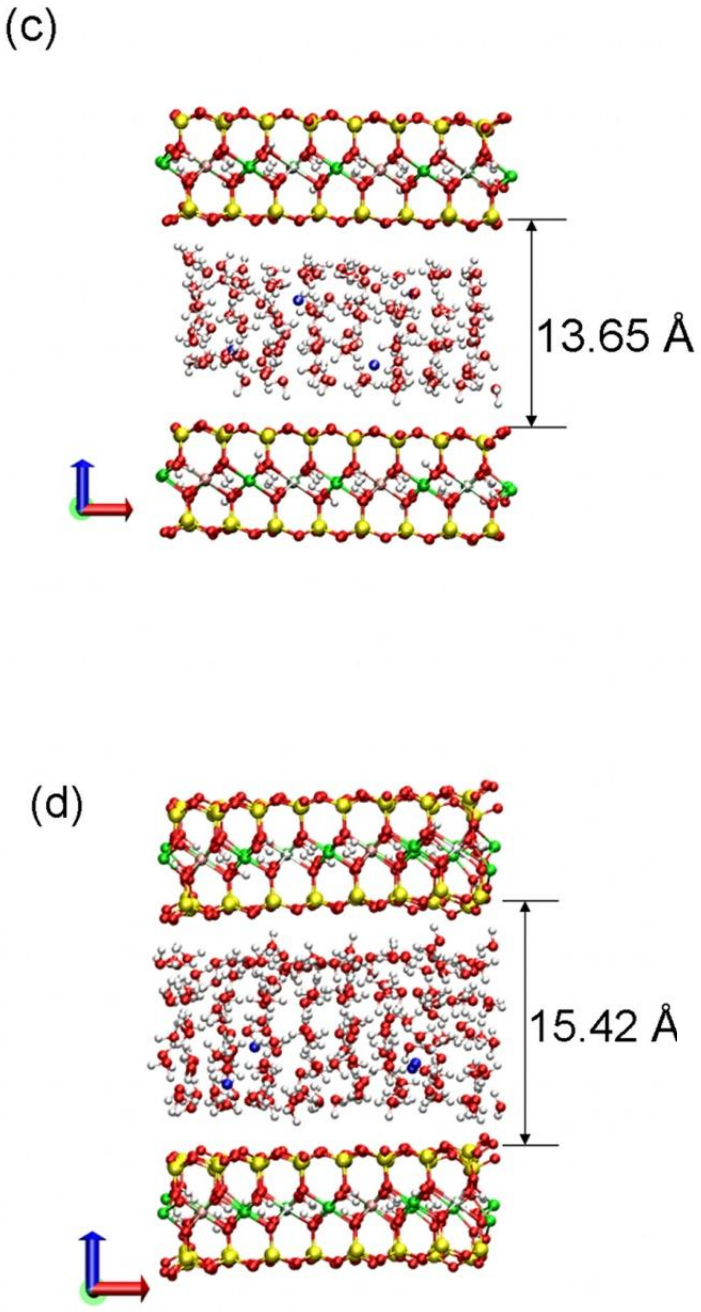

Figure 9.2. Montmorillonite models with different levels of interlayer hydration consisting of, (a) dry clay, (b) two layers, (c) four layers, (d) six layers, (e) eight layers, (f) ten layers of water. (Continued)

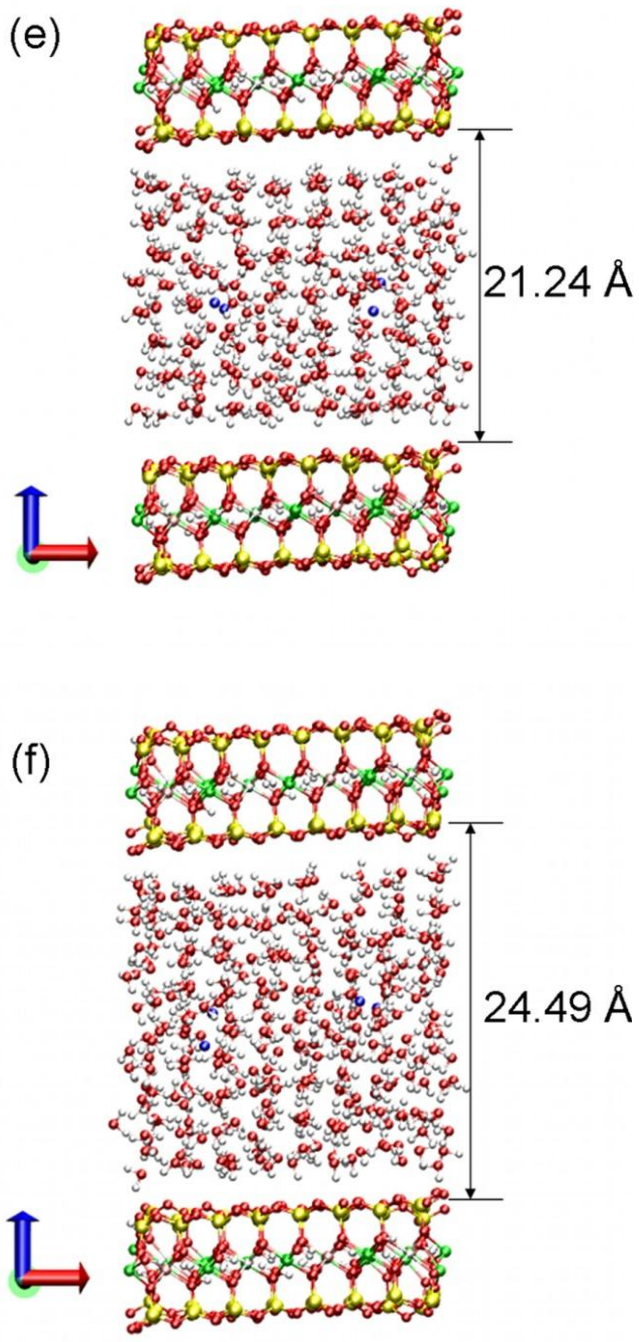

Figure 9.2. Montmorillonite models with different levels of interlayer hydration consisting of, (a) dry clay, (b) two layers, (c) four layers, (d) six layers, (e) eight layers, (f) ten layers of water. (Continued)

9.3. Simulation Details

We have used NAMD (22, 23) package developed by Theoretical and Computational Biophysics Group in the Beckman Institute for Advanced Science and Technology at the University of Illinois at Urbana-Champaign for carrying out our molecular dynamics study. Visual molecular dynamics (VMD) program (24), which is also developed by Theoretical and Computational Biophysics Group in the Beckman Institute was used for visualization and analysis. The hydrated clay was minimized using conjugate gradient method. All the molecular dynamics simulations were carried out at isothermal-isobaric (NPT) conditions. The temperature and pressure were increased in steps and equilibrated at 300 K and 1.01 bar respectively. The model was equilibrated for 400,000 steps (200ps), using the time step of 0.5 femtoseconds. Periodic boundary conditions were used in all the simulations. CHARMm (Chemistry at Harvard Macromolecular Mechanics) (25) force field is used for calculating energies. Parameters for CHARMm force field were derived from CFF parameters (26) as described in our previous study (15-17). The interaction energies between constituents were computed using NAMD Energy plugin of VMD software. For calculation of interaction energy, the last 20 picoseconds of simulation trajectory were used. All the simulations were carried out at the Center for High Performance Computing (CHPC) at North Dakota State University. The simulations were conducted on 96-node/192 processor (Dual 3.06 GHz Xeon-HT processors) distributed-memory Cluster.

9.4. Results

The interlayer spacing of dry montmorillonite and hydrated clay layers consisting different number of water monolayers are shown in figure 9.2. The interlayer spacing

corresponding to the dry montmorillonite is about 4.14 Å. The water which enters the interlayer is subject to the nonbonded interactions due to the clay layers and the sodium ions present in the interlayer. These nonbonded interactions are Van der Waals and Columbic in origin. The equilibrium of the nonbonded interactions between clay layers, water molecules, and cations at a given temperature and pressure determines the resultant interlayer spacing when different amounts of water enter the clay gallery. The interlayer spacing corresponding to two, four, six, eight, and ten monolayers of water are about 8.53 Å, 13.65 Å, 15.1 Å, 22.3 Å, and 24.50 Å respectively.

The hydrated clay is comprised of following components: clay layers, sodium, and water. The interactions between these components are collectively responsible for the swelling behavior of clay. These interactions are represented in the schematic diagram shown in figure 9.3. Specifically, the interaction energies between two adjacent clay layers, clay layers and sodium, clay and sodium-bound water, sodium and clay-bound water, and clay-bound water and sodium-bound water are presented. The interaction energy is defined as a negative of the energy that has to be expended in completely separating two objects. Therefore, negative interaction energy implies attractive interaction (especially if it is predominantly electrostatic in origin), whereas the positive interaction energy implies repulsion between two sets of atoms/molecules. The water molecules which are very close to the clay are capable of forming a strong bond with the negatively charged clay surface.

The evolution of interaction energies between various constituents and increasing hydration in the interlayer is shown in Figure 9.4. The figure also shows the increasing interlayer spacing with increasing hydration level. The figure indicates that the strongest

attractive interactions are between Na-ions and the clay sheets (predominantly electrostatic in nature) followed by clay-clay interactions (as a result of mainly Van der Waals interactions) for the dry condition (zero monolayers of water). It appears that for the dry condition, the sodium ions play a dominant role in keeping the stacked structure together. With the increase in hydration, the clay-clay attractive interactions rapidly decrease to almost zero for 4 monolayers of water. The Na-clay attractive interactions also show reduction in the interaction energies with increasing hydration, although at much smaller rate and are present even up to 10 monolayers of interlayer water. The Na-clay attractive interactions are predominantly electrostatic in nature for all levels of hydration.

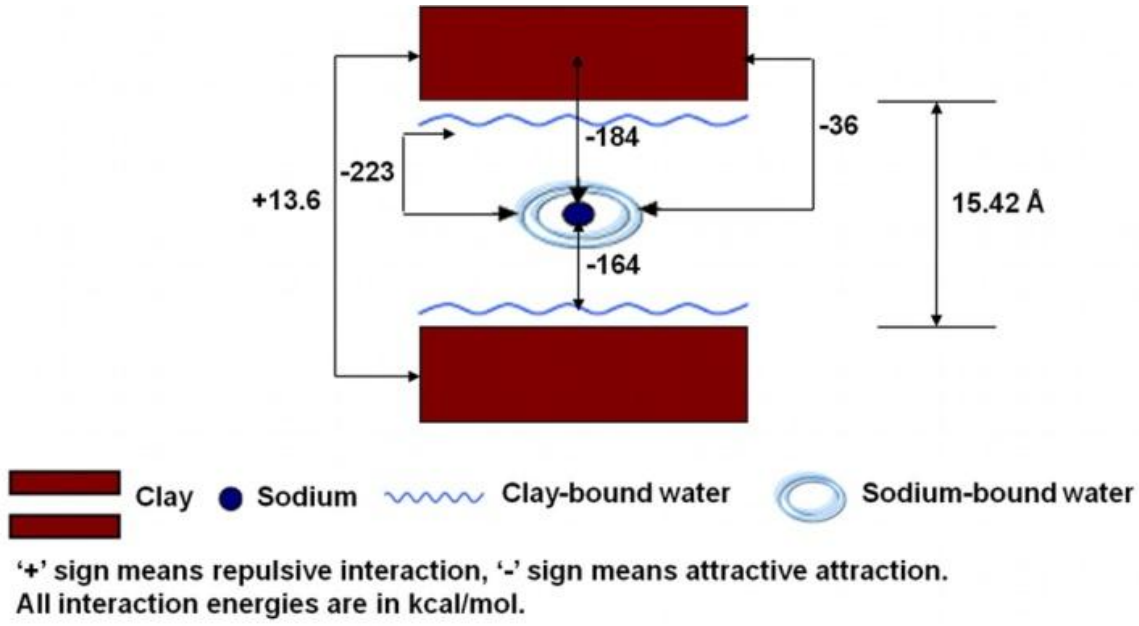

Figure 9.3. Schematic diagram showing various interactions calculated between adjacent clay layers, clay layers and sodium, clay and sodium-bound water, sodium and clay-bound water, and clay-bound water and sodium-bound water.

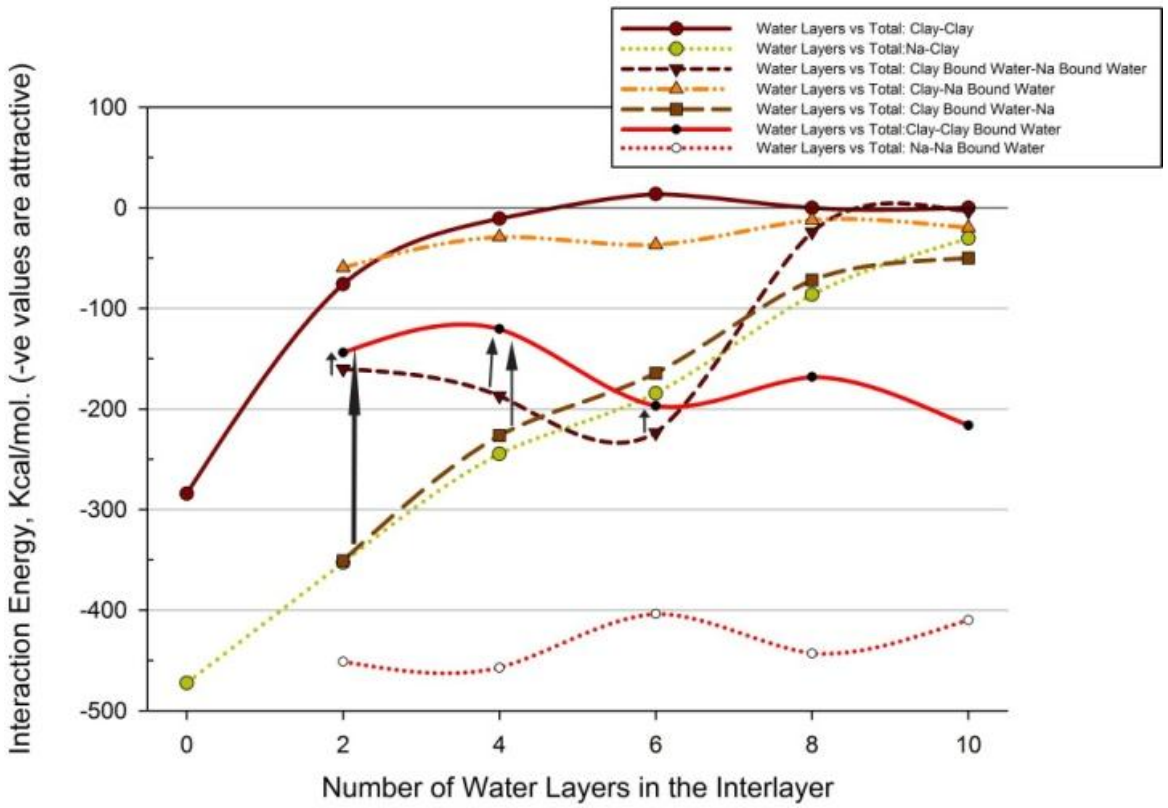

Figure 9.4. Evolution of interaction energies with increasing water layers in the interlayer. Positive values of interaction energies indicate attractive interactions. Large attractive interaction energies are observed between Na-ions and water molecules in their close proximity (≤ 3.5 Å) and clay and water molecules in their close proximity leading to the concept of bound water. Arrows show limits placed on the magnitude of clay bound water-Na bound water and clay bound water and Na-ions attractive interactions towards the stability of the clay structure due to clay bound water attractive interaction energies.

Water in the close proximity of Na-ions and clay surfaces show more organization compared to bulk water. We have defined the water molecules within a distance of 3.5 Å of clay surface and 3.5 Å of Na-ions as clay bound water and Na-bound water respectively. This magnitude of this distance is the typical range for hydrogen bond interactions (27-29). The authors have observed bound water phenomenon with mineral surfaces in other materials systems (30-33). In Figure 9.5, the variation of non-bonded interactions between Na-ions and Na-bound water with increasing hydration is shown. These interaction energies are among the largest attractive interactions among all interactions shown on the plot, for hydrated condition. The variation of these interactions with increasing water layers appear to be narrow. The water molecules in the Na-bound water are strongly attracted to the Na-ions. The plot also shows the variation of non-bonded molecular interactions between clay sheets and clay bound water molecules. The interactions are attractive in nature and are quite significant, although smaller in magnitude compared to Na-Na bound water interactions. These interactions show some increase in the magnitude of attractive interactions with hydration as a result of increasing number of water molecules interacting with the clay surfaces. Thus, the clay bound water is strongly attracted towards the clay surfaces. The bound water –Na or bound water-clay interactions are a result of both Van der Waals and electrostatic interactions.

In Figure 9.5, we have also plotted the variation of interactions between clay bound water and sodium bound water with hydration. These interactions are attractive in nature and become almost negligible at the hydration level of 10 layers of water in the interlayer. The plot shows the magnitude of these interactions to be larger than the clay-

clay bound water interaction energies for hydration levels of two to six monolayers of water, however, the clay-clay bound water attractive interaction energies will be the limiting attractive energy to hold the stacked structure together. A plot of clay bound water-Na ions interaction energies with increasing hydration is shown in the same figure. These interactions are also attractive in nature and decrease with increasing levels of hydration. Similar to the Clay bound water-Na bound water interactions, initially the magnitude of attractive energies of these interactions are larger than the clay-clay bound water interaction energies and thus the clay-clay bound water attractive interaction energies will be the limiting attractive energy to hold the stacked structure together. The clay-Na bound water interactions, although relatively smaller in magnitude compared to the other bound water interactions are also attractive in nature and are present for all levels of hydration used in the simulations.

The nature of non-bonded interactions, whether electrostatic or Van der Waals provide an insight into the role of molecular proximity and charge on the swelling behavior of the interlayer. In the dry state, the magnitude of attractive clay-clay (sheets) interactions are composed of -239.8 Kcal/mol. Van der Waals energy and -44.4 Kcal/mol. electrostatic energy for a total interaction energy of -284.2 Kcal/mol. For the same condition, the magnitude of Na ions-clay sheets interaction energy consists of +39 Kcal/mol. (repulsive) Van der Waals energy and -511.3 Kcal/mol. electrostatic energy for a total interaction energy of -472.3 Kcal/mol. It appears that in the dry state, the large attractive Na-clay interactions bring the clay sheets closer and those interactions provide the structural stability for stacking of the clay sheets.

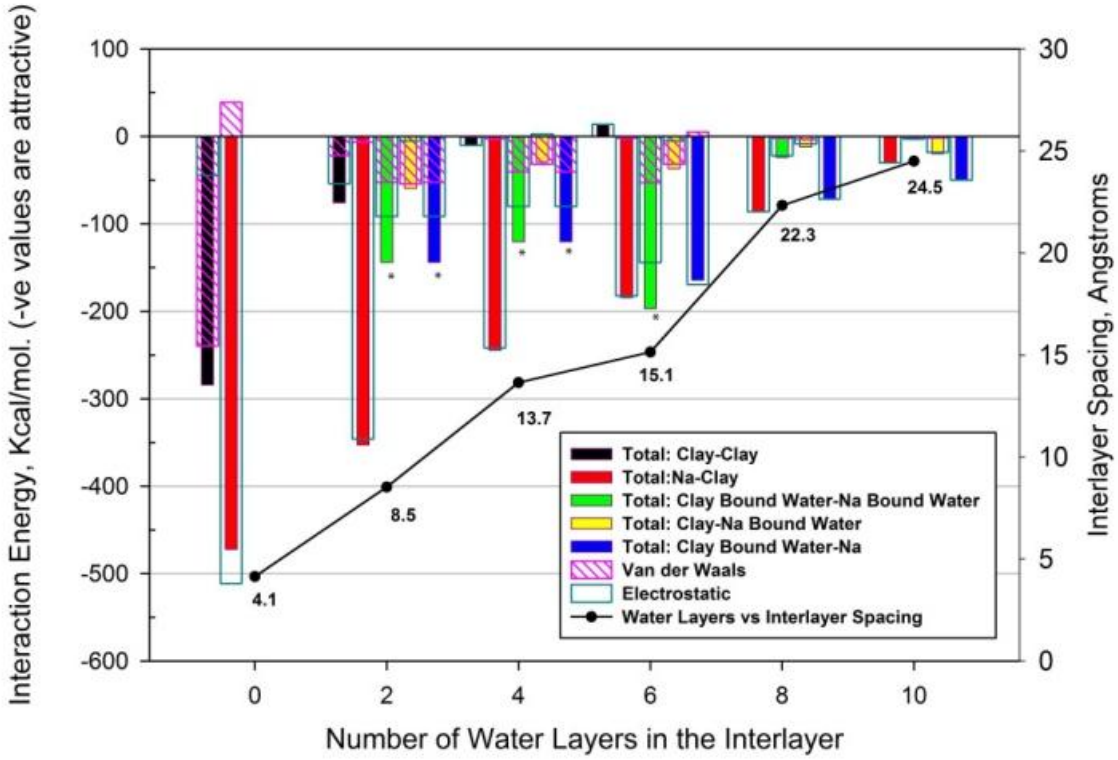

Figure 9.5. Increase in the interlayer spacing with increasing interlayer water and the corresponding interaction energies. The contribution of Van der Waals and electrostatic interactions on the interaction energy values are also shown. Stars below the bars indicate limiting interaction energy values.

With hydration, the Na ions- Na bound water interactions are initiated. These interactions are predominantly electrostatic in nature. For the Na-Na bound water interactions, for the two monolayer level of interlayer hydration, the total attractive interaction is -451.2 Kcal/mol. and comprises of +31.2 Kcal/mol Van der Waals energy and -482.4 Kcal/mol. electrostatic energy. These interactions do not change significantly

at 10 monolayer hydration level, where the total Na-Na bound water attractive interaction is -409.9 Kcal/mol. and comprises of +29.8 Kcal/mol. Van der Waals energy and -439.7 Kcal/mol. This suggests that the Na-ions are almost fully hydrated at the two monolayer hydration level. Also, the large electrostatic interactions hold the water molecules in the close proximity of Na-ions. Similarly, for the clay-clay bound water interactions, for the two monolayer water interlayer hydration level, the total interaction energy is -144 Kcal/mol. which comprises of -52.5 Kcal/mol. Van der Waals energy and -91.5 Kcal/mol. electrostatic energy. With increasing hydration, the tendency for this energy is to increase as a result of additional water molecules interacting with clay sheets and the magnitude of the interaction energy for 10 monolayer water interlayer hydration is -216.4 Kcal/mol. and comprises of -39 Kcal/mol. Van der Waals energy and -177.4 Kcal/mol. electrostatic energy. The large magnitude of attractive interactions between clay or Na and corresponding bound water molecules indicate that these water molecules are strongly bound. For the remaining interaction pairs, electrostatic interactions compared to Van der Waals interactions, play predominant role in the clay interlayer during hydration.

In figure 9.6, comparisons are made between the attractive interactions between Na-ions and clay sheets and cumulative bound water interactions (Clay bound water-Na bound water; Clay bound water-Na; and Clay-Na bound water). As observed in the schematic diagram in figure 9.3, all of these attractive interactions will contribute to maintaining the stacked structure of the clay together. For two, four, six, eight and ten monolayer interlayer hydration levels, the Na-clay attractive interaction values are -353 Kcal/mol., -245 Kcal/mol., -184.4 Kcal/mol., -86.3 Kcal/mol. and -30.3 Kcal/mol.. For

two, four, six, eight and ten monolayer interlayer hydration levels, the Bonded water-clay/Na cumulative attractive interaction values are -144 Kcal/mol., -120.5 Kcal/mol., -197 Kcal/mol. -95.6 Kcal/mol. and -53.5 Kcal/mol. Thus the contribution of attractive interactions in the interlayer by the bound water is significant. Relative to the Na-clay attractive interactions, the contribution of bonded interactions towards attractive interactions in the interlayer for two, four, six, eight and ten monolayer interlayer hydration levels are 40.79%, 49.18%, 106.83%, 110.78% and 176.56%. In fact, at six, eight and ten monolayer hydration levels, the attractive interactions from bonded water are higher than the Na-clay attractive interactions. Thus, the increasing water in the interlayer not only causes the interlayer to swell, but also contributes significantly to maintaining the intercalated structure for relatively large amount of hydration. Thus the bound water interactions along with other binding interactions allow for the stability of stacked clay structure at larger interlayer water content. Significant interlayer swelling at large water content has been observed experimentally by Foster etal. (34) and several other researchers. Beyond four monolayers of water, contribution of water in stabilizing the clay structure exceeds the contribution of Na-clay interactions. It should be noted that beyond 10 monolayers of water, the attractive interaction energies become negligible, leading to potential for exfoliation under free swelling condition.

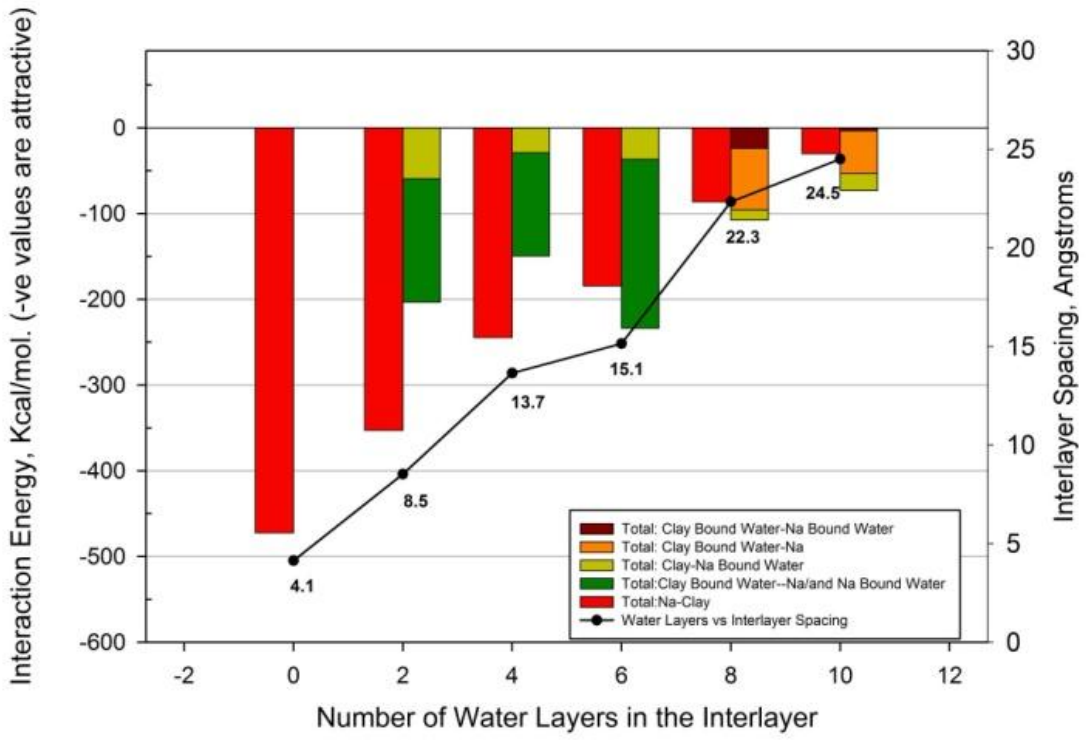

Figure 9.6. Plot shows the comparison of clay sheet- Na-ions interaction energies with increasing interlayer hydration and cumulative bound water binding interaction energies with increasing interlayer hydration. The bound water interactions contribute significantly to the binding interactions within the clay interlayer with increasing hydration.

Although the water is a neutral molecule, it consists of negative partial charge on the oxygen atom and positive partial charge on hydrogen atoms. This results in a permanent dipole moment of the water. The experimental dipole moment of individual water molecules is 1.85 D. Dipole moment of water is a vector pointing away from oxygen atom along the bisector of an angle between hydrogen, oxygen, and hydrogen.

The dipole moment is a vector defined as $P=\Sigma q\mathbf{r}$, where q is the charge and **r** is a position vector of the charge. For our simulations we have used TIP3P model of water and assume that the dipole moment of each water molecule remains constant during simulation. The water molecules in a solution interact with each other due to the partial charges on oxygen and hydrogen atoms through dipole-dipole interactions. In addition, the dipole moment of water also interacts with the electrostatic field of clay and cations to orient themselves in a certain direction. We can add the dipole moment vectors of each water atoms to obtain the total dipole moment. The direction of the total dipole moment vector can tell us about the general orientation of the water molecules in an average sense. The dipole moment of the upper and lower layers of water molecules separated by an equatorial plane is shown in figure 9.7 for different number of water monolayers. In case of clay with two layers of the water all of the water molecules are under the combined influence of both clay layers and sodium ions. The clay sheets have a net negative charge (due to isomorphous substitution), which attracts hydrogen atom of water while repelling oxygen atom. At small separation between clay layers, as in case of two layers of water, the opposite clay layers compete with each other to attract hydrogen atoms of water molecule towards themselves. At the same time, the Na-ions have strong attractive interactions with the water molecules. These interactions result in the net direction of dipole moment of water to become relatively horizontal (Fig. 9.7). However, when the number of water layers increase, leading to the greater separation between clay layers, the water molecules above the equatorial plane are influenced more by the upper clay layer and the water molecules below the equatorial plane are influenced more by the lower clay layer. In such a situation, the net dipole moment of upper and lower water starts pointing

towards clay sheets as seen in figure for four, six, and eight layers of water. This implies that at larger separation between clay sheets the water molecules above and below the equatorial plane point in opposite directions in an average sense, i.e. the conformations of upper and lower water layers are different. Such effect of clay sheet on water molecules is evident even at an interlayer spacing as large as 24.5 Å corresponding to 10 layers of water, although the dipole vectors begin to point away from the clay sheets, possibly indicating that some of the water molecules may be outside of the significant influence of either clay sheets or the Na-ions. Furthermore, the evolution of the direction of net dipole moment of water molecule with increasing volume of water in the interlayer has important implication for the interaction among clay, sodium, and bound-waters.

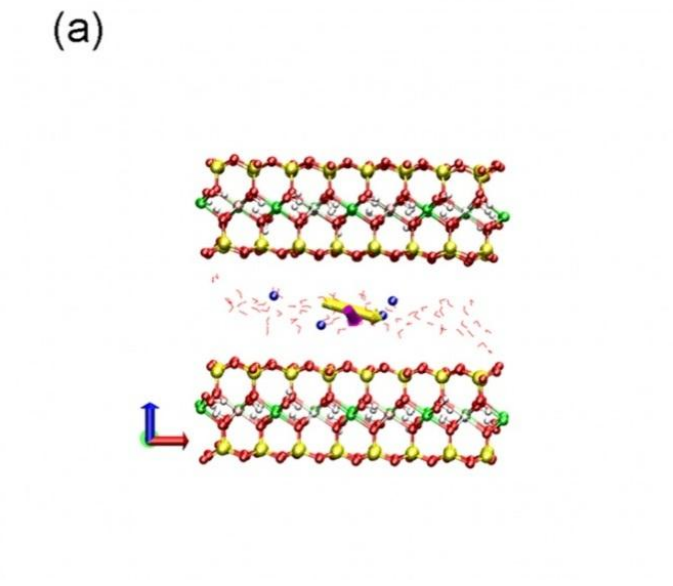

Figure 9.7. Total dipole moment of water above and below the middle plane for different amounts of interlayer water: (a) two layers, (b) four layers, (c) six layers, (d) eight layers, (e) ten layers of water.

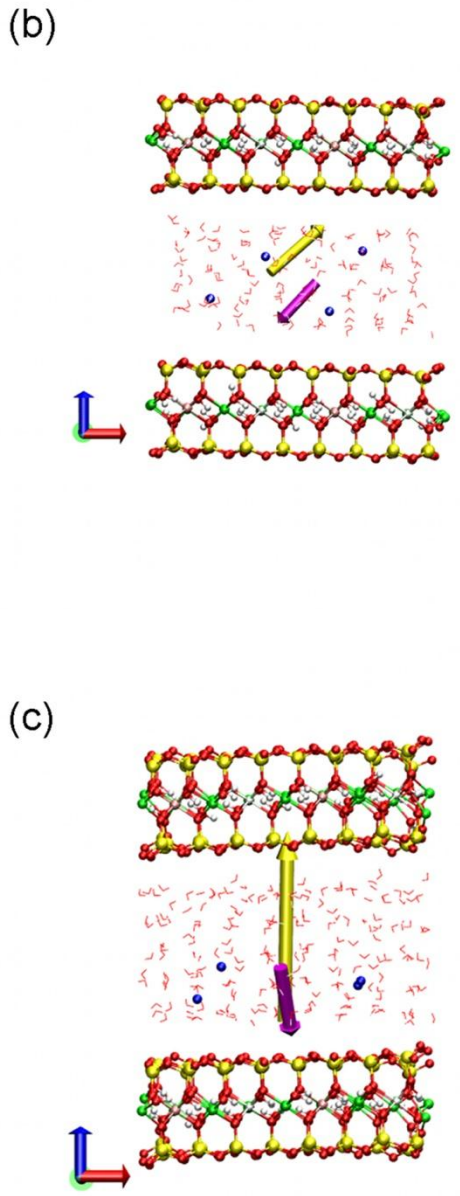

Figure 9.7. Total dipole moment of water above and below the middle plane for different amounts of interlayer water: (a) two layers, (b) four layers, (c) six layers, (d) eight layers, (e) ten layers of water. (Continued)

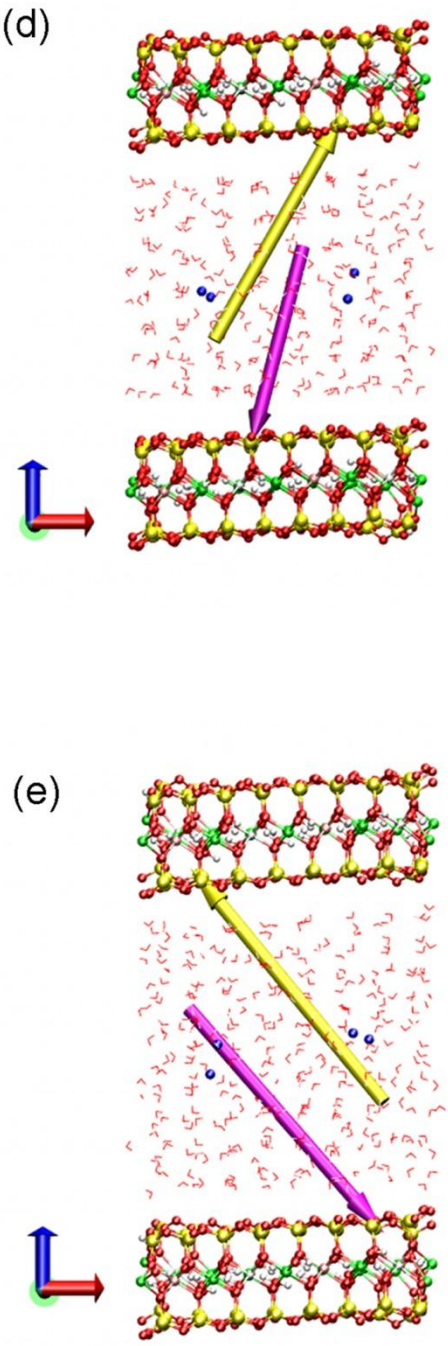

Figure 9.7. Total dipole moment of water above and below the middle plane for different amounts of interlayer water: (a) two layers, (b) four layers, (c) six layers, (d) eight layers, (e) ten layers of water. (Continued)

The planar view of the conformation of water molecules with different number of water layers is shown in figure 9.8. The figures show an interesting pattern formed by the conformation of water molecules corresponding to four, six, eight, and ten water layers. The water molecules appear to align in a semi-hexagonal pattern which seems to mimic the arrangement of oxygen atoms on the clay surface. This kind of behavior is not prominent in case of two layers of water. This observation suggests an interesting ability of clay sheets to act as a template and organize water molecules in the vicinity.

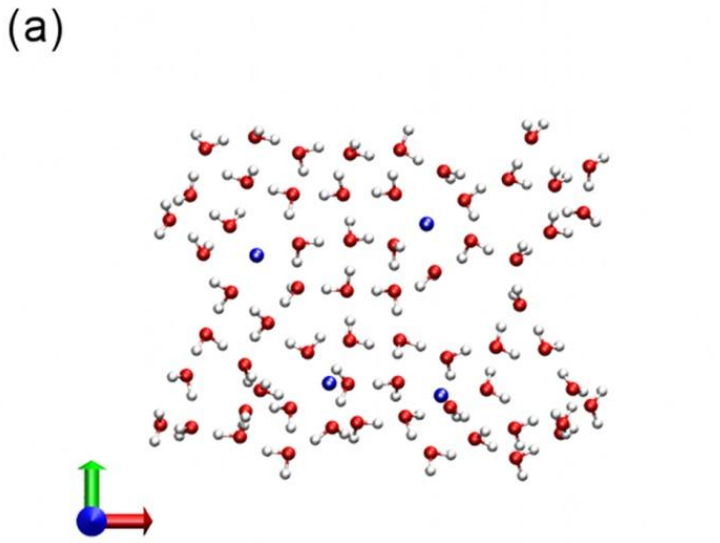

Figure 9.8. Planar view showing conformations of water molecules corresponding to different number of water layers: (a) two layers, (b) two layers, (c) six layers, (d) eight layers, (e) ten layers of water.

(b)

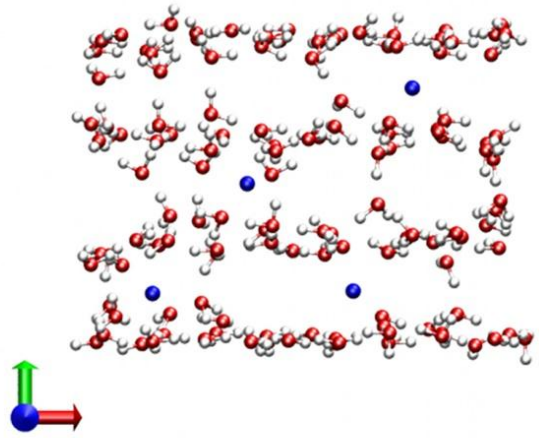

(c)

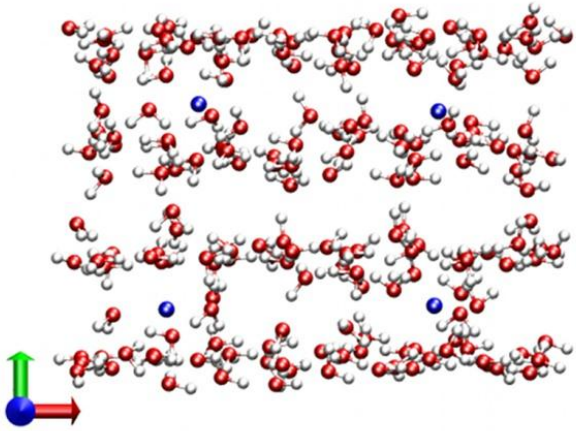

Figure 9.8. Planar view showing conformations of water molecules corresponding to different number of water layers: (a) two layers, (b) two layers, (c) six layers, (d) eight layers, (e) ten layers of water. (Continued)

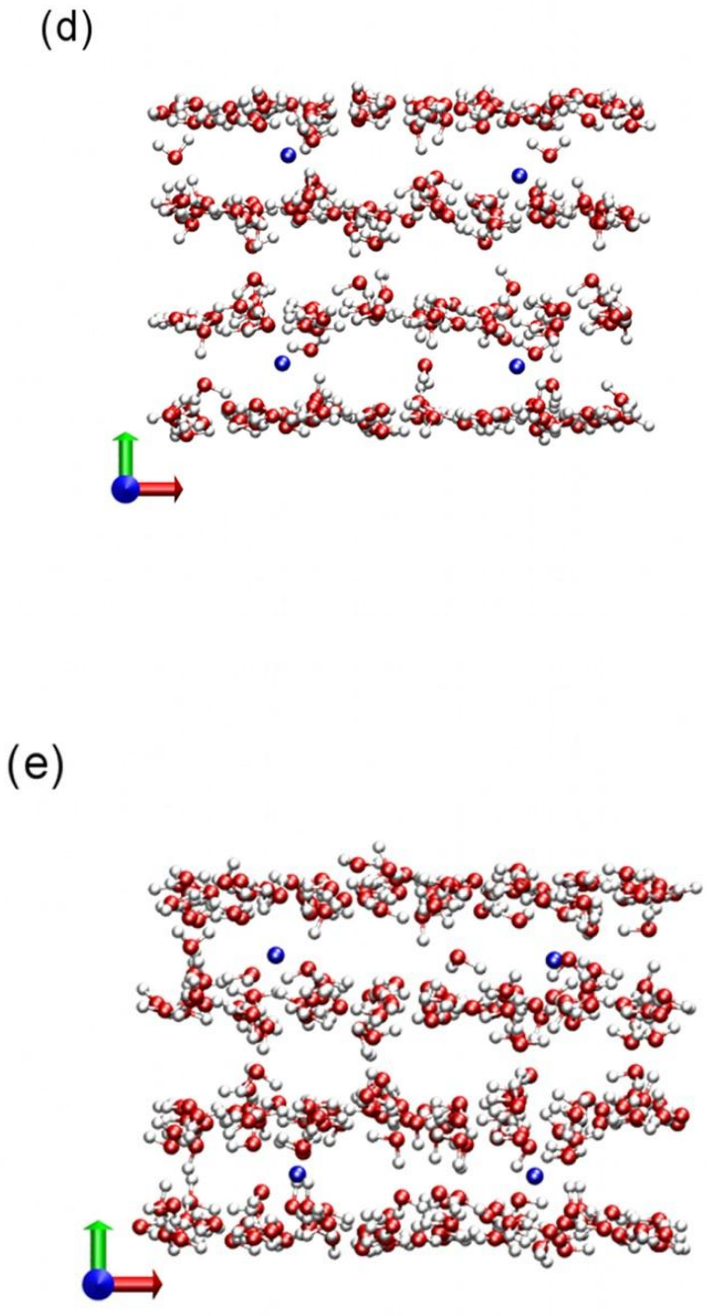

Figure 9.8. Planar view showing conformations of water molecules corresponding to different number of water layers: (a) two layers, (b) two layers, (c) six layers, (d) eight layers, (e) ten layers of water. (Continued)

9.5. Conclusions

Molecular dynamics study of dry clay and hydrated clay with increasing levels of interlayer hydration was carried out to investigate swelling behavior of Na-montmorillonite. This work captures the evolution of interaction energies in the interlayer of Na-montmorillonite swelling clay with increasing hydration and provides an insight into swelling mechanisms. It is found that the Van der Waals interactions between adjacent clay sheets play an important role in case of dry clay, however, with increased hydration and interlayer spacing the columbic interactions become more dominant. The dry clay is held together by attractive interactions between clay sheets and interlayer sodium ions and between the clay sheets. The interaction energy between clay sheets rapidly drops with increase in the number of water layers and becomes negligibly small beyond about four monolayers of interlayer water. The attractive interactions between clay and sodium ions play an important role in case of dry clay as well as hydrated clay at all levels of hydration. The water bound to clay sheets as well as sodium ions play an important role for hydrated clay to help maintain the stability of intercalated clay structure. The interaction energies due to clay-bound and sodium bound water peaks around 6 layers of water and rapidly diminish with increasing hydration and interlayer spacing. However, the rate of decrease in the cumulative attractive interaction energies as result of bound water is less than that of clay and sodium ions. The increase in attractive interaction energy resulting from bound water between 6 and 10 layers of water greatly compensates for the rapid drop in attractive interaction between clay and sodium ions. Thus, the bound water appears to greatly contribute to the stability of hydrated clay even at large interlayer separation between clay sheets.

The non-bonded interaction of clay appears to have a significant impact on the conformation of water. The net dipole moments of the upper and lower water molecules are roughly horizontal at for two monolayers of water, however at higher levels of hydration the net dipole moment point towards the clay sheets. This implies that the conformations of water molecule above and below the middle plane are significantly different. In addition to this, the planar view of water shows a very interesting conformation of water molecules. The water molecules appear to have an organized pattern approximately mimicking the arrangement of surface oxygen atoms on the clay sheets. The results and insight provided by this work will help in modeling and predicting exfoliation and resulting particle breakdown in swelling clays in addition to expounding the key role of interlayer interactions in swelling in smectite clays.

9.6. Acknowledgements

The authors acknowledge the support of National Science Foundation grant # 0556020 and Dr. Richard Fragaszy, the cognizant program director. The authors acknowledge computational resources at NDSU center for high performance computing (CHPC). The authors thank Dr. Greg Wettstein for hardware and software support. The authors also acknowledge computational support from XCEDE/TeraGrid computational grant for use of their supercomputing facilities. Author SMP acknowledges support from ND EPSCOR.

9.7. References

1. Jo HY, Katsumi T, Benson CH, & Edil TB (2001) Hydraulic conductivity and swelling of nonprehydrated GCLs permeated with single-species salt solutions. *Journal of Geotechnical and Geoenvironmental Engineering* 127(7):557-567.

2. Verwey EJW (1945) THEORY OF THE STABILITY OF LYOPHOBIC COLLOIDS. *Philips Research Reports* 1(1):33-49.

3. Verwey EJW (1947) Theory of the stability of lyophobic colloids. *Journal of Physical and Colloid Chemistry* 51(3):631-636.

4. Skipper NT, Refson K, & McConnell JDC (1991) Computer-simulation of interlayer water in 2-1 clays. *Journal of Chemical Physics* 94(11):7434-7445.

5. Skipper NT, Chang FRC, & Sposito G (1995) Monte-carlo simulation of interlayer molecular-structure in swelling clay-minerals .1. Methodology. *Clays and Clay Minerals* 43(3):285-293.

6. Skipper NT, Sposito G, & Chang FRC (1995) Monte-carlo simulation of interlayer molecular-structure in swelling clay-minerals .2. Monolayer hydrates. *Clays and Clay Minerals* 43(3):294-303.

7. Karaborni S, Smit B, Heidug W, Urai J, & vanOort E (1996) The swelling of clays: Molecular simulations of the hydration of montmorillonite. *Science* 271(5252):1102-1104.

8. Tambach TJ, Hensen EJM, & Smit B (2004) Molecular simulations of swelling clay minerals. *Journal of Physical Chemistry B* 108(23):7586-7596.

9. Smith DE, Wang Y, & Whitley HD (2004) Molecular simulations of hydration and swelling in clay minerals. *Fluid Phase Equilibria* 222:189-194.

10. Smith DE, Wang Y, Chaturvedi A, & Whitley HD (2006) Molecular simulations of the pressure, temperature, and chemical potential dependencies of clay swelling. *Journal of Physical Chemistry B* 110(40):20046-20054.

11. Delville A (1991) Modeling the clay water interface. *Langmuir* 7(3):547-555.

12. Delville A (1992) Structure of liquids at a solid interface - an application to the swelling of clay by water. *Langmuir* 8(7):1796-1805.

13. Shroll RM & Smith DE (1999) Molecular dynamics simulations in the grand canonical ensemble: Application to clay mineral swelling. *Journal of Chemical Physics* 111(19):9025-9033.

14. Smith DE (1998) Molecular computer simulations of the swelling properties and interlayer structure of cesium montmorillonite. *Langmuir* 14(20):5959-5967.

15. Katti DR, Schmidt SR, Ghosh P, & Katti KS (2005) Modeling the response of pyrophyllite interlayer to applied stress using steered molecular dynamics. *Clays and Clay Minerals* 53(2):171-178.

16. Katti DR, Schmidt SR, Ghosh P, & Katti KS (2007) Molecular modeling of the mechanical behavior and interactions in dry and slightly hydrated sodium montmorillonite interlayer. *Canadian Geotechnical Journal* 44(4):425-435.

17. Schmidt SR, Katti DR, Ghosh P, & Katti KS (2005) Evolution of mechanical response of sodium montmorillonite interlayer with increasing hydration by molecular dynamics. *Langmuir* 21(17):8069-8076.

18. Amarasinghe PM, Katti KS, & Katti DR (2012) Insight into Role of Clay-Fluid Molecular Interactions on Permeability and Consolidation Behavior of Na-Montmorillonite Swelling Clay. *Journal of Geotechnical and Geoenvironmental Engineering* 138(2):138-146.

19. Katti DR, Matar MI, Katti KS, & Amarasinghe PM (2009) Multiscale modeling of swelling clays: A computational and experimental approach. *Ksce Journal of Civil Engineering* 13(4):243-255.

20. Katti D & Shanmugasundaram V (2001) Influence of swelling on the microstructure of expansive clays. *Canadian Geotechnical Journal* 38(1):175-182.

21. Jorgensen WL, Chandrasekhar J, Madura JD, Impey RW, & Klein ML (1983) Comparison of simple potential functions for simulating liquid water. *Journal of Chemical Physics* 79(2):926-935.

22. Kale L, *et al.* (1999) NAMD2: Greater Scalability for Parallel Molecular Dynamics. *Journal of Computational Physics* 151(1):283-312.

23. Phillips JC, *et al.* (2005) Scalable molecular dynamics with NAMD. *Journal of Computational Chemistry* 26(16):1781-1802.

24. Humphrey W, Dalke A, & Schulten K (1996) VMD: visual molecular dynamics. *Journal of molecular graphics* 14(1):33-38, 27-38.

25. Brooks BR, *et al.* (1983) CHARMM: a program for macromolecular energy, minimization, and dynamics calculations. *Journal of Computational Chemistry* 4(2):187-217.

26. Teppen BJ, Rasmussen K, Bertsch PM, Miller DM, & Schaefer L (1997) Molecular Dynamics Modeling of Clay Minerals. 1. Gibbsite, Kaolinite, Pyrophyllite, and Beidellite. *Journal of Physical Chemistry B* 101(9):1579-1587.

27. Luzar A & Chandler D (1993) Structure and hydrogen-bond dynamics of water-dimethyl sulfoxide mixtures by computer-simulations. *Journal of Chemical Physics* 98(10):8160-8173.

28. Luzar A & Chandler D (1996) Hydrogen-bond kinetics in liquid water. *Nature* 379(6560):55-57.

29. Ferrario M, Haughney M, McDonald IR, & Klein ML (1990) Molecular-dynamics simulation of aqueous mixtures - methanol, acetone, and ammonia. *Journal of Chemical Physics* 93(7):5156-5166.

30. Ghosh P, Katti DR, & Katti KS (2007) Mineral Proximity Influences Mechanical Response of Proteins in Biological Mineral-Protein Hybrid Systems. *Biomacromolecules* 8(3):851-856.

31. Ghosh P, Katti DR, & Katti KS (2008) Mineral and protein-bound water and latching action control mechanical behavior at protein-mineral interfaces in biological nanocomposites. *Journal of Nanomaterials*.

32. Bhowmik R, Katti KS, & Katti DR (2009) Mechanisms of Load-Deformation Behavior of Molecular Collagen in Hydroxyapatite-Tropocollagen Molecular System: Steered Molecular Dynamics Study. *Journal of Engineering Mechanics-Asce* 135(5):413-421.

33. Katti DR, Pradhan SM, & Katti KS (2010) Directional dependence of hydroxyapatite-collagen interactions on mechanics of collagen. *Journal of Biomechanics* 43(9):1723-1730.

34. Foster WR, Savins JG, & Waite JM (1954) Lattice Expansion and Rheological Behavior Relationships in Water Montmorillonite Systems. *Clays and clay Minerals* 3:282-289.

CHAPTER 10. SUMMARY AND CONCLUSIONS

My doctoral research has made important contributions to the fundamental understanding of material behavior of natural nanocomposite–bone and swelling clay–montmorillonite at the molecular scale and the bridging of molecular properties of bone to the continuum scale through multiscale modeling. The research findings and methods developed in this study of provide important insights and direction for the investigation of other natural/synthetic materials that exhibit unique set of properties which have its origins at the molecular scale. The conclusions of my doctoral research work are as follows:

1. Directional dependence of collagen hydroxyapatite interactions on mechanics of collagen.
    a. Steered molecular dynamics study was carried out to investigate the mechanics of collagen in bone. The arrangement of collagen molecules and hydroxyapatite in collagen fibril gives rise to relative orientations between collagen and mineral leading to different types of nonbonded interactions at the interface, which directly affects the mechanical behavior of collagen. The two possible cases of the relative orientations between collagen and mineral resulting in different interfacial configurations are: (i) collagen molecules placed normal to the hydroxyapatite surface, and (ii) collagen molecules parallel to the mineral surface. In this study, the directional dependence of the mechanics of collagen is investigated by pulling it normal and parallel to the hydroxyapatite (0001) and $(10\bar{1}0)$ surfaces.

b. The collagen is pulled normal and parallel to the mineral (0001) surface at different velocities using a harmonic spring attached to its center of mass. The water molecules have strong interactions with both the mineral and collagen molecule, which allows it to act as an intermediary between them. The water is found to have a prominent effect on the initial region of the load-displacement response of collagen pulled normal to the surface as the collagen molecule has to overcome the attractive interaction of water strongly bound to HAP.
c. Load-deformation behavior of collagen perpendicular and parallel to HAP are different at different pulling velocities. The collagen molecule is stiffer at small displacement when pulled normal to HAP surface, whereas in the large displacement regime collagen pulled parallel to HAP surface is stiffer. This is a result of differences in deformation mechanisms of collagen when pulled in different directions, which is evident from the differences in the breaking of inter-chain hydrogen bonds that keep collagen triple-helix intact.
d. The collagen molecules show substantial enhancement in stiffness in the proximity of mineral compared to the absence of mineral. The increased stiffness results in the higher energy required to pull collagen molecule through a same displacement. This has important implications for the strength and toughness in bone as collagen is the only major component of bone capable of undergoing large deformation.
e. The collagen pulled parallel to $(10\bar{1}0)$ and (0001) surfaces exhibit characteristically different load-displacement response. This shows that the

deformation mechanism of collagen is also dependent on the type of mineral surface in the proximity.

2. Mechanical response of full length and short collagen molecules.
    a. The current studies of collagen rely on short molecule about 8.5 nanometers in length. The full length collagen measuring about 300 nanomeners and consisting of 1014 residues is built and investigated using steered molecular dynamics by pulling at different velocities and of harmonic spring different stiffness. The simulations show that the unfolding mechanisms of short and full length collagen molecules are significantly different.
    b. In case of both collagen molecules the elastic modulus was found to be higher when higher spring constants and velocities are used. Thus the stiffness response is dependent not only on the pulling rate but also on the stiffness of spring used to pull the molecule. Additionally, softer spring is necessary for pulling the full length collagen molecule to obtain stiffness response similar to short collagen molecule.
    c. At small pulling rate the elastic modulus of short and long collagen are comparable, however at large pulling rates the modulus of long collagen molecule is found to be higher. Furthermore, the load-displacement response of short collagen molecule show saw toothed features with large fluctuations in force, while in case of full length collagen such features are not observed.
    d. The above findings indicate that the deformation mechanisms of short and full length collagen are entirely different. The differences in deformation response of short and long collagen molecules are attributable to the coiled feature observed

for the first time in full-length collagen molecules and the differences in conformational changes evident from the nature of breaking and forming of hydrogen bonds in short and full length collagen.

3. The role of helical hierarchy on the deformation behavior of collagen molecule.
    a. The molecular mechanisms responsible for the deformation of collagen molecule are investigated by studying the conformational evolution of collagen helices when the full-length collagen molecule is extended. Collagen consists of a hierarchy of three helical levels: level-1 (left-handed helix formed by alpha chains), level-2 (right handed triple-helix formed by three alpha chains), and level-3 helix (helical turns along the length collagen molecule). The level-3 helix can be observed only in the full-length collagen molecule, which has been reported in our study for the first time.
    b. The deformation of collagen results from the collective extension of α-chain helices (the level-1 helix) and helical turns along the collagen length (the level-3 helix). The triple-helix (the level-2 helix) is found to have minimal contribution to deformation of collagen as it is relatively stable and does not exhibit much unfolding, even at large displacement, unlike reported in the literature (where the simulations are carried out using short collagen molecule).
    c. Despite the marginal contribution to deformation, the relative stability of triple helix (the level-2 helix) plays an important role in the conformational stability of collagen molecule. The level-2 helix allows collagen molecule to possess higher stiffness compared to three isolated α-chains, while retaining an ability to undergo large deformation through the extension of level-1 helix.

d. Two key mechanisms for the deformation and conformational stability of collagen molecule are proposed in this study: (i) interlocking gear analogy, (ii) interplay between level-1 and level-2 hierarchies. Both of these mechanisms are dependent on the hydrogen bonds between the α-chains, which demonstrate the importance of hydrogen bonds in the conformational stability of collagen.

e. The total energy of hydrogen bonds in the collagen molecule is significantly smaller than the attractive interaction energy between three α-chains. This shows the importance of nonbonded interactions in the mechanics of collagen, while interchain hydrogen bonds contribute to the preservation of triple helical confirmation of collagen.

4. Multiscale modeling of collagen fibril in bone: elastic response.

a. A multiscale model of collagen fibril is carried out using a hierarchical approach by combining molecular dynamics simulations and finite element method. The mechanical properties of collagen under various conditions that mimic organization of collagen molecules and mineral inside the collagen fibril is estimated from the steered molecular dynamics. These nanomechanical properties are then imported into the finite element model of collagen fibril. The finite element model mimics the staggered arrangement of collagen molecules and minerals resulting in the banded pattern consisting of gap and overlap regions along the fibril length.

b. The simulations show that the elastic modulus of collagen fibril is significantly influenced by the nonbonded molecular interactions between the collagen and hydroxyapatite. The collagen fibril that incorporates the influence of mineral

proximity on the mechanical response of collagen show 20% higher modulus compared to the collagen fibril that does not take into account of such interaction. The elastic moduli of fibril corresponding to these two cases are 4.01 GPa and 4.81 GPa, the higher modules being obtained when the interactions between collagen and mineral are taken into consideration.

c. The study of deformation mechanism that the most of the strain and strain energy density is localized in the overlap region of collagen fibril. This is a first multiscale model of collagen fibril that incorporates the effect of mineral on the mechanical response of collagen molecule. This work illustrates the importance of mineral-collagen interaction on the mechanics of collagen fibril.

5. Multiscale modeling of collagen fibril in bone at various crosslink densities: an insight into its deformation mechanism in the small and large displacement regime.

   a. The nonbonded molecular interactions between the collagen and hydroxyapatite are found to significantly enhance the elastic modulus of collagen fibril at all the crosslink densities (ranging from 1 to 5 crosslinks per end of collagen molecule) including the model no crosslink. In addition to the small displacement regime the enhancement in stiffness is also observed in the large displacement regime of upto 30%. This demonstrates the importance of incorporating the enhancement in mechanical property of collagen due to mineral proximity into the model of collagen fibril.

   b. The higher crosslinks densities contribute the enhancement in elastic modulus in the small displacement regime and higher stiffness in the large displacement regime. The enhancement in elastic modulus due to crosslinks range from 5-11%

for various crosslink densities as compared to the collagen fibril with no crosslink.

c. Two possible deformation mechanisms of collagen fibril are proposed. The deformation mechanism of collagen fibril depends on the characteristic length of fibril under consideration. The deformation of collagen fibril is governed by the pullout between the ends of collagen molecules, followed by straining of crosslinks, if the effective length is greater than the characteristic length. However, if the effective length is not greater than the characteristic length the deformation mechanism is governed by shearing between collagen molecules.

d. The highest magnitude of stress and strain in collagen fibril is found in the mineral and overlap zone respectively. In the overlap zone the end regions consisting of crosslinks are found to experience higher stress compared to the non-crosslinked section. Furthermore, the overlap zone due to its ability to undergo larger strain is found to have the higher concentration of strain energy compared to other regions of collagen fibril.

6. Evolution of molecular interactions in the interlayer of Na-montmorillonite swelling clay with increasing hydration.

   a. Molecular dynamics simulations of the dry clay and the clay with increasing levels of hydration are carried out to study its swelling behavior. The dry clay is seen to be held together by the attractive interactions between clay sheets and between clay and sodium ions.

   b. The evolution of interaction energies with increasing hydration show that the Van der Waals interactions between adjacent clay sheets play an important role in dry

clay, whereas, at increasing levels of hydration the columbic interactions are prominent. The attractive interactions energies between clay sheets decrease progressively with increasing hydration and become negligible beyond four monolayers of water. The attractive interactions between clay and sodium are relatively stronger than the clay-clay interactions and persist up very high levels of hydration of ten monolayers of water.

c. In addition to the clay and sodium, the water molecules bound to the clay and sodium also play important role in hydrated clay in maintaining the stability of intercalated clay structure. The role of bound waters becomes very important at higher levels of hydrations where the clay-clay and clay-sodium interaction are relatively weak. Thus the bound water significantly contributes to the stability of clay at higher interlayer spacing between clay platelets.

d. The nonbonded interaction between clay and interlayer water has a significant impact on the conformation of water. The water molecules above and below the equatorial plane of interlayer are aligned such that their dipole moments point in opposite directions towards the top and bottom clay sheets. This indicates that the clay layers have strong influence in the orientation of water molecules and that the conformations of water molecule above and below the middle plane are entirely different.

e. This study elucidates the key role played by interaction energies in the swelling behavior of Na-montmorillonite, as well as, provides important insights for modeling exfoliation and clay particle breakdown.

The major contributions from the studies are as follows:

1. It has been shown that the deformation behavior of collagen in the proximity of mineral depends on the type of collagen-mineral interface. The different types of interfaces in collagen fibril results in the directional dependence of mineral-collagen interactions.
2. First steered molecular dynamics simulation of full length collagen molecule is conducted. This study shows that short length collagen molecule models are incapable of predicting and modeling true behavior of full length collagen molecules.
3. It has been shown that helical hierarchy, consisting of three tiers of helices, controls the deformation behavior of collagen molecule.
4. Third level helical hierarchy is identified/discovered that has a major impact on collagen deformation.
5. It has been shown that the inter-chain hydrogen bonds in collagen are responsible for the conformational stability of α-chain helices and triple helix, whereas the large interaction energy between α-chains contribute to the keeping the chains together.
6. It is found that the deformation of collagen results from the extension of α-chain helices (level-1 helix) and helical features along the length (level-3 helix), while the triple helix (level-2 helix) only contributes marginally.
7. The two mechanisms responsible for the stability of collagen helices are proposed: (i) interlocking gear analogy, (ii) interplay between level-1 and level-2 hierarchies.
8. It has been demonstrated that the molecular interactions between collagen and mineral significantly affect the deformation response of collagen fibril. Therefore it is

necessary to incorporate molecular interactions for correctly modeling bone mechanics.

9. It has been found that the deformation mechanism of collagen fibril depends on the characteristic length.
10. During deformation of collagen fibril majority of strain and strain energy density is localized in the overlap zone.
11. It has been found that the attractive interactions between clay and sodium ions plays very important role in the stability of hydrated clay interlayer. At higher levels of hydration when the sodium-clay interactions become relatively weak, the bound water interactions play a dominant role in maintaining stability of stacked clay structure allowing for relatively large d-spacing.
12. It has been found that the clay platelets strongly affect the conformation of water molecules in the interlayer. And the conformations of water molecules above and below the equatorial plane of interlayer are different.

CHAPTER 11. FUTURE WORKS

The studies presented in this dissertation have provided unprecedented insight into the mechanics of material at the nanoscale and a new direction for multiscale modeling of wide ranges of nanoscale systems. This has opened up number of avenues for future research which are as follows:

1. The study of the interactions between type-I collagen and mineral may be carried out to obtain additional information about the bone mechanics.
2. The genetic mutation in collagen triple helix is known to cause global pathological conditions leading to diseases such as Osteogenesis Imperfecta (OI) and Ehlers Danlos Syndrome (EDS). The future studies on physiological and pathological collagen molecules is needed to better understand how the point mutations in α-chain sequence interfere with the proper folding/conformation of collagen molecule, stability of collagen, and fiber formation.
3. The results of our multiscale modeling of collagen fibril show that the deformation mechanism it strongly dependent on the fibril length and loading conditions. The finite element model of full length collagen fibril with different loading conditions is recommended for obtaining detailed picture of fibril mechanics.
4. Another step in the multiscale modeling of bone is to develop the model of collagen fiber. This will answer number of questions about the deformation mechanism of fibril, as well as, the mechanism of load transfer between the collagen fibrils.

5. More detailed theoretical and computational studies using larger clay models and more accurate force fields are needed to completely uncover the mechanisms of clay swelling.

APPENDIX

A.1. Sample NAMD configuration file for Steered Molecular Dynamics Simulation

```
coordinates          Collagen.coor;          # Coordinate file
structure            Collagen.psf;           # PSF file
parameters           par_all22_prot.inp;     # CHARMM parameter file
paratypecharmm         on;                   # Parameter type
velocities           Collagen.vel;           # Velocity file

set output           Collagen.out
outputname           $output;                # Output file
dcdfile              ${output}.dcd           # Trajectory file
xstFile              ${output}.xst           # eXtended System Configuration) file
dcdfreq              500
xstFreq              200
velDCDfile           ${output}.vel.dcd       #  Velocity trajectory filename
velDCDfreq           500

binaryoutput         no
binaryrestart        no
outputEnergies       100;                    # Timesteps between energy output
restartfreq          1000

exclude              1-3                     # Non-bonded exclusion policy
#1-4scaling          1
COMmotion            no                      # Do not allow initial center of mass
motion
dielectric           1.0

#Particle Mesh Ewald (PME grid in X, Y, Z directions)
PME                  on
PMEGridSizeX         50
PMEGridSizeY         50
PMEGridSizeZ         1000

switching            on
switchdist           9.00;          # Distance of switching for non-bonded  calculations
(Å)
cutoff               10.00;         # Cutoff distance
pairlistdist         11.00
#margin               2

firsttimestep         0             # First time step of simulation
timestep              0.5           # Time step in femtoseconds
```

```
# Temperature control
set temperature         300
#temperature            $temperature;          # initial temperature

# Langevin Dynamics
langevin                on;                    # do langevin dynamics
langevinDamping         5;                     # damping coefficient (gamma) of 5/ps
langevinTemp            $temperature;          # bath temperature
#langevinHydrogen       no;                    # don't couple langevin bath to hydrogens
seed                    12345

# Pressure control
langevinPiston          on;                    # use Langevin piston pressure control
langevinPistonTarget    1.01325;               # in bar -> 1.01325 bar = 1 atm
langevinPistonPeriod    300                    # oscillation period (fs)
langevinPistonDecay     100                    # damping time scale (fs)
langevinPistonTemp      $temperature
useFlexibleCell         no
useGroupPressure        no

# Periodic Boundary Conditions
cellBasisVector1   150.0     0         0
cellBasisVector2     0     150.0       0
cellBasisVector3     0       0      3500.0
#cellOrigin          10.5    20.2    136.7
#wrapAll             on
dcdUnitCell          yes


fixedAtoms              on
fixedAtomsForces        on
fixedAtomsFile          fixedatoms.pdb; # PDB file containing fixed atom parameters
fixedAtomsCol           B

SMD             on;                    # Activates steered molecular dynamics (SMD)
SMDFile         pullingCOM.pdb         # SMD constraint reference position
SMDk            4.0;                   # Force constant to use in SMD simulation
SMDVel          0.005;                 # Velocity of the SMD reference position
SMDDir          0 0 1;                 # Direction of the SMD center of mass movement
SMDOutputFreq   100;

# Scripting

run 2000000 ;                          # Number of steps to run
```

A.2. NAMD generated sample coordinate file (only 246 of 93750 atoms shown)

The columns 7, 8, and 9 represent x, y, and z coordinates.

```
REMARK  RESTART COORDINATES WRITTEN BY NAMD AT TIMESTEP 1447000
ATOM      1  N   GLY A   1       3.858  15.189 114.217  1.00  0.00      P1
ATOM      2  HT1 GLY A   1       3.645  16.219 114.087  1.00  0.00      P1
ATOM      3  HT2 GLY A   1       3.119  14.765 114.883  1.00  0.00      P1
ATOM      4  HT3 GLY A   1       3.710  14.698 113.251  1.00  0.00      P1
ATOM      5  CA  GLY A   1       5.186  14.956 114.788  1.00  0.00      P1
ATOM      6  HA1 GLY A   1       5.826  15.656 114.341  1.00  0.00      P1
ATOM      7  HA2 GLY A   1       5.452  13.966 114.477  1.00  0.00      P1
ATOM      8  C   GLY A   1       5.185  15.084 118.665  1.00  0.00      P1
ATOM      9  O   GLY A   1       4.031  14.737 118.730  1.00  0.00      P1
ATOM     10  N   PRO A   2       5.578  15.294 122.233  1.00  0.00      P1
ATOM     11  CA  PRO A   2       5.443  15.286 125.437  1.00  0.00      P1
ATOM     12  HA  PRO A   2       5.071  14.256 125.622  1.00  0.00      P1
ATOM     13  CD  PRO A   2       6.914  15.622 122.315  1.00  0.00      P1
ATOM     14  HD1 PRO A   2       7.580  14.710 122.279  1.00  0.00      P1
ATOM     15  HD2 PRO A   2       7.157  16.316 121.563  1.00  0.00      P1
ATOM     16  CB  PRO A   2       6.902  15.657 125.200  1.00  0.00      P1
ATOM     17  HB1 PRO A   2       7.423  14.689 125.249  1.00  0.00      P1
ATOM     18  HB2 PRO A   2       7.253  16.351 125.977  1.00  0.00      P1
ATOM     19  CG  PRO A   2       7.106  16.409 123.768  1.00  0.00      P1
ATOM     20  HG1 PRO A   2       8.153  16.791 123.757  1.00  0.00      P1
ATOM     21  HG2 PRO A   2       6.429  17.249 123.804  1.00  0.00      P1
ATOM     22  C   PRO A   2       5.673  15.536 129.283  1.00  0.00      P1
ATOM     23  O   PRO A   2       6.662  16.261 129.237  1.00  0.00      P1
ATOM     24  N   PRO A   3       5.584  15.551 132.860  1.00  0.00      P1
ATOM     25  CA  PRO A   3       5.712  15.776 136.082  1.00  0.00      P1
ATOM     26  HA  PRO A   3       5.774  16.824 136.003  1.00  0.00      P1
ATOM     27  CD  PRO A   3       4.612  14.476 132.978  1.00  0.00      P1
ATOM     28  HD1 PRO A   3       3.658  14.914 132.670  1.00  0.00      P1
ATOM     29  HD2 PRO A   3       4.987  13.548 132.444  1.00  0.00      P1
ATOM     30  CB  PRO A   3       4.456  14.966 135.794  1.00  0.00      P1
ATOM     31  HB1 PRO A   3       3.548  15.563 135.698  1.00  0.00      P1
ATOM     32  HB2 PRO A   3       4.277  14.298 136.628  1.00  0.00      P1
ATOM     33  CG  PRO A   3       4.481  13.978 134.502  1.00  0.00      P1
ATOM     34  HG1 PRO A   3       5.401  13.283 134.681  1.00  0.00      P1
ATOM     35  HG2 PRO A   3       3.563  13.269 134.528  1.00  0.00      P1
ATOM     36  C   PRO A   3       5.717  15.616 139.920  1.00  0.00      P1
ATOM     37  O   PRO A   3       5.022  14.560 139.891  1.00  0.00      P1
ATOM     38  N   GLY A   4       5.976  15.955 142.857  1.00  0.00      P1
ATOM     39  HN  GLY A   4       6.599  16.700 142.852  1.00  0.00      P1
ATOM     40  CA  GLY A   4       5.929  15.910 146.095  1.00  0.00      P1
ATOM     41  HA1 GLY A   4       5.971  14.831 146.059  1.00  0.00      P1
ATOM     42  HA2 GLY A   4       4.917  16.281 145.982  1.00  0.00      P1
ATOM     43  C   GLY A   4       6.071  16.219 149.966  1.00  0.00      P1
ATOM     44  O   GLY A   4       5.946  17.418 149.831  1.00  0.00      P1
ATOM     45  N   PRO A   5       6.242  16.083 153.568  1.00  0.00      P1
ATOM     46  CA  PRO A   5       6.188  16.355 156.767  1.00  0.00      P1
ATOM     47  HA  PRO A   5       5.172  16.700 156.820  1.00  0.00      P1
ATOM     48  CD  PRO A   5       6.473  14.633 153.722  1.00  0.00      P1
ATOM     49  HD1 PRO A   5       5.457  14.216 153.350  1.00  0.00      P1
ATOM     50  HD2 PRO A   5       7.264  14.337 152.939  1.00  0.00      P1
ATOM     51  CB  PRO A   5       6.175  14.762 156.613  1.00  0.00      P1
ATOM     52  HB1 PRO A   5       5.080  14.475 156.507  1.00  0.00      P1
ATOM     53  HB2 PRO A   5       6.627  14.193 157.464  1.00  0.00      P1
ATOM     54  CG  PRO A   5       6.932  14.372 155.241  1.00  0.00      P1
ATOM     55  HG1 PRO A   5       6.888  13.228 155.453  1.00  0.00      P1
ATOM     56  HG2 PRO A   5       7.972  14.743 155.391  1.00  0.00      P1
ATOM     57  C   PRO A   5       6.632  16.416 160.579  1.00  0.00      P1
```

```
ATOM     58  O   PRO A   5       7.837  16.335 160.534  1.00  0.00      P1
ATOM     59  N   PRO A   6       6.531  16.505 164.093  1.00  0.00      P1
ATOM     60  CA  PRO A   6       6.786  16.762 167.360  1.00  0.00      P1
ATOM     61  HA  PRO A   6       7.170  17.792 167.241  1.00  0.00      P1
ATOM     62  CD  PRO A   6       5.114  16.441 164.261  1.00  0.00      P1
ATOM     63  HD1 PRO A   6       4.568  16.898 163.427  1.00  0.00      P1
ATOM     64  HD2 PRO A   6       4.847  15.417 164.478  1.00  0.00      P1
ATOM     65  CB  PRO A   6       5.261  16.495 167.104  1.00  0.00      P1
ATOM     66  HB1 PRO A   6       4.622  16.811 167.991  1.00  0.00      P1
ATOM     67  HB2 PRO A   6       5.067  15.388 167.060  1.00  0.00      P1
ATOM     68  CG  PRO A   6       4.742  17.102 165.766  1.00  0.00      P1
ATOM     69  HG1 PRO A   6       5.116  18.134 165.730  1.00  0.00      P1
ATOM     70  HG2 PRO A   6       3.630  17.130 165.871  1.00  0.00      P1
ATOM     71  C   PRO A   6       6.771  16.677 171.217  1.00  0.00      P1
ATOM     72  O   PRO A   6       6.233  15.585 171.207  1.00  0.00      P1
ATOM     73  N   GLY A   7       6.986  17.032 174.085  1.00  0.00      P1
ATOM     74  HN  GLY A   7       7.490  17.939 174.120  1.00  0.00      P1
ATOM     75  CA  GLY A   7       7.115  16.961 177.436  1.00  0.00      P1
ATOM     76  HA1 GLY A   7       8.140  17.359 177.439  1.00  0.00      P1
ATOM     77  HA2 GLY A   7       6.933  15.886 177.406  1.00  0.00      P1
ATOM     78  C   GLY A   7       6.982  17.289 181.294  1.00  0.00      P1
ATOM     79  O   GLY A   7       5.868  17.746 181.248  1.00  0.00      P1
ATOM     80  N   PRO A   8       7.278  17.393 184.805  1.00  0.00      P1
ATOM     81  CA  PRO A   8       7.173  17.575 188.033  1.00  0.00      P1
ATOM     82  HA  PRO A   8       6.354  16.873 188.028  1.00  0.00      P1
ATOM     83  CD  PRO A   8       8.683  17.027 184.935  1.00  0.00      P1
ATOM     84  HD1 PRO A   8       8.856  16.016 184.781  1.00  0.00      P1
ATOM     85  HD2 PRO A   8       9.167  17.587 184.123  1.00  0.00      P1
ATOM     86  CB  PRO A   8       8.569  17.043 187.797  1.00  0.00      P1
ATOM     87  HB1 PRO A   8       8.531  15.943 187.556  1.00  0.00      P1
ATOM     88  HB2 PRO A   8       9.132  17.225 188.702  1.00  0.00      P1
ATOM     89  CG  PRO A   8       9.160  17.635 186.377  1.00  0.00      P1
ATOM     90  HG1 PRO A   8      10.245  17.435 186.485  1.00  0.00      P1
ATOM     91  HG2 PRO A   8       8.998  18.717 186.360  1.00  0.00      P1
ATOM     92  C   PRO A   8       7.372  17.932 191.839  1.00  0.00      P1
ATOM     93  O   PRO A   8       8.080  18.913 191.750  1.00  0.00      P1
ATOM     94  N   PRO A   9       7.273  17.890 195.357  1.00  0.00      P1
ATOM     95  CA  PRO A   9       7.308  18.091 198.607  1.00  0.00      P1
ATOM     96  HA  PRO A   9       6.766  19.008 198.697  1.00  0.00      P1
ATOM     97  CD  PRO A   9       6.352  16.723 195.545  1.00  0.00      P1
ATOM     98  HD1 PRO A   9       5.469  16.805 194.830  1.00  0.00      P1
ATOM     99  HD2 PRO A   9       6.921  15.812 195.463  1.00  0.00      P1
ATOM    100  CB  PRO A   9       6.623  16.700 198.399  1.00  0.00      P1
ATOM    101  HB1 PRO A   9       6.033  16.287 199.259  1.00  0.00      P1
ATOM    102  HB2 PRO A   9       7.386  15.976 198.285  1.00  0.00      P1
ATOM    103  CG  PRO A   9       5.718  16.736 197.072  1.00  0.00      P1
ATOM    104  HG1 PRO A   9       5.128  17.683 197.083  1.00  0.00      P1
ATOM    105  HG2 PRO A   9       5.124  15.840 197.055  1.00  0.00      P1
ATOM    106  C   PRO A   9       7.671  18.138 202.450  1.00  0.00      P1
ATOM    107  O   PRO A   9       8.847  17.795 202.443  1.00  0.00      P1
ATOM    108  N   GLY A  10       7.450  18.377 205.349  1.00  0.00      P1
ATOM    109  HN  GLY A  10       6.522  18.697 205.247  1.00  0.00      P1
ATOM    110  CA  GLY A  10       7.712  18.489 208.664  1.00  0.00      P1
ATOM    111  HA1 GLY A  10       8.156  19.445 208.642  1.00  0.00      P1
ATOM    112  HA2 GLY A  10       8.499  17.680 208.694  1.00  0.00      P1
ATOM    113  C   GLY A  10       7.580  18.631 212.486  1.00  0.00      P1
ATOM    114  O   GLY A  10       6.455  18.202 212.494  1.00  0.00      P1
ATOM    115  N   PRO A  11       7.836  18.922 216.069  1.00  0.00      P1
ATOM    116  CA  PRO A  11       7.631  19.006 219.300  1.00  0.00      P1
ATOM    117  HA  PRO A  11       7.491  17.943 219.303  1.00  0.00      P1
ATOM    118  CD  PRO A  11       9.138  19.479 216.289  1.00  0.00      P1
ATOM    119  HD1 PRO A  11       9.875  19.152 215.524  1.00  0.00      P1
ATOM    120  HD2 PRO A  11       9.031  20.592 216.397  1.00  0.00      P1
```

```
ATOM    121  CB  PRO A  11       9.083  19.550 219.102  1.00  0.00      P1
ATOM    122  HB1 PRO A  11       9.692  19.272 219.911  1.00  0.00      P1
ATOM    123  HB2 PRO A  11       9.217  20.638 219.189  1.00  0.00      P1
ATOM    124  CG  PRO A  11       9.735  19.039 217.706  1.00  0.00      P1
ATOM    125  HG1 PRO A  11       9.885  17.972 217.688  1.00  0.00      P1
ATOM    126  HG2 PRO A  11      10.763  19.474 217.701  1.00  0.00      P1
ATOM    127  C   PRO A  11       7.724  19.552 223.177  1.00  0.00      P1
ATOM    128  O   PRO A  11       7.685  20.772 223.027  1.00  0.00      P1
ATOM    129  N   PRO A  12       7.812  19.577 226.682  1.00  0.00      P1
ATOM    130  CA  PRO A  12       7.814  20.018 229.800  1.00  0.00      P1
ATOM    131  HA  PRO A  12       6.802  20.393 229.849  1.00  0.00      P1
ATOM    132  CD  PRO A  12       7.681  18.200 226.923  1.00  0.00      P1
ATOM    133  HD1 PRO A  12       7.091  17.734 226.045  1.00  0.00      P1
ATOM    134  HD2 PRO A  12       8.779  17.853 226.966  1.00  0.00      P1
ATOM    135  CB  PRO A  12       7.867  18.516 229.634  1.00  0.00      P1
ATOM    136  HB1 PRO A  12       7.531  17.976 230.545  1.00  0.00      P1
ATOM    137  HB2 PRO A  12       8.909  18.191 229.519  1.00  0.00      P1
ATOM    138  CG  PRO A  12       7.067  17.942 228.374  1.00  0.00      P1
ATOM    139  HG1 PRO A  12       6.845  16.857 228.453  1.00  0.00      P1
ATOM    140  HG2 PRO A  12       6.061  18.388 228.454  1.00  0.00      P1
ATOM    141  C   PRO A  12       8.034  20.159 233.719  1.00  0.00      P1
ATOM    142  O   PRO A  12       9.084  19.494 233.715  1.00  0.00      P1
ATOM    143  N   GLY A  13       7.810  20.560 236.627  1.00  0.00      P1
ATOM    144  HN  GLY A  13       6.888  20.987 236.547  1.00  0.00      P1
ATOM    145  CA  GLY A  13       8.062  20.688 239.851  1.00  0.00      P1
ATOM    146  HA1 GLY A  13       8.147  21.749 239.779  1.00  0.00      P1
ATOM    147  HA2 GLY A  13       8.949  20.004 239.753  1.00  0.00      P1
ATOM    148  C   GLY A  13       8.020  20.917 243.705  1.00  0.00      P1
ATOM    149  O   GLY A  13       8.109  19.674 243.851  1.00  0.00      P1
ATOM    150  N   PRO A  14       7.994  21.425 247.259  1.00  0.00      P1
ATOM    151  CA  PRO A  14       8.008  21.439 250.489  1.00  0.00      P1
ATOM    152  HA  PRO A  14       8.789  20.747 250.610  1.00  0.00      P1
ATOM    153  CD  PRO A  14       8.006  22.874 247.500  1.00  0.00      P1
ATOM    154  HD1 PRO A  14       8.589  23.198 246.651  1.00  0.00      P1
ATOM    155  HD2 PRO A  14       6.925  23.278 247.511  1.00  0.00      P1
ATOM    156  CB  PRO A  14       8.448  22.875 250.325  1.00  0.00      P1
ATOM    157  HB1 PRO A  14       9.209  23.182 251.012  1.00  0.00      P1
ATOM    158  HB2 PRO A  14       7.599  23.570 250.558  1.00  0.00      P1
ATOM    159  CG  PRO A  14       8.741  23.393 248.819  1.00  0.00      P1
ATOM    160  HG1 PRO A  14       9.784  23.226 248.491  1.00  0.00      P1
ATOM    161  HG2 PRO A  14       8.429  24.455 248.738  1.00  0.00      P1
ATOM    162  C   PRO A  14       7.832  21.881 254.314  1.00  0.00      P1
ATOM    163  O   PRO A  14       7.090  22.844 254.275  1.00  0.00      P1
ATOM    164  N   PRO A  15       7.929  21.917 257.858  1.00  0.00      P1
ATOM    165  CA  PRO A  15       7.656  22.075 261.027  1.00  0.00      P1
ATOM    166  HA  PRO A  15       6.735  21.584 260.980  1.00  0.00      P1
ATOM    167  CD  PRO A  15       9.295  21.366 258.151  1.00  0.00      P1
ATOM    168  HD1 PRO A  15       9.507  20.649 257.420  1.00  0.00      P1
ATOM    169  HD2 PRO A  15      10.034  22.185 258.218  1.00  0.00      P1
ATOM    170  CB  PRO A  15       9.096  21.432 260.938  1.00  0.00      P1
ATOM    171  HB1 PRO A  15       9.110  20.732 261.840  1.00  0.00      P1
ATOM    172  HB2 PRO A  15       9.892  22.214 261.064  1.00  0.00      P1
ATOM    173  CG  PRO A  15       9.298  20.664 259.552  1.00  0.00      P1
ATOM    174  HG1 PRO A  15       8.513  19.872 259.576  1.00  0.00      P1
ATOM    175  HG2 PRO A  15      10.223  20.038 259.594  1.00  0.00      P1
ATOM    176  C   PRO A  15       7.752  22.470 264.807  1.00  0.00      P1
ATOM    177  O   PRO A  15       8.495  23.463 264.682  1.00  0.00      P1
ATOM    178  N   GLY A  16       7.528  22.386 267.721  1.00  0.00      P1
ATOM    179  HN  GLY A  16       7.001  21.531 267.752  1.00  0.00      P1
ATOM    180  CA  GLY A  16       7.488  22.811 270.978  1.00  0.00      P1
ATOM    181  HA1 GLY A  16       6.451  23.162 270.999  1.00  0.00      P1
ATOM    182  HA2 GLY A  16       8.181  23.631 270.870  1.00  0.00      P1
ATOM    183  C   GLY A  16       7.424  22.853 274.761  1.00  0.00      P1
```

```
ATOM    184  O   GLY A  16       8.482  22.280 274.795  1.00  0.00      P1
ATOM    185  N   PRO A  17       7.028  23.123 278.257  1.00  0.00      P1
ATOM    186  CA  PRO A  17       7.091  23.195 281.446  1.00  0.00      P1
ATOM    187  HA  PRO A  17       8.103  23.495 281.507  1.00  0.00      P1
ATOM    188  CD  PRO A  17       5.991  24.180 278.342  1.00  0.00      P1
ATOM    189  HD1 PRO A  17       6.228  24.847 277.454  1.00  0.00      P1
ATOM    190  HD2 PRO A  17       5.041  23.753 278.013  1.00  0.00      P1
ATOM    191  CB  PRO A  17       5.996  24.301 281.131  1.00  0.00      P1
ATOM    192  HB1 PRO A  17       6.043  25.095 281.916  1.00  0.00      P1
ATOM    193  HB2 PRO A  17       4.994  23.933 280.999  1.00  0.00      P1
ATOM    194  CG  PRO A  17       6.164  25.038 279.754  1.00  0.00      P1
ATOM    195  HG1 PRO A  17       7.149  25.484 279.701  1.00  0.00      P1
ATOM    196  HG2 PRO A  17       5.330  25.793 279.811  1.00  0.00      P1
ATOM    197  C   PRO A  17       6.628  23.250 285.253  1.00  0.00      P1
ATOM    198  O   PRO A  17       5.430  23.127 285.128  1.00  0.00      P1
ATOM    199  N   PRO A  18       6.685  23.342 288.799  1.00  0.00      P1
ATOM    200  CA  PRO A  18       6.395  23.209 291.897  1.00  0.00      P1
ATOM    201  HA  PRO A  18       6.114  22.176 291.868  1.00  0.00      P1
ATOM    202  CD  PRO A  18       8.010  23.824 288.990  1.00  0.00      P1
ATOM    203  HD1 PRO A  18       8.717  22.959 288.891  1.00  0.00      P1
ATOM    204  HD2 PRO A  18       8.217  24.624 288.301  1.00  0.00      P1
ATOM    205  CB  PRO A  18       7.895  23.505 291.754  1.00  0.00      P1
ATOM    206  HB1 PRO A  18       8.548  22.544 291.757  1.00  0.00      P1
ATOM    207  HB2 PRO A  18       8.101  24.114 292.664  1.00  0.00      P1
ATOM    208  CG  PRO A  18       8.262  24.397 290.483  1.00  0.00      P1
ATOM    209  HG1 PRO A  18       9.305  24.681 290.534  1.00  0.00      P1
ATOM    210  HG2 PRO A  18       7.525  25.276 290.749  1.00  0.00      P1
ATOM    211  C   PRO A  18       6.244  23.474 295.699  1.00  0.00      P1
ATOM    212  O   PRO A  18       6.437  24.709 295.752  1.00  0.00      P1
ATOM    213  N   GLY A  19       6.006  23.186 298.645  1.00  0.00      P1
ATOM    214  HN  GLY A  19       5.939  22.211 298.532  1.00  0.00      P1
ATOM    215  CA  GLY A  19       5.798  23.377 301.848  1.00  0.00      P1
ATOM    216  HA1 GLY A  19       4.746  23.318 301.936  1.00  0.00      P1
ATOM    217  HA2 GLY A  19       6.110  24.395 301.871  1.00  0.00      P1
ATOM    218  C   GLY A  19       5.778  23.273 305.634  1.00  0.00      P1
ATOM    219  O   GLY A  19       6.997  23.446 305.585  1.00  0.00      P1
ATOM    220  N   PRO A  20       5.399  23.199 309.179  1.00  0.00      P1
ATOM    221  CA  PRO A  20       5.435  23.279 312.290  1.00  0.00      P1
ATOM    222  HA  PRO A  20       6.225  24.071 312.296  1.00  0.00      P1
ATOM    223  CD  PRO A  20       4.091  23.666 309.364  1.00  0.00      P1
ATOM    224  HD1 PRO A  20       4.182  24.738 309.452  1.00  0.00      P1
ATOM    225  HD2 PRO A  20       3.301  23.358 308.611  1.00  0.00      P1
ATOM    226  CB  PRO A  20       4.029  23.829 312.025  1.00  0.00      P1
ATOM    227  HB1 PRO A  20       4.150  24.922 311.873  1.00  0.00      P1
ATOM    228  HB2 PRO A  20       3.350  23.727 312.938  1.00  0.00      P1
ATOM    229  CG  PRO A  20       3.314  23.215 310.758  1.00  0.00      P1
ATOM    230  HG1 PRO A  20       2.291  23.551 310.663  1.00  0.00      P1
ATOM    231  HG2 PRO A  20       3.280  22.143 310.724  1.00  0.00      P1
ATOM    232  C   PRO A  20       5.122  23.016 316.037  1.00  0.00      P1
ATOM    233  O   PRO A  20       4.368  22.016 315.961  1.00  0.00      P1
ATOM    234  N   PRO A  21       5.119  23.114 319.505  1.00  0.00      P1
ATOM    235  CA  PRO A  21       5.063  22.780 322.656  1.00  0.00      P1
ATOM    236  HA  PRO A  21       5.843  22.061 322.703  1.00  0.00      P1
ATOM    237  CD  PRO A  21       5.368  24.543 319.780  1.00  0.00      P1
ATOM    238  HD1 PRO A  21       6.501  24.665 319.689  1.00  0.00      P1
ATOM    239  HD2 PRO A  21       4.900  25.232 319.003  1.00  0.00      P1
ATOM    240  CB  PRO A  21       5.367  24.409 322.456  1.00  0.00      P1
ATOM    241  HB1 PRO A  21       6.434  24.463 322.502  1.00  0.00      P1
ATOM    242  HB2 PRO A  21       4.981  24.867 323.378  1.00  0.00      P1
ATOM    243  CG  PRO A  21       4.710  24.931 321.155  1.00  0.00      P1
ATOM    244  HG1 PRO A  21       4.763  26.071 321.349  1.00  0.00      P1
ATOM    245  HG2 PRO A  21       3.647  24.703 321.227  1.00  0.00      P1
ATOM    246  C   PRO A  21       4.690  22.755 326.438  1.00  0.00      P1
```

A.3. Supplimentaty figures for chapter 6

(a)

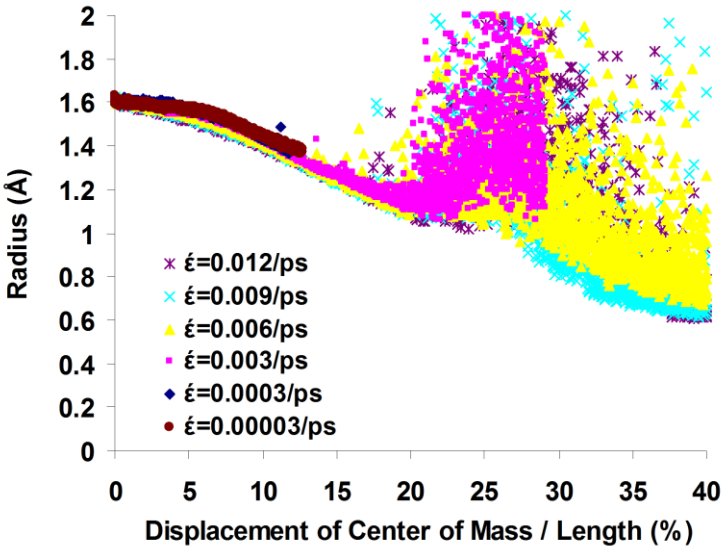

(b)

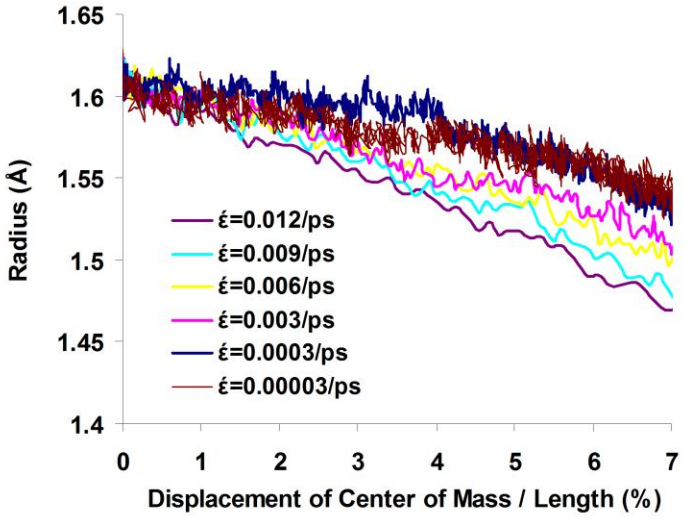

Figure A.3.1. Average radius of the level-1 helix (i.e. alpha chain) during extension of collagen at various pulling rates and spring constants: (a) large displacement (k = 0.1 kcal/mol/Å^2), (b) small displacement (k = 0.1 kcal/mol/Å^2), (c) large displacement (k = 0.1 kcal/mol/Å^2), (d) small displacement (k = 0.1 kcal/mol/Å^2).

(c)

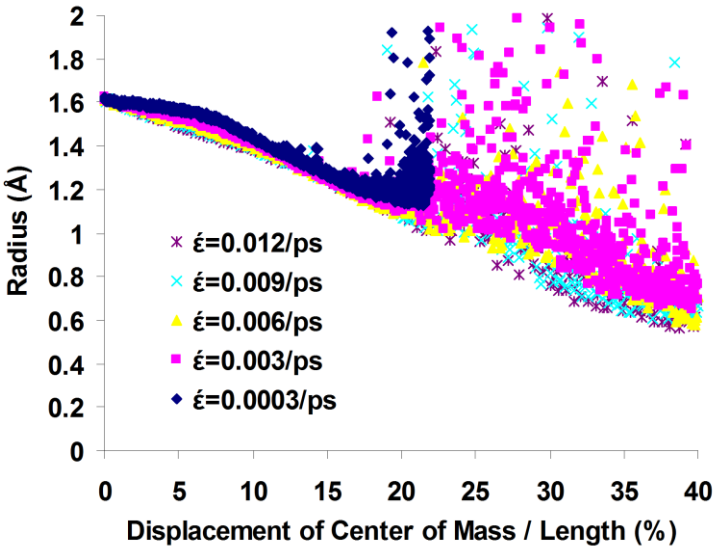

(d)

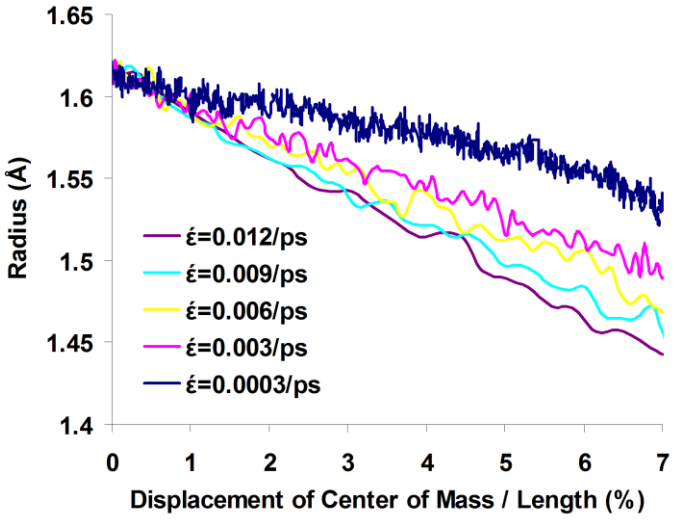

Figure A.3.1. Average radius of the level-1 helix (i.e. alpha chain) during extension of collagen at various pulling rates and spring constants: (a) large displacement (k = 0.1 kcal/mol/Å2), (b) small displacement (k = 0.1 kcal/mol/Å2), (c) large displacement (k = 0.1 kcal/mol/Å2), (d) small displacement (k = 0.1 kcal/mol/Å2). (continued)

(a)

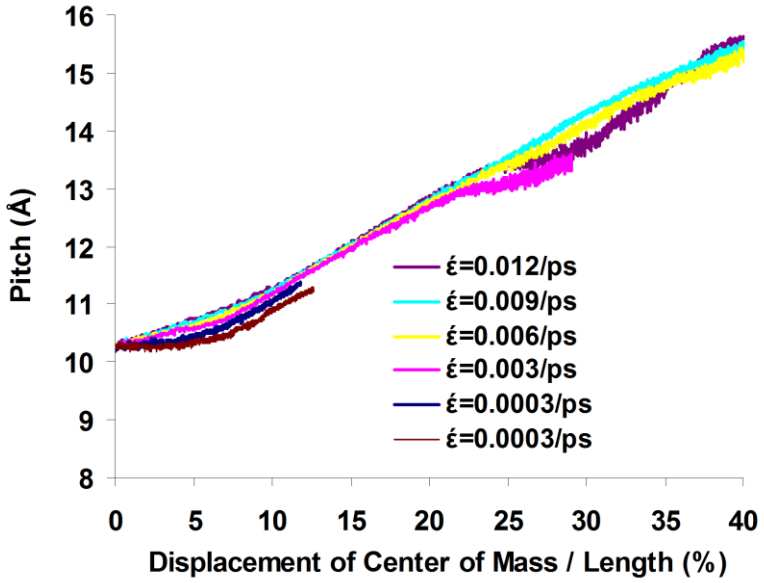

(b)

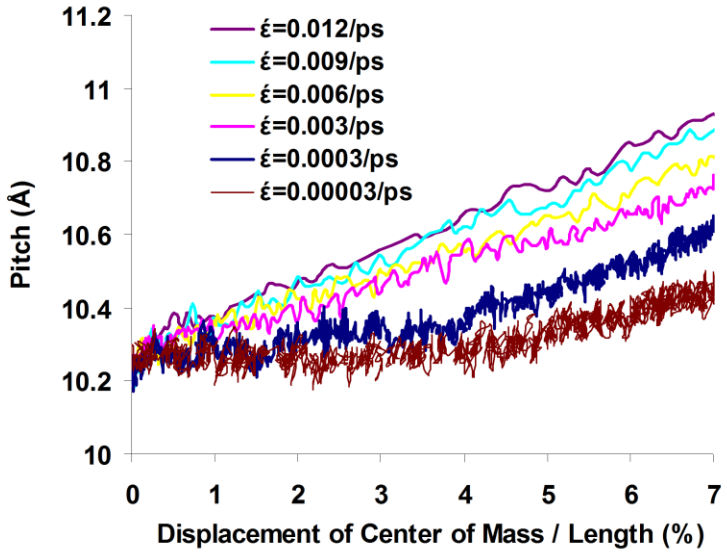

Figure A.3.2. Average pitch of the level-1 helix (i.e. alpha chain) during extension of collagen at various pulling rates and spring constants: (a) large displacement (k = 0.1 kcal/mol/Å^2), (b) small displacement (k = 0.1 kcal/mol/Å^2), (c) large displacement (k = 1.0 kcal/mol/Å^2), (d) small displacement (k = 1.0 kcal/mol/Å^2).

(c)

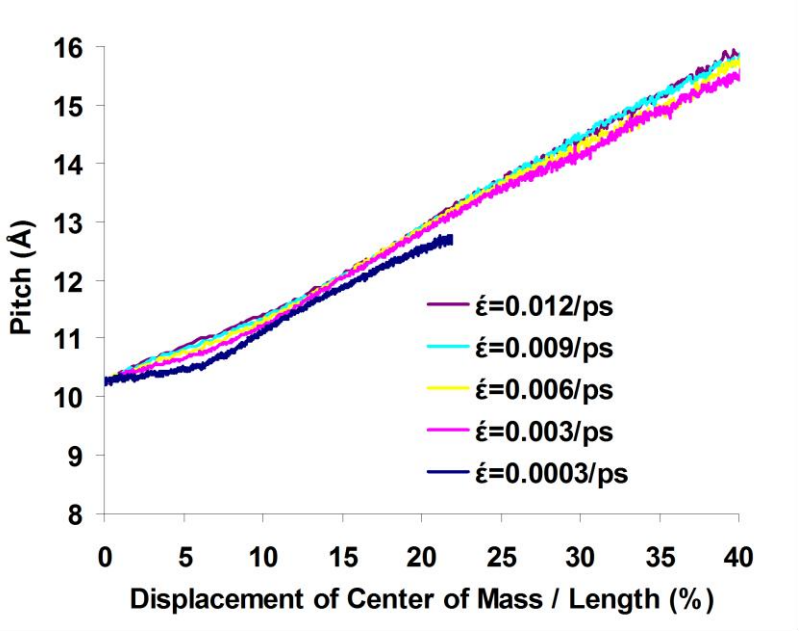

(d)

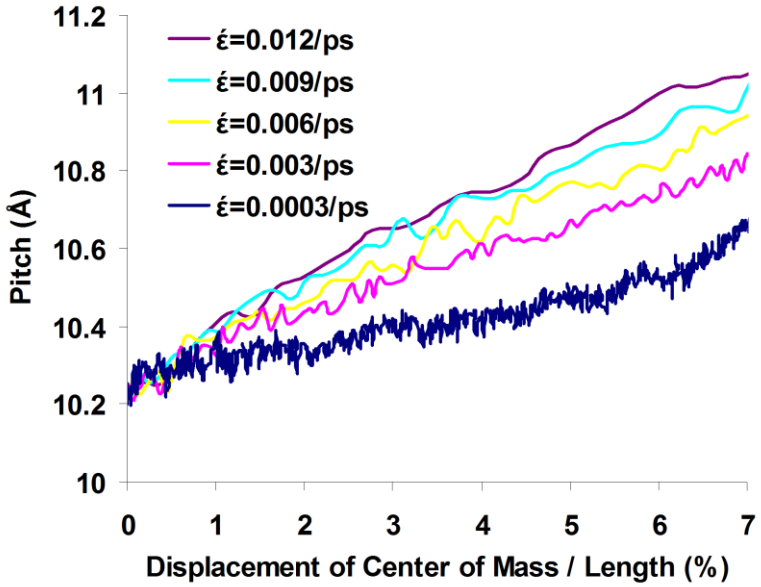

Figure A.3.2. Average pitch of the level-1 helix (i.e. alpha chain) during extension of collagen at various pulling rates and spring constants: (a) large displacement (k = 0.1 kcal/mol/Å^2), (b) small displacement (k = 0.1 kcal/mol/Å^2), (c) large displacement (k = 1.0 kcal/mol/Å^2), (d) small displacement (k = 1.0 kcal/mol/Å^2). (Continued)

(a)

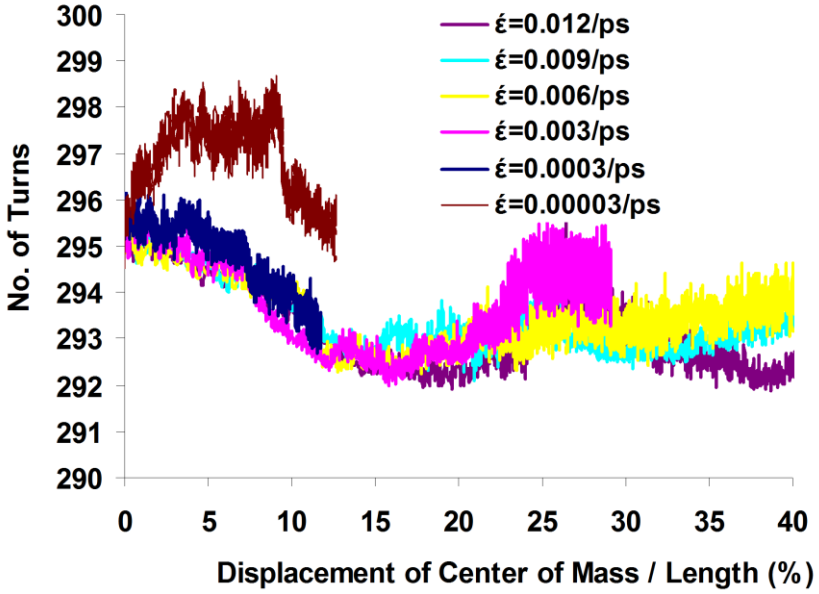

(b)

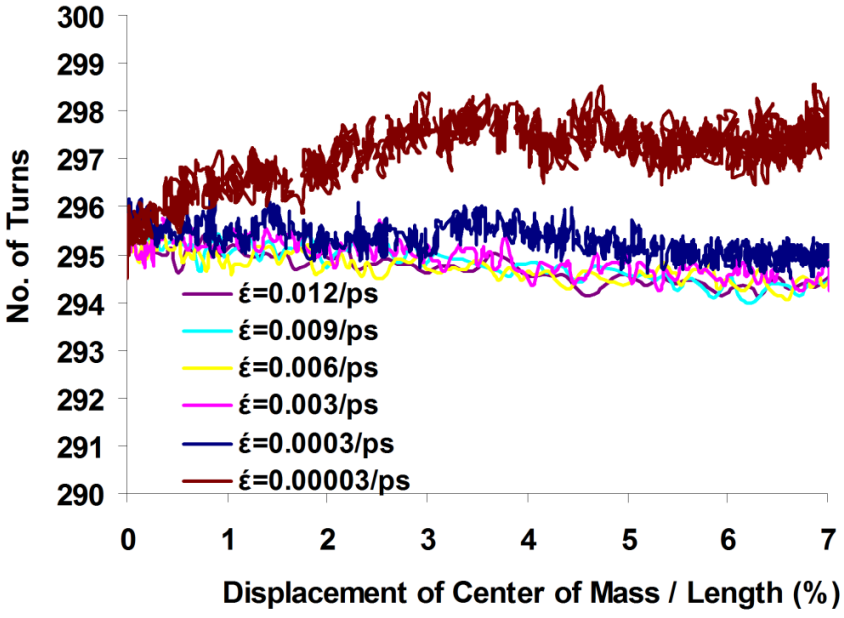

Figure A.3.3. Variation of the total number of turns along the length of the level-1 helix (i.e., α-chain) during loading: (a) large displacement (k = 0.1 kcal/mol/Å^2), (b) small displacement (k = 0.1 kcal/mol/Å^2), (c) large displacement (k = 1.0 cal/mol/Å^2), (d) small displacement (k = 1.0 kcal/mol/Å^2).

(c)

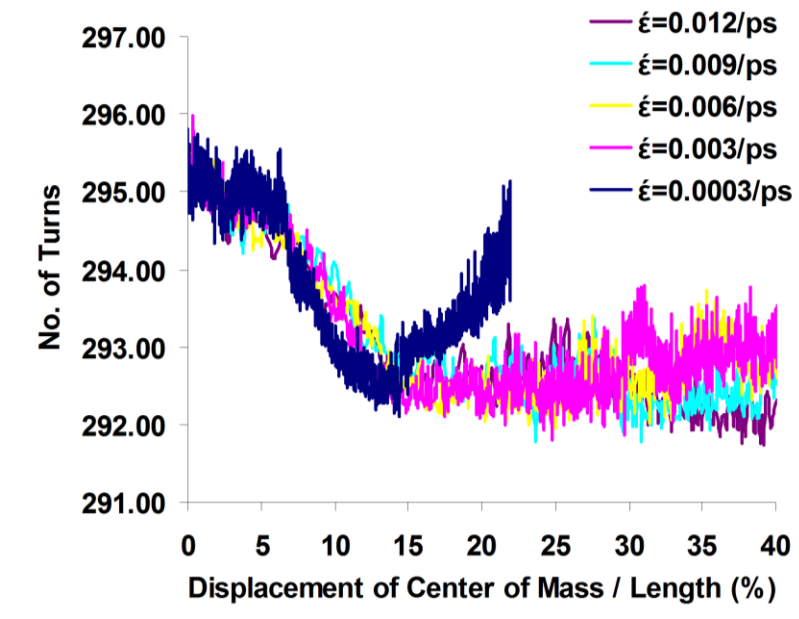

(d)

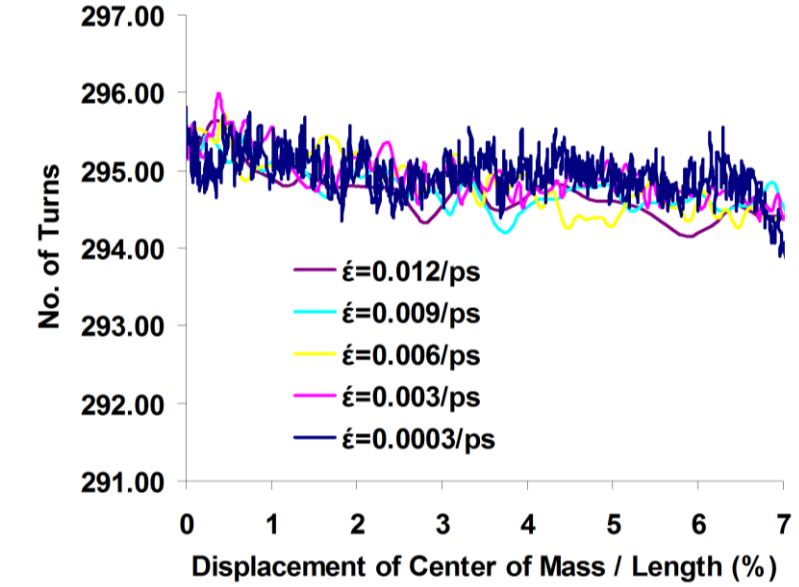

Figure A.3.3. Variation of the total number of turns along the length of the level-1 helix (i.e., α-chain) during loading: (a) large displacement (k = 0.1 kcal/mol/Å2), (b) small displacement (k = 0.1 kcal/mol/Å2), (c) large displacement (k = 1.0 cal/mol/Å2), (d) small displacement (k = 1.0 kcal/mol/Å2). (Continued)